UNIVERSITY OF L'AQUILA
DEPARTMENT of Physical and Chemical Sciences

PhD in Physical and Chemical Science

XXXIII Cycle

Thesis title

APPLICATIONS OF HYDROGELS: Surfactants and polysaccharides as highly versatile gelators

SSD CHIM/06

PhD Student

Gabriele Francesco

Course coordinator

Prof. Antonio Mecozzi

Tutor

Prof. Nicoletta Spreti

A.A. 2019/2020

Table of contents

Abstract

Hydrogels are unique materials composed of hydrophilic gelators linked together in a three-dimensional network capable of encapsulating large amounts of water. These materials are easily adaptable to different application areas i.e. biomedical areas, agriculture, removal of heavy metals from water or in food industry.

In this thesis, some eco-sustainable gelators have been selected as starting materials to develop hydrogels that possess characteristics related to the selected applications. For this purpose, zwitterionic amine oxide surfactants and polysaccharides, i.e. alginate and chitosan, were selected for their ability to form hydrogels by modulating their concentration or by adding crosslinking agents.

In Section B, several common techniques were selected to fully characterize the two polysaccharides in order to determine their structural features, which can affect the hydrogels properties.

In Section C, the hydrogels were prepared based on the selected application areas i.e. bioconversion, food packaging and cultural heritage.

The effect of surfactants structure and immobilization into hydrogel structure on the catalytic properties of Candida rugosa lipase (CRL) was investigated. The selected amine oxide surfactants exploited an improvement of the enzymatic activity as a function of the morphology of the micellar aggregates; in particular, by varying the headgroup size and the chain length, the micelles shift from spherical to rod-like leading to an increased hydrolytic activity. Furthermore, CRL was effectively entrapped in alginate hydrogel beads formed by ionotropic gelation induced by calcium ions. Different bead formulations were prepared and the effect of their morphology on the catalytic properties of CRL was assessed by studying two model reactions. The immobilized lipase showed noticeable recyclability and improved thermostability compared to the free enzyme.

Part of this study was addressed to the application of chitosan-based hydrogels to prepare membranes applicable as eco-friendly food packaging material. Chitosan-succinate films were prepared, starting by their hydrogel form, by solvent casting method using glycerol as plasticizer. The NaOH-neutralized membranes, compared to the non-neutralized ones, showed improved mechanical and physicochemical properties. The formation of amide bonds between chitosan and succinic acid, suggested by the FTIR analysis, was then confirmed by acid-base titration. The prepared membranes are currently under preliminary study as novel food packaging for pecorino cheese samples.

The last part of this thesis is included in a wider project focused on “Product and process innovation for maintenance, preservation and sustainable programmed restoration of cultural heritage” (Smart Cities and Communities and Social Innovation on Cultural Heritage project). It aimed at the improvement of the restoration and maintenance intervention on stone-based cultural heritages. For this purpose, novel approaches to reduce microbial colonization from stone materials were developed using classic oxidant biocidal agents supported in alginate hydrogels.

Novel ionically crosslinked alginate hydrogels, which contain oxidative biocides were developed and tested. All hydrogel formulations were able to eliminate biofilms from the stone surface, keeping the chromaticity and capillary properties of the cleaned stones unchanged. To assess the presence of residues, any type of surface alteration and to evaluate the hygroscopic behavior of the stone samples, microscopic techniques, colorimetry and 1H-NMR T2 relaxation measurements have been performed. They were applied both on a laboratory scale, using calcarenite specimens artificially colonized by filamentous cyanobacteria and green microalgae and “in situ” on stone artworks in rupestrian churches of “Sassi of Matera”.

Section A

Hydrogels

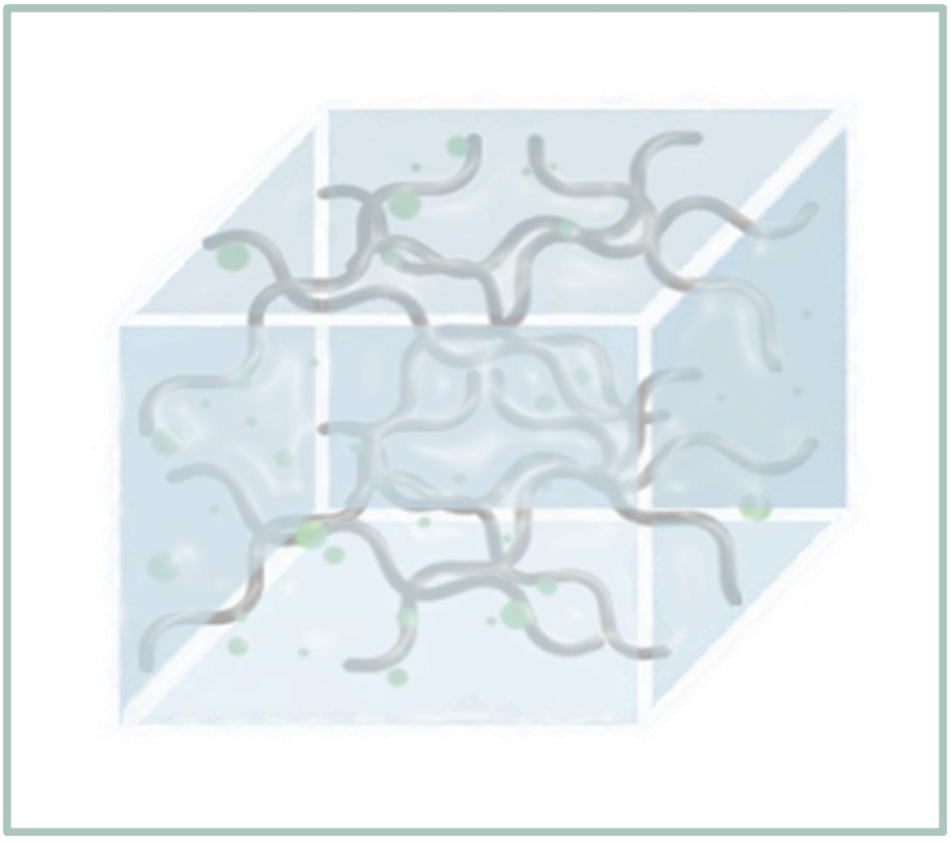

Chapter A 1

Introduction

A 1.1 Hydrogels: An overview

Hydrogels were discovered around the 1960s, when one of the first crosslinked hydrogels, hexamethyl methacrylate (HMMA), was prepared and tested for biological use. The authors of the time talked about the possible employment of "plastic" in permanent contact with living tissue.[1] This represents a contradictory concept if we think about the controversy over plastic materials and on the problems associated with them today. Nevertheless, some highly interactive hydrophilic materials can present intrinsic characteristics making that biocompatible. Extending this concept, it is possible to define a hydrogel as a three-dimensional crosslinked network of hydrophilic molecules or macromolecules that origin well organized supramolecular structures that swell in water without solubilize in short times.[2-4]

The great interest addressed after their discovery to these materials is due to their high similarity with living tissues: rubbery consistency, high water content, reactivity to stimuli and ability to absorb biological fluid.[5] These properties, in addition to the possibility of dispersing and diffusing substances and / or particles in their network, have made hydrogel very promising materials for biomedical and pharmaceutical applications. Nevertheless, even more studies show how they can be applied in many different scientific areas such as engineering, cultural heritage, food, water depuration and more.

The growing attention paid to hydrogels in most fields is clearly due to the possibility to design tunable, responsive and adaptable materials. In fact, there are a multitude of molecules capable of forming hydrogels and, at the same time, are

also able to respond at different chemical or physical stimuli such as magnetism, temperature, light, pH, ions and more.[2,6]

The properties of hydrogels as well as their tuneability depend on the nature of the components, on the nature of gelation process and on the degree of crystallinity of the three-dimensional network.

A 1.1.1 Classification of hydrogels

As well as for the definitions of hydrogel, the literature presents several different ways to classify these systems. Generally, is possible to regroup the classification based on the nature of constituents, crosslinking and structure. As shown in Figure A 1.1, each of them can be also divided into other subgroups.[3,6-8]

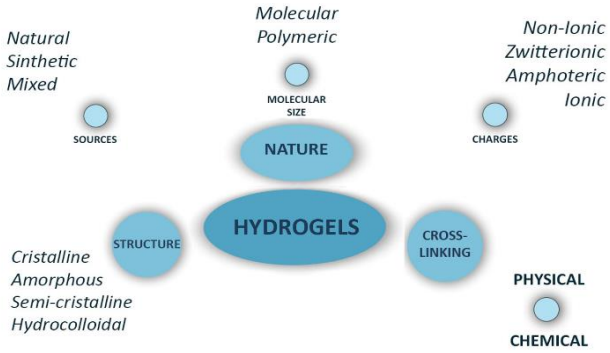

Figure A 1.1: Schematic representation of hydrogel classifications.

Nature of constituents

The classifications based on the nature of constituents can be divided in three macro-groups depending on their source, the size and the electrical charge. Hydrogels, for their definition, can be based on natural or synthetic constituents all characterized by many hydrophilic functions. Usually "natural" hydrogels are characterized by biodegradability and high biocompatibility but at the same time present worse mechanical properties than that made up by synthetic constituents. Moreover, a series of works talk about hydrogels in which the network is constituted by a mix of these classes.

Another way to classify these systems is based on their components charge. Indeed, hydrogels can consist of non-ionic, non-charged unit, ionic, anionic or

cationic units, amphoteric, which show anionic and cationic sub-units and zwitterionic components.[6] Furthermore, depending on the molecular size of constituents, hydrogels can be divided into molecular- and polymeric-based.

Molecular hydrogels are based on self-assembling non-covalent interactions that generate supramolecular structures capable of trapping water. The main representative driving force of the gelation process is usually represented by the interactions of the hydrogen bond between the gelators.[3] In addition, even amphiphilic molecules such as surfactants, through weak interactions, can aggregate into complex supramolecular structures, different from the classic micelle. Thus, gelation process arises when the little gelator molecules form entangled secondary structures (such as fibers, ribbon, worm, tube and others) able to entrap water via surface tension.[3,7] Moreover, as schematically reported in Figure A 1.2, some secondary structures are capable of forming chiral supramolecular aggregates, such as tape, ribbon, fibril and fiber, as the amount of gelator is increased.

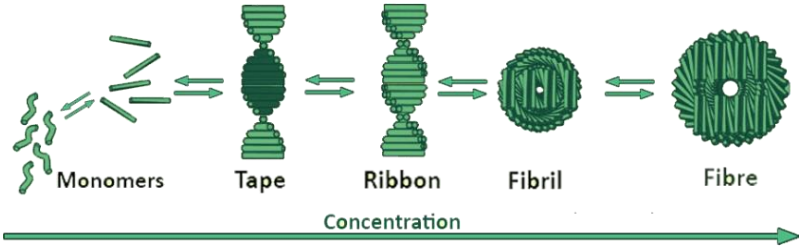

Figure A 1.2: Rod-like monomers organized in chiral supramolecular tertiary structures depending on the surfactant concentration.

On the other hand, polymeric hydrogels are defined as single- or multi-polymer systems in which the polymeric chains are entangled and crosslinked one another to constitute a 3D-network. Only polymers made up of a high amount of polar functions, such as -NH_2, -COOH, -OH, -$CONH_2$, and showing opportune degree of hydrophilicity are able to form hydrogels.[4,6,9] According to the component structures, it is possible to define the system as homo-polymeric, if the network

derives from a single monomer or copolymeric, if the monomers involved in the polymer chain formations are two or more.

Regardless of their structures, semi-interpenetrating (S-IPN) and interpenetrating (IPN) networks constitute another class of mixed polymeric hydrogels. The former is constituted at least of a cross-linked polymeric network in which a non-crosslinked polymer is dispersed; the other is formed by two crosslinked polymers having their network entangled in each other.[6]

Nature of crosslinking

The crosslinks represent a fundamental characteristic of hydrogels and once introduced into a network the system thus obtained will show elastic and / or viscoelastic properties. The nature of the crosslinking, both physical and chemical, defines the properties of the hydrogels and therefore their possible applications field.[4,10]

Physical hydrogels are characterized by non-covalent interactions between the components that constitute the network. Generally, it is achieved when weak interactions, such as hydrogen bonding, Van der Waals and hydrophobic interactions, or ionic interactions are formed. Physical gelation process is strictly related with the structure of hydrogel components and can be obtained in different ways. The main physical cross-links, shown schematically in Figure A 1.3, are easily reversible, therefore the cross-linking can be used as a phase transition switch SOL-GEL / GEL-SOL.[4,6,9,11,12]

Thermal condensation refers to those systems in which heat-sensitive components are present. These can be characterized by a lower critical solution temperature (LCST) or an upper critical solution temperature (UCST) below and above which the system is homogeneous, respectively.[9] Moreover, self-assembled hydrogels are formed by physical non-covalent interactions, that, once established, force the molecules to fold in a well-organized supramolecular structure. Another reversible gelation occurs when two opposing charge systems are brought into contact. This

kind of gelation process can be classified as ionic gelation, if a charged polymer was reticulated with a small counterion, or as electrostatic gelation when two oppositely charged polyelectrolytes are brought into contact.[11,12]

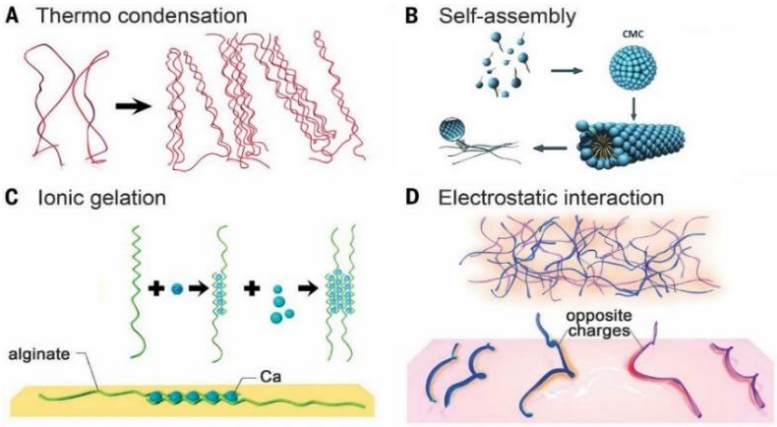

Figure A 1.3: Schematic representation of physical gelation: thermal (A), self-assembly (B), ionic (C) and electrostatic (D).

In addition, physical crosslinking is also possible through crystallization process. In this system high ordered interactions are established between components to form crystallite moieties that acts as physical crosslinker.[13,14]

On the contrary, chemical covalent crosslinking is not reversible but is more controllable and confer high order, tunable swelling and better mechanical properties to the hydrogels.[10-12] These reticulation methods are referred only to the polymer-based hydrogels. Covalent crosslinking can usually be made up by using crosslinking molecules, such as glutaraldehyde, formaldehyde, epoxy compounds and dialdehyde. These agents can link the hydrophilic moieties of polymers chains forming well-ordered network.[10] Another way to form chemical hydrogels is represented by the radical polymerization of soluble polymer functionalized with polymerizable groups. Using an opportune initiator, it was possible to control the polymerization process and, therefore, the hydrogels properties.[10,11]

Structures

Hydrogels are a 3D-structured material, then can be described by configuration and chemical composition of the components; these define the main properties of a hydrogel. Indeed, these systems can be classified according to the order of the system in their structures. Therefore, it is possible to define amorphous hydrogels as highly disordered systems in which components are randomly dispersed. On the contrary, in crystalline systems components and structured motifs are regularly repeated in space. Finally, semi-crystalline hydrogels are characterized by a complex mixture of amorphous and crystalline structures.[4,6, 15,16]

A 1.1.2 Eco-friendly hydrogels

One of the main advantages that led researchers to develop hydrogel-based systems in many scientific areas is the low environmental impact, biodegradability and biocompatibility that characterize these systems. Compared to polymeric hydrogel of a synthetic nature, natural hydrogels based on polysaccharides, proteins or DNA as constituents, are safer and also show greater hydrophilicity and water absorption capacity. In addition, these materials can be often recovered and extracted from secondary raw materials, further reducing their environmental impact.[17,18] Furthermore, depending on the origin of gelators, self-assembled three-dimensional networks are usually considered relatively safe and biocompatible too, due to the non-covalent interactions underlying the formation of the hydrogel. In fact, these supramolecular aggregates can be easily degraded, if compared to the polymeric materials. Nowadays, many classes of molecules capable of forming these types of safe hydrogels have been studied and employed for several applications, such as small peptides, derivatives of small natural molecules and surfactants.[3,7]

A 1.2 Surfactant-based hydrogels

The term surfactant, that derives from the surface-active-agent, is referred to amphiphilic molecules characterized by a polar head group and a hydrophobic tail capable of modifying the interfacial properties of liquids. Being the hydrophobic

tail of most surfactants a hydrocarbon chain, their classification generally is based on the nature of the head groups; therefore, they are classifiable as ionic (cationic or anionic), non-ionic or zwitterionic. Anionic amphiphiles represent the widely used surfactants because of their powerful detergent action. This class of amphiphilic molecules is usually characterized by different negatively charged head groups such as carboxylates, sulphates, sulfonate and phosphate. On the other hand, cationic surfactants consist in positively charged head groups generally based on quaternary ammonium salts. Neutral amphiphilic species are constituted by non-charged head groups (e.g. polyoxyethylene alkyl ethers). Finally, in zwitterionic surfactants, the head groups consists in both positive and negative portion such as betaine, sulfobetaine, amine oxide and others; depending on the pH of the solution the head group can exhibit only one charge (positive in acid media and negative in alkaline media) or both charge together(around the isoelectric point).[19,20]

A 1.2.1 Aggregation and morphologies of amphiphiles

Regardless of their classification, the amphiphilic molecules in solution will be positioned at the interface between the polar and non-polar phases. The hydrophilic group interacts with the water molecules while the hydrophobic tail will face the non-polar system (for example air or non-polar liquids), forming an oriented monolayer.[21] As long as this behavior is observed, a surfactant solution acts as an electrolytic solution capable of reducing the surface activities of the solvent. Once the concentration of amphiphilic molecules has exceeded the critical micellar concentration (CMC), well-ordered aggregates, called micelle, are formed. The driving force beside the formation of these amphiphilic aggregates lies in the soft interactions established between surfactant molecules such as hydrogen bonds, Van der Waals forces, hydrophobic effects and electrostatic interactions.[3,21] Although these interactions are weak, their large amount produces an overall effect that holds the amphiphiles together, ensuring the stability of the micelles in

solution. On the other hand, thanks to the soft interactions established in their formation, these aggregates turn out to be dynamic and flexible structures in which the building blocks are in dynamic equilibrium with the mass solution.

The formation of these ordered aggregates in solution can be explained thermodynamically considering both the favorable enthalpy contribution, due to the formation of new water-surfactant and surfactant-surfactant interactions, and the entropy of the system, which increases due to the hydrophobic effect induced by the interactions between the tails of the surfactant. Considering the overall interactions, the energy dissipated during the breakdown of the hydrogen bond network characteristic of bulk water, caused by the formation of micelles, is balanced by the new hydrogen bond interactions established between the polar head of amphiphiles and the molecules of water surrounding the aggregates. Furthermore, another contribution to be taken into consideration derives from the hydrophobic interactions formed between the tails of the surfactants inside the micelles. On the other hand, the formation of ordered aggregates is entropically unfavorable but is balanced by the distortion of the network of H-bonds around the micelle, to which is due an increase in the entropy of the system.[22]

The shape and the size of the micellar aggregates is strictly related to the solution conditions and can be estimated analyzing the critical packing factor (C_{pp}). This parameter, descripted in Figure A 1.4, represents the geometry hired by the surfactant molecules through which is possible to predict the micellar morphologies.

$$C_{pp} = \frac{V}{a_0 \cdot l_c}$$

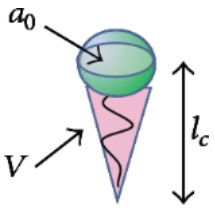

Figure A 1.4: Critical packing parameter equation its scheme in a generic amphiphile molecule.

As represented in the figure, V and l_c are referred to the hydrophobic chain and represent respectively its occupied volume and the maximum effective length. The parameter indicated as a_0 represents the effective surface of the hydrophilic head showed at the interface between the aggregate and the solution. As shown in Figure A 1.5, to an increment of the critical packing parameter, caused by the increase in the size of the tail (V and l_c) and/or the decrease in the surface of the head group (a_0), correspond a shift in the amphiphilic molecule from cone geometry until cylindric and inverted cone.

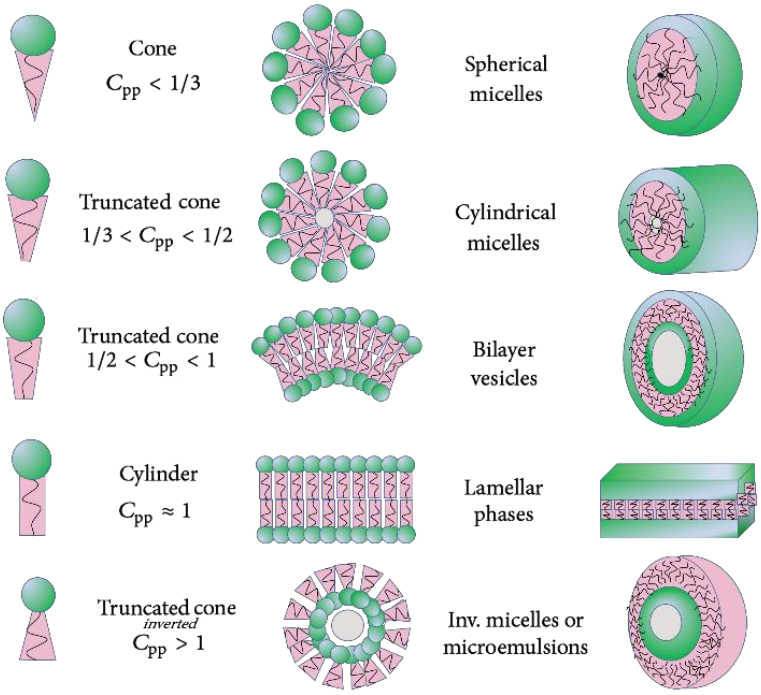

Figure A 1.5: Schematic representation of the main surfactant shape and the morphologies associated.

These estimated geometries well explain the pattern of possible secondary structures that can be obtained.[22,23] Indeed, increasing their concentration exceeding the CMC, amphiphilic molecules characterized by truncated cone geometry can form ellipsoidal micelles capable of further increase their longitudinal dimensions forming fibers as aggregates.[3] Moreover, if the packaging parameter tends to the unit, also vesicles and double layer can be formed.[22,23]

The shape of amphiphiles also affect the phase diagram of the binary mixture water-surfactant and its behavior. For instance, Figure A 1.6 shows a hypothetical phase diagram water-surfactant, in which the temperature was plotted as function of the amount of surfactant.

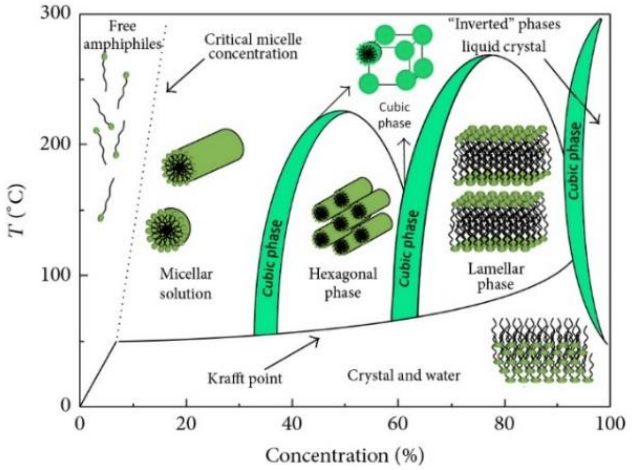

Figure A 1.6: Hypothetical phase diagram in which the positions of the cubic, hexagonal and lamellar phases are showed.

Depending on these it is possible to shift from one phase to another. For instance, cooling the two-component system below the Krafft point a heterogeneous system will be formed by water and hydrated amphiphilic crystals, while warming the system it is possible to shift from ordered to disordered phase.[22,24]

When the amount of the amphiphilic molecules largely increases and the temperature exceeds the Krafft point, liquid crystals phases can be observed. There are two main type of tertiary structures in which liquid crystal can exists, lamellar and hexagonal phases. The first mesomorphic phase is characterized by a series of double layers while the other is formed by linear rigid rod-like structures each one packed close to the other forming a hexagonal motif. Both the described mesomorphic phases are liquid, anisotropic and viscous.[22,24,25] Cubic arrangement is usually considered an intermediate phase between the two described liquid crystal aggregates. This phase, formed by densely packed spherical aggregates

ordered in cubic tertiary structures, is an isotropic liquid crystal. Surfactant-water binary mixtures organized in the cubic phase show glass-like viscoelastic behavior and high yield stress that are typical characteristics of a gel system.[24,26]

A 1.2.2 Molecular gel formations

Some micellar aggregates can change the rheological properties of their solution just at a low concentration, forming viscoelastic self-assembled hydrogel systems. As indicated above, depending on the critical packing parameter, C_{pp}, it is possible to predict from the geometry of the amphiphiles, the secondary structure in which they aggregate.[26] Furthermore, the packing parameter can be influenced by adding a cosurfactant to the amphiphilic solution; these kind of species, interacting with the head group or with the hydrophobic tail, are capable of modifying the geometry of the surfactant and, consequently, the secondary structure of the aggregates.[26-28]

In some cases, structural change of the aggregates can be induced simply varying the temperature. As shown in Figure A 1.7, adding 5-methyl salicylic acid (5mS) as cosurfactant to an aqueous solution of cetyltrimethylammonium bromide (CTAB) in equimolar ratio, worm-like micelles will be formed. Nevertheless, also vesicular aggregates can be obtained, only exceeding the amount of 5mS among CTAB.

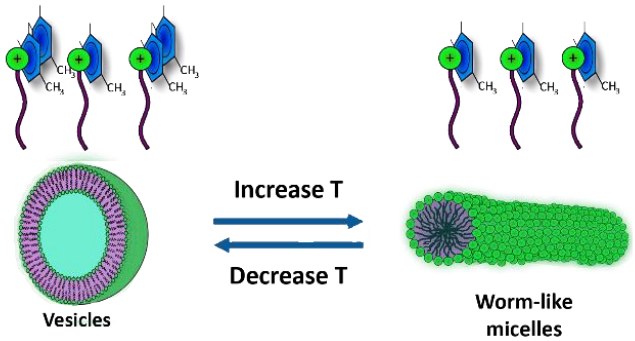

Figure A 1.7: Mechanism of the vesicle to worm-like micelles transition in the CTAB/5mS system.

In this condition, by changing the temperature of the system, the structure of the aggregates can easily shift from vesicles to worm-like micelles and vice versa as a result of a partial exchange of 5mS from the vesicles to water solution.[29]

Densely packed bilayer vesicle gels

Bilayer arrangement is a very common secondary structure observed in surfactant solutions, starting from the lamellar organization, typical of lyotropic liquid crystals, up to disk and vesicles. Compared to the micelles, the colloidal solutions composed by vesicles significantly vary the rheology of the solution considerably increasing its viscosity and conferring to it a viscoelastic behavior typical of a hydrogel system.[30] The vesicular aggregates, schematically represented in Figure A 1.8, are composed of closed double layer of surfactant that encapsulate a large amount of water and can be classified according to their stratification as unilamellar vesicles (ULV) and multilamellar vesicles (MLV).

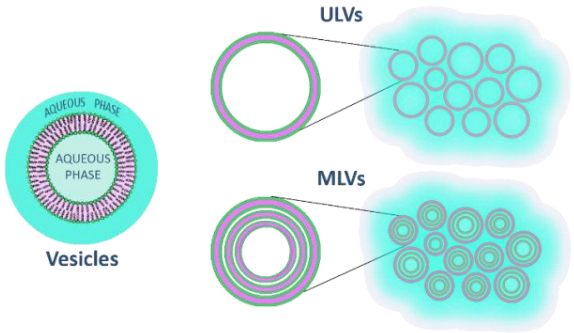

Figure A 1.8: Vesicles schematization: unilamellar (ULVs) and multilamellar (MLVs) densely packed vesicles.

ULVs are often obtained spontaneously when suitable cosurfactants are added to solution of anionic surfactants. Typically, they are spherical aggregates sized around 20 and 200 nm. Both classes of vesicles are capable of forming hydrogels due to their dense packing in solution as the concentration of surfactant, and often of cosurfactants, increases.[31] The higher viscosity observed for the ULVs compared to the micelles can be attributed to the volume fraction of the vesicles which far exceeds the effective surfactant fraction in solution, precisely because of the large

amount of water confined in these aggregates. On the other hand, the multilamellar systems are formed by concentric and multiple layers of vesicles. The secondary structures of these aggregates can change ranging from spherical to polyhedral shape increasing the surfactant concentration in order to allow a denser packaging.[28,31] Unlike ULVs, MLVs generally encapsulate less water due to the presence of multiple concentric vesicles. Furthermore, due to their stratification and larger size, their viscous behavior is very complex compared to that observed for the individual vesicles. However, many of these systems still could exhibit gel-like behavior also attributable to the dense aggregates packing.[28,30,31]

Worm-like micellar hydrogels

Another way to obtain high viscous surfactant-based hydrogel system is represented by the formation of the so-called rod- or worm-like micelles. These aggregates, as for the lamellar double layer, are characteristic of well-known phases (hexagonal phases) of liquid crystals, previously described, of which they are rigid components in an ordered mesh of fibers. At very low concentration worm-like micelles are much more flexible aggregates that can be formed when the amphiphilic molecules show a packing parameter that ranges above 0.5 and 0.3. As for the vesicular aggregates even this type of secondary structure can be reached by increasing the surfactant concentration or using appropriate cosurfactants.[27,31]

The formation of high viscous worm-like micellar hydrogels can be reached after increasing the concentration of surfactant or after the addition to the solution of appropriate additives. Figure A 1.9 schematically represents the formation of a worm-like supramolecular aggregates that can be obtained using an amphiphilic system.[31]

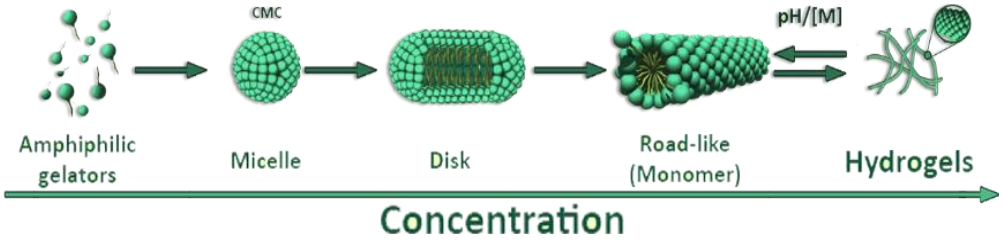

Figure A 1.9: Schematic representation of surfactant gelators capable of forming self-assembly hydrogels.

Although the rheological properties of these systems have been known for a long time, various hypotheses have been made in the last 30 years to justify their behavior; first of all, so formed hydrogels can be mainly divided into hard and soft. Regarding the former, in their intertwining, the fibers interact by means of crystalline junctions between the supramolecular aggregates. The others are characterized by weak interactions established between the entangled worm-like fibers.[32,33] Regardless the strength of the junctions, adjacent fibers can be superimposed in point splices, as if it were a cross-link between two aggregates, or in splice areas, in which the interaction is extended to a portion of two adjacent fibers, as shown in Figure A 1.10.[34]

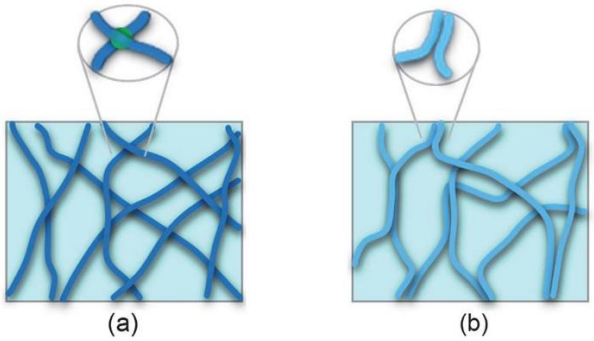

Figure A 1.10: Entangled worm-like micelles interacting: a) junction point, b) junction area.

A 1.3 Natural polymer-based hydrogels

Natural polymers are attracting more and more attention in the design of hydrogels. Although their chemical and physical properties are often less controllable than synthetic polymers, their intrinsic hydrophilic character,

biocompatibility and biodegradability make these system very interesting materials for many fields of application. Furthermore, both the possibility of chemically modifying their structure and the multitude of crosslinking methods increase the applicability, making them very versatile materials.[35]

As described for all polymers capable of forming hydrogels, natural polymers can be chemically or physically crosslinked. Physical polymeric natural hydrogels are reversible systems in which it is possible to swap quickly from the sol to the gel phases. Physical crosslinking can be exploited in many ways depending on the soft interactions established such as ionic interactions, formation of stereo complexes and hydrogen bond network.[36-39]

Although physical crosslinking is more biocompatible, due to the absence of toxic linkers, chemical crosslinking is often chosen due to the improved stability and mechanical properties of the resulting hydrogels. Chemical crosslinking is based on the formation of molecular bridges capable of covalently connecting the polymer chains together. Natural polymers are characterized by multiple polar functions such as alcoholic, carboxylic, thiol and amino groups capable of easily reacting with suitable crosslinkers. For example, some proteins are rich in amine functions on their surface that can undergo chemical crosslinking by adding formaldehyde to their solutions as shown in Figure A 1.11.[39]

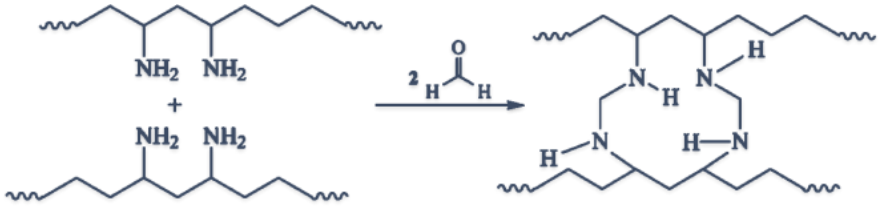

Figure A 1.11: Examples of chemical crosslinking of natural polymers.

A 1.3.1 Classification

This vast class of materials includes all those polymeric substances extracted directly from plants, animals or other living organisms. Biopolymers are generally classified according to their chemical architecture as polysaccharides, proteins,

polynucleotides, polyisoprenes, polyesters and lignin; only a part of them, however, are capable of forming hydrogels.[40]

Polysaccharides

Polysaccharides are natural macromolecules grouped biologically in the carbohydrate class. The monosaccharides, which also belong to the same class of molecules, represent the building blocks of this type of biopolymers which, bounded together during a condensation reaction, form the glycosidic bonds.

Natural polysaccharides can be divided according to their function in the organisms into structural or energetical polysaccharides. The former is synthetized by living organisms to contribute to the stability of the cellular wall. Among this class of polysaccharides, cellulose, alginate, lignin and pectin represent the most common structural carbohydrates that can be found in the plant kingdom, while hyaluronic acid and chitin play the same functions in animals. As regards the energetical reservoir functions, glycogen and starch, are the most abundant polysaccharides in many organisms. These biomolecules, after being extracted and purified, can be used to design both physical and chemical hydrogels. Thanks to their intrinsic properties, such as non-toxicity, high swelling, high mechanical properties, biocompatibility and biodegradability, polysaccharide hydrogels are the most studied and employed biopolymers in many different fields of application.[35,36,40]

Protein

If polysaccharides play a fundamental structural and energetic role, proteins in living organisms are the functional actuators in all biological systems. They are involved in a plethora of cellular and extracellular biological processes, starting from catalysis in metabolism up to cell signaling, molecular transport, DNA replication and more. They are biological macromolecules composed of amino acids such as monomers connected together by peptide bonds and arranged in long polypeptide chains. After synthesis, in the living organism, these biopolymers undergo a series of conformational changes that organize them into their active

tertiary structures. Proteins classification can be mainly conducted depending on the shape, size, solubility, composition, function and localization in the living organism.

Hydrogels designed on polypeptide macromolecules can be formed in many ways. As example, gelatin, a protein derived from the partial and irreversible hydrolysis of collagen, is probably one of the most popular polypeptides used to form physical and chemical hydrogels.[41,42] Moreover, proteins can be covalently bonded using polydentate crosslinkers, generating a long and orderly network of crosslinked polypeptides as shown in Figure A 1.12.[42]

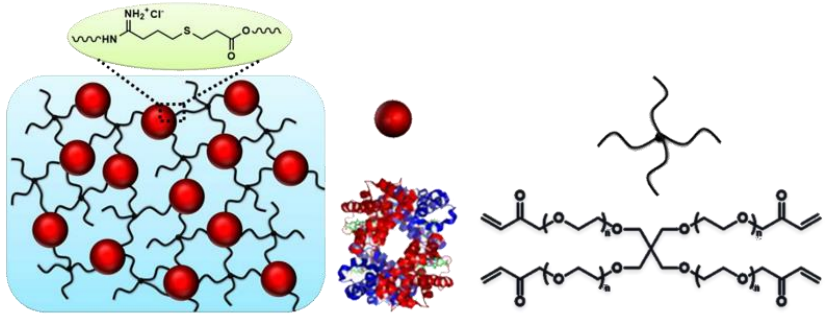

Figure A 1.12: Example of chemical cross-linking of hemoglobin forming a polypeptide-based hydrogel.

Nucleic Acid

Polynucleotides, in living organisms, are generally divided into ribonucleic acid (RNA) and deoxyribonucleic acid (DNA) which, together, make up the building block of life. These biomolecules contain all the information necessary to preserve and perform cellular functions. They are composed of nucleobases connected to a scaffold consisting of ribose (RNA) or deoxyribose (DNA) and phosphate anion which act as a binding agent between the sugar molecules.

Although DNA-based chemical hydrogels may form, the most common hydrogels based on this biopolymer are represented by physical entanglements. Physical interactions in this system can be mainly based on ionic interactions and hydrogen bonds. DNA is an anionic polyelectrolyte; therefore, it can strongly interact with

positively charged polyelectrolytes as well as with silver until the formation of physical DNA-based hydrogels.[35]

Moreover, some folded oligonucleotides, called aptamers, are able to selectively bind proteins or other molecules. Designing aptamers hydrogels, more attention is addressed to the typical hydrogen bonding interactions established between coupled nucleobases observed in DNA. In fact, exploiting the facile synthesis of oligomers it is possible to develop highly reactive physical hydrogels.[43,44]

A 1.4 Main applications

As mentioned above, there are a large number of compounds capable of forming safe hydrogels. This evidence, added to the possibility of modulating their chemical-physical properties simply varying their composition, allows to design a hydrogel that shows well-defined characteristics. Furthermore, the intrinsic water content, biocompatibility, biodegradability and low toxicity further extend their possible areas of application.

The biomedical and pharmacological areas represent the first fields of application of hydrogels; particular attention is paid to biopolymer-based hydrogels widely used for tissue engineering, the development of muscle-like systems, wound dressing.[18,45] In addition, the small-molecules based supramolecular hydrogels has proven to be efficient drug delivery systems, both using small peptide-based nanofiber as encapsulation of active principle and prodrugs able to self-assembly into a supramolecular network.[46,47]

Over the biomedical applications, hydrogels have been employed in many different fields like, as example, heavy metal ions removal during wastewater purification treatments. Several studies show how it is possible to reduce the amount of toxic metal ions from wastewater using hydrogel based on natural polymers. The excellent absorption rate of these hydrogels allows, over the water uptake, the network penetration by heavy metal ions. Once absorbed, heavy ions interact strongly with the polar functions of the hydrogels staying tied to the network.[48]

Hydrogels have also found applications in the agricultural field, as superabsorbent materials capable to act both as water reservoir and fertilizers carrier.[49] In food packaging industry, even more attention is paid to the replacement of classic packaging with hydrogels as new active packaging systems. Some hydrogels based on natural polymers, in which bacteriostatic nanoparticles are encapsulated in their structure, have recently been tested in in vitro experiments as packaging materials. This test showed good biological resistance against the tested bacterial strains indicating a possible improvement in food conservation.[50]

References

1- O. Wichterle, D. Lìm, Nature, **185**, 117-118 (1960);

2- N. Chirani, L.H. Yahia, L. Gritsch, F.L. Motta, S. Chirani, S. Faré, Journal of Medical Science, **4**, No. 2:13 (2015);

3- L.A. Estroff, A.D. Hamilton, Chemical Reviews, **104**, No. 3, 1201-1217 (2004);

4- E.M. Ahmed, Journal of Advanced Research, **6**, 105-121 (2013);

5- Q. Chai, Y. Jiao, X. Yu, Gels, **3**, 6 (2017);

6- M. Bahram, N. Mohseni, M. Moghtader, "*An introduction to hydrogels and some recent applications*" in "Emerging concepts in analysis and applications of Hydrogels", S.B. Majee Ed., Books on Demand, chap. 2, pp. 9-38 (2016);

7- A. Cesaretti, I. Di Guida, N. E. Caldero-Rodríguez, C. Clementi, R. Germani, P. L. Gentili, ACS Omega, **3**, 16777−16783(2018);

8- P.K. Sukul, P.K. Singh, S.K. Maji, S. Malik, Journal of Materials Chemistry B, **1**, 153-156 (2013);

9- W.A. Laftha, S. Hashim, A.N. Ibrahim, Polymer-Plastic Technology and Engineering, **50**, 1475-1486 (2011);

10- J. Maitra, V.K. Shukla, American Journal of Polymer Science, **4**, 25-31 (2014);

11- F. Ullah, M.B.H. Othman, F. Javed, Z. Ahmad, H.M. Akil, Materials Science and Engineering C, **57**, 414-133 (2015);

12- Y.S. Zhang, A. Khademhosseini, Science, **356**, eaaf3627 (2017);

13- C.M. Hassan, N.A. Peppas, Macromolecules, **33**, 2472-2479 (2000);

14- T. Li, B. Kumru, N. Al Nakeeb, J. Willersinn, B.V.K.J. Schmidt, Polymers, **10**, 576 (2018);

15- J.J. Yuan, R.H. Jin, Langmuir, **21**, 3136-3145 (2005);

16- B. Kurt, U. Gulyuz, D.D. Demir, O. Okay, European Polymer Journal, **81**, 12-23 (2016);

17- X. Cui, J.J.L. Lee, W.N. Cheng, Scientific Reports, **9**, 18166 (2019);

18- H. Du, W. Liu, M. Zhang, C. Si, X. Zhang, B. Li, Carbohydrate Polymers, **209**, 130-144 (2019);

19- L.O. de Guertechin, "*Surfactants: classification*" in "Handbook of detergents, Part A", G. Broze Ed., chap.2, pp. 7-46 (1999);

20- K.J.B. Holmberg, B. Kronberg, B. Lindman, "*Surfactants and polymers in aqueous solution*", John Wiley & Sons Ed. (2003);

21- L.L. Schramm, E.N. Stasiuk, D.G. Marangoni, Annual Reports Section C, **99**, 3-48 (2003);

22- D. Lombardo, M.A. Kiselev, S. Magazù, P. Calandra, Advances in Condensed Matter Physics, Article ID 151683 (2015);

23- J.N. Israelachvili, J. Mitchell, B.W. Ninham, Journal of the Chemical Society, Faraday Transactions 2: Molecular and Chemical Physics, **72**, 1525–1568 (1976);

24- H. Hoffmann, W. Ulbricht, Current Opinion in Colloid & Interface Science, **1**, 726-739 (1996);

25- F.B. Rosevear, Journal of the Society of Cosmetics Chemists, **19**, 581-594 (1968);

26- H. Rehage, H. Hoffmann, Molecular Physics, **74**, 933–973 (1991);

27- K. Trickett, J. Eastoe, Advances in Colloid and Interface Science, **144**, 66-74 (2008);

28- M. Gradzielski, Current Opinion in Colloid & Interface Science, **16**, 13–17 (2011);

29- T.S. Davies, A.M. Ketner, S.R. Raghavan, Journal of the American Chemical Society, **128**, 6669-6675 (2006);

30- P. Fernandez, N. Willenbacher, T. Frechen, A. Kuhnle, Colloids and Surfaces A, **262**, 204-210 (2005);

31- P.M. de Molina, M. Gradzielski, Gels, **3**, 30 (2017);

32- P. Terech, R.G. Weiss, Chemical Reviews, **97**, 3133-3159 (1997);

33- Y.E. Shapiro, Progress in Polymer Science, **36**, 1184-1253 (2011);

34- S.R. Raghavan, J.F. Douglas, Soft Matter, **8**, 8539-8546 (2012);

35- Z. Shi, X. Gao, M.W. Ullah, S. Li, Q. Wang, G. Yang, Biomaterials, **111**, 40-54 (2016);

36- K.I. Draget, G. Skjåk-Bræk, O. Smidsrød, International Journal of Biological Macromolecules, **21**, 47–55 (1997);

37- M. Ishihara, S. Kishimoto, S. Nakamura, Y. Sato, H. Hattori, Polymers, **11**, 679 (2019);

38- W.E. Hennink, S.J. De Jong, G.W. Bos, T.F.J. Veldhuis, C.F. van Nostrum, International Journal of Pharmaceutics, **277**, 99–104 (2004);

39- W.E. Hennink, C.F. van Nostrum, Advanced Drug Delivery Reviews, **64**, 223-236 (2012);

40- O. Olatunji, "*Classification of natural polymers*" in "Natural polymers", O. Olatunji Ed., Springer International Publishing, chap. 1, pp. 1-17 (2016);

41- V. Kulkarni, B. Kishor, R. Suddha, International Journal of Research in Pharmaceutical and Biomedical science, **3**, 1597-1613 (2012);

42- A.M. Jonker, D.W.P.M. Löwik, J.C.M. van Hest, Chemistry of Materials, **24**, 759-773 (2012);

43- B. Wei, I. Cheng, K.Q. Luo, Y. Mi, Angewandte Chemie International Edition, **47**, 331-333 (2008);

44- H. Yang, H. Liu, H. Kang, W. Tan, Journal of the American Chemical Society, ***130,*** 6320-6321

45- W. Kong, C. Wang, C. Jia, Y. Kuang, G. Pastel, C. Chen, G. Chen, S. He, H. Huang, J. Zhang, S. Wang, L. Hu, Advanced Materials, **30**, 1801934 (2018);

46- F. Zhao, M.L. Ma, B. Xu, Chemical Society Reviews, **38**, 883-891 (2009);

47- P.K. Vemula, N. Wiradharma, J.A. Ankrum, O.R. Miranda, G. John, J.M. Karp, Current Opinion in Biotechnology, **24**, 1174-1182 (2013);

48- S. Perumal, R. Atchudan, D.H. Yoon, J. Joo, I.W. Cheong, Industrial & Engineering Chemical Research, **58**, 9900-9907 (2019);

49- M.R. Guilherme, F.A. Aouada, A.R. Fajardo, A.F. Martins, A.T. Paulino, M.F.T. Davi, A.F. Rubira, E.C. Muniz, European Polymer Journal, **72**, 365-385 (2015);

50- R.A. Batista, P.J.P. Espitia, J.S.S. Quintans, M.M. Freitas, M.Â. Cerqueira, J.A. Teixeira, J.C. Cardoso, Carbohydrate Polymers, **205**, 106-116 (2019);

Chapter A 2

Surfactant & polysaccharide-based hydrogels

In recent years, hydrogels have found increasing applications in many scientific areas. Particular attention is addressed to those materials, capable of forming hydrogels, which can be easily degraded, such as natural polymers or small molecules with self-assembly abilities. Thanks to their properties and wide availability, these systems could be considered the basis for the design of new smart eco-compatible materials.

The research activities performed in this work by our group are centered on the study of two types of hydrogel characterized by a low environmental impact. On one hand, our attention has been focused on those systems capable of forming supramolecular hydrogels; in particular, amine oxide surfactants with gelling ability have been employed. On the other hand, research has been extended to two of the most common used natural biopolymers, sodium alginate and chitosan. In this section the main structural features and the methods to obtain hydrogels based on those starting materials will be provided.

A 2.1 Amine oxide surfactants

The surfactants known as amine oxides are a restricted class of compounds belonging to the broader class of zwitterionic surfactants. These particular species are studied since the beginning of the 20th century but have been recognized as surfactants only after the 1939.[1] Some alkyl amine oxides with a tail length usually ranged between 8 and 20 carbon atoms, also called fatty alkyl dimethyl amine oxides are commercially available. They are generally employed in addition to other surfactants in household cleaning, in personal care and in industrial products.[2-4]

A 2.1.1 Properties of amine oxides

Amine oxides represent a very interesting class of zwitterionic surfactants because of their intrinsic properties, deriving by the presence of a small but highly polar head group.[1,5] In addition, varying the pH of the media from acid to alkaline their character can be shifted from ionic to zwitterionic, depending on the protonation of the head groups. The pK_a value for most amine oxides surfactants is around 5, thus in distilled water the presence of both protonated and non-protonated amine oxides can be expected.[5] Moreover, the small dimension of the head group of most amine oxides could favor the formation of elongated aggregates, conferring to their solutions viscoelastic properties as described in the previous chapter.

The great importance given to these surfactants lies mainly in their intrinsic properties, such as thickener and emollient activities, foam stabilizer and/or booster, skin compatibility and biodegradability.[1-4] Amine oxide safety studies have shown their low bioaccumulation potential in the organisms.[6] Furthermore, these surfactants can be easily degraded under aerobic conditions in carbon dioxide, water and biomass; otherwise, depending on their structures, some amine oxide can also be degraded under anaerobic conditions.[7-9]

Another important feature of amine oxide is their increasing antimicrobial activity versus a large number of microorganisms which occurs as the chain length increase. This effect, already observed for some other surfactants, it has been attributed to their perturbating effect towards the cell wall.[1]

A 2.1.2 Amine oxide synthesis

Amine oxides are generally synthetized by the oxidation of tertiary amines with concentrated hydrogen peroxide, usually greater than 35% by performing the reaction at a temperature generally comprised between 60 and 100 °C.[1,3]

It has been suggested that the kinetic of the oxidation process take place through the ammonium peroxide as reversible intermediate; showing, for the amine oxides formation, an overall order of 2.[1,10] Figure A 2.1 shows the scheme of the general

reactions in which a tertiary amine is involved, highlighting reversibility of the formation of the intermediate.

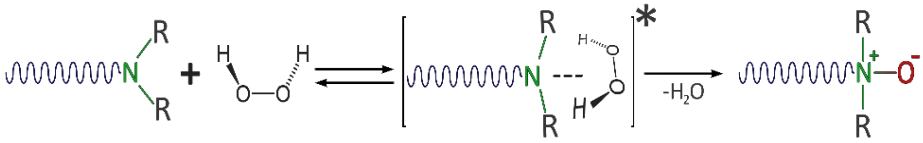

Figure A 2.1: Schematic representation of the formation of amine oxide surfactants.

For instance, Toney and coworkers synthetized three N-lauryl amine oxides with different head groups (dimethyl, piperidine and morpholine) both in distilled water and isopropyl alcohol, using hydrogen peroxide 51% in molar ratio 1:1 with the tertiary amine and an operating temperature of 75 °C. Although the morpholine and piperidine derivatives have similar steric constrain, the kinetic of reaction evidences for the N-laurylmorpholine oxide an increased rate constant compared to the piperidine derivative. This evidence confirms the formation of a reversible intermediate between the reagents; in fact, in the case of the laurylmorpholine the intermediate can be stabilized by the formation of hydrogen bond which involves the oxygen of the morpholine, as represented in the scheme showed in Figure A 2.2.[11]

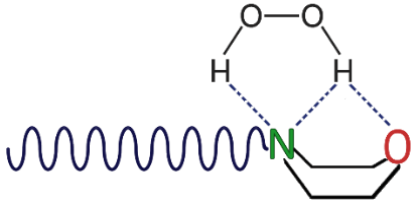

Figure A 2.2: Schematic representation of the hypothetical stabilization via hydrogen bond formation between the oxygen of morpholine ring and the hydrogen peroxide.

A different procedure has been adopted by Goracci and coworkers who synthetize an ammine oxide surfactant that includes an aromatic ring in its structures. The reaction was performed firstly solubilizing the tertiary amine in anhydrous ethanol and, subsequently, an excess of hydrogen peroxide was slowly added allowing the reaction to proceed for 14 hours. In order to remove the excess hydrogen

peroxide, MnO_2 is added to the resulting solution until oxygen development stops.[12] This step is fundamental because, after their synthesis, the most common impurities that can be found in the amine oxide, are traces of residual hydrogen peroxide, added to free amines, even if usually in very small amount. It has been observed that the yield of amine oxide formations is strongly affected by the purity of the tertiary amine. In fact, after the recrystallization of the tertiary amine the degree of conversion can be increased up to the 99%.[1]

A 2.1.3 p-Alkoxy benzyl amine oxides

Aromatic moieties can be relevant in the supramolecular aggregate formations of amphiphiles, especially by ruling the shape of the aggregates and the properties of their solutions. In the past years many surfactants have been developed with rigid aromatic system incorporated in different ways. As reported in Figure A 2.3, the aromatic moieties can be included among or at the end of the hydrophobic tail as well as between the charged head group and the tail.

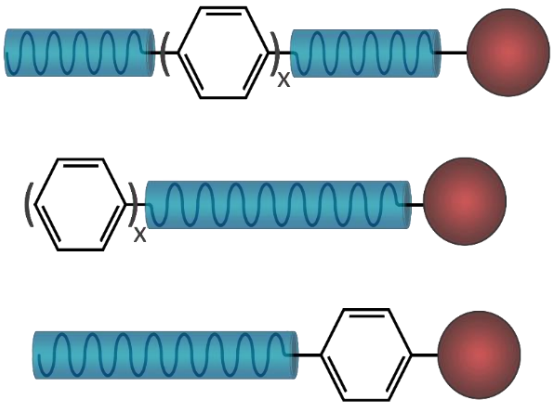

Figure A 2.3: Structures of surfactants that include aromatic moieties into their structure.

The main effect observed concerns the staking π-π between the amphiphiles into the micellar structure which increases their packaging ability, promoting their longitudinal growth and, in some cases, the formation of hydrogels.[13]

Since the early 80's the role of aromatic moieties in the shape of amphiphilic aggregates has been highlighted. Kunitake and coworkers synthetized many of

these systems analyzing the resulting structures of the aggregates. The main results observed are that amphiphiles which incorporate two aromatic rings preferably form discoidal, worm-like or tubular aggregates.[14] Other examples derive from the amphitropic molecules, which are amphiphilic molecules with thermotropic abilities. In these systems, aromatic functions, such as mesogenic units or azobenzene, are connected to the end of the hydrophobic tail. The favorable effect of the aromatic interactions leading to the formation of elongated aggregates, bilayers or vesicles was observed.[15,16] More recently, sodium dodecylbenzene sulfonate (SDBS), coupled with benzylamine hydrochloride (BzCl), has been employed in order to obtain organized self-assembled structures based on aromatic interactions. In this anionic surfactant the benzene ring act as a bridge between the charged head group and the hydrophobic tail. The packaging abilities of the surfactant are varied using the hydrotropic salt BzCl. Thanks to the π-π interactions established between the surfactant and the salt, vesicles (both ULV and MLV) and ultralong self-assembled fibers are obtained.[17]

Similar systems can be achieved when a *p*-alkoxy benzyl ring is added between the hydrophobic tail and the charged headgroup of amine oxides, as for the *p*-dodecylbenzyl dimethyl amine oxides (*p*DOAO). The π-π interactions established by this surfactant are the main responsible of the formation of giant elongated micelles at relatively low concentration (about 0.05 M). Furthermore, as seen also for other amine oxide surfactants, the viscoelastic properties of *p*DOAO solutions are sensitive to pH variations and, as showed in Figure A 2.4, the system can be shifted from gel to sol phase and vice versa, simply by adding an acid or a base.[18]

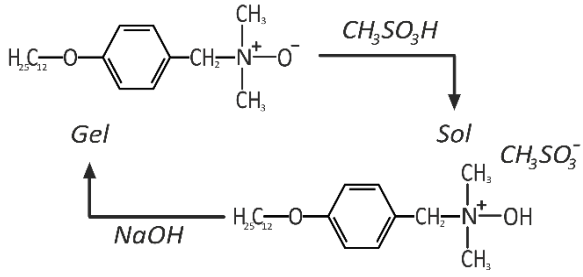

Figure A 2.4: SOL-GEL transition in pDOAO induced by pH shift.

A 2.2 Alginate

Alginate is a polysaccharide extracted mainly from the cell wall of brown algae, of which it represents about 40% of their dry weight. The cell wall of brown algae consists of a rigid internal matrix of microfibril covered of a mainly amorphous external matrix. Although the cellulosic microfibrils represent the main structural constituents, alginate gives them elasticity.[19,20]

The extraction of alginate is carried out only from few algal species, in which it can be found in the form of a mixture of calcium, strontium, magnesium and sodium salts. As it is shown in Figure A 2.5, the extraction of alginate starts with the washing and grinding procedure after which, the brown algae are treated in a warm alkaline solution.

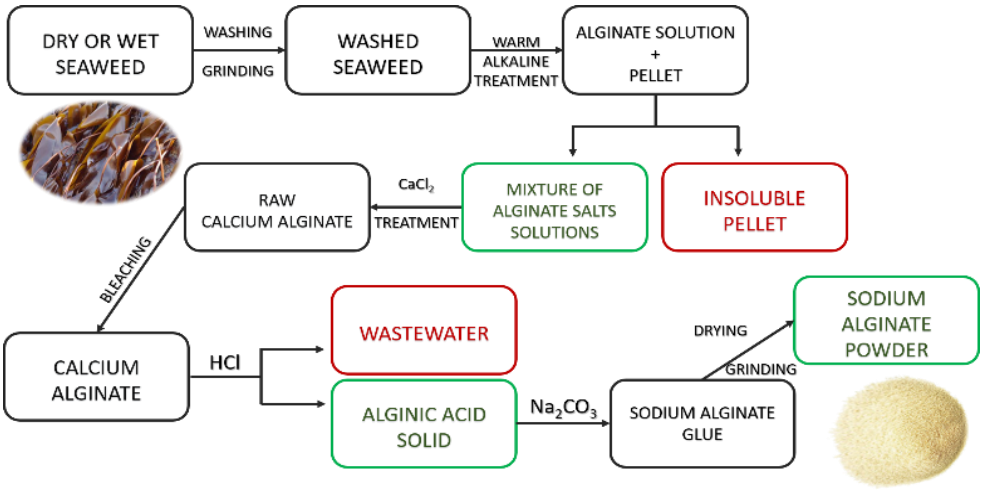

Figure A 2.5: Schematization of the steps of the extraction and purification process of the sodium alginate from the brown algae

Afterwards, the supernatant is separated by the solid pellet and added with calcium chloride to precipitate the alginate as calcium salts. The so-obtained salt is firstly beached and therefore treated with hydrochloric acid until the impurities are dissolved and alginic acid is formed as a precipitate. Lastly, the residual alginic acid after neutralization with a sodium carbonate solution is dried and ground to obtain the sodium alginate powder.[21]

Alginate may be also derived by some bacteria (e.g. *Azotobacter vinelandii* and *Pseudomonas aeruginosa*) which synthesize this biopolymer in acetylated form. The bacterial production of alginate can be employed in order to obtain alginates with a more defined structure and therefore improved physico-chemical properties.[19,22]

A 2.2.1 Alginate structure

Alginate is a linear copolymeric polysaccharide composed of β-D-mannuronic acid and α-L-guluronic acid organized in a block structure. The monomers are linked together by α and β 1-4 glycosidic bonds both in homopolymer (GGG or MMM) and heteropolymer (MGMG) blocks as showed in Figure A 2.6.

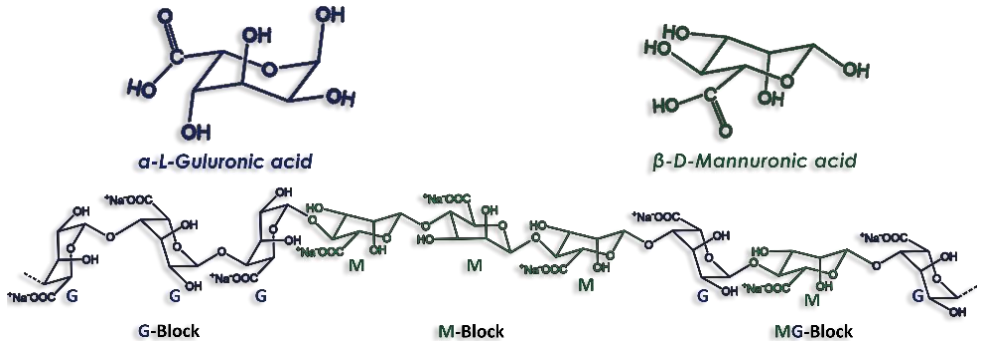

Figure A 2.6: Structures of the monomers on the top of the figure and below their block organization.

Each monomeric unit adopts a specific conformation regardless of its neighbors, always maintaining the carboxyl group in a favorable equatorial orientation. Focusing on the heteropolymer blocks, their structure is not well defined because it can be changed depending on the conformation assumed by all the single monomers. On the contrary, both homopolymer blocks are characterized by well-defined conformation. The mannuronic homo-blocks assume a ribbon structure while the guluronic homo-blocks are characterized by a typical "buckled" chain conformation.[23,24]

The molecular weight, the relative amount and organization of the blocks vary according to the sources of extraction. Generally, the average molecular weight of the commercially available alginates is between 40 and 100 kDa.

Regarding the monomeric composition, some brown algae such as *Ascophyllum nodosum* and *Macrocystis pyrifera* generally show a low content of guluronate, between 32 and 45%, while in others, such as *Laminaria hyperborea*, guluronic acid is the main constituent (over the 65%).[21] There exists a deep relationship between the composition, the organization of blocks and the properties of the alginates. In fact, these parameters can affect their abilities in metal ions complexation, the formation of crosslinking, the gelation process as well as their physico-chemical properties. There are many ways to determine these properties and they can usually be divided into chemical and physical methods.

Chemical analysis consists in the fragmentation of the alginate chain in its constitutive subunit via acid hydrolysis. Although this methodology is simple and cheap, the drastic condition reached can promote the partial decarboxylation of the monomeric unit over the long experimental time and the use of dye can misrepresent the real amount of guluronic and mannuronic acid. Regarding the physical methods, they include the nuclear magnetic resonance, circular dichroism, viscosimetry and infrared spectroscopy.[25-28]

A 2.2.2 Alginate hydrogels

Alginate is usually used in its hydrogel form, a dense three-dimensional network of connected polymer chains capable of retaining large amounts of water. The gelation process can be achieved in many different ways, according to which the properties of the resulting hydrogels are strongly influenced. The most commonly used crosslinking methods, some of which are briefly described below, can involve both chemical and physical interactions.

Covalent gelation

Chemical hydrogels are generally stable system in which the alginate chains are crosslinked together with a suitable molecular bridge. The inter-chain bonds are mainly established between the crosslinking agent and the carboxylate groups of the monomers. In Figure A 2.7 some strategies used to chemically crosslink alginates are schematically represented.

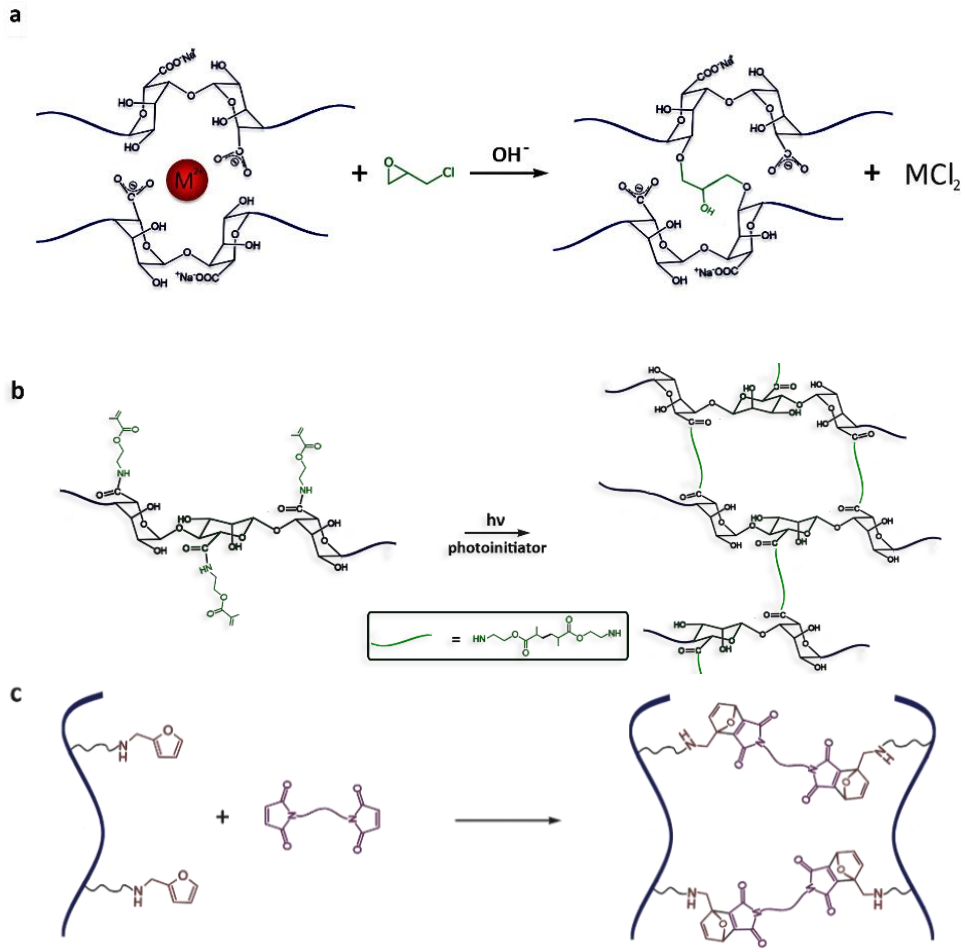

Figure A 2.7: Chemical cross-linking employed using: epichlorohydrin (a); photoradicalic reaction (b); click reaction (c).

For instance, epichlorohydrin can be used as crosslinking for ionically cross-linked alginates (Figure A 2.7-a).[29] Moreover, using poly (ethylene glycol)-diamine as

crosslinker, the properties of the hydrogels can be easily tuned by varying the length of the linkers.[30]

Crosslinking can also be obtained following a previous functionalization of the biopolymer. For example, by modifying the alginate structure to form its methacrylate derivative, a radical gelling triggered by ultraviolet light can be obtained. This functionalization is carried out by reacting the biopolymer with 2-aminoethyl methacrylate; subsequently, using a photoinitiator and an electromagnetic radiation of adequate energy, the three-dimensional network will be formed (Figure A 2.7-b).[31,32]

More recently, click reactions has been involved in the chemical reticulation of alginates. For instance, this gelation process can be obtained via Diels Alder reaction, by previously modifying the alginate backbones adding a furanic ring as diene. In a second step, the Diels Alder reactions are performed by adding the double dienophile bismaleimide to the modified alginates (Figure A 2.7-c).[31,33]

If on the one hand, chemical crosslinking confers to the hydrogel greater stability and better mechanical properties, on the other the employed crosslinkers are often considered toxic. Therefore, if they are not properly removed from the gel structure, the application of these systems will be drastically reduced.

Thermal gelation

Thermal crosslinking is a way in which alginates can form hydrogels. This process cannot be properly considered as chemical crosslinking, since the interactions involved are soft, without the formation of covalent bonds. However, this is not even a physical transition because the backbone of the biopolymer must be functionalized with suitable functions so that it can be made thermoresponsive. One way consists in the use of γ-radiation to graft the thermoresponsive poly(N-isopropylacrylamide) (PNIPAAm) on the alginates.[34] Figure A 2.8 shows the PNIOAAm-alginate that can shift from sol to gel by increasing the temperature of the system above its characteristic LCST.

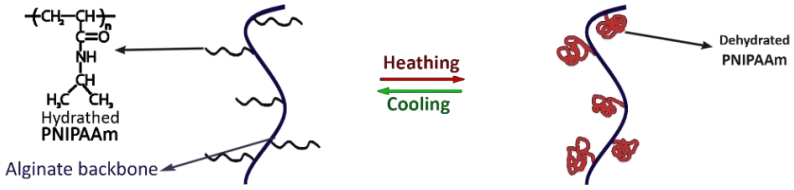

Figure A 2.8: Schematization of the thermal behavior of thermoresponsive alginate grafted with PNIPAAm chains.

By increasing the temperature, the water molecules are expelled from the PNIPAAm branches, which curl up as a result of the establishment of a greater number of hydrophobic interactions, leading to the formation of a hydrogel.[31,34]

Ionic gelation

This reticulation represents one of the most common used methods to form physical alginate hydrogels. The gelation involves an ionic exchange reaction, in which the divalent cations, that act as crosslinkers, are able to interact strongly with the carboxylate moieties, replacing the sodium. Although both mannuronic and guluronic acid are capable of interacting with these cations, mainly the guluronic homo-blocks significantly contribute to the reticulation. This evidence can be attributable to the spatial organization of the homo-blocks; the orientation of the carboxylate groups in the G-blocks leads to the establishment of interchain interaction between adjacent chains. As a result, the divalent cations are chelated in a typical structure called egg-box, shown in Figure A 2.9.[21]

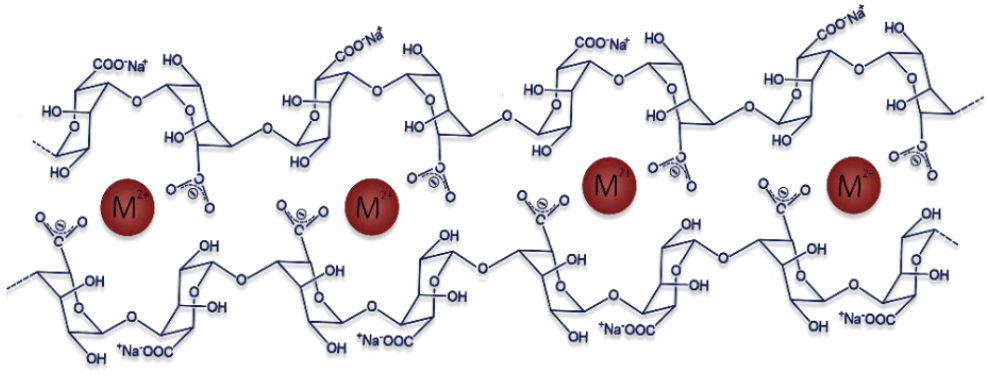

Figure A 2.9: Representation of the egg-box structures.

Not all divalent cations are able of inducing the formation of hydrogels; moreover, as previously described, the crosslinking process can be affected by the extraction sources of the polysaccharide.

Although alginate can be crosslinked with several divalent cations, Ca^{2+} ions are the most used and generally added to the alginate in the form of its chlorine salt.[31] However, since it is a very soluble salt, crosslinking may occur rapidly and consequently it is very difficult to control the gelation and properties of the resulting hydrogels. In order to limit this drawback, crosslinking can usually be performed at lower temperatures, as well as using less soluble salts, such as $CaCO_3$ and $CaSO_4$.[35]

A 2.3 Chitosan

Chitosan is a biopolymer derived by partial deacetylation of chitin which, together with cellulose, is one of the most abundant polysaccharides in nature. It is the fundamental constituent of the insect exoskeleton as well as of the crustaceous shell, from which it is mainly extracted.[36]

Chitin extraction, schematically reported in Figure A 2.10, consists of a two-step process, in which the ground raw materials are subjected to demineralization and deproteinization.

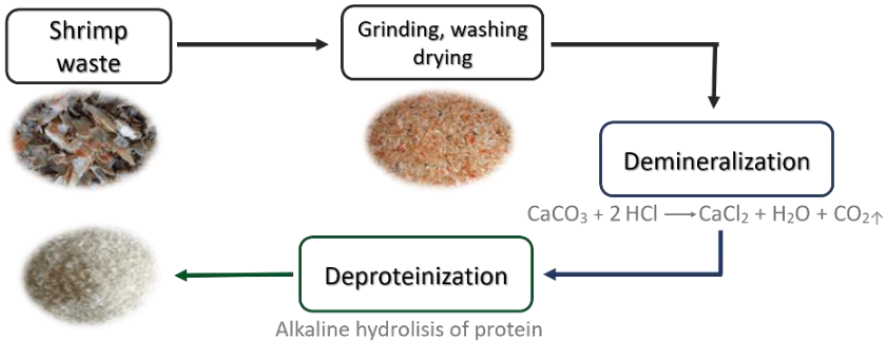

Figure A 2.10: Step schematization of the extraction process of chitin.

The first step consists of a treatment with a dilute hydrochloric acid solution to promote the decarbonation of the mineral constituents. Subsequently, a dilute

alkaline treatment is performed at various temperature to hydrolyze and remove the protein components and thus release the chitin.[36-38] Following, the partial deacetylation of the chitin can be carried out to partially release the acetyl groups, thus obtaining the chitosan.

There are several methods currently adopted to promote the deacetylation of chitin such as alkaline, enzymatic and steam explosion method, of which the main operative condition is showed in Figure A 2.11.[39]

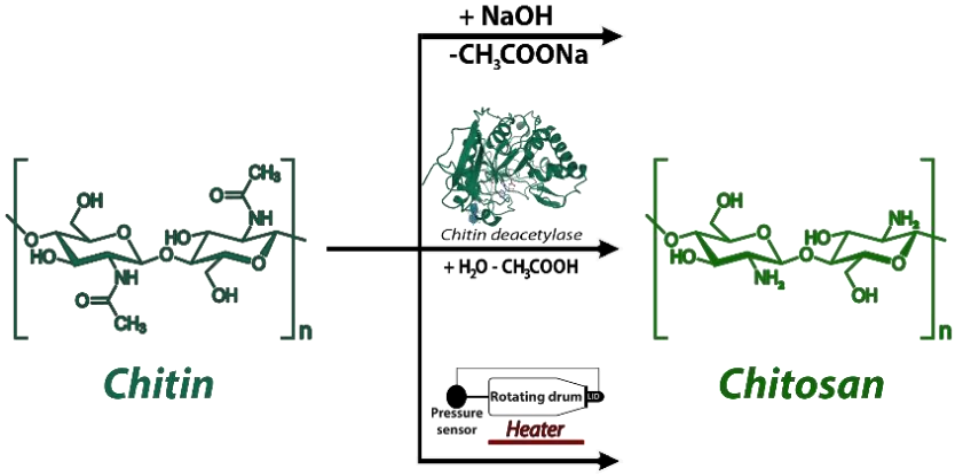

Figure A 2.11: Representation of alkaline, enzymatic and steam explosion process used in chitin deacetylation.

Alkaline deacetylation

Alkaline treatment is the most used method for performing the deacetylation of chitin to form chitosan. This is carried out adding chitin to a solution of concentrated NaOH solution (50 wt%). Generally, both the reaction time and the temperature can be varied in order to modulate the degree of deacetylation (DD) and the degradation of the polysaccharide.[40,41] The resulting biopolymer is rinsed many times with hot distilled water and then dried. It has been observed that after 24 hours of treatment at 100 °C in 50 wt% NaOH a deacetylation of about 82% is obtained. By increasing the time at 48 hours under the same conditions, the chain degradation overcomes, decreasing the average molecular weight of the polysaccharide.[39-41]

The alkaline deacetylation process has been also performed using microwave as source of energy. In this case, the sample undergoes a series of pre-treatments of chitin in acid media (3N HCl) and subsequent neutralization by dialysis. Successively chitin is treated with 40 wt% of aqueous NaOH in a microwave chamber (400 W and 2.45 GHz) under a nitrogen atmosphere. The DD achieved in a short time with this procedure is higher than the classical alkaline treatment.[39]

Enzymatic deacetylation

Another powerful method is represented by the enzymatic deacetylation performed using chitin deacetylase, an enzyme extracted by some fungi or insects. By using the enzymatic cleavage of the acetylated groups of chitin it is possible to obtain a high DD and to minimize the depolymerization. Moreover, compared to the previous one, it is an eco-friendly method since no alkaline media and high temperature must be reached; however, because of the high cost of the chitin deacetylase, this method is much more expensive.[42]

Steam explosion

The steam explosion method represents another green technique which consists in the employment of a puffin gun to promote deacetylation. The extracted chitin is previously immersed in water and then injected in a puffin gun. Subsequently, the apparatus is warmed up to about 180°C until the internal pressure reached a suitable value of 9 Kg/cm^2. At this time the gun lid was opened inducing the steam explosion capable of destroying the crystalline structure of chitin. It has been observed that the higher is the moisture content of chitin, the greater the resulting DD. This evidence was attributed to the higher amount of hydroxyl groups in a more wetted system.

Although this represents an eco-friendly process, the degree of deacetylation obtained is far lower than those obtained with the enzymatic and alkaline methods, previously described.[39,43]

A 2.3.1 Chitin and chitosan structures

Chitin is a linear and highly crystalline biopolymer consisting of monosaccharide units of 2-(acetylamino)-2-deoxy-D-glucose linked together by β 1-4 glycoside bond.

There exist three different polymorphic form of chitin (α, β and γ), which are schematically represented in Figure A 2.12.[44]

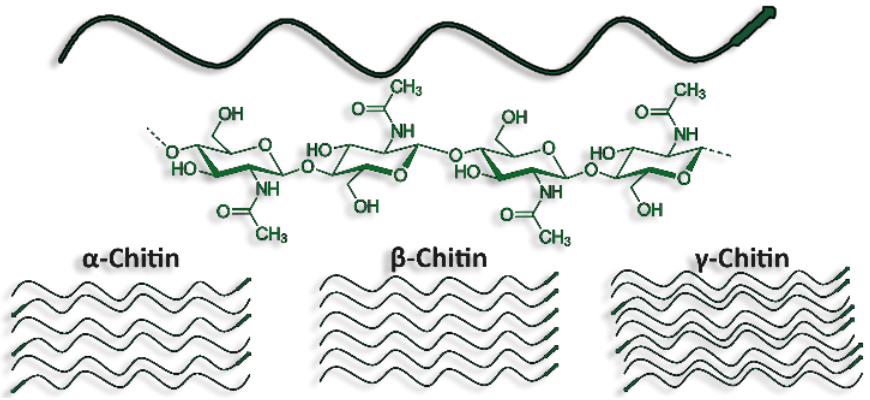

Figure A 2.12: Representation of a chitin chain and its possible crystalline polymorph form.

α-Chitin is the most abundant allomorph; in this form the polysaccharide chains are spatially oriented in an antiparallel way. The β allomorph is instead characterized by a parallel arrangement of the polymer chains and is less stable than the α arrangement. Furthermore, in a strong acidic environment β-chitin undergoes to a partial hydrolysis of the polysaccharide chains which promote a spontaneous transition from β to α.[44,45] Finally, the γ arrangement is the least common; in its structure, similar to that observed for the α allomorph, there are two adjacent parallel chitin chains that alternate with a chain oriented in the opposite direction.[44]

The difference between chitin and chitosan lies in the degree of acetylation (DA) of amino groups. It has been established that over a 50% DA the polysaccharide is chitin otherwise can be considered chitosan. The crystallinity of the deacetylated biopolymer depends on the degree of deacetylation; DD close to 100% corresponds to a high crystalline chitosan.[41] Commercially available chitosan is only

partially deacetylated, so it has a rigid and semi-crystalline structure. Therefore, crystallinity and degree of deacetylation, added to the average molecular weight, strongly affects the properties of this biopolymer, e.g. solubility, viscosity and mechanical properties.[41,44]

A 2.3.2 Chitosan hydrogels

Chitosan hydrogels have gained great interest because of the unique properties shown by this polysaccharide, such as low toxicity, biocompatibility, sorption ability, biodegradability and antibacterial activity. Nowadays in the literature there are a plethora of different methods involving chitosan as component of hydrogel used for the most widespread application. All these methods employ a different interaction between the chitosan polysaccharide chains, conferring many different properties to the resulting hydrogels.[46]

H-bonding and coordination

If on the one hand the low solubility in neutral and alkaline solutions can represent a disadvantage, on the other hand this property can lead to the formation of hydrogels without using any type of crosslinker. In fact, by neutralizing an acid aqueous dispersion of this polysaccharide, a physical hydrogel will be formed. This evidence can be explained by taking into account the fact that many protonated amine (ammonium) functions generate a series of repulsive forces between the chitosan chain, hindering their association. Considering that, during the reaction with a base, the repulsive forces are lowered, leading to the formation of a dense network of tangled polysaccharide chains capable of trapping the water.[47-49]

The physical hydrogel of chitosan can be also obtained by coordination of metal ions, ionic interactions with small molecules. Moreover, a polyelectrolytic complex can also be formed.

Transition metal ions, such as Ag^{+}, Zn^{2+}, Cu^{2+}, Co^{2+}, Ni^{2+}, Cd^{2+}, and Pd^{2+}, can induce the rapid gelation of chitosan solutions. The effect is the same previously

mentioned, the metal ions show repulsive forces against the ammonium groups; while, after their deprotonation, the amino groups rapidly coordinate the metal ions, forming a hydrogel.[49,50]

Electrostatic interactions

The formation of ionic interactions between anionic species, both small polyanions and polyelectrolyte, leads instead to the formation of ionic crosslinking, as reported in Figure A 2.13.

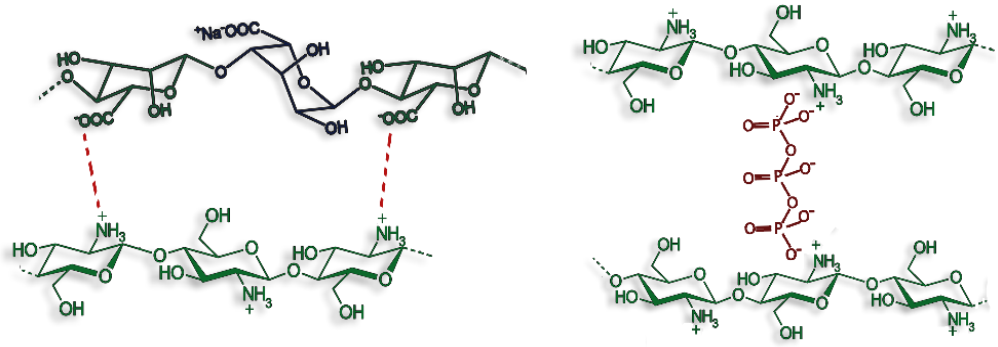

Figure A 2.13: Representation of: the formation of a polyelectrolytic complex (PEC) between sodium alginate and chitosan on the left; formation of ionic crosslinking employing the tripolyphosphate polyanion on the right.

It has been observed that employing citrate, sulphate or tripolyphosphate it is possible to induce the gelation of this biopolymer.[48,49,51] However, by mixing these gelators with a chitosan solution an inhomogeneous hydrogel can be obtained because of the rapid kinetics of gelation. To overcome this drawback the chitosan solution can be placed between two dialysis membranes in order to slowly spread the gelators.[49]

Compared to the ionic crosslinking in which a small crosslinker is employed, the driving force of PEC-based hydrogel formation is the multitude of electrostatic interactions formed along the chains of the two poly-ions. In fact, when a polyanion is mixed with a polycation their association is very fast. As described for

the ionic crosslinking, slow diffusion through a permeable membrane can also be employed in the PEC formation in order to obtain a homogeneous hydrogel.[52]

Most anionic polysaccharides, proteins and synthetic polymers are capable of forming PEC-based hydrogels with chitosan as polycation. During their formation, no other auxiliary chemicals are needed. Therefore, the biocompatibility of the hydrogels is improved as the matrix purification process is avoided. The chemical and physical characteristic of this type of chitosan-based materials can be varied according to the polyanionic partner.[53]

Chemical hydrogels

The characteristics as well as the main differences between physical and chemically crosslinked hydrogels have already been widely discussed and can also be extended to the chemically crosslinked chitosan hydrogels. Chitosan can be chemically crosslinked employing many different types of linkage, some of which are schematically described in Figure A 2.14.[49]

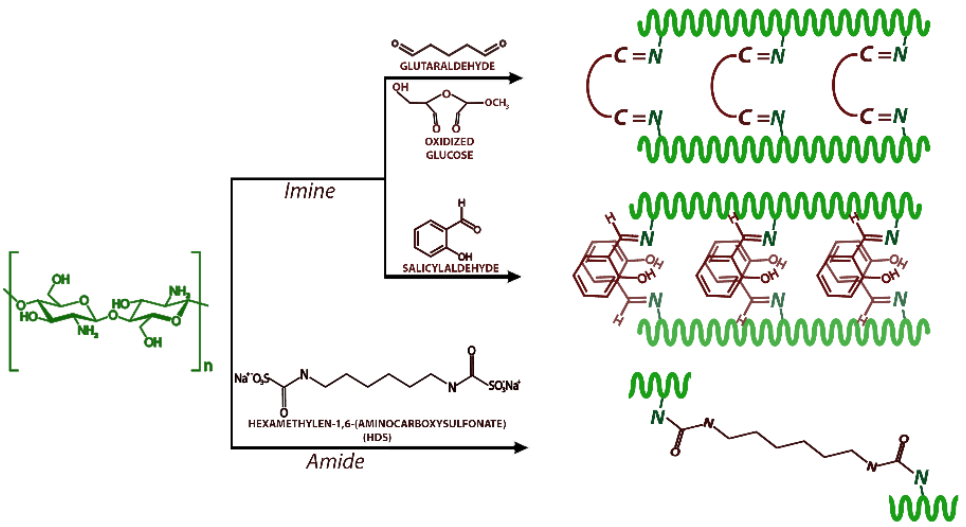

Figure A 2.14: Examples of some covalent crosslinkers employed in the formation of chitosan hydrogel.

Covalent imine bond is mainly used in the formation of a crosslinked network of chitosan. Schiff bases can be easily formed when an aldehyde group reacts with an

amine. In the case of chitosan, being a polyamine, it reacts with dialdehydes, of which the most used is glutaraldehyde, leading to the formation of double imine crosslinking. The mild experimental conditions, easiness and rapidity of hydrogel formation, added to the possibility to easily modulate its properties are the main advantage obtained by using glutaraldehyde. Nevertheless, the main problem remains the removal of the excess of this neurotoxic crosslinker from the 3D network.[54] To overcome this issue, natural derived dialdehyde can be involved in substitution of classical crosslinkers. The diols present in many saccharides can be easily oxidized using periodate, thus forming a dialdehyde.[55] An example is represented by the employment of previously oxidized glucose as a crosslinker in hydrophobized chitosan.[56]

Recently some monoaldehydes, much safer than glutaraldehyde, are involved in the formation of chitosan hydrogels. These hydrogels should be considered hybrids because of the combinate chemical and physical nature of their reticulation process. In facts, chitosan backbone is chemically modified by the formation of Schiff bases, while the intra- and inter-molecular interactions involved in the hydrogel network formation are soft. For instance, using salicylaldehyde to form the imine groups, a large amount of π-π associations will be established between the modified polysaccharide chains.[57]

In addition to the imine formations, using carboxylic acids and their derivates, chemical crosslinked chitosan by amidic bond has been developed. Regarding this last type of crosslinking, chitosan has been effectively crosslinked using hexamethylene-1,6-(aminocarboxysulfonates) (HDS). The degree of swelling as well as the mechanical properties of the resulting hydrogel are strongly related to the amount of crosslinking.[49]

References

1- S.K. Singh, M. Bajpai, V.K. Tyagi, Journal of Oleo Science, 55, 99-119 (2006);

2- H. Sanderson, C. Tibazarwa, W. Greggs, D.J. Versteeg, Y. Kasai, K. Stanton, R.I. Sedlak, Risk Analysis, **29**, 857-867 (2009);

3- L.O. de Guertechin, "*Surfactants: classification*" in "Handbook of detergents, Part A", G. Broze Ed., chap.2, pp. 7-46 (1999);

4- H. Sanderson, J.L. Counts, K.L. Stanton, R.I. Sedlak, Risk Analysis, **26**, 1637-1657 (2006);

5- L. Goracci, R. Germani, J.F. Rathman, G. Savelli, Langmuir, **23**, 10525–10532 (2007);

6- B. Sansoni, Journal of Surfactants and Detergents, **7**, 347 (2004);

7- M.T. García, E. Campos, I. Ribosa, Chemosphere, **69**, 1574-1578 (2007);

8- F. Ríos, M. Lechuga, M. Fernández-Serrano, A. Fernández-Arteaga, Chemosphere, **171**, 324-331 (2017);

9- F. Ríos, M. Lechuga, A. Fernández-Arteaga, E. Jurado, M. Fernández-Serrano, Biodegradation, **28**, 303-312 (2017);

10- A.A. Ostwald, D.L Guertin, Journal of Organic Chemistry, **28**, 651-657 (1963);

11- C.J. Toney, F.E. Friedli, P.J. Frank, Journal of the American Oil Chemists' Society, **71**, 793-794 (1994);

12- L. Goracci, R. Germani, G. Savelli, D.M. Bassani, ChemBioChem, **6**, 197 – 203 (2005);

13- G. Wang, A.D. Hamilton, Chemical Communications, 310-311 (2003);

14- T. Kunitake, Y. Okahata, M. Shimomura, S. Yasunami, K. Takarabe Journal of the American Chemical Society, **103**, 5401-5413 (1981);

15- A.C. Nieuwkerk, A.T.M. Marcelis, A. Koudijs, E.J.R. Sudholter, Liebigs Annalen, 1719-1724, (1997);

16- M.D. Everaars, A.T.M. Marcelis, A.J. Kuijpers, E. Laverdure, J. Koronova, A. Koudijs, Langmuir, **11**, 3705-3711 (1995);

17- Y. Lin, Y. Qiao, X. Cheng, Y. Yan, Z. Li, J. Huang, Journal of Colloid and Interface Science, **369**, 238–244 (2012);

18- L. Brinchi, R. Germani, P. Di Profio, L. Marte, G. Savelli, R. Oda, D. Berti, Journal of Colloid and Interface Science, **346**, 100-106 (2010);

19- D.F. Day, "*Alginates*", in "Biopolymers from Renewable Resources", D.L. Kaplan Ed., Springer-Verlag Berlin Heidelberg, chap. 5, pp. 119-143 (1998);

20- T.A. Davis, B. Volesky, A. Mucci, Water Research, **37**, 4311-4330 (2003);

21- K.Y. Lee, D.J. Mooney, Progress in Polymer Science, **37**, 106-126 (2012);

22- C.M. Ott, D.F. Day, Trends In Polymer Science, **3**, 402-406 (1995);

23- J.W. Rhim, LWT- Food Science and Technology, **37**, 323-330 (2004);

24- O. Smidsrød, Faraday Discussion of the Chemical Society, **57**, 263-274 (1974);

25- E.R. Morris, D.A. Rees, D. Thom, Carbohydrate Research, **81**, 305-314 (1980);

26- M.A. Masuelli, C.O. Illanes, International Journal of BioMaterials Science and Engineering, **1**, 1-11 (2014);

27- H. Grasdalen, B. Larsen, O. Smidsrød, Carbohydrates Research, **89**, 179-191 (1981);

28- E. Gómez-Ordóñez, P. Rupérez, Food Hydrocolloids, **25**, 1514-1520 (2011);

29- A. Merakchi, S. Bettayeb, N. Drouiche, L. Adour, H. Lounici, Polymer Bullettin, Issue 7/2019 (2018);

30- P. Eiselt, K.Y. Lee, D.J. Mooney, Macromolecules, **32**, 5561-5566 (1999);

31- J. Sun, H. Tan, Materials, **6**, 1285-1309 (2013);

32- O. Jeon, K.H. Bouhadir, J.M. Mansour, E. Alsberg, Biomaterials, **30**, 2724–2734 (2009);

33- C. García-Astrain, L. Avérous, Carbohydrate Polymers, **190**, 271-280 (2018);

34- M.M.S. Lencina, C. Rizzo, C. Demitri, N. Andreucetti, A.Maffezzoli, Radiation Physics and Chemistry, **156**, 38-43 (2019);

35- C.K. Kuo, P.X. Ma, Biomaterials, **22**, 511-521 (2001);

36- W. Arbia, L. Arbia, L. Adour, A. Amrane, Food Technology and Biotechnology, **51**, 12-25 (2013);

37- A. Khanafari, R. Marandi, S. Sanatei, Journal of Environmental Health Science & Engineering, **5**, 19-24 (2008);

38- A. Percot, C. Viton, A. Domard, Biomacromolecules, **4**, 1380-1385 (2003);

39- P.R. Sivashankari, M. Prabaharan, "*Deacetylation modification techniques of chitin and chitosan*" in "Chitosan Based Biomaterials Volume 1", J.A. Jennings and J.D. Bumgardner Ed., Woodhead Publishing, chap. 5, 117-133 (2017);

40- E.S. Abdou, K.S.A. Nagy, M.Z. Elsabee, Bioresource Technology, **99**, 1359-1367 (2008);

41- J.K.F. Suh, H.W.T. Matthew, Biomaterials, **21**, 2589-2598 (2000);

42- M.B. Kaczmarek, K. Struszczyk-Swita, X. Li, M. Szczęsna-Antczak, M. Daroch, Frontiers in Bioengineering and Biotechnology, **7**, 243 (1-26) (2019);

43- T.S. Tan, H.Y. Chin, M. Tsai, C. Liub, Carbohydrate Polymers, **122**, 321-328 (2015);

44- J.C. Roy, F. Salaün, S. Giraud, A. Ferri, G. Chen, J. Guan, "*Solubility of chitin: solvents, solution behaviors and their related mechanisms*" in "Solubility of Polysaccharides", Z. Xu Ed., IntechOpen, chap. 7, 109-127 (2017);

45- M. Ioelovich, Journal of Chemistry, **3**, 7-14 (2014);

46- F. Croisier, C. Jérôme, European Polymer Journal, **49**, 780–792 (2013);

47- Y. Xu, J. Han, H. Lin, Carbohydrate Polymers, **156**, 372–379 (2017);

48- J. Fu, F. Yanga, Z. Guo, New Journal of Chemistry, **42**, 17162-17180 (2018);

49- P. Sacco, F. Furlani, G. de Marzo, E. Marsich, S. Paoletti, I. Donati, Gels, **4**, 67 (2018);

50- Z. Sun, F. Lv, L. Cao, L. Liu, Y. Zhang, Z. Lu, Angewandte Communications International Edition, **54**, 7944-7948 (2015);

51- J. Berger, M. Reista, J.M. Mayera, O. Feltb, N.A. Peppasc, R. Gurny, European Journal of Pharmaceutics and Biopharmaceutics, **57**, 19-34 (2004);

52- M. Ishihara, S. Kishimoto, S. Nakamura, Y. Sato, H. Hattori, Polymers, **11**, 672 (2019);

53- D. Hermanto, M. Mudasir, D. Siswanta, B. Kuswandi, N. Ismillayli, Journal of Mathematical and Fundamental Science, **51**, 309-319 (2019);

54- A. Ou, I. Bo, Journal of Physical Chemistry & Biophysics, **7**, 3 (2017);

55- K.A. Kristiansen, A. Potthast, B.E. Christensen, Carbohydrate Research, **345**, 1264-1271 (2010);

56- F. Li, W.G. Liu, K. De Yao, Biomaterials, **23**, 343–347 (2002);

57- M. Iftime, S. Morariu, L. Marin, Carbohydrate Polymers, **165**, 39-50 (2017).

Section B

Polysaccharide characterization

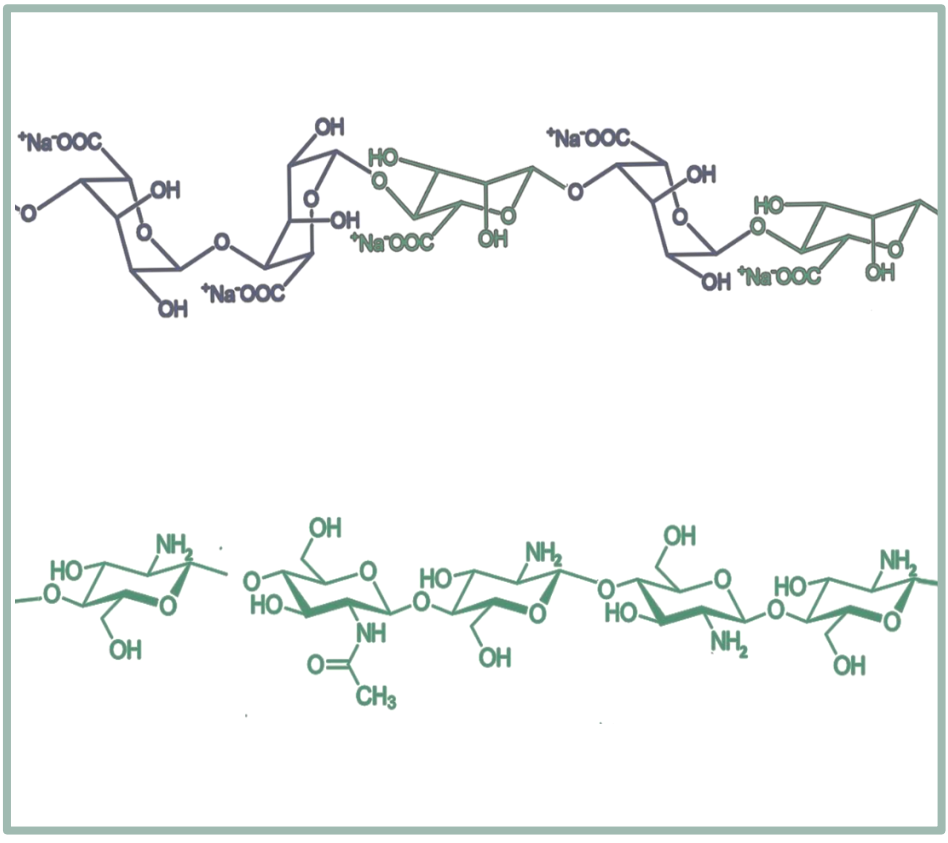

Chapter B

Alginate & chitosan characterization

The preparation and application of the polysaccharide hydrogels studied in this work has been preceded by the characterization of the biopolymers performed to fully understand their behavior during the applications. Chitosan and sodium alginate have been characterized employing the most common techniques used for the determination of their intrinsic properties. At this purpose, infrared spectroscopy, conductimetry nuclear magnetic resonance and viscosimetry were selected in order to determine the structural features and molecular weight of both the biopolymer as well as M/G ratio and DD concerning respectively alginate and chitosan.

B 1.1 Materials and methods

Alginic acid sodium salt low viscosity and chitosan low viscosity purchased by Sigma Aldrich were selected as starting material for the preparation of the hydrogels studied in this work.

B 1.1.1 Infrared spectroscopy

In order to characterize the structure of the polysaccharides selected as starting materials the FTIR-UATR analysis for both the biopolymers was performed. Moreover, this technique allows to estimate approximately the value of the M/G ratio for the alginates through the ratio by the absorbance ratio of the two IR bands cantered respectively at 1030 and 1080 cm^{-1}.[1] The IR spectrum of sodium alginate and chitosan powders were acquired at room temperature in a scan range between 4000 and 450 cm^{-1}, with 4 accumulations and at a resolution of 4 cm^{-1}. In particular, FTIR Spectrum Two (Perkin-Elmer) equipped with a UATR module, for the attenuated total reflectance, was employed.

B 1.1.2 Conductometric titration

Conductometric analysis was performed in order to determine the degree of deacetylation of the chitosan sample following the procedure already reported in literature by Crofton and coworkers. Chitosan (0.1 g) was dissolved in 10 mL of 0.1 M HCl and then 90 mL of distilled water was added. The solution was titrated with a standard 0.1 M NaOH solution using a 25 mL buret.[2]

The conductivity of the solution was monitored with an Orion Research conductivity meter (Mod. 101) equipped with an Orion conductivity cell (Mod. 012001). The degree of deacetylation was calculated by using the following relation:

$$DD\% = \frac{(V_2 - V_1)(L) \times C_{NaOH}\left(\frac{mol}{L}\right) \times 161{,}16\left(\frac{g}{mol}\right)}{\text{mass of chitosan (g)}}$$

where (V_2 - V_1) is the difference between the two deflection points expressed in liters, C_{NaOH} is the molar concentration of NaOH solution and 161.16 is the molar mass of chitosan deacetylated monomer.

B 1.1.3 Nuclear magnetic resonance (NMR)

The nuclear magnetic resonance spectra have been acquired using the Bruker Avance III Ascend 400 MHz spectrometer in order to evaluate the M/G ratio during the characterization of alginate and the degree of deacetylation DD% related to the studies on the chitosan sample.

^{13}C-NMR

In this work we have applied the experimental procedure proposed and reported by Grasdalen and coworkers.[3] An alginate solution 100 mg/ml were prepared in deuterated water (D_2O) at pD=7 and placed in an NMR tube; the NMR spectrum has been acquired at the frequency of 50 MHz with pulse duration of 0.8 s and 40000 scans. Moreover, in order to minimize the drawbacks related to the viscosity of the alginate sample, the temperature of the probe has been set at 90 °C. The

M/G value was obtained from the average between the integral ratios of all the individual carbon peaks of the mannuronate subunit and the guluronate ones.

^{1}H-NMR

^{1}H-NMR analysis was accomplished in order to determine the degree of deacetylation of the selected chitosan according to the procedure reported by Lavertu and coworkers.[4] At this regard, 10 mg of chitosan powder was solubilized in a solution composed of 1.96 mL of D_2O and 0.04 mL of DCl under magnetic stirring.

The sample tube was inserted into the probe and the experiment was performed at a single pulse sequence at 90°, with solvent presaturation. The delay before the application of the pulse was 6 seconds and the acquisition time was 2 seconds, for a total relaxation time of 8 seconds.

The suppression of the solvent signal, obtained by saturation, takes place by irradiating the decoupler set to the solvent resonance frequency using low power during the 6 seconds delay before the 90° pulse. The total time for acquisition of the data was about 30 minutes. Finally, the degree of deacetylation was calculated applying the relationship reported below.

$$\mathrm{DD}(\%) = \left(\frac{\mathrm{H1\text{-}D}}{\mathrm{H1\text{-}D} + \mathrm{H1\text{-}A}}\right) \times 100$$

Where H1-D and H1-A were the areas of the peaks observed for the hydrogen bounded to the carbon C1 of the deacetylated and acetylated monomer respectively.

B 1.1.4 Viscosimetric analysis

A Fungilab Viscolead ADV "L" rotational viscosimeter has been used to determine the viscosities of the polysaccharide solutions. This instrument is equipped by a rotating cylindrical element which must be immersed in the solution. When the rotation is started the torque required to reach a certain rotational speed is measured and directly related to the viscosity of the solution.

The determination of the average molecular weight of the two polysaccharides employed in this work was obtained adopting the viscosimetric approach based on the Mark-Houwink-Sakurada:

$$[\eta] = K \cdot \overline{MW}^{a}$$

Where MW is the average molecular weight while *K* and *a* are empirical constants. As reported by Masuelli and co-worker the values of K and a for the alginate correspond to 7.3×10^{-5} and 0.92, for the measurements carried out at 25 °C in a 0.1 M sodium chloride aqueous solution and 1.23×10^{-4} and 0.96 in distilled water.[5] Therefore, the viscosity of alginate solutions has been measured by ranging the biopolymer concentration from 0.1 to 7 g/dL.

On the other hand, the intrinsic viscosity of chitosan was determined dispersing the polysaccharide in two different acetate buffer solutions, 0.25 and 0.5 M. The viscosimetric analysis was performed under these conditions for chitosan solutions whose polysaccharide concentration was ranged between 0.05-2.0 g/dL. In these experimental conditions the values of the viscometric constants used are K=199 $\times10^{-5}$ dL/g, a=0.59 and K=15.7×10^{-5} dL/g, a=0.79 in 0.5 M and 0.25 M acetate buffer, respectively; as reported by Kasaai these parameters accords to the degree of deacetylation calculated for the chitosan used in this work.[6] The so obtained viscosity values were firstly converted in reduced viscosity values ($\frac{\eta_{rel}-1}{C}$) for both polysaccharides and, then, plotted as function of the biopolymer concentration expressed in g/dL. The reduced viscosity of the solutions of both polysaccharides increased exponentially by increasing their concentration. The intrinsic viscosity for both biopolymers was extrapolated taken into account only the most dilute point of the exponential functions which, by applying the linear regression, shows R^2 correlation factor always higher than 0.98. The y-intercept values for the two biopolymers and the standard error associated with them were taken as the intrinsic viscosity used for the molecular weight calculation with the Mark-Houwink-Sakurada equation.

B 1.2 Sodium alginate characterization

B 1.2.1 Structural features

By analyzing the IR spectrum reported in Figure B 1.1 acquired according to the procedure described before, the structure and typical functional groups of the sample were evaluated and compared with those reported in the literature.

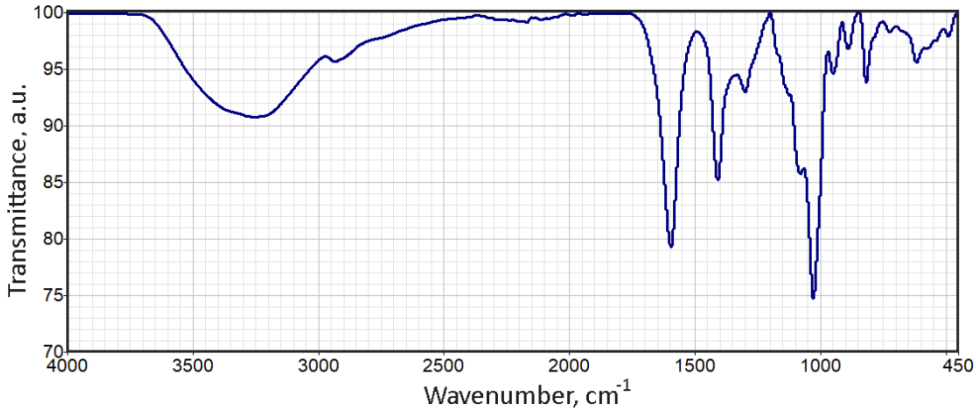

Figure B 1.1: ATR-infrared spectra of alginic acid sodium salt low viscosity powder.

In the region between 3700 and 2970 cm^{-1} there is a typical intense and broad peak due to the O-H stretching vibrations. Near this region a weak peak attributable to the C-H stretching of the methylene groups appears at the turn of the previous one and extends up to 2850 cm^{-1}.

The two sharp peaks centered at 1600 cm^{-1} and 1410 cm^{-1} may be due to the asymmetric and symmetric carboxylate (O-C-O) stretching, respectively. Moreover, the weak peak observed around 1300 cm^{-1} is generally assigned to the C-C-H and C-O-H bending vibrations.

The latter peak, added to the shoulder and the more intense peaks observed at 1077 and 1030 cm^{-1}, due to the C-O and C-C stretching, represent the vibration of the pyranose ring. The peak attribution in the fingerprint region is not properly easy. The shoulder which appears at 950 cm^{-1} is generally attributed to the guluronic residues while the peaks at 885 and 815 cm^{-1} are characteristic of the mannuronic residues.[1,7]

B 1.2.2 M/G ratio

The ratio between the mannuronic and guluronic monomers that characterize an alginate strongly affects its intrinsic properties. Its determination can be performed in various way, some more accurate than others. An approximative evaluation of the relative amount of the monomers can be obtained by the absorbance ratio of the two IR bands at 1030 and 1080 cm^{-1}, typically assigned to the mannuronic and guluronic subunits respectively. In Table B 1.1 the values of the maximum intensity of the peaks, centered at 1030 and 1080 cm^{-1}, of four acquired spectra are reported.

Table B 1.1: Maximum intensity of IR absorption bands A_{1030} and A_{1080}, corresponding to O-H bending of mannuronate and C-O-C stretching of guluronate respectively.

A_{1030}	A_{1080}	A_{1030}/A_{1080}
1.27	0.67	1.9
0.97	0.57	1.7
0.89	0.51	1.7
Average M/G ratio		1.8 ± 0.1

Therefore, the IR spectra showed in the previous section has been converted in absorbance, then the M/G ratio of 1.8±0.1 was calculated from the indicated absorbance ratio (A_{1030}/A_{1080}).[1]

A more accurate evaluation of the ratio between the two saccharides of the alginates can be extrapolated by the ^{13}C-NMR spectra. The first results obtained using this spectroscopic technique were disappointing due the broad and less resolute peaks and the high viscosity of the polysaccharide solution. However, some strategies have been developed to improve these drawbacks. There are two main process both employed to reduce the viscosity of the alginate solutions. The first involves the depolymerization of alginates in drastic condition; otherwise, the temperature of the samples can be raised up to about 100°C. Despite the high timing usually related to the ^{13}C-NMR spectroscopy, this represents one of the most accurate methods in determining the M/G ratio. In Figure B 1.2 the acquired

spectrum is reported; the assignment of each carbon was attributed according to the spectrum reported by Grasdalen and coworkers.[3]

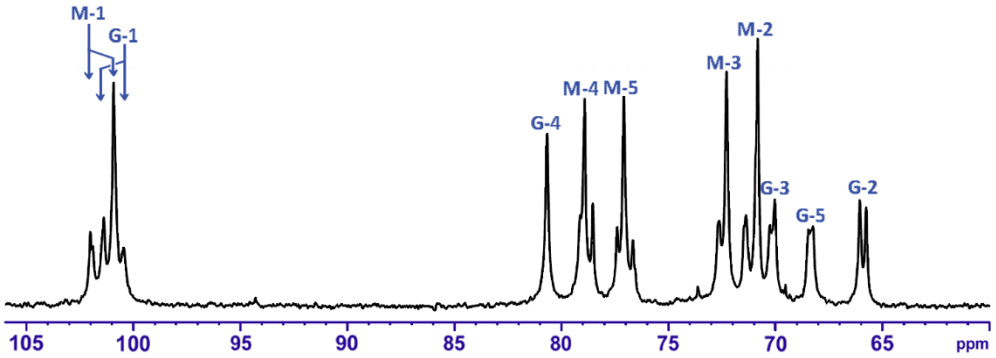

Figure B 1.2: Acquired ^{13}C-NMR spectra of sodium alginate 100 mg/ml in D_2O, pD=7.

As can be seen, the spectrum is sufficiently resolved to distinguish each carbon well and in Table B 1,2 the integral values of each carbon of the mannuronate and guluronate subunits are reported. Moreover, in table the M/G ratios calculated for each one carbon and their average value are also indicated.

Table B 1.2: Carbon integrals values of mannuronate and guluronate subunits, obtained from ^{13}C NMR analysis; each and average M/G ratio are reported.

	C1	C2	C3	C4	C5
M	2629.99	3416.12	2508.90	2519.38	2444.70
G	1488.36	1232.44	1711.23	1439.38	1364.14
M/G	1.77	1.71	1.82	1.75	1.79
Average M/G ratio				**1.77±0.04**	

This procedure makes it possible to determine the M/G ratio thanks to the different chemical shifts associated with the carbon nuclei of the two monomeric units and to the high resolution of the peaks associated with them. Therefore, monomeric composition can be derived from the ratio of the integrals of the carbon nuclei relative to the mannuronic and guluronic residues. The M/G ratio calculated with this method is equal to 1.77±0.04, a value that perfectly matches the previous data obtained using the IR spectra (1.8±0.1).

B 1.2.3 Molecular weight

As previously stated, the average molecular weight is an important parameter that affects the properties of a polymer. In this study the molecular weight of the alginate has been extrapolated using the Mark-Houwink-Sakurada relationship, discussed before. The values of many empirical Mark-Houwink-Sakurada coefficients (K and a) for alginates are listed in the literature. As reported, these parameters generally depend both on the source of alginate and on the solvent, on the temperature and on the ionic strength of the medium used in the viscosimetric analysis.

As shown in Figure B 1.3, the viscosity of the alginate increases exponentially increasing its concentration therefore, in order to extrapolate the intrinsic viscosity only the first stroke of the curve, comprise between 0.1 and 1.5 g/dL was considered.

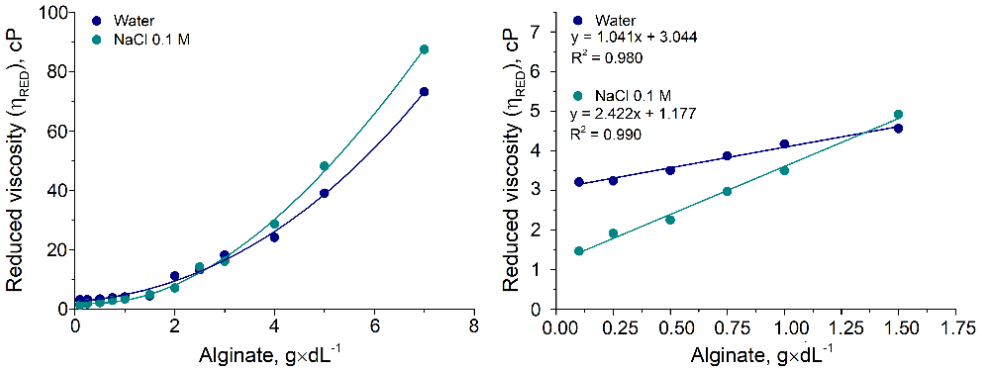

Figure B 1.3: Reduced viscosity plotted as function of the concentration of alginate dissolved in water (●) and in sodium chloride 0.1 M (●) and extrapolation of the intrinsic viscosity.

In these condition intrinsic viscosity values of 1.177 and 3.044 dL/g were extrapolated for the alginate solution in sodium chloride 0.1 M and in water respectively. In the graph the reduced viscosity values were plotted as a function of the concentration of polysaccharide. Therefore, the average molecular weight of 37.6±0.2 kDa has been obtained by applying the reverse formula of the Mark-Houwink relation, using the parameters found in the literature.

B 1.3 Chitosan characterization

B 1.3.1 Structural features

Regarding the characterization of chitosan, the same guidelines adopted for the alginate characterization were followed. In a first step, the IR analysis via FTIR-ATR was employed in order to obtain a structural characterization of the polysaccharide. Figure B 1.4 shows the IR spectra acquired with 4 accumulation at a resolution of 4 cm^{-1}, at room temperature in the spectral region between 4000 and 450 cm^{-1}.

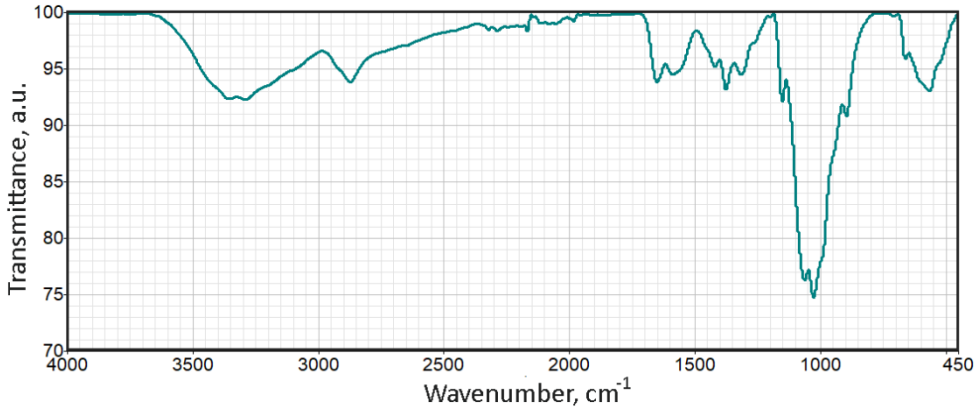

Figure B 1.4: ATR-infrared spectra of the powder of low viscous chitosan.

The region between 3680 and 2980 cm^{-1} is characterized by the O-H stretching vibration which overlaps the N-H stretching of the amino group of chitosan. The stretching vibrations of the C-H bond both of methyl and methylene groups occur around 2900 cm^{-1}. In the middle of the analyzed spectral region, the stretching of the carbonyl group, also called amide I (Am I), occurs at 1650 cm^{-1}, while at 1590 cm^{-1} a peak relative to the H-N-H in plane bending can be observed. The presence of amidic groups is confirmed by the shoulder at approximately 1550 cm^{-1} due to the bending of the C-N-H groups, called amide II (Am II).

Regarding the two peaks centered at 1420 and 1375cm^{-1}, they can be assigned to the bending vibrations of a series of groups, such as methyl, methylene and hydroxyl. Moreover, close to them, the band of amide groups III, due to the C-N bond stretching, appears. Finally, the broad band observed between 1190 and 760

cm^{-1} is the results of the overlap of a series of peaks typical of the polysaccharides, as stated for the alginates. The main vibrations that occurs in this region are the stretching of both C-O-C, C-O-H added to a series of out-of-plane bending and the skeletal vibrations involving the C-O bond. The remaining region of the fingerprint is a complex combination of bending vibrations both in- and out-of-plane.[8,9]

B 1.3.2 Degree of deacetylation

The degree of deacetylation (DD) is an important parameter for characterizing chitosan. During this work the DD of the chitosan was determined using two methods: conductometric titration and ^{1}H-NMR spectroscopy. Conductometric analysis was performed in triplicate following the procedure reported in the material and methods section and in Figure B 1.5 the average values of the conductivity, together with the standard deviation, are reported.

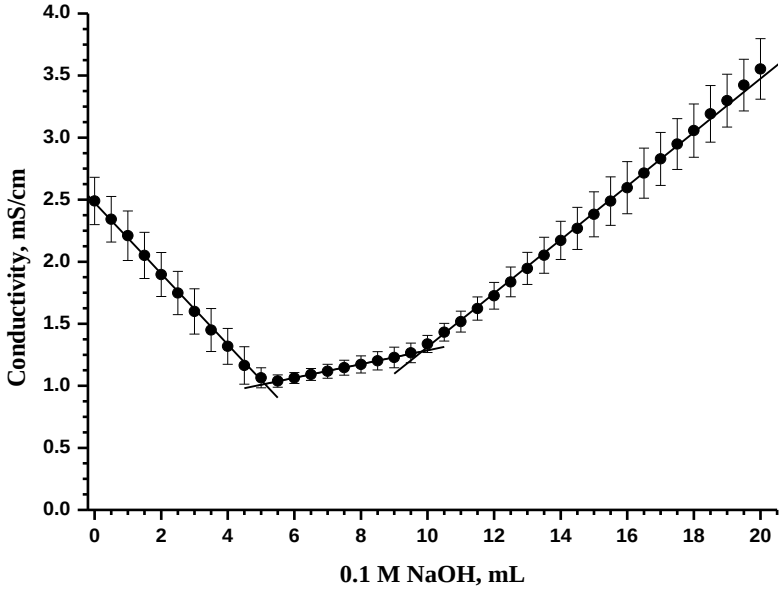

Figure B 1.5: Conductometric titration curve of chitosan sample.

The titration curve is characterized by the presence of a first rapid descending branch, which corresponds to the neutralization of excess H^{+} ions of added HCl. The first deflection point can be attributed to the initial dissociation of the weak acid, the protonated amino groups of the chitosan. When the ammonium groups

are completely neutralized, the final upward branch corresponds to the increase in conductance due to an excess of added base.

The equivalence was calculated by determining the positions of intersection of the three branches of the titration curve and the difference between the two intersection points corresponds to the volume of base required to neutralize the amino acid groups. Replacing the data obtained after the titration in the equation reported before, a DD of 76.6% ± 0.5 was calculated.

Another very suitable method for the determination of the DD % of chitosan is ^{1}H-NMR spectroscopy. This technique does not need an accurate weighting of chitosan, sample preparation is easy, and no calibration curve is required. Moreover, if the impurity peaks do not overlap with the relevant peaks of chitosan, its purity must not be determined. In Figure B 1.6 is shown the ^{1}H-NMR spectrum of chitosan, registered at 70 °C to improve chitosan water solubility.

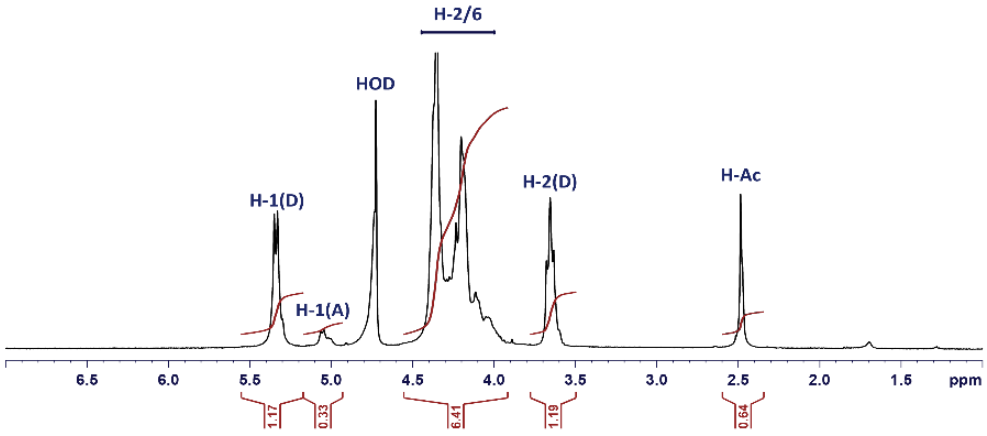

Figure B 1.6: Chitosan ^{1}H-NMR spectrum acquired at 70 °C.

The peaks used to determine the degree of deacetylation are well resolved and the integration of these peaks is simple. Therefore, the deacetylation degree can be easily calculated by using the areas of the peaks of protons H1 of both deacetylated and acetylated monomer (H1-D, H1-A). The DD% was found to be 78.0%, a value very similar to that determined by the conductometric titration.

B 1.3.3 Molecular weight

Much importance is paid in investigating the molecular weight of chitosan inasmuch, can strongly affect the characteristic of its hydrogels. As observed for the alginate, in this work the molecular weight of the chitosan it has been extrapolated using the Mark-Houwink-Sakurada relation.

The chitosan solution was prepared in acetate buffer both 0.25 M and 0.5 M. As described previously the intrinsic viscosity was extrapolated by plotting the reduced viscosity as function of the biopolymer concentration. As shown in Figure B 1.7, the viscosity of the chitosan increases exponentially increasing its concentration therefore, in order to extrapolate the intrinsic viscosity only the first stroke of the curve, comprise between 0.05 and 0.25 g/dL was considered.

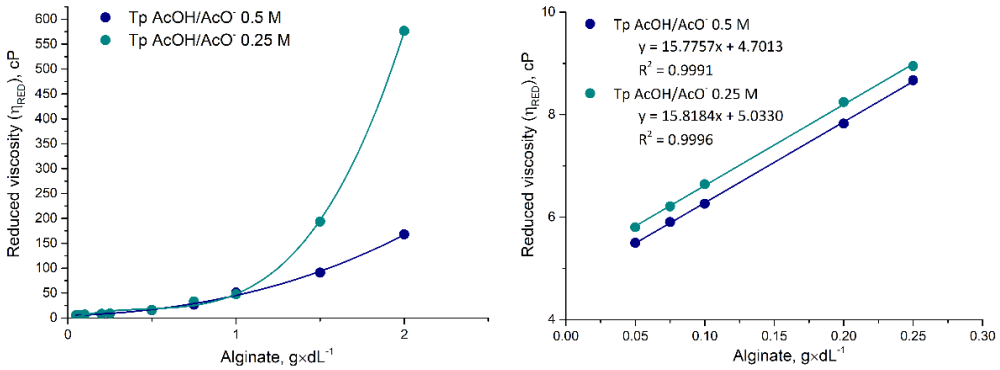

Figure B 1.7: Reduced viscosity data plotted as function of the concentration of chitosan for the extrapolation of the intrinsic viscosity.

In these condition intrinsic viscosity values of 4.7013 and 5.0330 dL/g were extrapolated for the chitosan solutions prepared in acetate buffer 0.5 and 0.25 M respectively. For the chitosan, in addition to the temperature, the pH and the ionic strength of the medium, the constants K and α depend on the degree of deacetylation (% DD) of the polysaccharide. In fact, the chitosan conformation and its interactions with the solvent depend on the number of ammonium groups along the chain, which increases as the deacetylation degree increases. For these reasons, viscosimetric analysis must be carried out under selected experimental conditions according to the DD % previously obtained. Therefore, applying the

Mark-Houwink-Sakurada relation for both the experimental condition was obtained an average molecular weight of 513,7±11.6 KDa.

References

1- E. Gómez-Ordóñez, P. Rupérez, Food Hydrocolloids, **25**, 1514-1520 (2011);

2- A.R. Crofton, S.M. Hudson, K. Howard, T. Pender, A. Abdelgawad, D. Wolski, W.M. Kirsch, Carbohydrates Polymer, **146**, 420-426 (2016);

3- H. Grasdalen, B. Larsen, O. Smidsrød, Carbohydrates Research, **89**, 179-191 (1981);

4- M. Lavertu, Z. Xia, A.N. Serreqi, M. Berrada, A. Rodrigues, D. Wang, M.D. Buschmann, A. Gupta, Journal of Pharmaceutical and Biomedical Analysis, **32**, 1149-1158 (2003);

5- M.A. Masuelli, C.O. Illanes, International Journal of BioMaterials Science and Engineering, **1**, 1-11 (2014);

6- M.R. Kasaai, Carbohydrate Polymers, **68**, 477-488 (2007);

7- D. Leal, B. Matsuhiro, M. Rossib, F. Caruso, Carbohydrate Research, **343**, 308-316 (2008);

8- J. Brugnerotto, J. Lizardi, F.M. Goycoolea, W. Argülles-Monal, J. Desbrières, M. Rinaudo, Polymer, **42**, 3569-3580 (2001);

9- A. Zając, J. Hanuza, M. Wandas, L. Dymińska, Spectrochimica Acta Part A: Molecular and Biomolecular Spectroscopy, **134**, 114-120 (2015).

Section C

Hydrogel applications

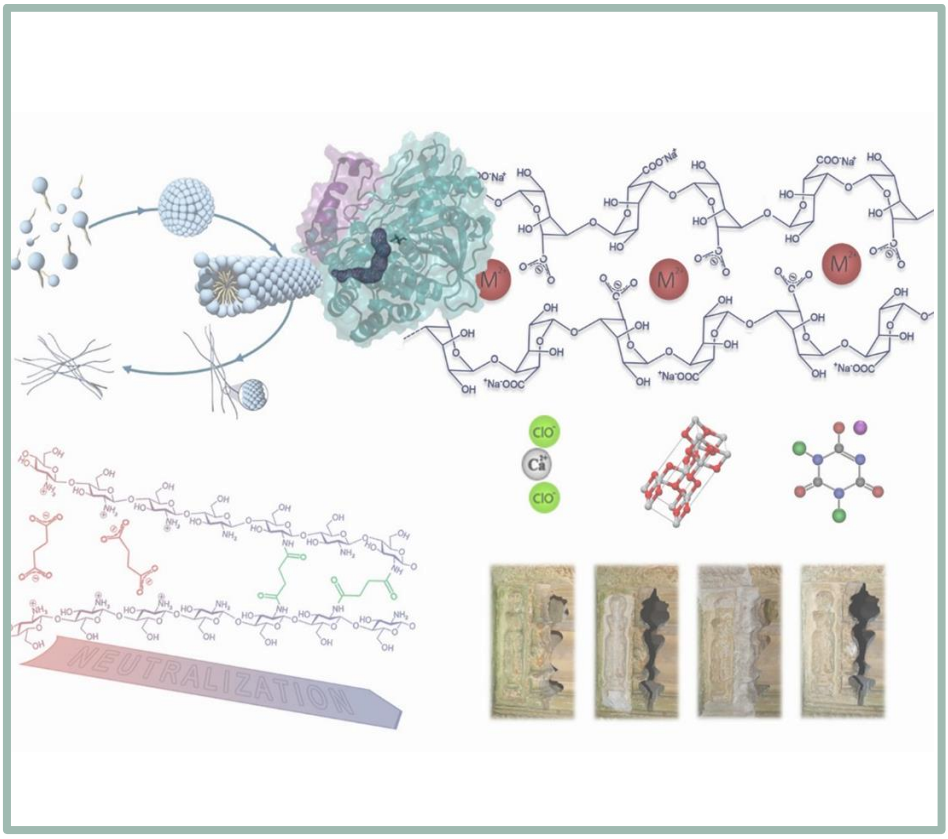

Chapter C 1

Enzyme in surfactant & hydrogel

C 1.1 Bioconversion

Enzymes are proteins with outstanding catalytic activity, regiospecificity and stereospecificity. Properly thanks to these features high interest is paid in the application of enzymes in synthetic processes termed *bioconversion*. The main challenge in this field of catalysis is the improvement of the methodologies aimed to the enzyme stabilization also in non-physiological environment. For this purpose, the addition of suitable additives or the entrapment of enzymes in solid matrices could improve the enzymatic stability and, in some cases, can also increase its activity. Moreover, through immobilization of enzyme good enzyme recycle can be obtained.[1,2]

C 1.1.1 Bioconversion in aqueous surfactant solution

Surfactant solutions are a promising alternative for solubilizing hydrophobic chemicals in aqueous media avoiding the employment of organic solvents, which are known to rapidly deactivate enzymes. Furthermore, thanks to their amphiphilic character, as described in Chapter A 1, they can form micellar aggregates when the surfactant concentration overcome the CMC. Lipophilic substrates are generally confined inside the hydrophobic microenvironment of the micellar aggregate, dispersed in water as for the enzyme. The bioconversion frequently occurs in the proximity of the hydrophobic/hydrophilic interface of such aggregates.[1] In the past decades, the effect of surfactants on the catalytic activity of enzymes has been widely studied for various field of research and applications such as drug delivery, cosmetics and detergency.[3-6] For a long time surfactants have been considered non-specific denaturants for proteins, including enzymes. In fact, the denaturation induced by sodium dodecyl sulphate (SDS) to globular proteins was exploited in gel

electrophoresis.[7] The role of the surfactants during protein denaturation was extensively studied in the past years; the first studies reported in this sense are date back to the early 70's.[8,9] The structure of surfactants and enzymes plays a key role as regards the interactions established between them leading to denaturation. Indeed, firstly the charged headgroups strongly interact with the ionic residues on the protein surface. These electrostatic interactions lead to the exposition of the hydrophobic amino acid residues. Therefore, the interaction between hydrophobic moieties of the protein and the alkyl chain of amphiphiles induce the loss of the tertiary structure. On the other hand, non-ionic surfactants generally do not induce the denaturation of proteins because of the absence of such strong electrostatic interactions. These "soft" surfactants also include the zwitterionic amphiphiles such as betaines, sulfobetaines and amine oxides.[3,10]

In the literature, several examples of surfactants able to enhance activity and or stability of enzymes are also reported. In some cases, this effect can be ascribed to positive interactions established between surfactant and substrate or products. The increased solubility or availability of the substrate can increase the turnover of the enzymes as well as the surfactants can lead to the dissociation of enzyme-product complex, rapidly reestablishing the catalytic site.[11,12] Moreover, free surfactant monomers or micellar aggregates can induce some conformational change on the tertiary structure of the enzyme that allow to increase its catalytic properties both in term of activity and stability.[13-16]

C 1.1.2 Enzyme immobilization

In addition to the great activity and stability, in industrial processes the recycling of the catalysts is required to limit the cost of the process. In the past years several implementations were developed, aimed at increasing the reusability and stability of enzymes, including immobilization. Enzyme immobilization allows the biocatalyst to be applied in more drastic operating conditions, by increasing their stability in term of pH, temperature and reaction time. Moreover, being confined to a solid

phase with respect to substrate and product, the inhibition effect is usually reduced.[17] On contrast the time required for the immobilization and its cost must be taken into account; in fact, this process is particularly useful when the enzyme is expensive. Nowadays, several methods and procedure to immobilize enzymes on a wide range of supports (organic and inorganic) were developed, allowing to choose the suitable immobilization condition. Immobilization methods can be grouped according to the interaction established between enzyme and support in chemical and physical immobilization, each of which presents advantages and drawbacks.[18,19] In Figure C 1.1 the main immobilization methods are schematically showed.

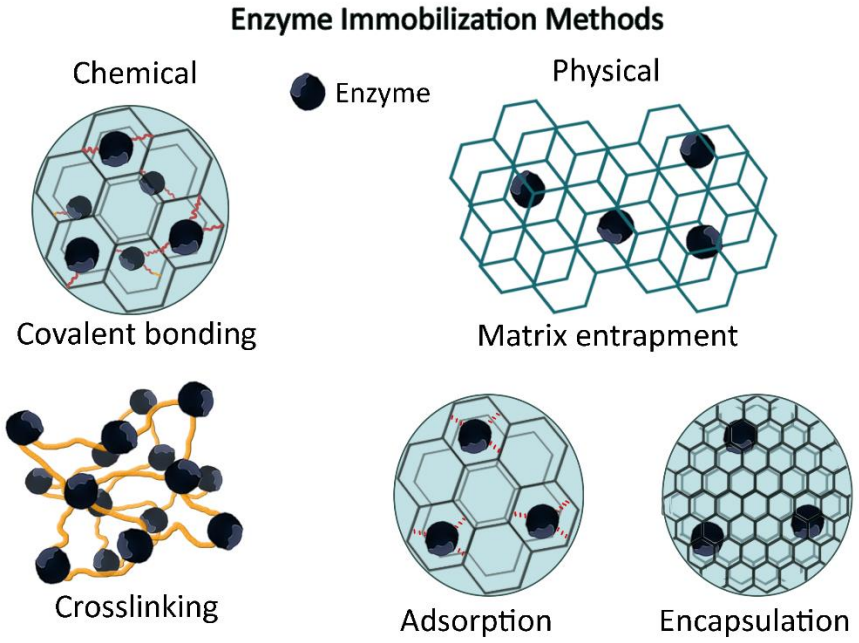

Figure C 1.1: Chemical and physical method of enzyme immobilization.

Chemical immobilization

Chemical methods of immobilization refer to the establishment of covalent bonds between the enzyme and a support or other enzymes. Firstly, covalent bonding consists in the multiple linkage of the protein to the matrix by exploiting the functional groups of both constituents. Alternatively, small crosslinking agents, *i.e.* glutaraldehyde, can be used as "small spacer" between matrix and protein. Using

this method, the stability of enzymes is generally improved also under harsh conditions such as drastic pH or temperature. However, this approach can induce irreversible conformational changes of the protein or may force the enzyme in position that hinders the access of the substrate to its catalytic site. These effects result in a loss of the total enzymatic activity which must be considered for application purposes.[19-21]

The second method involves the use of crosslinking agents, mainly glutaraldehyde, able to bind the biomacromolecules together by exploiting the lysine residues, thus forming the crosslinked enzyme aggregates (CLEAs). These aggregates are formed by adding both precipitating and crosslinking agents to the enzyme solution. The crosslinker avoids the enzyme dissolution after the removal of the precipitants from the CLEAs. The main advantages of these immobilization methods lie alongside the ease of the crosslinking process added to low costs, reduced diffusion problems, less conformational stress, easy recovery and good reusability. However, using this immobilization techniques, the crosslinking can be ineffective when the enzyme surface presents a low amount of lysine residues. Moreover, as also described for covalent immobilization, crosslinking can involve amino acid residues close to the catalytic site, hampering the formation of the enzyme-substrate complex.[19]

Physical immobilization

Physical methods provide enzymatic immobilization due to the establishment of weak enzyme-support interactions, such as Van Der Waals forces, hydrophobic interactions, hydrogen bonds and electrostatic interactions. This process is reversible and can be modulated according to the chemical-physical parameters. The different techniques are affected by the same drawbacks, which mainly includes the easy desorption of the protein or the poor diffusivity of the substrate. However, these techniques allow to maintain the active form of the enzymes, without inducing irreversible conformational change; moreover, they are generally simple, fast, reversible and do not require any dangerous crosslinker. Physical immobilization

methods can be mainly divided into adsorption, entrapment and microencapsulation.

Surface adsorption was the first methods used to confine an enzyme and exploit solid supports with suitable surface characteristics are able to adsorb high enzyme amounts establishing strong electrostatic interactions. The most used matrices can be organic such as cellulose, gelatin, dextran or inorganic such as alumina, activated carbon and glass.[22] The immobilization through physical entrapment within a polymeric lattice (alginate, polyacrylamide etc.) allows good substrate permeation and product release, ensuring a continuous transformation.[23]

Finally, the microencapsulation of enzymes refers to the entrapment within semipermeable spherical membranes with controlled porosity (1-100 μm). Such semipermeable membranes can be permanents or not, depending on their constituents. Regardless of their nature, microcapsules containing enzymes have a very high surface area, which favors the development of the catalytic process.[24]

C 1.2 Lipases

Lipases are serine hydrolases defined as triacylglycerol acyl hydrolase, which differ from esterase for the nature of their substrate. These two subclasses can be also distinguished for the phenomenon of interfacial activation. In fact, in the absence of an interface between the organic and aqueous phase, the active site of lipases is covered by a secondary structure that hinder access to the substrate. Instead, when the lipase was exposed to such interface, it undergoes an important conformational rearrangement, switching to the active state. This phenomenon, not observable for esterase, allows lipases to exploit their catalytic activity even in organic solvents.[25] Moreover, according to the nature of the organisms from which they were extracted, these enzymes can operate in extreme conditions of temperature (thermophiles), pH (acidophilic and/or alkaliphilic) and high saline concentrations (halophiles).[26-28]

The ability to catalyze reactions other than physiological ones, with non-model substrates, is quite widespread in enzymology and has recently been defined as "*enzymatic promiscuity*". However, the activity of enzymes in the catalysis of promiscuous reactions is generally lower than the physiological one.[29,30] As reported in Figure C 1.2, lipases can catalyze many reactions such as esterification, transesterification, interesterification.

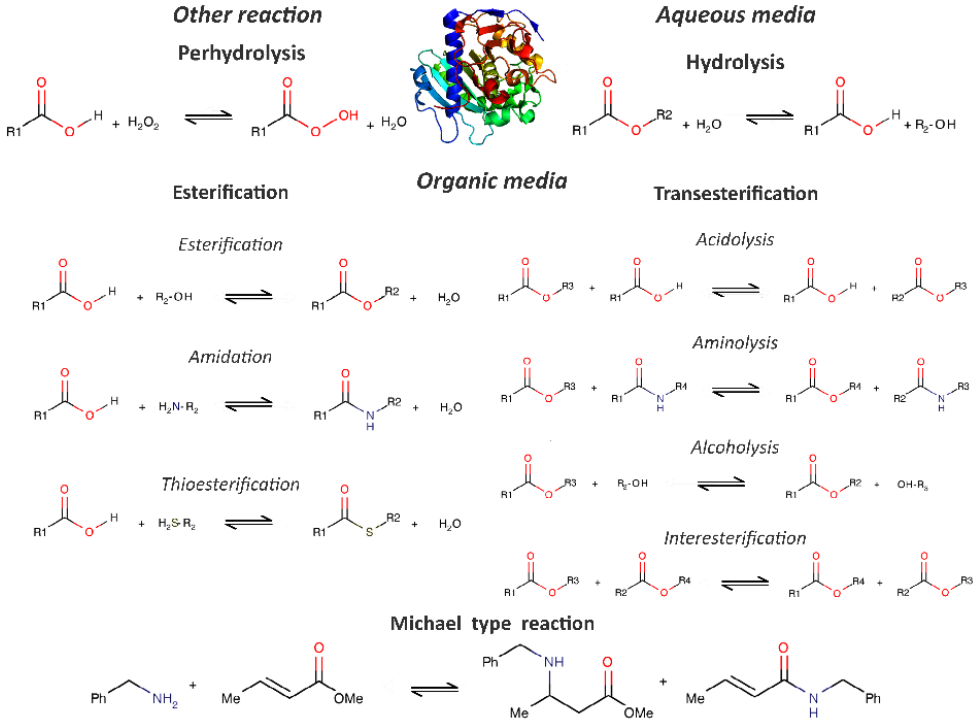

Figure C 1.2: Reactions catalyzed by lipases.

The promiscuity of lipases and their stability under drastic conditions (pH, temperature, non-aqueous media) added to the good regio- and stereoselectivity make this class of enzymes very attractive in many research fields, with particular regard to the pharmacological field.[31]

C 1.2.1 Structural features of lipases

Lipases are members of the enzyme superfamily of α/β-hydrolase and consist of a core with filaments having a secondary β-strands structure surrounded by α-helices.

All lipases, with the exception of lipase B from *Candida antarctica*, have a conservative pentapeptide sequence Gly-X-Ser-X-Gly around the active nucleophilic serine residue, which forms a characteristic β-turn-α motif called "*nucleophilic elbow*".[32] The active site of lipases is formed by a catalytic triad consisting of serine, histidine and aspartic or glutamic acid. For a chemical point of view, lipases are quite similar to proteases except for the different structure of the active sites; this difference lies in the orientation of the hydroxyl group of the catalytic serine which involves an inverse stereochemistry of the respective catalytic triads.[33] The lid domain represents a functional and structural feature that can be observed in all lipases, but its structure can be very different.[34] Figure C 1.3 shows the common structural properties of lipases.

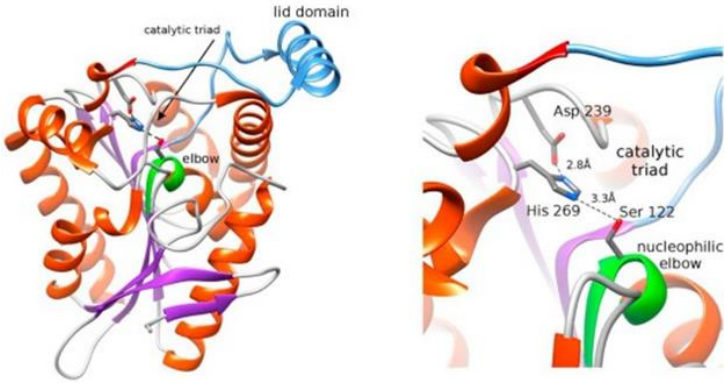

Figure C 1.3: Lipase structure: catalytic triad, nucleophilic elbow and lid domain.

In addition, there are four different binding pockets for triglycerides. The first one is an oxyanion hole, which is formed by the two backbone amides of a residue in the N-terminal region of the lipase and the neighboring C-terminal of the catalytic serine. The other three remaining pockets allow the entrance of the fatty acids by binding them in positions Sn-1, Sn-2 and Sn-3.[35] In the literature, a classification of lipases made according to the geometry of the binding site is reported. In this regard, they are generally divided into slit-like hydrophobic (lipases from *Rhizomucor* and *Rhizopus*), funnel-like (for example lipases from *Candida antarctica*) and tunnel-like (lipase from *Candida rugosa*) binding site.[36]

C 1.2.2 Catalytic mechanism of lipases

Based on the similarity of the catalytic triads of lipase and proteases, it is common to expect an analogy in the catalytic mechanism. As shown in Figure C 1.4, lipases exhibit a catalytic mechanism similar to that of serine proteases, which provide the formation of two tetrahedral intermediates.

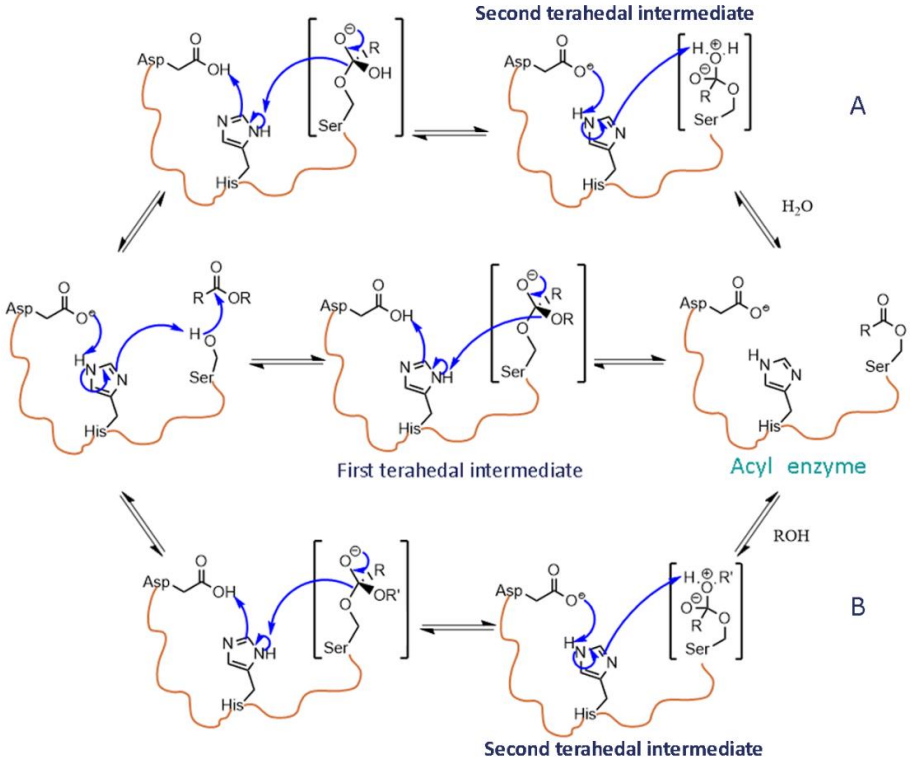

Figure C 1.4: Catalytic mechanism of hydrolysis (A) and esterification (B) of lipases.

The mechanism provides a transfer of charges between the catalytic residues to make the hydroxyl group of the serine more nucleophilic. Then, the nucleophilic attack by the serine hydroxyl group on the carbonyl carbon of the ester substrate takes place by forming the first tetrahedral intermediate; this, by losing an alcohol molecule, gives rise to the acyl-enzyme. Subsequently, a water molecule attacks the acyl-enzyme forming the second tetrahedral intermediate, which, by losing a carboxylic acid molecule, regenerates the enzyme in its native form.

As for the esterification reaction, in the transesterification catalytic cycle following the formation of the acyl-enzyme, an alcohol molecule replaces the water and carries out its nucleophilic action.[37]

C 1.2.3 Candida rugosa lipase

Candida rugosa lipase (CRL) is one of the most used enzymes of its class to implement biotransformations. This type of enzyme was first described in the 1960s by isolating yeast from natural soils. Two isoenzymes, initially called LipA and LipB, were subsequently identified, purified and genetically characterized. This nomenclature was then replaced by a numerical one starting from Lip1 up to Lip7. At least seven genes are involved in the production of CRL, five of which (Lip1 - Lip5) are fully characterized.[38,39]

All the isoenzymes characterized so far are composed of 534 amino acids and have a structural homology greater than 70%. Like the other lipases all the isoenzymes belong to the α/β-hydrolase family with a catalytic triad (Ser-209, Glu-341 and His-449) and a lid that protects the active site when the enzyme is in its inactive form.[40] However, the lid structure is mainly based on a disulphide bond, between Cys-60 and Cys-97, and on an ionic interaction, established between Glu-96 and Arg-37. Figure C 1.5 shows the conformational changes induced by the opening of the lid.

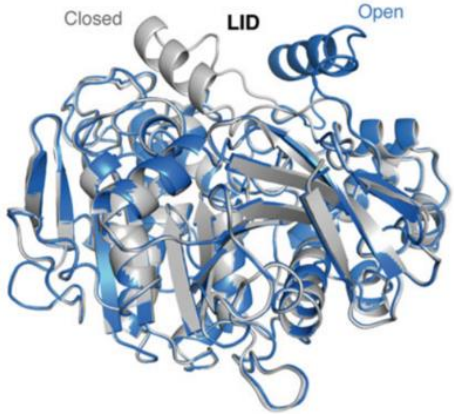

Figure C 1.5: Overlap of the CRL in its active form (lid opened-blue) and its inactive form (lid closed-grey).

There is a rotation of the amino acids Glu-66 and Pro-92, which can take place thanks to a *cis-trans* isomerization of the peptide bond of Pro-92.[41] The lid in its open form has greater thermodynamic stability thanks to the hydrophobic interactions established between lid amino acids and external lipophilic environment. The structure of the lid shows differences between the various isoforms which can lead to different catalytic activities.[42] These differences can be well observed by comparing the lid structure of Lip1 and Lip3. The π-staking interactions between Phe-344 and Phe-87 and between Phe-344 and Tyr-69 are present only in the Lip1 isoenzyme. Moreover, the hydrogen bond between Ser-84 and Ser-450 present in Lip1 cannot be established in the case of Lip3 due to the replacement of Ser-450 with Ala-450 in this isoenzyme.[43] Due to these differences, the lid of Lip1 is more stable than that of Lip3, which however is more flexible. In fact, Lip1 is generally more effective on esterification of simple substrates, such as fatty acids, while Lip3 shows esterase cholesterol activity.[44]

As described above, CRL is characterized by a tunnel, used for the recognition of the hydrophobic chain of the substrate, which starts in conjunction with Ser-209 and extends inward under the cover. This L-shaped cavity has a total length of about 25 Å and is capable to adapt to different type of substrates.

Figure C 1.6 shows the 3D structure of the Lip3 isoenzyme from *C. rugosa* (CRL3).[45,46]

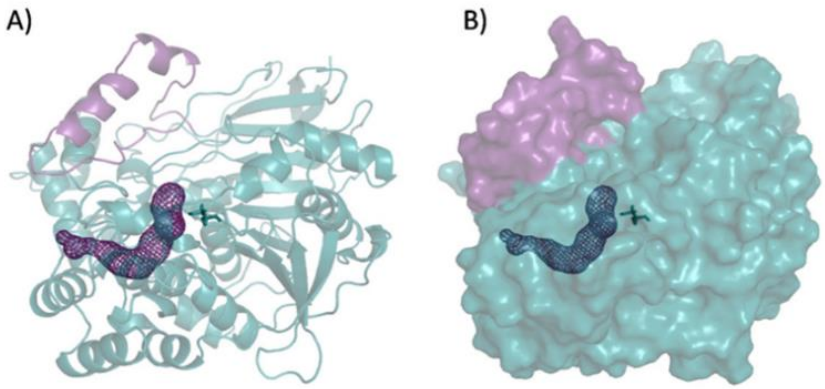

Figure C 1.6: 3D Structure of CRL3, the α-helices forming the lid are colored in magenta and the intramolecular tunnel is represented by a mesh.

Thanks to its broad substrate specificity, *Candida rugosa* lipase has acquired importance in the industrial sector where it is successfully used for hydrolysis and esterification reactions, including enantioselective ones; thanks to these characteristics it is a biocatalyst used in the synthesis of drugs, in the production of aromas and in the perfumery and cosmetic industries.[47]

The here presented work, is divided in two parts in which the activity of the *Candida rugosa* lipase was evaluated in different media. On one hand has been evaluated the effects of surfactant structure on the hydrolytic activity of CRL. The charge of the headgroup of the amphiphiles and, for the selected zwitterionic amine N-oxide surfactants, the dimension of the hydrocarbon chain and headgroup was investigated. This part of study is aimed to well understand the CRL-surfactant interactions highlighting the role of the amphiphile structures and the shape of the aggregates on the enzymatic activity.

On the other hand, the CRL has been encapsulated into calcium alginate hydrogel beads in order to study this very promising method of immobilization. This second part of the work is aimed at the improvement of enzyme stability and recyclability. In this sense, the effect of composition and morphology of different beads formulations on the CRL activity was investigated using different model substrates. Moreover, in this second part of work the selected beads were used in a preliminary study on the kinetic resolution of a racemic ester mixture.

C 1.3 Effect of surfactants structure on catalytic activity of CRL

The effect of surfactants on enzymatic performances in aqueous solutions was widely investigated and studied in the literature: both hydrophobic and electrostatic interactions can occur between protein and surfactant. [3-6,10] However, only a few studies were addressed to understand the effect of surfactant structure on the catalytic properties of CRL in aqueous solution.[48,49] This topic is relevant considering the different effects that could be obtained by changing the molecular structures of the amphiphiles.[50]

Anionic and nonionic surfactants interact with the isoforms of CRL in a different way. Lipase B was more sensitive than Lipase A to the presence of sodium dodecyl sulfate (SDS) and Triton X-100 and its deactivation was rapid. Goswami et al. reported the effects of different cationic, anionic and nonionic surfactants on castor oil hydrolysis catalyzed by CRL. The authors argued that the nonionic surfactant Span 80 resulted the most suitable because it did not denature the enzyme and it acted as stabilizer for water/oil emulsions, promoting the substrate hydrolysis.[49]

The presence of amphiphiles might be responsible for the conformational changes of the protein that lead to enzyme activation.[51] For instance, surfactants can induce the conformational changes in lipase that open the lid and give access to its active site. On the other hand, surfactants can interact with the enzyme, and such interactions can have various consequences on protein structure and activity, depending on the nature of the surfactant and on its concentration.

In this part of the work, the effect of differently structured surfactants (anionic, cationic, and zwitterionic) on the catalytic properties of CRL in aqueous media was studied. Structures and acronyms of all the additives employed in this section are reported in Figure C 1.7.

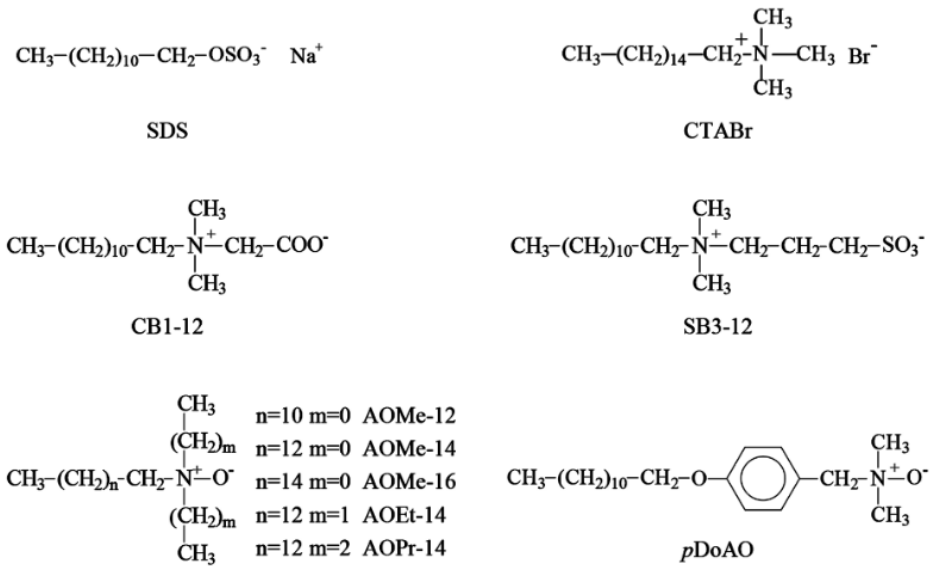

Figure C 1.7: Structure of the surfactants used in this work.

C 1.3.1 Materials and methods

Lipase type VII from *Candida rugosa* (CRL, type VII, > 1000 U/mg solid) and *p*-nitrophenyl acetate (*p*NPA) were purchased from Sigma-Aldrich and were used with no further purification. The commercial grade surfactants, SDS, CTABr, and SB3-12 were also supplied by Sigma-Aldrich and purified by recrystallization in acetone/methanol or ethyl acetate/methanol mixtures.

CB1-12 and the amine N-oxides, provided by Prof. Germani and coworkers from the University of Perugia, were prepared starting from the corresponding tertiary amines. CB1-12 was synthesized by the reaction of N,N-dimethyldodecylamine with the sodium chloroacetate to reflux in acetonitrile-ethanol mixture for 48 hours.

For the N-oxides, the tertiary amines were dissolved in ethanol, then 1.5 eq of H_2O_2 (30% water solution) were added; the mixtures were stirred at 70°C for 6-8 hours. All surfactants were purified as reported in literature.[52-54]

The purities of all the surfactants were verified via surface tension measurements with a Sigma 700 Force Tensiometer with a platinum ring (diameter 1.9 cm).

CRL catalytic assay

The hydrolysis of *p*-nitrophenyl acetate (*p*NPA), reported in Figure C 1.8, was selected as a model reaction to evaluate the enzymatic activity.

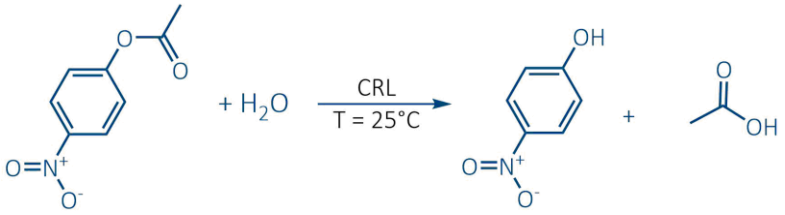

Figure C 1.8: Scheme of p-nitrophenyl acetate hydrolysis.

The CRL activity measurements were carried out spectrophotometrically at 25.0 ± 0.1 °C, following the increase in the absorbance at 348 nm, which corresponds to the isosbestic point of *p*-nitrophenol/*p*-nitrophenoxide (*p*NP), taking the molar extinction coefficient as 5400 M^{-1} cm^{-1}. Measurements were performed with a

Shimadzu UV-160A UV-VIS spectrophotometer equipped with a thermostatic cell using 3 mL quartz cuvette with 1 cm of pathlength.

CRL activity assay mixture was prepared in 0.01 M phosphate buffer at pH 7.0; the enzyme concentration was always 0.05 mg/ml (0.83 µM). The substrate *p*NPA was prepared in CH_3CN:H_2O (50:50 v/v) mixtures and its concentration in the assay mixture was 1×10^{-3} M (5% CH_3CN). The reaction starts by enzyme addition from a stock solution (0.2 mg/ml) to a thermostated solution of substrate in pure buffer or at different surfactant concentrations. The linear increase of absorbance at 348 nm due to *p*NP formation was then recorded as a function of time for five minutes; reaction rate of CRL, defined as moles of *p*NP formed per unit of time, was calculated from the slope of the initial linear curve of *p*NP concentration vs. time.

When autohydrolysis of *p*NPA (*p*NP formation in the presence of surfactants but without enzyme in the cuvette) was detected, reaction rates were calculated by subtracting the reaction rates in the absence of enzyme at the enzyme-catalyzed hydrolysis rates in surfactant solution.

Kinetic parameters k_{cat} and K_M in pure buffer and in presence of surfactants were obtained from the linear regression analysis of the double reciprocal Lineweaver-Burk plots in a range of substrate concentration between 1×10^{-4} M and 2.0×10^{-3} M. Regression coefficient was always higher than 0.99. All sets of experiments were reproduced at least three times and the differences between duplicates in each experiment were always below 5%.

C 1.3.2 Effect of ionic surfactants

The effect of the anionic sodium dodecyl sulfate (SDS) and of the cationic cetyltrimethylammonium bromide (CTABr) were investigated to evaluate the effect of the head group surfactant charge on CRL activity. In fact, it is well known that the surfactant head group has a crucial role in protein-surfactant interactions because of strong ionic interactions between the surfactant polar groups and specific charged sites on the protein surface.

Figure C 1.9 shows profiles of enzyme activity in the presence of SDS and CTABr as a function of surfactant concentration. In this plot, as in the following ones, the enzyme activity is reported as the ratio between the reaction rate in the surfactant solution and in pure buffer ($r_{surfactant}/r_{buffer}$).

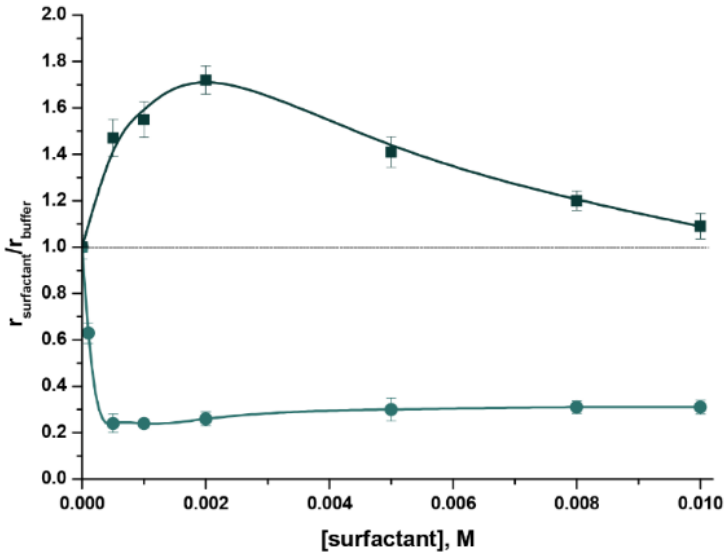

Figure C 1.9: Effect of surfactant concentration on CRL activity in 0.01 M phosphate buffer, pH 7.0 at 25.0 °C; [pNPA] = 1×10^{-3} M, [CRL] = 0.05 mg/ml (0.83 μM). (■) SDS, (●) CTABr.

As highlighted from the figure, the catalytic activity of CRL strongly depends on the charge of the surfactant head group. In fact, in the presence of SDS, the relative activity showed a bell-shaped trend as the additive concentration increased. Reaction rate reached a maximum at [SDS] = 2×10^{-3} M, with an enzyme activation of 1.72, and then decreased, but still remained higher than that in buffer.

On the contrary, CTABr showed a strong deactivating effect and CRL lost more than 70% of its activity already at a concentration of 5×10^{-4} M, a value below the critical micelle concentration (CMC), *i.e.* 8.7×10^{-4} M; then, the enzymatic activity remained almost constant as the surfactant concentration increased. The negative effect of CTABr could be explained considering that CRL have an isoelectric point located at pH 4.65, since its surface is characterized by the presence of 31 acidic and 18 basic amino acid residues.[55] Thus, in our experimental conditions (pH 7.0), lipase has an

overall negative charge and the cationic head groups of CTABr can establish strong electrostatic interactions with the protein that promotes enzyme deactivation.

A similar behavior can be found in the literature; it has been reported that the activity of *Rhizomucor miehei* lipase is much lower in the presence of a cationic surfactant than in anionic or nonionic one. Moreover, positively charged surfactants form a complex with the enzyme in solution at pH values both above and slightly below the isoelectric point of the lipase and the complex formation is due to both electrostatic and hydrophobic interactions.[56,57]

Nevertheless, the reduced enzyme activity may not be due to conformational changes of the protein, but to the binding of the surfactant with one or more lipase binding sites close to the active site.

C 1.3.3 Effect of zwitterionic surfactants

Carboxy- and sulfobetaines

An interesting category of surfactants, widely used in cosmetic for hair and skin care and as biological carriers for hydrophobic drugs, is the zwitterionic one. This class is characterized by the presence of both a positive and a negative charge, that makes the molecule overall neutrally charged at neutral pH.

Some types of zwitterions are susceptible to pH changes in a solution and may become completely cationic or anionic in acidic or basic environments. The positively-charged portion in these molecules is typically a quaternary ammonium ion, while the negatively charged portion can be a sulfate, a carboxylate, or a sulfonate.

Two betaines having the same alkyl chain, but that differ for both the type of anionic group and for the inter-charge distance (dodecyldimethylammonium methanecarboxylate (CB1-12) and dodecyldimethylammonium propanesulfonate (SB3-12)), were studied. The effect of betaine concentration on CRL activity is reported in Figure C 1.10.

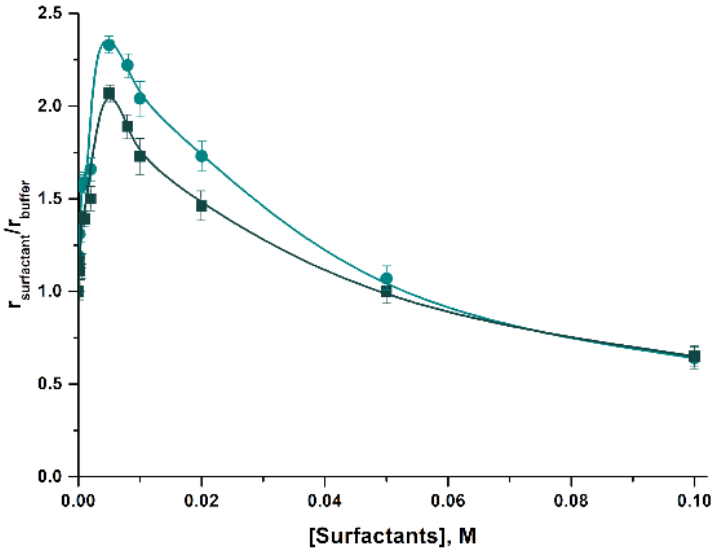

Figure C 1.10: Effect of surfactant concentration on CRL activity in 0.01 M phosphate buffer, pH 7.0 at 25.0 °C; [pNPA] = 1×10^{-3} M, [CRL] = 0.05 mg/ml (0.83 µM). (■) CB1-12, (●) SB3-12.

As it is clearly showed in the figure, both CB1-12 and SB3-12 enhance the enzyme activity with a similar behavior. In fact, CRL activity showed a bell-shaped trend, a two-fold enzyme superactivity occurred at the same surfactant concentration, equal to 5×10^{-3} M, and it was rapidly weakened at betaine concentrations higher than 5×10^{-2} M. Therefore, in this case, the nature of betaine head group appeared to have no effect on the interaction between the additive and the enzyme.

Amine oxides

As described in Chapter A 2, amine oxides are a particularly interesting class of zwitterionic surfactants because of their small but highly polar head group and the ability to protonate it by varying the pH, leading to cationic species. Their pK_a in bulk solution is about 5, therefore in pure water a mixture of neutral and ionic amine oxide molecules can be expected. Surfactants possessing smaller head group area are favored to form cylindrical rod-like micelles, and their mean aggregation number is sensitive to the total surfactant concentration. Therefore, they can form long flexible aggregates depending on the structure of the monomers; in this case their

solutions can exhibit viscoelastic properties. For these reasons, several amine oxide surfactants with different alkyl chain length and head group size were chosen: dodecyldimethylamine N-oxide (AOMe-12), tetradecyldimethylamine N-oxide (AOMe-14), esadecyldimethylamine N-oxide (AOMe-16), tetradecyldiethylamine N-oxide (AOEt-14) and tetradecyldipropylamine N-oxide (AOPr-14). These surfactants have a very similar molecular structure and the effect of slight structural changes on the hydrolysis rate of *p*NPA catalyzed by CRL was therefore evaluated.

In this case, unlike the other additives considered till now, amine oxide surfactants showed a moderate nucleophilic power. Then, relative reaction rates ($r_{surfactant}/r_{buffer}$) were calculated by subtracting the reaction rates in the absence of enzyme at the enzyme-catalyzed hydrolysis rates in surfactant solution ($r_{surfactant}$) and the obtained data was divided by the reaction rate in pure buffer. In Figure C 1.11 the effect of hydrocarbon chain length of amine oxide surfactants on CRL activity is reported.

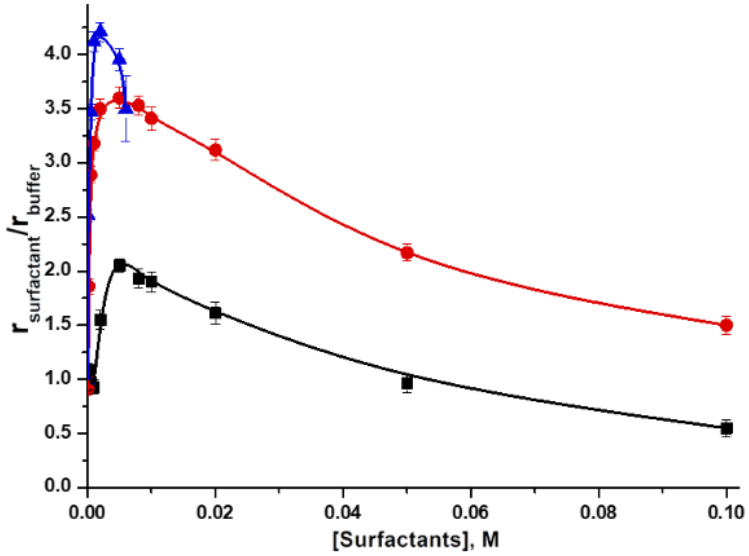

Figure C 1.11: Effect of surfactant concentration on CRL activity in 0.01 M phosphate buffer, pH 7.0 at 25.0 °C; [pNPA] = 1×10^{-3} M, [CRL] = 0.05 mg/ml (0.83 µM). (■) AOMe-12, (●) AOMe-14, (▲) AOMe-16.

As observed for the other zwitterionic surfactants, a rapid increase in the relative activity at low amine oxide concentrations was observed. This activation effect is higher with longer alkyl chains. The effect of AOMe-12 was very similar to those

observed with CB1-12 and SB3-12, with a maximum at a concentration of 5×10^{-3} M, at which the enzymatic activity was twice compared to that in pure buffer. The chain elongation caused a further increase in the relative activity and the superactivity reached 3.6 at 5×10^{-3} M of AOMe-14 and 4.2 at 2×10^{-3} M of AOMe-16. At higher surfactant concentrations, a decrease in enzyme activity was observed, but in the presence of 0.1 M AOMe-14 the enzyme activity remained higher than that in pure buffer, ($r_{surfactant}/r_{buffer}$ = 1.5), while with AOMe-12 a deactivation was observed for concentrations greater than 0.05 M. As regards AOMe-16, an increase in the viscosity of the solution was attained at 6×10^{-3} M and an accurate and reproducible measurement of the reaction rate was not allowed. For these reasons, the effect of head group size was evaluated with amine oxide surfactants having a tetradecyl hydrocarbon chain, and the effect of AOEt-14 and AOPr-14 on CRL activity was compared with that obtained with AOMe-14. Results are shown in Figure C 1.12, where the enzyme activity is again reported as $r_{surfactant}/r_{buffer}$.

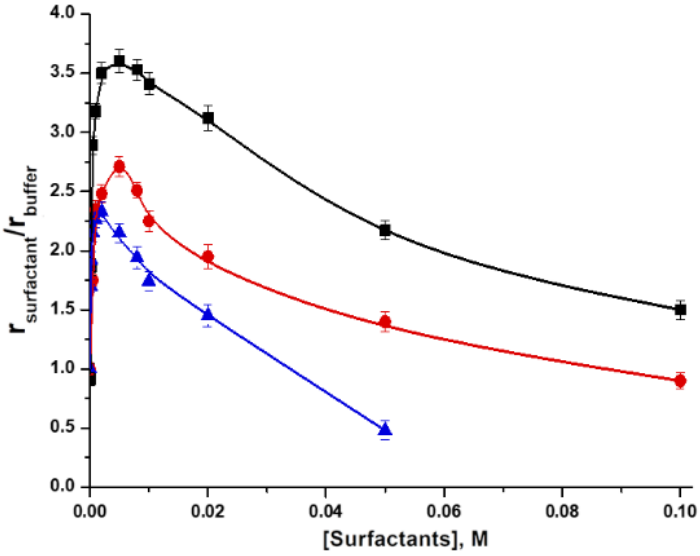

Figure C 1.12: Effect of surfactant concentration on CRL activity in 0.01 M phosphate buffer, pH 7.0 at 25.0 °C; [pNPA] = 1×10^{-3} M, [CRL] = 0.05 mg/ml (0.83 µM). (■) AOMe-14, (●) AOEt-14, (▲) AOPr-14.

Here again, differences in the surfactant head group did not change the relative rate trends. With both additives, in fact, the profiles showed a bell shape, even if the maximum activation was observed at different concentrations. In particular, in the presence of AOEt-14, the maximum of activity (2.7-fold) was obtained at additive concentration of 5×10^{-3} M, while in 2×10^{-3} M AOPr-14 enzyme activity was 2.3 times higher than in buffer. Anyway, enzyme activity lowered as the head group size increase.

All the amine oxides used in this work showed a superactivation of lipase and the concentration at which the maximum activity occurred was greater than the corresponding CMC. It therefore seemed evident that, in order to best perform their activating action, they must be in the form of micellar aggregates. The reduction of activity observed at high surfactant concentrations could be attributed to substrate subtraction by micellar aggregates. Therefore, if on one hand micelles were required to increase the activity of lipase, on the other they decreased the amount of substrate available for the enzymatic reaction. The collected results indicated that slight changes on the monomer structure can significantly affect enzyme-surfactant interactions and consequently enzyme activity. We therefore thought to correlate the hydrophobicity of the surfactant with the induced superactivity.

The hydrophobicity of surfactants can be evaluated both by their critical micelle concentration value (CMC) and partition coefficient (logP). The tendency of amphiphilic molecules to form micelles in aqueous solution is a consequence of the hydrophobic effect and then CMC decreases with increase in hydrophobicity of surfactant molecules.

The logarithm of the 1-octanol/water partition coefficient (logP) is a well-known measure of molecular hydrophobicity and several useful computational methods for estimating logP values of organic compounds were developed. Here, the Ghose-Crippen-Viswanadhan approach (AlogP), one the most widely used methods of predicting partition coefficient, was used to calculate the partition coefficient of the amine oxide surfactants.[58,59] For each compound, logP was calculated by using the

software Dragon as the sum of the number of all atoms, multiplied by their corresponding hydrophobicity constants.[60] The relative hydrolysis rate catalyzed by CRL, at the surfactant concentration at which superactivity is obtained, was therefore correlated with the hydrophobicity of surfactant, as reported in Table C 1.1.

Table C 1.1: Correlation between surfactant hydrophobicity and enzyme superactivity.

Amine oxide	CMC, M	AlogP	$r_{surfactant}/r_{buffer}$
AOMe-12	1.2×10^{-3}	3.047	2.05
AOMe-14	1.4×10^{-4}	3.960	3.60
AOMe-16	2.5×10^{-5}	4.872	4.21
AOMe-14	1.4×10^{-4}	3.960	3.60
AOEt-14	1.1×10^{-4}	4.657	2.71
AOPr-14	5.4×10^{-5}	5.705	2.33

As expected, both CMC and AlogP values seemed to indicate that hydrophobicity increases with increasing the length of the surfactant chain and the size of the head group. However, this increase had opposite effects on the enzyme activity. Indeed, CRL superactivity doubled passing from AOMe-12 to AOMe-16; on the other hand, it decreased as the head group size increases, being 3.60 and 2.33 in AOMe-14 and AOPr-14, respectively.

To explain these results, we hypothesized that the shape of colloidal aggregates affected lipase structure and activity and the morphological changes from spherical to rod-like micelles improved its catalytic properties. As already mentioned, amine oxide surfactants exist as either a nonionic or a cationic species and short-range attractive interactions, e.g. hydrogen bonds, between deprotonated and protonated forms remarkably affects the structure of the aggregate. Indeed, intermolecular hydrogen bonding could decrease the area of the head group and the dimers thus formed behave like double chain amphiphiles.[61] Sphere-rod transition of surfactant micelles is clearly affected by the hydrocarbon chain length and the longer the chain, the greater the tendency to form rod-like structures. Therefore, AOMe-12 forms spherical aggregates, while AOMe-14 and AOMe-16 are favored to form rod-like

micelles. A bulky head group increases the distance between polar head groups, thus weakening the hydrogen bond between the monomers; consequently, it can be hypothesized that, even in the presence of a long alkyl chain, AOEt-14 and AOPr-14 prefer spherical aggregates.

Other experimental evidences confirm that an increase in the alkyl residues of the head group can influence the ability of morphological growth from spherical micelles towards rod-like micelles. In the case of cationic surfactants of the family of cetyltrialkyl ammonium bromide (CTRABr; R = methyl, ethyl, n-propyl, n-butyl) the gelling induced by the *trans*-o-methoxycinnamate (*trans*-OMCNa) anion is strongly reduced by the increase in alkyl residues (R). In fact, while the CTABr / *trans*-OMCNa system forms worm-like micelles, the substitution of the methyl groups with the other alkyl groups produces an immediate reduction in the viscosity of the solution.[62] Similar observations emerged with zwitterionic surfactants of the *p*-dodecyloxybenzyldialkylamine N-oxide family (*p*DoRAO; R = methyl, ethyl, n-propyl, n-butyl). While the surfactant *p*DoAO (R = methyl) forms viscous aqueous solutions already at 0.01M concentration, the substitution of the methyl groups with more voluminous groups drastically reduces the viscosity of the solution at the same surfactant concentration.

p-Dodecyloxybenzyldimethylamine oxide (pDoAO)

As previously stated, the amine oxide surfactants give rise to aggregates sensitive to the increase in concentration, since they lead to an increase in the size due to the sphere-rod transition, without adding any type of additive. The zwitterionic surfactant *p*-dodecyloxybenzyldimethylamine N-oxide (*p*DoAO) has the ability to form highly viscous solutions at relatively low concentrations. This behavior could be due to strong interactions among the tails whereas the phenyl group plays an important role in the aggregation by π-π stacking. It has been reported that small micelles grow in length (wormlike or threadlike micelles) as *p*DoAO concentration increases and, at high surfactant concentrations, large aggregates and smaller

micelles coexist. Moreover, worm-like micelles are present already at low surfactant concentrations, and the entanglement starts at higher concentrations, when the system gets viscoelastic.[63]

The introduction of an aromatic residue in the hydrophobic moiety induces a large decrease of the CMC with respect to AOMe-12 (1.6×10^{-5} M vs. 1.2×10^{-3} M) and it is very similar to that of AOMe-16 (2.5×10^{-5} M), indicating its high tendency to form colloidal aggregates. The effect of *p*DoAO concentration on CRL activity (as r_{pDoAO}/r_{buffer}) was investigated and results are shown in Figure C 1.13.

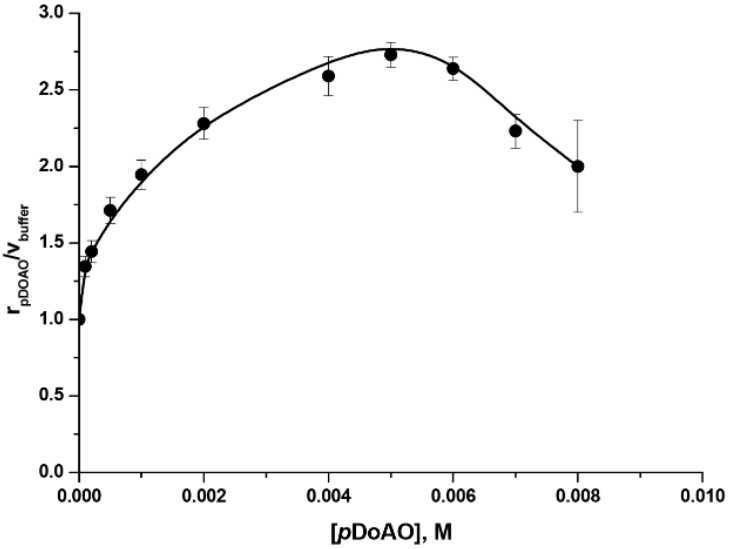

Figure C 1.13: Effect of pDoAO concentration on CRL activity in 0.01 M phosphate buffer, pH 7.0 at 25.0 °C; [pNPA] = 1×10^{-3} M, [CRL] = 0.05 mg/ml (0.83 µM).

Even in the presence of *p*DoAO, CRL activity showed a bell-shaped trend, and the maximum of activity (2.7-fold) was attained at a concentration of 5×10^{-3} M. At surfactant concentration higher 8×10^{-3} M, the solution became too viscous and it is no longer possible to obtain reproducible measurements of the reaction rate.

C 1.3.4 Determination of kinetic parameters

To attain a deeper understanding of the activating effect produced by amine oxides, the kinetic parameters of CRL were determined. Measurements were performed at the additive concentrations that induced the maximum of superactivity. All data

points obeyed to Michaelis-Menten kinetics and could be correlated in the Lineweaver-Burk plot for an estimation of the kinetic parameters, reported in Table C 1.2.

Table C 1.2: Effect of amine oxide surfactants on kinetic parameters of CRL in 0.01 M phosphate buffer solution, pH 7.0 at 25.0 °C. [CRL] = 0.05 mg/mL (0.83 μM).

Amine oxide	10^3 K_M, M	k_{cat}, s^{-1}	$k_{cat(surfactant)}/k_{cat(buffer)}$
Buffer	2.08	0.57	-
AOMe-12	1.04	0.80	1.40
AOMe-14	1.42	1.52	2.67
AOMe-16	1.75	1.99	3.49
AOMe-14	1.42	1.52	2.67
AOEt-14	2.83	1.89	3.32
AOPr-14	4.28	1.91	3.35
*p*DoAO	1.13	1.02	1.79

Regardless of the surfactant used, it is evident that enzyme activation was mainly due to an increase in the turnover number (k_{cat}) and, in some cases, to an increase in the enzyme-substrate affinity (lowering of K_M). The addition of surfactant to the buffer increased the hydrophobicity of the reaction microenvironment and this greater lipophilicity may explain the observed effects on enzyme activity. In fact, the first step in CRL catalysis involves the nucleophilic attack of the hydroxyl group of Ser 209 to the carbonyl carbon on the ester substrate to form an enzyme-substrate tetrahedral intermediate and a more hydrophobic microenvironment enhances the nucleophilicity of the catalytic serine residue. Moreover, the enzyme interaction with a hydrophobic phase can cause the opening of the lid, making the active site accessible. As regards the enzyme-substrate affinity, both the lengthening of the alkyl chain and the increase of the head group size enhanced K_M value.

In presence of alkyldimethylamine oxide, the enzyme affinity for the substrate was always higher than in pure buffer, even if the lengthening of the chain produced an increase in K_M. This trend could be explained with the different tendency of surfactants to form micelles. In fact, as previously reported in Table C 1.1, the longer

the alkyl chain the lower the CMC and then, at the same surfactant concentration, the higher the number of micellar aggregates.

Micelles seemed to have a dual role: on the one hand, they activate the enzyme, on the other they could partially subtract the substrate making it not available for catalysis. It is therefore evident that in AOMe-16 solution (CMC = 2.5×10^{-5} M) the amount of free substrate will be much lower than that in AOMe-12 solutions (CMC = 1.2×10^{-3} M), with a consequent increase in K_M. Kinetic parameters measured at 5×10^{-2} M AOMe-14 confirmed this hypothesis: k_{cat} remains unchanged if compared to the value at 5×10^{-3} M concentration, while K_M is almost doubled, being 2.6×10^{-3} M vs. 1.42×10^{-3} M, due to a greater subtraction of the substrate by micellar aggregates. With surfactants with the same chain length, *i.e.* tetradecyl, the enzyme superactivity decreased by increasing bulk hydrophobicity of alkyl head groups, following the series methyl < ethyl < n-propyl; this was due to the increase in K_M, which in AOPr-14 doubles compared to the buffer. Therefore, the lowering of enzyme superactivity with the increase of the head group size, shown in Figure C 1.13, can be ascribed to a real low affinity of CRL for the substrate. Indeed, in this case, the difference between the CMC of AOMe-14 and AOPr-14 was much smaller (≈ 2.5 times), if compared to that between AOMe-12 and AOMe-16 (≈ 500 times) and then the amount of free substrate available for the reaction should be very similar. It was evident that slight changes on the molecular structure of the surfactant can greatly influence CRL catalytic properties.

Finally, the activation induced by *p*DoAO was due both to an increase in enzyme-substrate affinity and to a higher turnover number, since K_M and k_{cat} were approximately half and twice of those obtained in buffer. It was therefore evident that the presence of the aromatic residue in the hydrophobic chain did not significantly influence the catalytic properties of CRL.

C 1.3.5 Conclusion

The present study showed that the catalytic activity of lipase from *Candida rugosa* can be significantly modulated by selecting suitable additives with certain structural features. In fact, the enzyme hydrolytic activity was enhanced in the presence of all the zwitterionic surfactants selected, and the effect of several amine N-oxide showed that slight changes on the monomer structure significantly affected enzyme-surfactant interactions, and consequently enzyme superactivity. In particular, enzyme activity increased by lengthening the alkyl chain of the surfactant and it lowered as the head group size increased. These results were interpreted assuming that the hydrolytic activity of lipase was improved by the sphere-rod transition of N-oxide micelles. Amine N-oxides can, indeed form rod-like structures and this feature depends on monomer structure: the longer the chain, the greater the tendency to form cylindrical aggregates; on the other hand, increasing the distance between the polar head groups, as in the presence of bulky head group, the monomers are expected to form spherical aggregates. Kinetic parameters showed that the enzyme activation was mainly due to an increase in the turnover number, probably due to a more hydrophobic microenvironment; this enhanced the nucleophilicity of the catalytic serine residue and could have caused the opening of the lid, making the active site accessible to the substrate. The decrease of enzyme-substrate affinity by lengthening the alkyl chain could be attributed to substrate subtraction by micellar aggregates, while its reduction increasing the surfactant head group size could be ascribed to a real low affinity of lipase for the substrate, since the amount of free substrate did not significantly change.

C 1.4 Characterization of CRL entrapped in alginate beads

As described previously, entrapment is a physical immobilization technique that can be obtained for example through a gelation process. Alginate is one of the most used polymers for physical entrapment, thanks to its biocompatibility and biodegradability, together with the ability to easily form the desired three-

dimensional structures in an aqueous environment (hydrogel) by coordinating divalent cations. Many alginate-based supports have been developed for enzyme immobilization and the enhancement of enzyme properties, in terms of operational stability and reusability, together with their biotechnological applications, have been recently reviewed by Bilal and coworker.[64]

In this section of the work, CRL was immobilized in alginate beads prepared by dropwise addition of an aqueous sodium alginate solution and the biocatalyst to a Ca^{2+} salt solution. When the droplets of alginate solution containing enzyme enter the crosslinking solution, beads are formed with the biocatalyst molecules entrapped inside them thanks to the ionotropic gelation, as schematically represented in Figure C 1.14.[65]

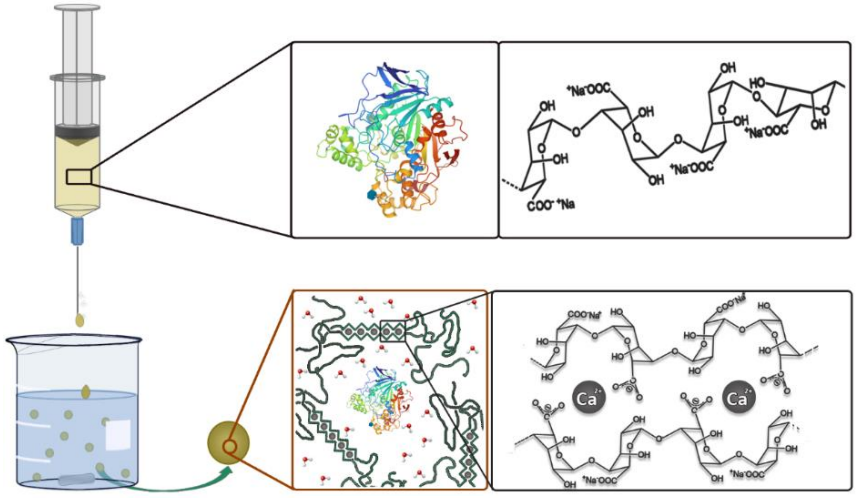

Figure C 1.14: Preparation of alginate beads by ionotropic gelation.

The effect of operating conditions, such as the concentration of $CaCl_2$ and the residence time in the aqueous salt solution, on the loading efficiency of the different beads, on their structural features and on the activity of the entrapped CRL were studied. This last parameter was evaluated by monitoring the previously reported hydrolysis reaction, using *p*NPA as model substrate. The selected biocatalyst formulation was then used to evaluate enzyme reusability, its tolerance to high

temperature and its efficacy towards a more hydrophobic substrate, *p*-nitrophenyl dodecanoate (*p*NPD), and to perform the kinetic resolution of the racemic ester (±)-1-phenylethyl acetate to form alcohol with high enantiomeric purity.

C 1.4.1 Materials and methods

Lipase from *Candida rugosa* (CRL), *p*-nitrophenyl acetate (*p*NPA) and alginic acid sodium salts were the same used in previous sections; *p*-nitrophenyl dodecanoate (*p*NPD), racemic (±)-1-phenylethanol and (*R*)-(-)-1-phenylethanol were purchased from Sigma Aldrich. Racemic (±)-1-phenylethyl acetate was obtained from Merck. Coomassie Brilliant Blue G-250 dye was supplied by Bio-Rad. Enzyme and substrate were used with no further purification and all other chemicals used were of analytical grade.

CRL entrapment in Ca-alginate beads

Six different formulations of beads (Table C 1.3) were prepared which differ from each other in the concentration of the calcium chloride solution and in the residence time in the solution itself. CRL (2 mg/ml) was added in a 5% (w/v) alginate aqueous solution and the mixture was stirred thoroughly to ensure complete mixing. Two ml of the resulting solution were withdrawn with a syringe with a 23G needle (inner diameter 600 μm) and dropped at a distance of about 2 cm into a 2% or 5% calcium chloride solution, maintained under magnetic stirring at 50 rpm, obtaining about 120 beads with a total weight of 1.2÷1.4 g. After the formation of the beads, they were left in the calcium chloride solution for a time ranging from 10 minutes to an hour, to increase their mechanical strength. Finally, the beads were filtered under vacuum and rinsed with distilled water to remove the excess of calcium chloride.

Table C 1.3: Composition of alginate bead formulations. Sodium alginate 5% wt, CRL 2mg/ml.

Beads N°	1	2	3	4	5	6
$CaCl_2$, % (w,v)	2	5	2	5	2	5
Residence time (min)	10	10	30	30	60	60

Immobilization efficiency

Loading efficiency was determined by checking the amount of CRL in both the bead preparation and washing solutions using the Bradford method.[66] A calibration curve was obtained by measuring the absorbance of solutions containing from 0 to 0.3 mg, prepared from a stock one with an enzyme concentration of 2 mg/ml of CRL, at λ = 595 nm. The resulting calibration curve has a R^2 correlation coefficient of 0.99. The loss of enzyme from beads over time was assessed similarly.

CRL activity assay

The hydrolysis of *p*NPA selected as a model reaction was followed using the UV/VIS spectrophotometry as previously described in paragraph C 1.3.1. However, in this case, being the biocatalysts encapsulated into hydrogel beads, the reaction was performed quite differently. In fact, beads (1.2÷1.4 g - 4 mg CRL) were placed in a reaction vessel contained 9 ml of distilled water. The substrate was added by using a 1 ml double notch pipette from a substrate stock solution (100 mM *p*NPA in CH_3CN) to start the reaction. The reaction was carried out at room temperature and under mild stirring and monitored at different time intervals, taking 20 microliters from the reaction solution, placing them in the 1 ml cuvette, where 0.98 ml of distilled water were already present. Spectrophotometric measurements were performed at λ = 348 nm, which corresponds to the isosbestic point of the equilibrium between *p*-nitrophenol/*p*-nitrophenoxide (*p*NP), with a molar extinction coefficient as 5400 M^{-1} cm^{-1}. Once the reaction was completed, the beads were filtered under vacuum, washed, placed in a container with distilled water and stored at 4 °C.

Activity of encapsulated lipase was also determined with a more hydrophobic substrate, *p*-nitrophenyl dodecanoate (*p*NPD), dissolved in acetonitrile, taken with a 1 ml double notch pipette from a 100 mM stock solution and placed in the reaction vessel containing 9 ml of *tert*-butyl alcohol as a solvent and the beads containing the enzyme (1.2÷1.4 g - 4 mg CRL). The reaction, reported in Figure C 1.15, was monitored at different time intervals following the appearance of *p*NP at 348 nm.

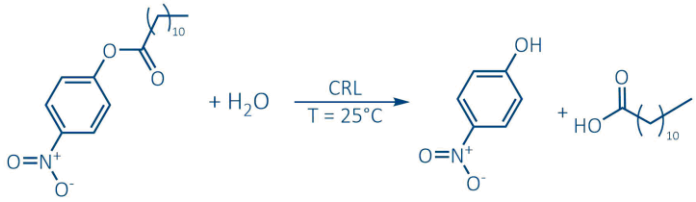

Figure C 1.15: Scheme of p-nitrophenyl dodecanoate hydrolysis.

CRL reusability

The stability of the encapsulated CRL and its reuse were tested under the same conditions described in the previous section. After each cycle, the biocatalyst was filtered, washed with water several times to remove any product adsorbed on the beads and reintroduced into a fresh reaction medium. The substrate hydrolysis reaction was assayed at appropriate time intervals up until its complete conversion to product.

CRL thermostability

Thermal stability of free and immobilized CRL was studied at 25 and 50 °C. Both forms of the enzyme were incubated in water for various periods, from 8 h up to one week. The *p*NPA hydrolysis reaction was carried out for 30 min to measure the initial rate and the remaining activity was determined.

Kinetic resolution of racemic 1-phenylethyl acetate

Hydrolysis reaction of (±)-1-phenyethyl acetate, illustrated in Figure C 1.16, was performed by placing 1 ml double notch pipette from a stock solution (100 mM in CH_3CN) into the reaction vessel containing 9 ml of water and 1.2÷1.4 g of beads.

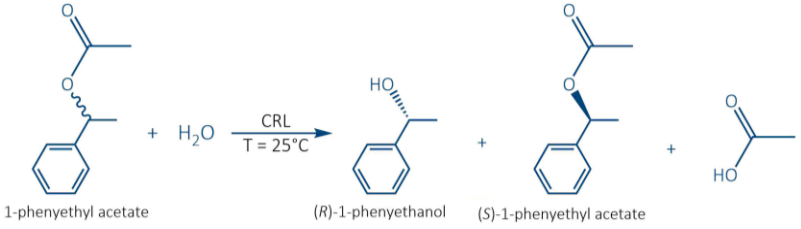

Figure C 1.16: Scheme of the kinetic resolution of 1-phenylethyl acetate racemic ester.

At different time intervals, the beads were separated by filtration under vacuum, the aqueous phase was extracted with ethyl ether and, after the solvent was removed, isopropanol was added to the flask. The hydrolysis degree determination was accomplished by HPLC analyses with an Agilent – 1220 Infinity II instruments equipped with a chiral column (Lux Cellulose-1) using 99:1 hexane/isopropanol as eluent at a flow rate of 0.6 ml/min.

The percentage enantiomeric excesses of the substrate (ee_s) and product (ee_p), conversion (c) and enantioselectivity (E) were calculated by applying the following equations:[67]

$$ee_s = \frac{|R\text{-}S|}{|R+S|} \times 100\% \qquad ee_p = \frac{|R\text{-}S|}{|R+S|} \times 100\%$$

$$c = \frac{ee_s}{ee_s + ee_p} \times 100\% \qquad E = \frac{\ln[(1-c)(1+ee_s)]}{\ln[(1-c)(1-ee_s)]}$$

where R was values of peak areas for (*R*)-1-phenylethanol (in ee_p and ee_s respectively) and its ester, whereas S was values of peak areas for (*S*)-1-phenylethanol and its ester (in ee_p and ee_s respectively).

Morphological characterization

The shape and size of the beads were analyzed using Leica S8APO stereoscopic microscope with EC3 camera connected to a computer. The diameters distribution of the beads was evaluated by using the variance coefficient (CV), which indicates the deviation of each diameter (D_n) from the average value (D_m), and was determined as follows:

$$CV = \frac{1}{D_m} \sqrt{\frac{\sum_{n=1}^{n} (D_n - D_m)^2}{n-1}}\, x\, 100$$

Generally, with a CV less than 5%, 20 beads are sufficient for measurement of sphericity indicator because they are generally uniform in size. Sphericity factor (SF), indicating the roundness of the beads, was determined by using the following equation: [68,69]

$$SF = \frac{d_{max} - d_{min}}{d_{max} + d_{min}}$$

where d_{max} and d_{min} are the maximum and the minimum diameter of Feret, respectively. This factor varies from zero, for a perfect sphere up to unity for an elongated particle.

The aspect ratio (AR) gives a good description of large bead deformations but is less accurate on smaller ones. AR varies from unity for a sphere to infinity for an elongated particle and was determined using the following equation where d_{max} and d_{min} have been previously described.

$$AR = \frac{d_{max}}{d_{min}}$$

The surface morphology and the internal structure of the hydrate systems was investigated using a scanning electron microscope (SEM) equipped with a Peltier cooling-device MK3 Cool stage Carl Zeiss SUPRA with a working distance of about 8 mm and high voltage of 10 KV. Analyses were done around zero Celsius degrees in variable pressure mode (20 Pa) using a BSE detector (Signal A BSD4).

C 1.4.2 Immobilization of CRL onto Ca-alginate beads

Different experimental conditions were tested to optimize the best composition to obtain stable Ca-alginate beads. Both their size and shape have a noticeable effect on their chemical and mechanical stability and the production of monodisperse and spherical beads is preferable. The main factors affecting the size and shape of Ca-alginate beads have been previously reported and reviewed.[68]

Being alginate a family of linear binary copolymers of mannuronic (M) and guluronic (G) acids, the chemical properties of the commercial alginate used to prepare the beads, namely the molecular weight (MW = 37.6 ± 0,2 kDa) and the composition (M/G = 1.77) influenced their crosslink ability; the characterization of the used alginate is reported in Chapter B 1. Various concentrations of sodium alginate were tested to obtain beads with good mechanical strength, and 5% (w/v) was selected.

Among the other parameters that affect the size and shape of the beads, the concentration of calcium chloride in gelation solution and the polymerization time in the gel bath play an important role. The beads were prepared by extrusion dripping, one of the most popular methods, in which an alginate solution containing the enzyme is extruded through a capillary and dropped into a calcium chloride solution. Briefly, CRL was dispersed in the aqueous alginate solution, added dropwise in two different calcium chloride solutions, *i.e.* 2 and 5% (w/v), and maintained under magnetic stirring at 50 rpm for 10, 30 or 60 min, in order to obtain six different formulations indicated as Beads 1-6, as reported in Table C 1.3.

C 1.4.3 Immobilization efficiency

The amount of the enzyme in the alginate beads, its loss in the preparation procedure and over time were evaluated using the Bradford method for all six different types of beads. To assess the loss of enzyme during the entrapment procedure, the concentration of CRL in the preparation solution and in washing water was measured. In these solutions, the amount of lipase from *Candida rugosa* turned out to be zero for all bead formulations, indicating that with our preparatory method all the enzyme was entrapped. As regards the enzyme loss over time, withdrawals of the storage water were taken at different time intervals for one month and subjected to the Bradford assay. The only preparations that had a detectable enzyme loss after 48 h of storage in the aqueous solution, which remained fairly constant over time, were Beads 1 (1 %) and Beads 2 (0.6 %), *i.e.* those with a shorter residence time (10 min) in the calcium chloride solution. In the other cases, there was an oscillation of the absorbance values that were below the sensitivity of the detection method, which turns out to be 22 µg/ml.

C 1.4.4 Hydrolytic activity of enzymatic Ca-alginate beads

Before evaluating the hydrolytic activity of CRL in alginate beads, tests were performed to verify that enzyme-free beads did not catalyze the hydrolysis reaction

of the model substrate *p*-nitrophenyl acetate. In fact, alginate has terminal carboxylate groups which could attack the carbonyl group of the substrate causing its hydrolysis. However, no reaction occurred, probably because most of the alginate carboxylates are involved in the chelation of the calcium ion, *i.e.* the cross-linking agent used.

Once it was established that the matrix did not cause substrate hydrolysis, activity tests were performed with the CRL-containing beads in pure water, instead of buffer solution. Indeed, notwithstanding the pH of the medium is a critical parameter in enzymatic reactions since it affects ionization state of enzyme and then leads to the change of active site,[70] the presence of salts in the reactor vessel could lead to corrosion issues in view of industrial applications, as biofuel production.[71]

The first catalytic tests were performed with all the bead formulations with the model substrate *p*-nitrophenyl acetate at a concentration of 10 mM. Figure C 1.17 shows the conversion percentage of the substrate over time for the six type of beads.

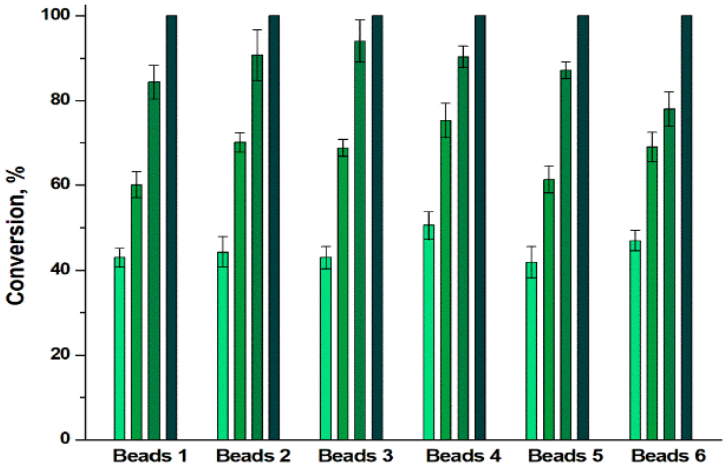

Figure C 1.17: Substrate conversion percentages for all types of beads at 30 min (■), 1 h (■), 2 h (■) and 3 h (■); [p-NPA] = 10 mM

The figure clearly shows that, regardless of the bead formulation, all reactions were complete within three hours and only slight differences were observed during the course of the reaction between the different types of beads. Therefore, it was not

possible to discriminate them in terms of conversion efficiency if used immediately after their preparation.

In the previous section, we proved that there was no leakage of enzyme from the beads during long-term storage, with the exception of Beads 1 and Beads 2, where the loss was still less than or equal to 1%, but we had no information regarding its activity after a month of permanence in water. Therefore, a reaction cycle was performed one month after preparation to evaluate whether the enzyme in the beads was still active. For all types of beads, complete substrate conversion was achieved within four hours, a result that differs slightly from that obtained with the freshly prepared beads; therefore, there were no significant changes in the activity of CRL after a month of storage.

C 1.4.5 CRL recyclability

One of the most useful advantages of enzyme immobilization is its reusability, which is of great importance in the production of biocatalysts. For this reason, many papers in the literature deal with the stability and recyclability of CRL immobilized on solid supports by adsorption,[72-74] cross-linking,[75] covalent binding[76-78] or entrapment.[79-81] Although in most of them the enzyme showed significant stabilization and recyclability, the deactivation of proteins can frequently occur. This effect is often due to the leakage of enzyme from the support or to its conformational limitation; furthermore, the low substrate diffusion can also contribute to the loss of catalytic activity.

To test the effectiveness of our Ca-alginate beads in terms of CRL reusability, the two extreme formulations, Beads 1 and Beads 6, were chosen to perform ten catalytic cycles with the aim of evaluating whether the difference in calcium chloride concentration and residence time in the solution itself influenced the reuse of the biocatalyst. These tests were carried out with 10 mM substrate and reactions were followed until to completion. After each catalytic cycle, Ca-alginate beads were recovered by filtration and washed to remove any product adsorbed on the bead

surface. Then, the reaction medium was replaced with a fresh one. Figure C 1.18 shows the results of repeated uses obtained after 3 h of reaction, which is the time required to the biocatalyst to complete the first cycle.

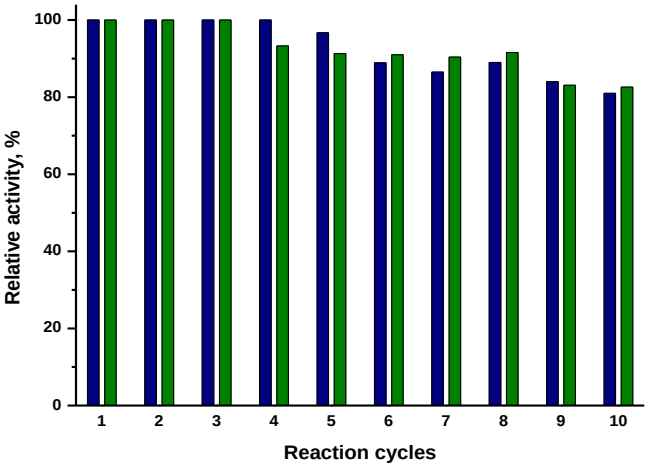

Figure C 1.18: Residual activity of immobilized CRL in Ca-alginate beads in water after 3 h of reaction: Beads 1 (■) and Beads 6 (■); [pNPA] = 10 mM.

The data obtained clearly indicated that the biocatalyst was able to convert all the substrate into product for the first four (Beads 1) and three (Beads 6) cycles and, at the tenth cycle, for both formulations the loss of activity was less than 20%. Furthermore, in order to achieve the complete hydrolysis of the substrate, a time of 4, 6 and 7 h were required for the fourth, sixth and tenth cycles respectively. The results obtained so far showed that there were no differences in terms of catalytic efficiency and recyclability between the different formulations.

C 1.4.6 Morphological studies

The morphological characterization was performed with the aim of determining if there are structural differences between beads prepared with different concentrations of calcium chloride and different residence times in its solution and, also in this case, Beads 1 and Beads 6 were chosen.

Analyses were initially performed using the stereomicroscope and the results are shown in Figure C 1.19.

BEADS 1	BEADS 6
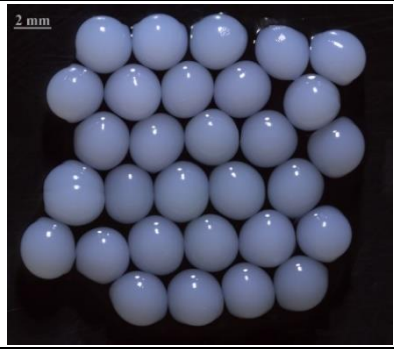	

Figure C 1.19: Stereomicroscope images at 1x magnification of Beads 1 and Beads 6.

Both Beads 1 and Beads 6 showed fairly uniform dimensions and the size distribution of 25 beads was measured, since the variance coefficient (CV) was 0.9 and 3.7%, respectively. Table C 1.4 reports some of the dimensionless shape indicators.

Table C 1.4: Average diameters of Beads 1 and Beads 6 and their sphericity indicator.

	Beads 1	Beads 6
Average diameter (Dm)	3.2 mm	3.4 mm
Sphericity Factor (SF)	0.031	0.069
Aspect ratio (AR)	1.06	1.15

Both beads formulations have similar dimensions of about 3 mm, but better spherical shape was obtained with Beads 1, that is those prepared with lower calcium chloride concentration and shorter hardening time, since SF < 0.05 and AR is slightly higher than unity.[69] On the other hand, Beads 6, as already visible from the stereomicroscope image, are less spherical; their SF value is very similar to that of alginate particles reported in literature and prepared with our same parameters, i.e. concentration of alginate and $CaCl_2$ and hardening time.[82]

Then, the analyses by the electron scanning microscope were performed on both the external surface and the internal structure (by cutting them with a scalpel). To avoid water evaporation and the consequent dehydration of the samples, the application of variable-pressure equipment (VP-SEM) and Peltier cooling-device allows the investigation of wet samples and hydrated systems in SEM. [83]

The SEM images were acquired at different magnifications and the most significant at 70x and 300x are shown in Figure C 1.20.

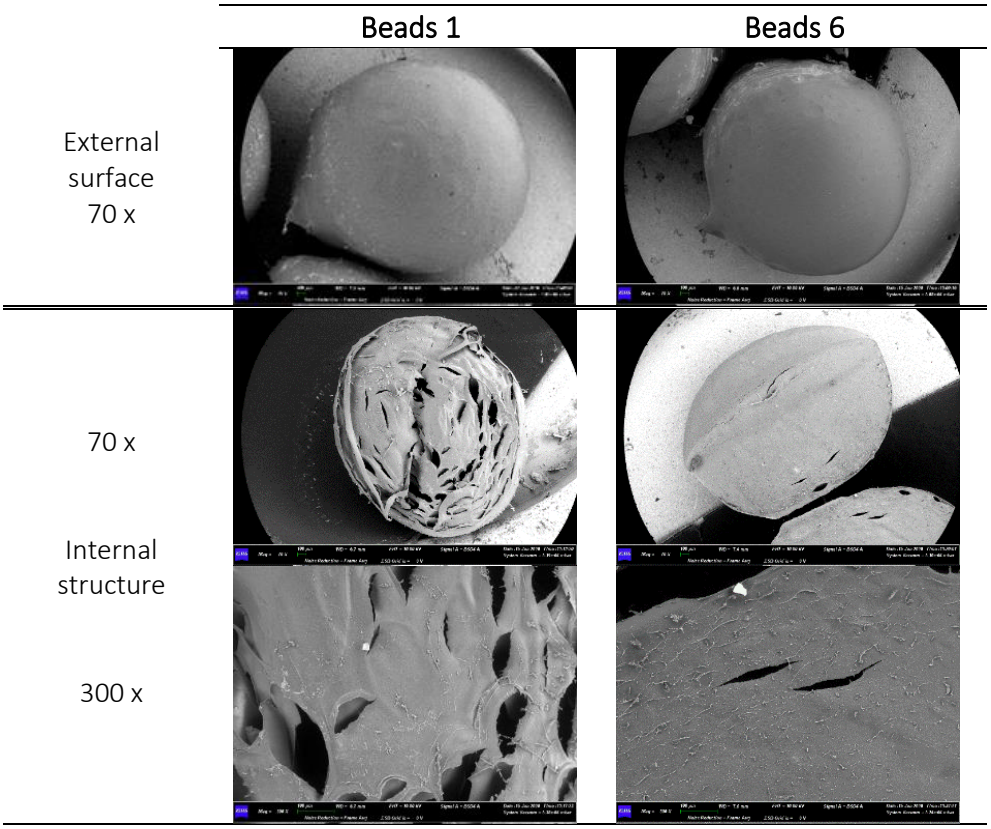

Figure C 1.20: SEM images at 70x magnification of the external structure and at 70x and 300x magnifications of the internal structure of Beads 1 and Beads 6.

Their external surface appeared smooth and that of Beads 1 seemed more porous than that of Beads 6. The addition of the enzyme did not appreciably change the shape and appearance of the corresponding alginate particles, indicating that the enzyme encapsulation did not significantly change the morphology of the beads (data not shown). The main differences are related to the internal structure of the two formulations, in terms of porosity. In particular, Beads 1 showed a significantly greater internal porosity than Beads 6, which seemed denser and more homogeneous. Further SEM analyses were then performed to understand if the cause of this different internal porosity was due to the calcium chloride

concentration and/or to the hardening time. For these analyses, Beads 2 ($CaCl_2$ 5%, 10 min) and Beads 5 ($CaCl_2$ 2%, 60 min) were selected and SEM images of both the whole beads and the internal structure (Figure C 1.21) highlighted that the internal compactness depends on the gelation time and not on $CaCl_2$ concentration.

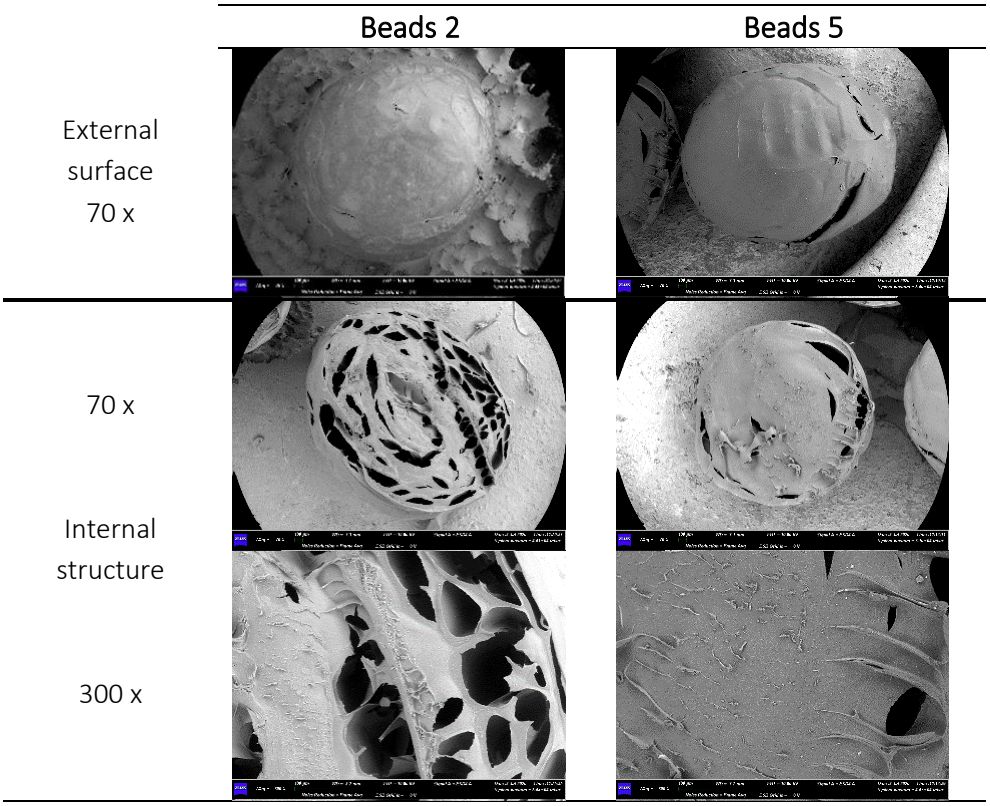

Figure C 1.21: SEM images at 70x magnification of the external structure and at 70x and 300x magnifications of the internal structure of Beads 2 and Beads 5.

C 1.4.7 Reaction with p-nitrophenyl dodecanoate

The *p*-nitrophenyl dodecanoate (*p*NPD) has been chosen to evaluate the efficiency of CRL immobilized on Beads 1 and 6 on a more hydrophobic substrate. Being poorly soluble in water, *p*NPD hydrolysis reaction was carried out in a sterically hindered alcohol, *i.e. tert*-butyl alcohol, in order to avoid or at least reduce the competitive transesterification reaction rate. In this case, the conversion efficiency of the two formulations was very different. In fact, Beads 1 were able to complete hydrolyze the substrate in 6 h, while the reaction rate catalyzed by Beads 6 was very low: after

6 h, little more than 40% of product was formed and increased slowly over time. The reaction did not complete even after 24 h, being the conversion equal to 80%. This result clearly indicated that the greater compactness of Beads 6 compared to Beads 1 limited the mass transfer of reagents and/or products in the reaction medium and this drawback was evident with large, hydrophobic substrates and therefore much more similar to natural ones. On the other hand, Beads 1, despite their greater internal porosity, were able not only to efficiently entrap the enzyme, but also to ensure the free diffusion of reagents within their porous structure.

Furthermore, the time taken by Beads 1 to completely hydrolyze *p*NPD was twice that required for the reaction with *p*NPA. Then, to determine if the increase in reaction time was due to the substrate or to the solvent, the reaction of *p*NPA in *tert*-butyl alcohol was performed for comparison purpose. After 48 h, only 50% of conversion was achieved, and this result can be explained by the dehydration of the beads that became smaller and smaller over time.

The loss of water from the confined environment in which the enzyme is located led to the observed slowdown of the reaction. This hypothesis was confirmed by experiments performed by varying the amount of water inside the reaction medium, in which the complete hydrolysis of *p*NPA required 7 and 4 h when 25% and 75% of water was added to *tert*-butyl alcohol, respectively.

Therefore, given all the considerations made so far, the Beads 1 formulation, being one of the fastest preparations and ensuring better mass transfer, thus allowing their possible use of a wide range of substrates, has been chosen to perform thermostability tests and kinetic resolution of (±)-1-phenylethyl acetate.

C 1.4.8 CRL Thermostability

One of advantages of enzyme immobilization is the improvement in thermal stability. Therefore, the stability of lipase immobilized in Ca-alginate beads (Beads 1) was determined at 25 and 50 °C and compared with that obtained with the free CRL (Figure C 1.22).

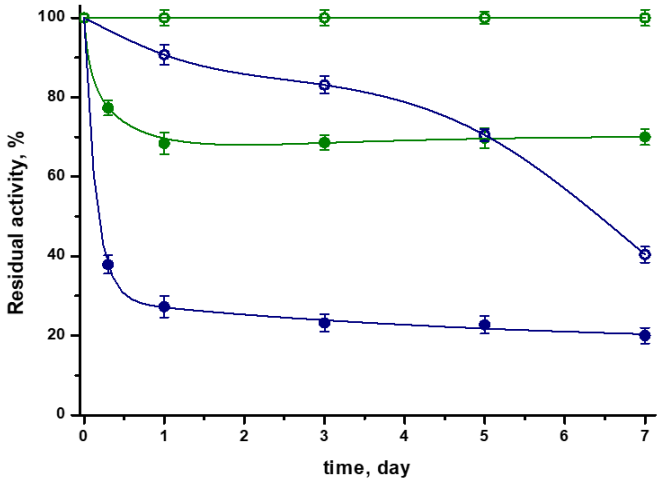

Figure C 1.22: Thermal stability of free (●/○) and immobilized lipase (●/○) at 25 °C (empty symbols) and 50 °C (closed symbols).

The effect of immobilization on Ca-alginate beads on CRL stability is clearly highlighted by the figure at both investigated temperatures. As seen above (Paragraph C 1.4.3), at 25 °C the immobilized CRL activity did not decrease even after one month of incubation, while the free form lost 30% of its initial activity after 5 days and 60% after one week. Even more evident is the stabilization effect at 50 °C. In fact, the residual activity of free lipase, after only 8 h, was lower than 40% and continued to decrease over time until reaching a value of about 20% after one week of incubation. On the other hand, the remaining activity of immobilized CRL was about 70% after 1 day of heat treatment at 50 °C and remained unchanged throughout the week.

Moreover, stability tests carried out with Beads 6 at 50 °C showed that the different operational conditions used in the preparation of the two formulations did not affect the stability of the enzyme, being the loss of activity after 24 hours equal to 66%.

The data reported in the figure show the trends of residual activity over time, but do not take into account the differences in the reaction rate catalyzed by the free and immobilized enzyme determined before incubation. In particular, hydrolysis rate with free CRL was 40% higher than that of immobilized one both at 25 °C (183 vs.

132 μM/min) and at 50 °C (520 vs. 370 μM/min). The lower reaction rate of the enzyme encapsulated in beads could be due to a slower diffusion of the substrate inside the support.

Despite the lower initial activity, the hydrolysis reaction rate of Beads 1 at 50 ° C was 45% and 2.2 times higher after 8 h and one week, respectively, than that of the free enzyme, thanks to the improvement in enzymatic stabilization following the immobilization.

C 1.4.9 Kinetic resolution of (±)-1-phenylethyl acetate

Numerous studies have been devoted to the kinetic resolution of substrates with pharmacological activity, such as naproxen[75,84,85] and ibuprofen[78] using immobilized CRL, since the enantiomers of these non-steroidal anti-inflammatory drugs demonstrate different therapeutic activities.

Given the excellent recyclability and thermal stability of Beads 1, and therefore their possible application in industrial processes, they have been used in preliminary tests for the resolution of (*R*)-1-phenylethanol in aqueous solution starting from racemic 1-phenylethyl acetate, as model substrate. In the literature, several papers report about the stereoselective kinetic resolution of *rac*-1-phenylethyl acetate catalyzed by other lipases[86-90], in which very high enantiomeric excess towards the (*R*)-enantiomer was obtained, but with not too satisfying yields. More recently, marine microbial GDSL lipase MT6 showed opposite stereoselectivity, as it hydrolyzed racemic 1-phenylethyl acetate to generate (*S*)-1-phenylethanol instead of (*R*)-1-phenylethanol.[91] During reaction course, as the conversion increased, the ee of the product decreased and, at the optimal reaction time (12 h), a conversion of 28.5% with an ee value higher than 97% was obtained. On the other hand, CRL solubilized in phosphate buffer at pH 7.2 showed no enantiopreference for the (*R*)-acetate with an ee value of only 44% and an enantioselectivity factor of 4.[92]

Here, the course and selectivity of the kinetic resolution of *rac*-1-phenylethyl acetate catalyzed by Beads 1 were checked by sampling the reaction mixture at different

time by chiral HPLC. The retention times were 3.6, 3.9, 14.7, 18.5 min for (*R*)-1-phenylethyl acetate, (*S*)-1-phenylethyl acetate, (*R*)-1-phenylethanol, and (*S*)-1-phenylethanol, respectively. To determine the optical purity and the enantioselectivity of the reaction, the equations reported in the materials and methods section were used. The calculations were performed on the basis of the peak areas of the chromatograms obtained from the separation of (*R,S*)-1-phenyethyl acetate and its hydrolyzed forms. In Figure C 1.23 the chromatogram of the reference and the reaction controlled at different time.

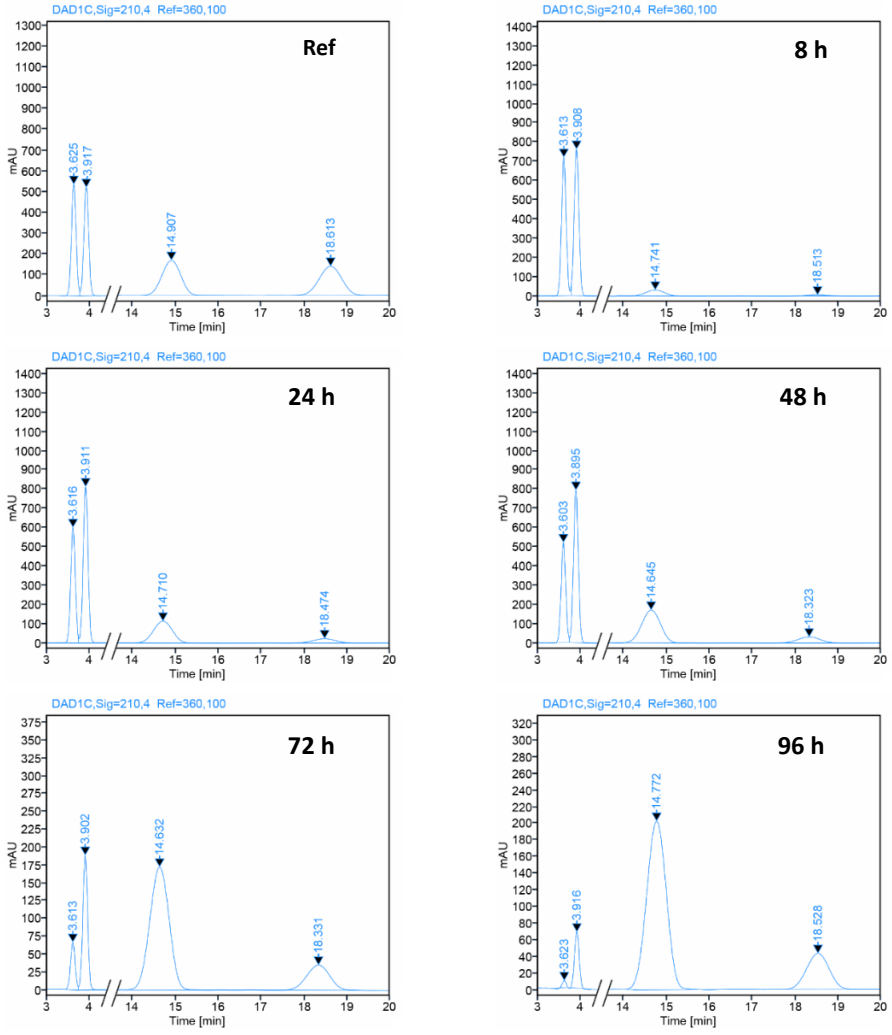

Figure C 1.23: Different time chromatograms of the kinetic Resolution of rac-1-phenylethyl acetate catalyzed by Beads 1.

The percentage of enantiomeric excesses of the substrate (ee_s) and product (ee_p), conversion (c) as well as enantioselectivity (E) are reported in Table C 1.5.

Table C 1.5: Enantiomeric excesses of substrate (ee_s) and product (ee_p), conversion (c) and enantioselectivity (E) of the hydrolysis reaction of (R,S)-1-phenylethyl acetate using Beads 1.

Reaction time (h)	ee_s	ee_p	c	E
8	3.5%	61.5%	5.3%	4.3
24	17.6%	62.8%	21.9%	5.2
32	18.1%	61.9%	22.6%	5.1
48	23.1%	64.5%	26.4%	5.8
72	49.5%	61.7%	44.5%	6.8
96	83.3%	60.9%	57.8%	10.3

As observed from these results, while the enantiomeric excess of the substrate (ee_s) increases with reaction time and conversion, to reach 83% after 96 h of reaction, the enantiomeric excess of the product remains almost constant around 60%. After 96 h of the reaction the highest values of enantioselectivity (E = 10.3), conversion (c = 57.8%) and enantiomeric excesses of substrate (ee_s = 83.3%) were observed. These values just described are slightly higher but do not differ so much from those reported in the literature regarding free lipase in phosphate buffer, which showed an ee value of 44% and an enantioselectivity factor of 4.[92] Further studies will be performed in different conditions in order to improve both yield and enantioselectivity.

C 1.4.10 Conclusion

In this study, lipase from *Candida rugosa* was efficiently trapped in Ca-alginate beads prepared using different operating conditions. All types of beads, which differed from each other in the concentration of calcium chloride in the gelation bath and in the hardening time, were able to catalyze the complete hydrolysis of the model substrate, i.e. *p*-nitrophenyl acetate, within three hours. After one month of storage at 4 °C in distilled water, no or very little loss of enzyme from the beads was observed and furthermore the immobilized enzyme was still active, converting all the

substrate into product in four hours. The reusability of the biocatalyst was tested for the two extreme formulations and the encapsulated lipase proved to be stable and lost little activity when subjected to repeated uses, having residual activity greater than 80% at the tenth reaction cycle.

The lower internal porosity of the Beads 6 compared to the Beads 1, revealed by SEM analyzes on these hydrated systems, limits the mass transfer significantly affecting the hydrolysis reaction rate. In fact, although using the two formulations the same activity in the hydrolysis of *p*NPA was revealed, using a more hydrophobic substrate, *i.e. p*NPD, Beads 1 show greater activity than Beads 6. A significant improvement in thermal stability was also achieved and, at 50 °C, the residual activity of the immobilized CRL was approximately 70% after one day and remained unchanged throughout the detection time, while the activity of free enzyme decreased over time to a value of about 20% after one week of incubation.

Finally, the immobilized lipase effectively hydrolyzed the more hydrophobic substrate, *p*-nitrophenyl dodecanoate, in *tert*-butyl alcohol, while the kinetic resolution of rac-1-phenylethyl acetate requires further studies to improve both yield and enantioselectivity.

References

1- Y. Li, G. Li, C. Ma, Journal of Dispersion Science and Technology, **21**, 409-432 (2000);

2- A.A. Homaei, R. Sariri, F. Vianello, R. Stevanato, Journal of Chemical Biology, **6**, 185-205 (2013);

3- G. Savelli, N. Spreti, P. Di Profio, Current Opinion in Colloid & Interface Science, **5**, 111-117 (2000);

4- M.A. Biasutti, E.B. Abuin, J.J. Silber, N. Mariano Correa, E.A. Lissi, Advances in Colloid and Interface Science, **136**, 1-24 (2008);

5- D. Otzen, Biochimica et Biophysica Acta, **1814**, 562-591 (2011);

6- T.E. Sintra, S.P.M. Ventura, J.A.P. Coutinho, Journal of Molecular Catalysis B: Enzymatic, **107**, 140-151 (2014);

7- D. Friefelder, "*Physical biochemistry. Applications to biochemistry and molecular biology*", W.H. Freeman and Company. San Francisco (1976);

8- M.N. Jones, H.A. Skinner, E. Tipping, A. Wilkinson, Biochemical Journal, **135**, 231-236 (1973);

9- C. Blinkhorn, M.N. Jones, Biochemical Journal, **135**, 547-549 (1973);

10- K. Holmberg, Colloids and Surfaces B: Biointerfaces, **168**, 169-177 (2018);

11- M.D. O'Donnell,K.F. McGeeney, Enzyme, **18**, 356-367 (1978);

12- L.J. Kricka, M. De Luca, Archives of Biochemistry and Biophysics, **217**, 674-681 (1982);

13- Y.K. Rao, P. Bahadur, A. Bahadur, S. Ghosh, Indian Journal of Biochemistry & Biophysics, **26**, 390-393 (1989);

14- J. Lalitha, V.H. Mulimani, Biochemistry and Molecular Biology International, **41**, 797-803 (1997);

15- M.N. Jones, A. Finn, A. Mosavi-Movalhedi, B.J. Waller, Biochimica et Biophysica Acta, **913**, 395-398 (1987);

16- M. Goldfeder, A. Fishman, Applied Microbiology and Biotechnology, **98**, 545-554 (2014);

17- C. Mateo, J.M. Palomo, G. Fernandez-Lorente, J.M. Guisan, R. Fernandez-Lafuente, Enzyme and Microbial Technology, **40**, 1451-1463 (2007);

18- M. Bilala, M. Asgherb, H. Chengc, Y. Yand, H.M.N. Iqbale, **39**, 1-18 (2018);

19- M.L.E. Gutarra, L.S.M. Miranda, R.O.M.A. de Souza, "*Enzyme immobilization for organic synthesis*" in "Organic synthesis using biocatalysis", A. Goswami, J.D. Stewart Ed., Elsevier, Amsterdam, chap. 4, pp. 99-126 (2016);

20- M.D. Trevan, "*Enzyme immobilization by covalent bonding*" in "Methods in molecular biology", J.M. Walker Ed., Humana Press, Clifton, chap. 37, pp. 495-510 (1988);

21- A. Pollak, R.L. Baughn, O. Adalsteinsson, G.M. Whitesides, Journal of the American Chemical Society, **100**, 302-304 (1978);

22- W.A. Alloue, J. Destain, T. El Medjoub, H. Ghalfi, P. Kabran, P. Thonart, Applied Biochemistry and Biotechnology, **150**, 51-63 (2008);

23- N. Das, A.M. Kayastha, A.P. Malhotra, Biotechnology and Applied Biochemistry, **27**, 25-29 (1998);

24- M. Iso, T. Shirahase, S. Hanamura, S. Urushiyama, S. Omi, Journal of Microencapsulation, **6**, 165-176 (1989);

25- S.H. Krishna, N.G. Karanth, Catalysis Review, **44**, 499-591 (2002);

26- E. Castillo, L. Casas-Godoy, G. Sandoval, Biocatalysis, **1**, 178-188 (2015);

27- N.A. Soliman, M. Knoll, Y.R. Abdel-Fattah, R.D. Schmid, S. Lange, Process Biochemistry, **42**, 1090-1100 (2007);

28- E. Lesuisse, K. Schanck, C. Colson, European Journal of Biochemistry, **60**, 155-213 (1993);

29- K. Hult, P. Berglund, Trends in Biotechnology, **25**, 231-238 (2007);

30- A. Babtie, N. Tokurik, F. Hollfelder, Current Opinion Chemical Biology, **14**, 1-8 (2010);

31- A. Houde, A. Kademi, D. Leblanc, Applied Biochemistry and Biotechnology, **118**, 155-170 (2004);

32- J.D. Schrag, M. Cygler, Methods in Enzymology, **284**, 85-107 (1997);

33- G.G. Dodson, D.M. Lawson, F.K. Winkler, Faraday Discussion, **93**, 95-105 (1996);

34- A. Hjorth, F. Carriere, C. Cudrey, H. Woldike, E. Boel, D.M. Lawson, Biochemistry, **32**, 4702-4707 (1993);

35- D.A. Lang, B.W. Dijkstra, Chemistry and Physics of Lipids, **93**, 115-122 (1998);

36- J. Pleiss, M. Fischer, R.D. Schmid, Chemistry and Physics of Lipids, **93**, 67-80 (1998);

37- K.E. Jaeger, B.W. Dijkstra, M.T. Reetz, Annual Review of Microbiology, **53**, 315-351 (1999);

38- S. Brocca, R. Grandori, D. Breviario, M. Lotti, Current Genetics, **28**, 454-457 (1995);

39- C. Lopez, N.P. Guerra, M.L. Rua, Biotechnology Letters, **19**, 303-306 (2000);

40- D.L. Ollis, E. Cheah, M. Cygler, B. Dijkstra, F. Frolow, S.M. Franken, Protein Engeneering, **5**, 197-221 (1992);

41- M. Cygler, J.D. Schrag, Biochimica et Biophysica Acta, **1441**, 205-214 (1999);

42- N.A. Turner, E.C. Needs, J.A. Khan, E.N. Vulfson, Biotechnology Bioengeering, **72**, 114-118 (2001);

43- M.A. Pernas, C. Lopez, L. Pastrana, M L. Rua, Journal of Biotechnology, **84**, 163-174 (2000);

44- M. Pernas, C. Lopez, A. Prada, J. Hermoso, M.L. Rua, Colloids and Surfaces B: Biointerfaces, **26**, 67-74 (2002);

45- P. Domınguez de Maria, J.M. Sanchez-Montero, J.V. Sinisterra, A.R. Alcantara, Biotechnology Advances, **24**, 180-196 (2006);

46- J. Barriuso, M.E. Vaquero, A. Prieto, M.J. Martínez, Biotechnology Advances, **34**, 874–885 (2016);

47- S.H. Hung, M.H. Liao, D.H. Chen, Biotechnology Progress, **19**, 1095-1100 (2003);

48- M.V. Calvo, F.J. Plou, A. Ballesteros, Biocatalysis and Biotransformation, **13**, 271-285 (1996);

49- D. Goswami, R. Sen, J.K. Basu, S. De, Bioresource Technology, **101**, 6-13 (2010);

50- L. Corte, M. Tiecco, L. Roscini, S. De Vincenzi, C. Colabella, R. Germani, C. Tascini, G. Cardinali, PLoS ONE, **10**, 1-15 (2015);

51- V. Belle, A. Fournel, M. Woudstra, S. Ranaldi, F. Prieri, V. Thomé, J. Currault, R. Verger, B. Guigliarelli, F. Carrière, Biochemistry, **46**, 2205-2214 (2007);

52- G.L.K. Hoh, D.O. Barlow, A.F. Chadwick, D.B. Lake, S.R. Sheeran, Journal of the American Oil Chemists' Society, **40**, 268-271 (1963);

53- L. Brinchi, C. Dionigi, P. Di Profio, R. Germani, C.A. Bunton, "Journal of Colloid and Interface Science, **211**, 179-184 (1999);

54- L. Goracci, R. Germani, J.F. Rathman, G. Savelli, Langmuir, **23**, 10525-10532 (2007);

55- L. Izrael-Zivkovic, L. Zivkovic, B. Jokic, A. Savic, I. Karadzic, Journal of the Serbian Chemical Society, **80**, 1113-1125 (2015);

56- P. Skagerlind, K. Holmberg, Journal of Dispersion Science and Technology, **15**, 317-322 (1994);

57- B. Folmer, K. Holmberg, M. Svensson, Langmuir, **13**, 5864-5869 (1997);

58- A.K. Ghose, G.M. Crippen, Journal of Computational Chemistry, **7**, 565-577 (1986);

59- A. Ghose, V. Viswanadhan, J. Wendoloski, Journal of Physical Chemistry A, **102**, 3762-3772 (1998);

60- Talete srl. DRAGON for Windows (Software for Molecular Descriptor Calculations). Version 5.4 http://www.talete.mi.it/;

61- H. Maeda, R. Kakehashi, Advances in Colloid and Interface Science, **88**, 275-293 (2000);

62- P. Baglioni, E. Braccalenti, E. Carretti, R. Germani, L. Goracci, G. Savelli, M. Tiecco, Langmuir, **25**, 5467-5475 (2009);

63- L. Brinchi, R. Germani, P. Di Profio, L. Marte, G. Savelli, R. Oda, D. Berti, Journal of Colloid and Interface Science, **346**, 100-106 (2010);

64- K. Won, S. Kim, K.J. Kim, H.W. Park, S.J. Moon, Process Biochemistry, **40**, 2149-2154 (2005);

65- M. Bilal, H.M.N. Iqbal, International Journal of Biological Macromolecules, **130**, 462-482 (2019);

66- M.M. Bradford, Analytical Biochemistry, **72**, 248-254 (1976);

67- C.S. Chen, Y. Fujimoto, G. Girdaukas, C.J. Sih, Journal of the American Chemical Society, **104**, 7294-7299 (1982);

68- B.B. Lee, P. Ravindra, E.S. Chan, Chemical Engineering and Technology, **36**, 1627-1642 (2013);

69- E.S. Chan, B.B. Lee, P. Ravindra, D. Poncelet, Journal of Colloid and Interface Science, **338**, 63-72 (2009);

70- Y. Liu, Q. Jin, L. Shan, Y. Liu, W. Shen, X. Wang, Ultrasonics Sonochemistry, **15**, 402-407 (2008);

71- E. Torsner, Corrosion Engineering Science and Technology, **45**, 42-48 (2010);

72- H. Aghaei, M. Ghavi, G. Hashemkhani, M. Keshavarz, International Journal of Biological Macromolecules, **162**, 74-83 (2020);

73- L.T. Izrael Živković, L.S. Živković, V.P. Beškoski, K.R. Gopčević, B.M. Jokić, D.S. Radosavljević, I.M. Karadžić, Journal of Molecular Catalysis B: Enzymatic, **133**, S533-S542 (2016);

74- L.T. Izrael Živković, L.S. Živković, B.M. Babić, M.J. Kokunešoski, B.M. Jokić, I.M. Karadžić, Biochemical Engineering Journal, **93**, 73-83 (2015);

75- S. Salgın, M. Çakal, U. Salgın, Preparative Biochemistry and Biotechnology, **50**, 148-155 (2020);

76- B. Zou, L. Zhang, J. Xia, P. Wang, Y. Yan, X. Wang, I.O. Adesanya, Applied Biochemistry and Biotechnology, **192**, 132-145 (2020);

77- F.N.N. Mohd Hussin, N. Attan, R.A. Wahab, Enzyme and Microbial Technology, **136**, 109506 (2020);

78- M.P. Marszałł, T. Siódmiak, Catalysis Communications, **24**, 80-84 (2012);

79- E. Ozyilmaz, K. Etci, M. Sezgin, Preparative Biochemistry and Biotechnology, **48**, 887-897 (2018);

80- E. Ozyilmaz, S. Sayin, M. Arslan, M. Yilmaz, Colloids and Surfaces B: Biointerfaces, **113**, 182-189 (2014);

81- C.H. Yang, C.C. Yen, J.J. Jheng, C.Y. Wang, S.S. Chen, P.Y. Huang, K.S. Huang, J.F. Shaw, Molecules, **19**, 11800-11815 (2014);

82- A.K. Tamo, I. Doench, A.M. Helguera, D. Hoenders, A. Walther, A.O. Madrazo, Polymers, **12**, 1-24 (2020);

83- A. Wassilkowska, T. Woźniakiewicz, Solid State Phenomena, **231**, 139-144 (2015);

84- E. Yilmaz, M. Sezgin, M. Yilmaz, Journal of Molecular Catalysis B: Enzymatic, **69**, 35-41 (2011);

85- E. Yilmaz, K. Can, M. Sezgin, M. Yilmaz, Bioresource Technology, **102**, 499-506 (2011);

86- I. Bustos-Jaimes, Y. García-Torres, H.C. Santillán-Uribe, C. Montiel, Journal of Molecular Catalysis B: Enzymatic, **89**, 137-141 (2013);

87- F. Kartal, A. Kilinc, Biotechnology Progress, **28**, 937-945 (2012);

88- I. Bustos-Jaimes, W. Hummel, T. Eggert, E. Bogo, M. Puls, A. Weckbecker, K.E. Jaeger, ChemCatChem, **1**, 445-448 (2009);

89- Y. Gao, R. Zhong, J. Qin, B. Lin, Chemistry Letters, **38**, 262-263 (2009);

90- E.M. Hill, J.M. Broering, J.P. Hallett, A.S. Bommarius, C.L. Liotta, C.A. Eckert, Green Chemistry, **9**, 888-889 (2007);

91- D. Deng, Y. Zhang, A. Sun, Y. Hu, Chinese Journal of Catalysis, **37**, 1966-1974 (2016);

92- F. Bellezza, A. Cipiciani, G. Cruciani, F. Fringuelli, Journal of the Chemical Society, Perkin Transactions, **1**, 4439-4444 (2000).

Chapter C 2

Food packaging

C 2.1 Role, issues and improvement of food packaging

Since its first application, the role of food packaging has been clear, it must reduce the loss of food during its supply and transport, and also act as a barrier to prevent, as far as possible, the contamination of food products by environmental factors, in order to preserve food integrity. The continuous rise in world's population and the consequent increase in food demand has led to the development of even more sophisticated food packaging materials able of extending the shelf life of perishable foods.[1]

Nowadays single-use food packaging is at the center of controversy due to the known environmental impact attributed to both its production and its incorrect disposal. However, the role of packaging is often overlooked because if on the one hand it represents an undisputed source of pollution, on the other its use has become increasingly essential to reduce the production of food waste that can have dangerous effects on the environment and human health.[2] In fact, packaged foods are less subject to all those oxidative processes which are responsible for unpleasant flavors, color changes and loss of their nutritional and energetical values. Moreover, a proper packaging can prevent and delay the growth of pathogenic microorganisms that increase the risk of food-borne diseases.[3] This evidence highlights even more the importance of food packaging in the improvement of the shelf life of foods as well as in the reduction of their disposal. Therefore, in order to obtain a correct and complete analysis of their environmental impact, the life cycle assessment (LCA) of packaging materials cannot only consider their life cycle, as it has been regarded until now, but it should be improved by including the prevention of food waste by using proper food packaging.[2,4]

What has just been said does not mean that food packaging is harmless or even eco-friendly but that it cannot be avoided. In fact, especially in recent years, the scientific community has focused its attention on the improvement of food packaging materials in terms of technology, additives and materials.[2,5-7] Regarding the implementation of technology and additives, the concept of smart and active packaging has been coined in order to limit food waste as much as possible.[5] On the other hand, the optimization and selection of suitable raw materials allows to reduce the environmental impact due to the production of packaging both in terms of total CO_2 emitted into the atmosphere and in terms of waste production for the end of the life cycle of the packaging.[2,6,7]

C 2.1.1 Active food packaging

During its evolution several strategies have been developed to improve food packaging in terms of food storage. In this sense, particular attention is paid to the use of additives applied in the packaging materials able to delay the degradation processes that the food will inevitably undergo.

Probably the earliest modern forms of active packaging date back to the early days of the era of plastic packaging. At that time, the orientation of the polypropylene chains, obtained after stretching the film in the length and width directions, and the metallization of the polymer films led to an improvement in the gas and vapor barrier properties of the resulting packaging.[1,8]

Nowadays exists a plethora of compounds commonly used in food packaging for their antimicrobial activity to prevent the growth of pathogenic microbes on food products. These substances can be placed inside the packaging in sachets or directly encapsulated in the structure of the packaging materials. Another alternative of this type of active packaging is food coating with edible materials to which some antimicrobial chemicals are added.[5,9] The main antimicrobial products used can be classified as non-volatile and volatile substances. The former are generally enzymes, organic acids, metal oxides nanoparticles, bacteriocins, bacteriophages, etc. bound

or encapsulated in the packaging material, as described above, and placed in direct contact with the food product.[10]

C 2.1.2 Common materials in food packaging

In addition to the implementation with active substances, the evolution of food packaging has also involved the development of suitable materials which can better play the role of barrier to protect food products from physical damage, dust, light and other forms of contamination. Nowadays the main materials used for food packaging, some of which reported in Figure C 2.1, are glass, metals, paper, plastics or multimaterials.[8]

Figure C 2.1: Common materials employed in food packaging.

Incorrect disposal of single-use food packaging is an increasingly critical issue linked to the environment; so, more and more scientists are focusing on developing more effective waste recycling. In these terms, packaging materials can be divided into permanent and non-permanent materials. The first includes those materials which, under ideal conditions following the transformations induced by the recycling process, will not change their initial physicochemical properties, and therefore they can be completely restored. To this class can be ascribed metals and glass packaging which should be indefinitely recycled and reused. On the contrary, the structure of non-permanent materials undergoes some chemical changes during processing; therefore, after their recycling, they must be added to the fresh materials to be used

for food packaging. Paper, cardboard and thermoplastics are generally materials commonly used for food packaging belonging to the latter class.[8,11]

Nevertheless, the use of recycled materials to make newer food packaging is generally subject to strong regulation to guarantee their safeness. This is due, regardless of the class of materials, to the recycling process which can result in inclusion of "non-intentionally added substances" (NIAS). The most common substances are additives, dyes, degradation products and products resulting from improper use of packaging or accumulated during previous recycling cycles. These chemicals can migrate through the recycled material and contaminate the food product.[11] Unfortunately, together with the discussed difficulties in producing safe recycled food packaging, their dispersion into the environment causes serious problems. For this purpose, biomaterials are considered an increasingly popular alternative to classic petroleum-based polymers. But what does the term biomaterials mean?

As schematized in Figure C 2.2, there are two classes of polymeric materials which are referred to as biopolymers; the first are the classic polymeric materials (polyethylene, polypropylene, polyethylene terephthalate, etc.) obtained by renewable sources.[2]

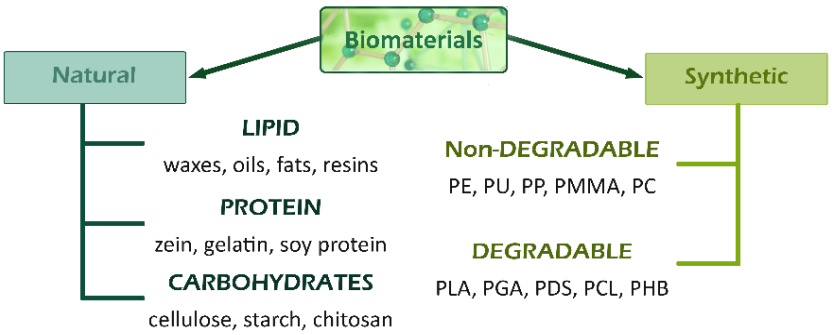

Figure C 2.2: Classification of biomaterials for food packaging.

Therefore, carbon dioxide emissions commonly attributed to the production and disposal of petroleum-based plastics can be drastically reduced while the physicochemical properties of the polymer remain unaffected. However, the other

main environmental issues ascribed to plastic food packaging can be reduced by using this class of bioplastic materials; in fact, their incorrect disposal should generate the same problems associated with petroleum-derived polymers.[2,12]

The other class of biopolymers includes all those polymers extracted from natural sources (chitosan, alginic acid, gelatin, starch, etc.) or synthetized starting from natural products (polylactic acid, polyhydroxy butyrate, polyhydroxy valerate, etc.). This class of biomaterials differs significantly from classical synthetic polymers with particular regard to their physicochemical properties, but they have proved to be a promising alternative to classical plastics thanks to their high biocompatibility and biodegradability.[13]

C 2.1.3 Natural biopolymers for food packaging

In the last few years, highly eco-friendly natural polymers have been considered a valid alternative to classic polymers from both renewable and non-renewable sources in the field of food packaging.[6] In particular, there is growing interest in the application of natural polymers for the development of edible packaging. For this purpose, edible coatings and films are often considered to be equivalent in terms of shelf life of the product despite significant differences in their preparations.[14]

Figure C 2.3 shows the formation of coatings and films starting from their common preparation which begins by dispersing the polymer in a solvent (commonly aqueous solutions of suitable additives), which is subsequently homogenized and degassed.

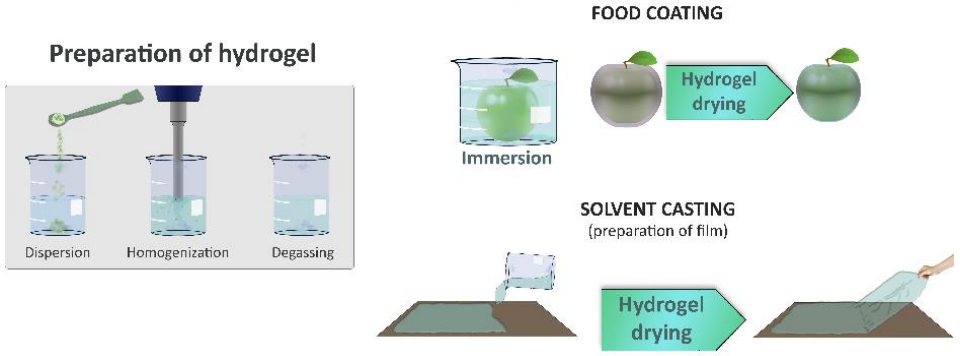

Figure C 2.3: Representation of the common preparation of food packaging methods by coating or film.

This process usually leads to the formation of a hydrogel that can be sprayed directly on the foods, which are subsequently dried at room temperature, thus obtaining the coating process. Otherwise, the solvent casting method is applied by pouring the hydrogel onto a rigid support until the solvent has evaporated and the film is formed. The starting materials commonly used for this purpose can be classified depending on their nature as lipids and hydrocolloids (protein, and polysaccharides) each of which presents peculiar characteristics.[14,15]

Among natural biopolymers, polysaccharides have acquired increasing importance due to their intrinsic and modulable properties. Polysaccharide films or coatings commonly exhibit excellent barrier properties against oxygen and other gases but, properly due to their hygroscopic nature, have a poor ability to hinder moisture exchange. Nevertheless, in the field of food packaging these materials represent one of the most accredited alternatives to replace common packaging materials.[16] For this purpose, cellulose probably represents the most widespread vegetable polysaccharide studied and applied in the field of food packaging. This biopolymer is a linear polysaccharide constituted by two anhydrous glucose rings linked together by β 1-4 glycosidic bond.[17] Cellulose is the most abundant renewable polymer found in nature and also exhibits low cost and good chemical stability. Because of its well-known insolubility in common polar solvents, to employ this polysaccharide as a raw material, many strategies have been developed to dissolve it, some of which involve ionic liquids or deep eutectic solvents.[15,17]

Starch from different sources is widely applied in food packaging thanks to its availability, cheapness, biodegradability, non-toxicity and high compatibility for food contact applications.[17] This material consists of a combination of two main polysaccharides, amylopectin and amylose of which relative composition varies depending on the source of extraction. During the development of starch-based packaging, some limiting issues have been encountered, such as low thermal and water vapor stability.[18] These disadvantages are more or less the same for all the polysaccharide-based materials and can be modulated by adding suitable

plasticizers, such as glycerol, alcohols and glycols. However, these reported are just a few examples of polysaccharides applied in this field; among other common carbohydrates that have gained more interest as food packaging materials, chitosan is one of the most studied.

C 2.1.4 Chitosan in food packaging

As stated before, several natural materials have recently been investigated with the aim of improving their physicochemical properties and optimizing what could represent the new frontier of food packaging. In this regards, chitosan has attracted attention mainly thanks to its intrinsic antimicrobial activity exploited against several species of fungi, yeasts and bacteria.[19] This property has not been fully understood, however the main hypothesis attributes the antimicrobial activity of chitosan to the interactions established between the negatively charged microbial membrane and the ammonium groups of the biopolymer; such interactions lead to a change in the permeability of the microbial membrane.[19,20] Furthermore, as shown in Figure C 2.4, the interest aroused in chitosan for this field is also due to the properties of the package such as edibility, biodegradability and therefore the possibility of developing an active packaging.

Figure C 2.4: Various application of chitosan in food packaging.

Chitosan film or coating preparation involves the solubilization of the biopolymer in slightly acidified water added with the selected additives. The hydrogel thus prepared can be applied directly on the food product for immersion or spraying or,

by means of the solvent casting method, it is deposited on a rigid support until a film is formed (as previously schematized in Figure C 2.3).

The thermal processes on pure chitosan cannot be exploited because this polysaccharide is not a thermoplastic material as its melting temperature is higher than the decomposition one, hence it cannot be thermally extruded.[21]

The properties of the resulting films or coating membranes are strongly affected by the structure of chitosan, which has been extensively discussed in the chapter A 2. For example, water vapor permeability can be reduced by selecting a low deacetylated chitosan. This evidence has been justified considering the greater water affinity and higher polarity observed for most deacetylated polymer.

Moreover, the properties of chitosan can be enhanced by using plasticizer and crosslinkers added during the preparation of the hydrogel; the additives allow to further reduce the water permeability of the resulting membranes and to improve their physical properties such as thermal stability and mechanical behaviour.[17,19]

Other interesting properties of chitosan are represented by its intrinsic antioxidant activity and its chelating properties which can be further improved by implementing the biopolymer film with some natural antioxidant species.[17,22]

Therefore, chitosan, used both as a co-material and as a pure polymeric constituent, has shown very promising applications in food packaging. This biopolymer can commonly be found mixed with other biomacromolecules, in order to combine the different properties of the biomaterials, or also combined with synthetic polymers as an antimicrobial and antioxidant agent.[21] On the other hand, pure chitosan films also found good application as packaging materials. During their preparation, some active substances can be added to the dispersion of the biopolymer to enhance its properties such as plasticizer, surfactant, antioxidant species and/or crosslinker.[20] For instance, extracts from bee secretion, such as propolis and beeswax, are usually added to edible food packaging to improve their antimicrobial properties. Hence, the incorporation of these complex substances should allow an improvement in the shelf life of the food product. Moreover, the addition of suitable natural plant

extracts can be exploited to reduce the application limits of chitosan by improving its mechanical, antioxidant and water barrier properties.[21]

C 2.2 Aim of the work

Over the last years, the use of natural polymers has emerged as alternatives to synthetic petroleum-based ones to reduce the environmental impact of plastic wastes.[23] With particular regard to the bio-based polymers extracted directly from biomass, polysaccharides display remarkable biodegradability, renewability and availability. Moreover, these class of biopolymers are generally inexpensive, non-antigenic, immunogenic and more stable to drastic condition than other.[24]

As described in Chapter A 2, among polysaccharides, chitin, poly (β-(1→4)-N-acetyl-D-glucosamine), is the second most abundant polysaccharide after cellulose and its main commercial sources are crab and shrimp shell. Chitin is poorly soluble in water and this is a major problem in the development of both its processing and its use. For this purpose, through deacetylation process chitin is converted into chitosan, a family of polymers characterized by deacetylation degree greater than 50% which are soluble in aqueous acid solutions.

However, films consisting of pure chitosan present some drawbacks, such as poor mechanical properties, poor elasticity, swelling and subsequent dissolution in an aqueous environment. To improve their chemical and mechanical resistance, different strategies could be followed. Crosslinking agents, like glutaraldehyde, 1-ethyl-3-(3-dimethylaminepropyl)carbodiimide (EDC) and N-hydroxysulfosuccinimide (NHS), or epichlorohydrin, trimethylpropane triglycidyl ether, and ethylene glycol diglycidyl ether have been used to covalently link polysaccharide chains, producing a more inert and stable chitosan structure even in a very acidic medium.[25-27] Alternatively, chitosan could be dissolved in organic acid solutions; they can provide the acid medium required to dissolve the polysaccharide and they can also form ionic bonds with ammonium groups of chitosan.[28] Moreover, dicarboxylic acids could also act as ionic-crosslinking agents among chitosan molecules and it has been

demonstrated that membrane functional properties are greatly improved if dicarboxylic acids replace acetic acid or inorganic ones.[29,30]

The formation of amide linkage between chitosan and carboxylic acids has been reported in the literature, when films were exposed to moist heat treatments or produced by freeze drying of chitosan solutions. In both cases, the covalent crosslinking was revealed by FTIR spectroscopy.[31,32]

In this work different chitosan-dicarboxylic acid membranes were prepared by casting method and their physicochemical and mechanical properties were compared. Glycerol has been added to the hydrogel mixtures to reduce the stiffness of the resulting film, because it inserts between the adjacent chains of the polymer, decreasing the intermolecular attractions. Furthermore, the effect of the neutralization process on both the structural features of the resulting membranes and their properties was evaluated. For this purpose, the comparison between the prepared membranes was extended to non-neutralized films and to those neutralized with NaOH.

The physicochemical and mechanical properties, and the water vapor permeability of the prepared films have been studied using different techniques, in order to highlight the effect of neutralization on the resulting films. The neutralization of the hydrogel could in fact induce the establishment of amide bonds between the chitosan chains improving their physicochemical properties.

C 2.3 Materials and methods

The chitosan powder is the same characterized in the previous section (Chapter B). Glycerol, malonic, succinic and glutaric acids were obtained from Sigma-Aldrich. All reagents and chemicals were used as received.

C 2.3.1 Preparation of chitosan solutions and gel films

Chitosan (2% w/v) was dissolved in a previously prepared aqueous solution of dicarboxylic acid (2% w/v) containing glycerol (5% w/v) as a plasticizer. The mixture

was kept under constant stirring until complete dissolution of the chitosan. Ten mL of solution were spread in polystyrene Petri-dishes (100 mm diameter) and dried in an oven for 12 h at 45 °C. After, these films were neutralized in the corresponding buffer solution, *i.e.* malonate, succinate and glutarate buffers, (0.2 M, pH 6.0) for 30 min and dried at room temperature.

Alternatively, neutralized films were prepared by slowly dripping 3 M NaOH to the chitosan solution under constant stirring until reaching a pH of about 5.5. Then, the chitosan hydrogels thus formed were poured onto Petri-dishes (100 mm diameter) and allowed to dry in an oven for 12 h at 45 °C.

C 2.3.2 Characterization of chitosan films

Thickness

The film thickness was measured at ten different points, taken randomly, using a digital micrometer (Mitutoyo) with range 0-25 mm and accuracy of 0.001 mm.

Degree of swelling and water solubility

Water solubility and swelling are important properties for the characterization of biodegradable films. To determine the water solubility, dried film samples (20 mm × 30 mm) were weighted (W_i) and immersed in distilled water (10 mL per 100 mg of sample) for 6 h. Afterwards, the samples were withdrawn from the medium, the excess of water removed with a filter paper and their wet weight immediately determined (W_w) to calculate the degree of swelling. The samples were then dried at room temperature and at relative humidity of about 50% until constant weight (W_f), to determine the solubilized mass. Degree of swelling (DS%) and water solubility (WS%) were determined by the following equations respectively.

$$DS\% = \left[\frac{W_w - W_i}{W_i}\right] \times 100 \qquad WS\% = \left[\frac{W_i - W_f}{W_i}\right] \times 100$$

To assess the water solubility and swelling behavior, at least five samples were tested.

FTIR-UATR spectroscopy

FTIR spectra of chitosan films prepared with succinic acid were evaluated with a Perkin-Elmer spectrometer (Spectrum Two FT-IR) equipped with a universal attenuated total reflectance accessory (UATR). Scans were performed in the spectral range 400-4000 cm^{-1} with a resolution of 4 cm^{-1}.

Titration of succinic acid/succinate in chitosan film

In order to determine the amount of succinic acid in non-neutralized films, a weighed sample of about 1 g was immersed for one day at room temperature in 25 mL of deionized water and the resulting solution was titrated with 0.1 M NaOH.

In order to determine the amount of succinate anions balancing the charge of the ammonium groups in the neutralized films, a weighed sample of about 1 g was immersed for one day at room temperature in 25 mL of deionized water (so as to remove succinic acid) and then put for another day in 25 mL of a 0.01 M HCl solution. 10 mL of this solution was withdrawn and 1 M HCl was added, drop by drop, so that the final pH was 2. The resulting solution was titrated with 0.1 M NaOH.

Differential scanning calorimetry

Thermal analyses were performed using a Mettler Toledo DSC 3 differential scanning calorimeter. All samples were placed in pierced lid aluminum pans and DSC scanning were accomplished under a nitrogen atmosphere with a flow rate of 50 mL/min. The pure component, *i.e.* chitosan and succinic acid powder and glycerol were heated from 25 to 350 °C with a heating rate of 10 °C/min, while for films a scan rate of 1 °C/min with a temperature range of 25-450 °C was used.

Mechanical properties

The mechanical properties of the films were evaluated by tensile tests using a Zwick Roell Z1.0 testing machine, with a 200 N static load cell following the procedure reported by Sood and coworkers.[33] Young's modulus, tensile strength at break and elongation at break were measured on rectangle shaped film stripes, obtained by a cutting machine, length and width of which were 100 and 5 mm, respectively. All

tests were carried out at a crosshead speed of 100 mm min^{-1} at room temperature (20–23 °C) and 40% RH. At least three replicate film stripes were analyzed. The data were elaborated by the TestXpert V11.0 Master software. The samples were conditioned at ambient conditions and over P_2O_5 for a week before to be tested.

Water vapor permeability

Water vapor permeability (WVP) was determined according to the ASTM E96 standard method with some modifications.[34] The method is performed by sealing a film to the open mouth (3 cm diameter) of a Payne cup containing water (10 g) and placing the assembly into a controlled climatic chamber at 30% RH and 30 °C in order to maintain a 70% RH gradient across the film. The system was weighed, placed in the climate chamber and then reweighed after 24 hours. The WVP was calculated by using the following formula:

$$WVP = \frac{\Delta_w \times T}{A \times t \times \Delta P}$$

Where ΔW is the weight loss by the assembly (g) during the test, T is the film thickness (cm), A is the permeation area of the exposed film surface (cm^2), t is the test time (h) and ΔP is partial pressure difference of water vapor through the film (atm). For each measurement, three replications were made.

C 2.4 Preparation and characterization of chitosan films

In a preliminary screening, three dicarboxylic acids with different chain length, *i.e.* malonic, succinic and glutaric acids, have been selected. Their function is not only to dissolve chitosan, but also to improve functional properties of chitosan through crosslinking because the intermolecular space between the polymer chains could have a notable role.

Regardless of the acid used, however, chitosan films initially swelled and then quickly dissolved in water. The instability of chitosan films prepared with inorganic or organic (monocarboxylic) acids in water is already reported in literature.[29,31,35-38] In this case, despite the presence of two carboxylic groups, the ionic interactions

between the selected diacids and the positively charged amino groups of chitosan were not so strong to prevent the initial swelling of the film and its following dissolution in water.

To limit the water solubility and improve the stability of the films, neutralization could be performed by treating the film with a buffer solution, as already reported in the literature.[37] Therefore, films prepared with malonic, succinic and glutaric acids have been washed with the corresponding buffer solution and then dried to obtain the final films. As a result of the washing treatment of the dry film with the buffer solution, there is a partial loss of glycerol, with a consequent decrease in the elasticity of the film itself. Moreover, when the buffer was poured onto the film, it caused swelling and stripes that made the surface uneven. The water solubility of the new neutralized films was then tested and, despite the treatment with the buffer solution, the neutralized chitosan malonate films dissolved. Therefore, this kind of film was not further investigated.

In literature, another method to neutralize the ammonium groups of chitosan, which consists in the use of basic solutions, was reported.[29,38-41] The basic solution could be used after the film preparation, that is by soaking the film in a NaOH aqueous (or ethanolic) solution, or during its preparation by slow drip of basic solution to the hydrogel. In our experiments, neutralization was carried out by adding sodium hydroxide to the hydrogel. In detail, a few drops of 3 M NaOH solution was added to the solution, consisting of chitosan, succinic or glutaric acids, and glycerol, very slowly and under magnetic stirring so as to reach a pH equal to the pKa_2 of the acid, *i.e.* 5.6 and 5.4 for succinic and glutaric acids respectively. In this way, both an excessive dilution of the polymer and a loss of the glycerol during the immersion in the basic solution and in the washing were avoided.

C 2.4.1 Thickness swelling and solubility of chitosan films

Different amount of hydrogel (10, 15, 20 and 25 mL) were poured onto plastic Petri dishes (∅ 10 cm) and dried in an oven at 45 °C until they reached a constant weight

(about 12-15 h). In Table C 2.1, the thickness of the films and their water solubility and swelling properties were reported; S refers to chitosan films prepared with succinic acid while G indicates the chitosan films prepared with glutaric acid.

Table C 2.1 – Thickness, degree of swelling (DS%) and water solubility (WS%) of chitosan films prepared with different amounts of hydrogel: 10 mL (S10/G10), 15 mL (S15/G15), 20 mL (S20/G20) and 25 mL (S25/G25) in 10 cm diameter Petri dishes.

Sample code	Thickness (μm)	DS%	WS%
S10	87 ± 3	66.8	73.4
S15	110 ± 6	81.5	73.4
S20	175 ± 8	87.9	73.5
S25	210 ± 10	70.0	74.0
G10	70 ± 2	86.8	69.6
G15	97 ± 5	179.6	69.7
G20	130 ± 7	188.2	69.5
G25	180 ± 9	240.6	68.2

As regard the thickness of the films, as expected, it increased with increasing the amount of the hydrogel used for their formation. The high value of swelling showed in the table was due to the hydrophilic characteristic of chitosan films and, those prepared with glutaric acid absorbed much more water than chitosan-succinic ones. Moreover, films prepared with glutaric acid adhered strongly to polystyrene the Petri-dishes and are therefore more difficult to handle. Nevertheless, all films did not break after studying the swelling index, which is the result of the film's water resistance. In all the samples there was a great loss of material, represented by the percentage of weight lost by partial solubilization of the film (WS%), equal to about 70%. It was assumed that this weight decrease was due to a loss of glycerol and then films were immersed in glycerol/water mixtures. As the percentage of glycerol increased, WS% value decreased and, when the amount of plasticizer in the mixture was significant, around 70%, it was adsorbed by the sample, with a consequent increase in membrane weight.

Among the tested samples, S10 was selected for further characterizations.

C 2.4.2 FTIR-UATR spectroscopy

FTIR spectroscopy was used in order to obtain information on the interactions between chitosan and succinic acid before and after the neutralization of the ammonium groups of chitosan with the basic treatment. In Figure C 2.5 the FTIR spectra of the chitosan film prepared with succinic acid before (A) and after (B) the neutralization with NaOH were compared.

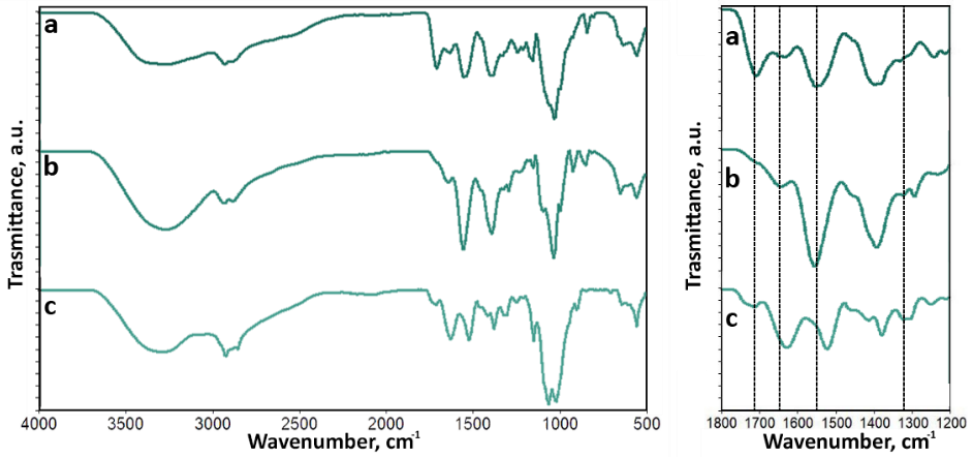

Figure C 2.5: FTIR spectra of chitosan film before (a) and after (b) the neutralization with NaOH; spectrum of neutralized film after acid treatment (c).

All chitosan samples showed broad infrared absorbance greater than 3000 cm^{-1} due to the stretching vibration of O-H superimposed to the N-H stretching. The films also displayed the characteristic C-H stretching (a doublet at 2921 and 2867 cm^{-1}) and the absorption bands at 1150 cm^{-1} (anti-symmetric stretching of the C-O-C bridge) and 1040 cm^{-1} (skeletal vibrations involving the C-O stretching), characteristics of chitosan polysaccharide structure (Figure C 2.8 a).[38,40] The main differences were observed in the medium infrared region between 1200 and 1800 cm^{-1} (Figure C 2.8 b), where the characteristic bands of carbonyl (C=O), amine (NH_2) and ammonium (NH_3^+) functionalities are present.

The spectrum registered on the sample before the treatment with NaOH (curve a) showed a band at 1710 cm^{-1}, related to the carbonyl stretch C=O of the succinic acid. The two bands at 1630 and 1550 cm^{-1}, which corresponded to NH_3^+ and COO^- groups,

overlapped to amide functions bands of the polysaccharide, indicated the formation of electrostatic interactions between chitosan and the acid.[31]

After the addition of NaOH to the hydrogel (curve b), the band at 1557 cm^{-1} could be attributed to N-H bending vibration (amide II), whose intensity increased with respect to untreated film because of an overlap with the asymmetric stretching of carboxylate groups of succinate ions, which absorb at around 1560 cm^{-1}. The C=O stretching (amide I band), symmetric stretching of carboxylate groups of succinate and C-N stretching (amide III band) appeared at 1643, 1392 and 1320 cm^{-1}, respectively. The intensity of the band of COOH groups of succinic acid at 1710 cm^{-1} decreased significantly and the peak became a shoulder at 1716 cm^{-1}.

Both films were then immersed in a 2 M HCl solution. If the chitosan-succinic acid interactions were only of the acid-base type (with formation of electrostatically interacting carboxylate and ammonium groups), then HCl should protonate the carboxylate groups and remove succinic acid from the film. After the acid treatment, the non-neutralized film dissolved completely in the acid solution, while the neutralized film underwent only a moderate swelling; its spectrum is reported in Figure C 2.8 c.

Several differences can be noted with respect to the previous spectra. In agreement with the above considerations the peak at 1550 cm^{-1} decreases while a slight increase in carbonyl stretching (although much less intense and defined than that of the non-neutralized film) can be seen at 1716 cm^{-1} due to residual succinic acid. Peaks of amide I and amide II shifted at lower wavenumber, *i.e.* 1628 and 1521 cm^{-1}, respectively, probably due to the overlap with the ammonium groups formed after acid treatment, which absorb at 1626 and 1518 cm^{-1}.[31,32] Moreover, the C-N stretching band (amide III) appeared better defined. Such outcomes suggest that interactions between diacid and chitosan may be either electrostatic or covalent, and then it is possible to hypothesize the formation of an amide bond.

C 2.4.3 Titration of succinic acid/succinate in chitosan film

In order to prove the formation of amide bonds, we estimated the amount of succinate anions balancing the charge of the ammonium groups (hereafter NH_3^+ succinate) so as to compare it with the overall amount of nitrogen atoms in the film (1.07 meq g^{-1}).

After neutralization with NaOH, the chitosan film contains (besides glycerol) monosodium and disodium succinate and chitosan-NH_3^+ succinate. Washing the film with water should remove quantitatively only monosodium and disodium succinate, without altering significantly the concentration of chitosan-NH_3^+ succinate. Accordingly, after washing with water, a non-neutralized film (containing only succinic acid and NH_3^+ succinate) releases an amount of succinic acid (2.55 meq g^{-1}) which is close to that (2.67 meq g^{-1}) expected after treatment of 1 g chitosan (possessing 1.07 meq g^{-1} of $–NH_2$ groups) with 3.74 meq of succinic acid.

On the basis of these considerations, a neutralized film was first washed with water to remove monosodium and disodium succinate, and then treated with a 0.01 M HCl solution so as to exchange the succinate with the chloride ion and remove it from the film in the form of succinic acid. After this treatment the film released 0.59 meq g^{-1} of succinic acid thus suggesting that a significant amount of nitrogen atoms (1.07 – 0.59 = 0.48 meq g^{-1}, *i.e.* ≈ 45% of the nitrogen atoms) forms amide bonds.

C 2.4.4 Differential scanning calorimetry analysis

The thermal transition characteristics of these biopolymeric systems, analyzed by differential scanning calorimetry, could provide useful information on the interactions established between the single constituents. Therefore, DSC analysis was firstly performed for the components of the films and subsequently on both the non-neutralized and neutralized films; the data reported in Figure C 2.6 represent the thermal transitions observed for all the studied samples.

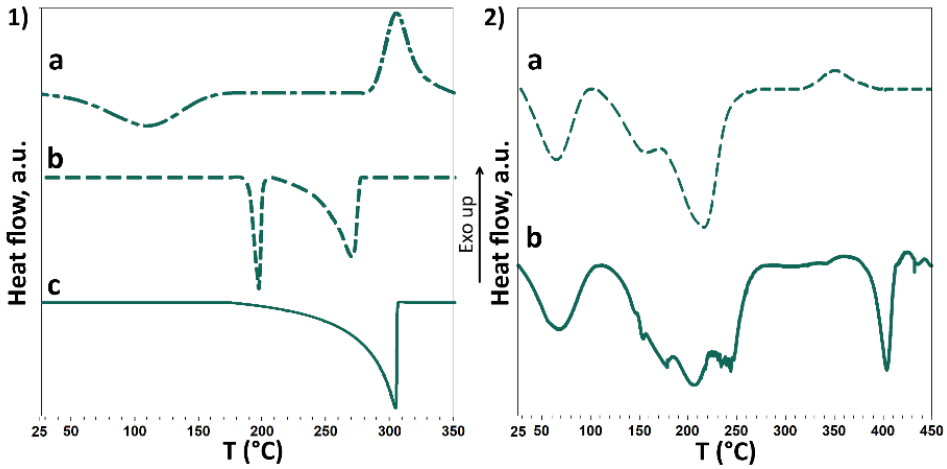

Figure C 2.6: DSC curves of (1): chitosan powder (a), succinic acid (b), glycerol (c) and (2): non-neutralized (a) and neutralized chitosan films (b).

According to the literature data, chitosan powder is characterized by two peaks, centered at 108.5 °C (endothermic) and 304.7 °C (exothermic).[31] The wide endothermic transition can be associated to the loss of bounded water while the sharper exothermic peak corresponds to the decomposition of the biopolymer. For succinic acid two endothermic peaks at 195.8 and 269.3 °C correspond to melting and boiling point respectively, while glycerol showed a sharp endothermic transition at 286.8 °C corresponding to its boiling point.

The DSC thermograms of chitosan films exhibited noteworthy differences; in fact, apart from the band associated to the loss of bounded water, observed for both films around 70 °C, other transitions occurred at different temperatures. The first endothermic peak, due to the loss of the bounded water, can provide useful information on the residual water content of non-neutralized and neutralized films. In fact, as reported by Cavallaro and coworkers[42], combining the area of the peak related to the loss of the bounded water and the enthalpy of water evaporation (2259 J g^{-1}), the water content of the membrane can be calculated, and it was found to be equal to 7±2% and 4±1% for the non-neutralized and the neutralized film, respectively.

As temperature raises beyond the dehydration process, films showed broad endothermic transitions in the temperature range of around 110-240 °C, for the non-neutralized sample, and of around 130-260 °C for the neutralized one. These transitions are probably due to a sum of thermal processes, which involve the single components. In this thermal region glycerol, succinic acid, and its salts, could show shifted phase transitions in comparison with the pure components caused by the interactions that they establish both in non-neutralized and neutralized samples. After these wide and noisy thermal transitions, both films showed an exothermic transition at 348.9 and 362.5 °C which corresponds to the decomposition process. It is evident that the formation of strong interactions between the chitosan chain and the succinate ion as "ionic crosslinker" increased the thermal stability of the film, if compared to the chitosan powder, increasing the degradation temperature. Furthermore, the greater thermal stability of the neutralized sample with respect to the non-neutralized one can suggest the formation of much more strong interactions between the chitosan chains and the succinic acid. At least, the endothermic transitions that occur for the neutralized film at 404.1 °C can be related to the disodium succinate fusion process.[43]

C 2.4.5 Mechanical properties

Performing packaging materials should possess high mechanically properties especially in terms of mechanical strength and flexibility.

Figure C 2.7 shows the stress-strain curves obtained from the tensile stress of S10 and, for comparison, of a chitosan film prepared with acetic acid (CH) and of an ionically crosslinked succinic acid-chitosan film that was not treated with NaOH (CH/S).

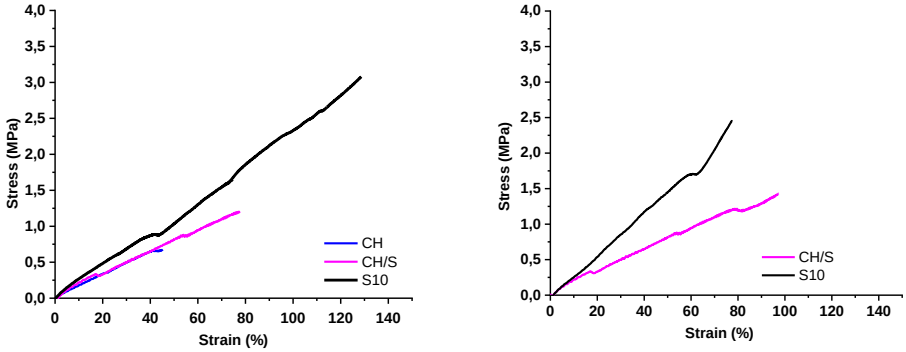

Figure C 2.7: Stress-strain curves on samples kept at RH=40% on the left and kept at RH=0% on the right.

Table C 2.2 reports the Young's Modulus (E), Tensile Strength at break (TS) and strain at break (ε) of the three films.

Table C 2.2: Elastic modulus (E), tensile strength at break (TS) and elongation at break of chitosan based-films.

	40% RH			0% RH		
Sample code	E (MPa)	TS (MPa)	ε (%)	E (MPa)	TS (MPa)	ε (%)
CH	1.62 ± 0.23	0.58 ± 0.14	42±4	–	–	–
CH/S	3.28 ± 0.12	0.55 ± 0.15	77 ± 15	2.22 ± 0.41	1.38 ± 0.56	97 ± 12
S10	3.50 ± 0.19	3.02 ± 0.20	164 ± 7	3.13 ± 0.19	2.45 ± 0.36	72 ± 10

As it can be seen from the values reported in table, the S10 film had higher E, TS and ε than the other two films. This improvement in mechanical properties of chitosan films may be ascribed to the presence of covalent crosslinking between succinic acid and chitosan. In particular, the covalently crosslinked films had significantly higher TS and ε also with respect to the ionically crosslinked films, which means that a more resistant and at the same time a more flexible network results from the formation of amide bonds.

The mechanical tests were also carried out in dry condition on films kept at 0% RH for a week (as reported in Table C 2.2). In general, although the difference is not significant, covalent crosslinking enhanced the E and TS likewise to the 40% RH conditions. The mechanical properties of the acetic acid-chitosan sample had not determined because of poor mechanical stability of this film.

C 2.4.6 Water vapor permeability

The Water Vapor Permeability (WVP) of control film without succinic acid was about 8.2 $x10^{-4}$ g cm^{-1} h^{-1} atm^{-1}. Films showed a decrease in WVP after inclusion of dicarboxylic acid due likely to additional attractive interactions between chitosan chains, which might cause the decrease of interchain spacing between chitosan chains as a result of ionic crosslinking. The WVP was further decreased after treatment with NaOH (Figure C 2.8).

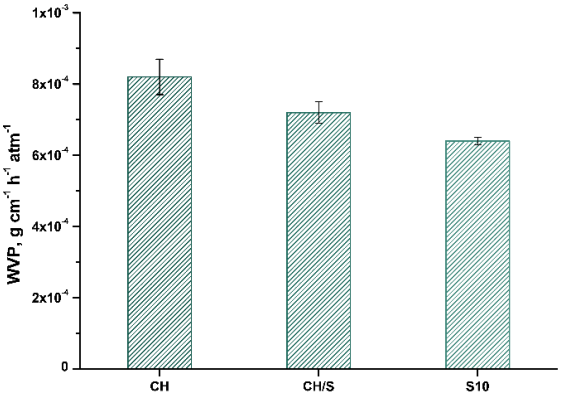

Figure C 2.8: WVP of chitosan-based films.

This additional WVP reduction could be explained considering that NaOH promotes the formation of a denser crosslinked network with a reduced free volume. This evidence well agrees with DSC results related to a lower water content of neutralized film with respect to non-neutralized ones.

C 2.5 Conclusion

In this study, several techniques have been used to compare the main features of non-neutralized and NaOH-neutralized chitosan-succinic acid films. The neutralization process has proven to improve the functional properties of the prepared films in terms of water solubility, mechanical strength, flexibility, water-vapor permeability and thermal stability. Tensile tests, water vapor permeability measurements and DSC analysis suggested the possibility that, as a result of treatment with NaOH, chitosan and succinic acid may be covalent bonded, since

both stronger interactions with each other and a denser crosslinked network are formed. Moreover, also FTIR spectra revealed the possible formation of amide bonds between the two components, but acid-base titration allowed us to confirm that a significant amount of nitrogen atoms, approximately 45%, forms amide bonds. The optimized film has shown good flexibility and resistance. These properties added to the intrinsic antibacterial activity of chitosan itself along with the possibility of incorporating drugs, enzymes, essential oils, antioxidants, etc. into the hydrogel make it a very promising membrane for many applications. Some preliminary tests were performed in our laboratory on different varieties of cheese using S10 membrane, pure and added with nisin, a well-known antibacterial peptide, as active packaging materials. The preliminary results showed an increased cheese shelf-life when compared to commercial PVC films. Moreover, further experiments will be carried out with the aim of replacing the glycerol, used to reduce the stiffness of the film, with other less water-soluble plasticizers to decrease the loss of material following washing treatments.

References

1- S.J. Risch, Journal of Agricultural and Food Chemistry, **57**, 8089–8092 (2009);

2- K. Molina-Besch, F. Wikström, H. Williams, International Journal of Life Cycle Assessment, **24**, 37-50 (2019);

3- J.W. Han, L. Ruiz Garcia, J.P. Qian, X.T. Yang, Comprehensive Reviews in Food Science and Food Safety, **17**, 860-877 (2018);

4- K. Verghese, H. Lewis, S, Lockrey, H. Williams, Packaging Technology and Science, **28**, 603-620 (2015);

5- T. Huang, Y. Qian, J. Wei, C. Zhou, Polymers, **11**, 560 (2019);

6- Y. Zhong, P. Godwin, Y. Jin, H. Xiao, Advanced Industrial and Engineering Polymer Research, **3**, 27-35 (2020);

7- J. Zheng, S. Suh, Nature Climate Change, **9**, 374–378 (2019);

8- K. Marsh, B. Bugusu, Journal of Food Science, **72**, R39-R35 (2007);

9- C.B. Contreras, G. Charles, R. Toselli, M.C. Strumia, "*Antimicrobial Active Packaging*" in "Biopackaging", M.A. Mauselli Ed., CRC Press, chap. 3, 36-58 (2017);

10- N. Emanuel, H.K. Sandhu, Journal of Thin Films, Coating Science Technology and Application, **6**, 13-29 (2019);

11- B. Geueke, K. Groh, J. Muncke, Journal of Cleaner Production, **193**, 491-505 (2018);

12- N. Peelman, P. Ragaert, B. De Meulenaer, D. Adons, R. Peeters, L. Cardon, F. Van Impe, F. Devlieghere, Trends in Food Science & Technology, **32**, 128-141 (2013);

13- S. Mehdi Emadian, T.T. Onay, B. Demirel, Waste Management, **59**, 526-536 (2017);

14- S. Galus, E.A. Arik Kibar, M. Gniewosz, K. Kraśniewska, Coatings, **10**, 674 (2020);

15- S.A.A. Mohamed, M. El-Sakhawy, M.A. El-Sakhawy, Carbohydrates Polymers, **238**, 116178, (2020);

16- A.R.V. Ferreira, V.D. Alves, I.M. Coelhoso, Membranes, **6**, 22 (2016);

17- P. Cazón, G. Velazquez, J.A. Ramírez, M. Vázquez, Food Hydrocolloids, **68**, 136-148 (2017);

18- H. Samsudin, N.M. Hani, "*Use of starch in food packaging*" in "Starch-Based Materials in Food Packaging", M. Vilar, S.E. Barbosa, M.A. García, L. Castillo, O.V. Lopez Ed., Academic Press, chap. 8, 229-256 (2017);

19- S. Kumar, A. Mukherjee, J. Dutta, Trends in Foods Science & Technology, **97**, 196-209 (2020);

20- S. Tripathi, G.K. Mehrotra, P.K. Dutta, e-Polymers, **8**, 1 (2013);

21- H. Wang, J, Qian, F. Ding, Journal of Agricultural and Food Chemistry, **66**, 395-413 (2018);

22- M. Yen, J. Yang, J. Mau, Carbohydrate Polymers, **74**, 840-844 (2008);

23- F. Galiano, K. Briceño, T. Marino, A. Molino, K.V. Christensen, A. Figoli, Journal of Membrane Science, **564**, 562-586 (2018);

24- M.J. Fabra, A. López-Rubio, J.M. Lagaron, "*Biopolymers for food packaging applications*", in "Smart polymers and their applications" M.R. Aguilar, J. San Román Eds., Woodhead Publishing, Cambridge, chap. 15, pp. 476-509 (2014);

25- Beppu M.M., Vieira R.S., Aimoli C.G., Santana C.C., Journal of Membrane Science, **301**, 126-130 (2007);

26- T. Jóźwiak, U. Filipkowska, P. Szymczyk, J. Rodziewicz, A. Mielcarek, Reactive and Functional Polymers, **114**, 58-74 (2017);

27- C.T. Tsao, C.H. Chang, Y.D. Li, M.F. Wu, C.P. Lin, J.L. Han, S.H. Chen, K.H. Hsieh, Journal of Bioactive and Compatible Polymers, **26**, 519-536 (2011);

28- S.Y. Cheng, B.J. Wang, Weng Y.-M., LWT- Food Science and Technology, **63**, 115-121 (2015);

29- P.H. Chen, T.Y. Kuo, F.H. Liu, Y.H. Hwang, M.H. Ho, D.M. Wang, J.Y. Lai, H.J. Hsieh, Journal of Agricultural and Food Chemistry, **56**, 9015-9021 (2008);

30- R. Medimagh, H. Aloui, M. Jemli, H. Chaabane, F. Belkahla, K. Khwaldia, Polymer Science, Series A, **58**, 409-418 (2016);

31- G.C. Ritthidej, T. Phaechamud, T. Koizumi, International Journal of Pharmaceutics, **232**, 11-22 (2002);

32- A. Ghosh, M.A. Ali, Journal of Materials Science, **47**, 1196-1204 (2012);

33- R. Sood, A. Donnadio, S. Giancola, A. Kreisz, D.J. Jones, S. Cavaliere, ACS Applied Materials & Interfaces, **8**, 16897-16906, (2016);

34- F. Ortega, L. Giannuzzi, V.B. Arce, M.A. García, Food Hydrocolloids, **70**, 152-162 (2017);

35- M. Hejazi, T. Behzad, P. Heidarian, B. Nasri-Nasrabadi, Composites Part A: Applied Science and Manufacturing, **109**, 221-231 (2018);

36- M. Kaya, P. Ravikumar, S. Ilk, M. Mujtaba, L. Akyuz, J. Labidi, A.M. Salaberria, Y.S. Cakmak, S. K. Erkul, Innovative Food Science and Emerging Technologies, **45**, 287-297 (2018);

37- I.C. Libio, R. Demori, M.F. Ferrão, M.I.Z. Lionzo, N.P. da Silveira, Materials Science and Engineering C, **67**, 115-124 (2016);

38- E.A. Takara, J. Marchese, N.A. Ochoa, Carbohydrate Polymers, **132**, 25-30 (2015);

39- Q. He, Q. Ao, Y. Gong, X. Zhang, Journal of Materials Science: Materials in Medicine, **22**, 2791-2802 (2011);

40- J.H.R. Llanos, L.C. de Oliveira Vercik, A. Vercik, Journal of Biomaterials and Nanobiotechnology, **6**, 276-291 (2015);

41- W. Chang, F. Liu, H.R. Sharif, Z. Huang, H.D. Goff, F. Zhong, Food Hydrocolloids, **90**, 50-61 (2019);

42- G. Cavallaro, G. Lazzara, S. Milioto, Langmuir, **27**, 1158-1167 (2011);

43- F.J. Caires, L.S. Lima, C.T. Carvalho, M. Ionashiro, Eclética Química, **35**, 73-80 (2010).

Chapter C 3

Cultural heritage

The combination of natural landscapes and cultural heritages represents the charm and wealth of a country. Works of art not only enrich the environment in which they are immersed but are also an indelible sign of the culture of ancient communities which, through their artistic expression, have helped to build modern societies. Therefore, in order to pass on these heritages for as long as possible, their conservation and maintenance plays an important role both for our society and for future ones. Unfortunately, the deterioration processes of work of arts are unavoidable and begin after their realization. Furthermore, type, entity and rate of these processes depend on several factors related to the artwork, such as the nature of the constituent material, its shape and physicochemical properties, the environmental conditions under which the works of art are subject, and also on anthropogenic activity (war, vandalisms, etc.).[1]

Conservation interventions of precious works of art can be divided into cleaning, restoration, consolidation and protection, all exploited in order to reduce the natural degradation of the artworks. Whatever the intervention on an artwork must be studied in all its single aspects to avoid damages to the work and undesirable future decay. In this context, adequate preliminary studies must be carried out to know the material nature and its fragility. At the same time, the study of the environmental condition as well as the comprehension of the causes and the extent of deterioration must be known to design the best intervention on the artefact.

The following sections will be focused on stone materials with particular regard to biodeterioration. The growth of microbial contaminants, their degradative action and the treatments, both common and novel, employed to reduce the biodegradation of stone materials will also be briefly discussed.

C 3.1 Stone artefacts and their biodeterioration

Rocks are the constituent elements of the earth's crusts and of the building materials most used by man. Moreover, stone materials are also the most common constituent of which the tangible cultural heritage is made up. Hence, the knowledge of their structure and composition is a fundamental aspect to fully understand the causes of the deterioration of the stone heritage and the optimal method of intervention. In fact, according to their origin, natural stone materials change in their morphological structure, *i.e.* in granulometry, pore size, pore distribution and texture. Instead, regarding their composition, stone materials greatly differ from each other. Through a preliminary rough classification, they can be divided into silicates or calcareous stones. However, this type of classification does not provide a well division between the large varieties of stone materials because they are commonly formed by multiple minerals encapsulated together in very complex structures. For example, igneous silicates are classified according to the amount of silica that confers to the material different characteristics. A high content of SiO_2 corresponds to acid materials while, on the contrary, the lower the amount of silica much more basic the material is considered.[2] Consequently, the composition plays an important role in terms of physicochemical properties of the stone material as well as its weakness against external agents.

C 3.1.1 Decay of stone artefacts

Artificial and natural stone materials can be classified according to their intrinsic properties such as mineral composition, petrographic structure and color. These properties are directly related to the decay processes, affecting causes and entities. Regardless of the causes, the deterioration of stone material can manifest itself in different forms such as loss of material, discoloration or deposits, cracks or deformations, detachments, crusts and erosions. Figure C 3.1 illustrates some of the most common forms of decay cited above, founded on the east tower of the Chambord castle in France.

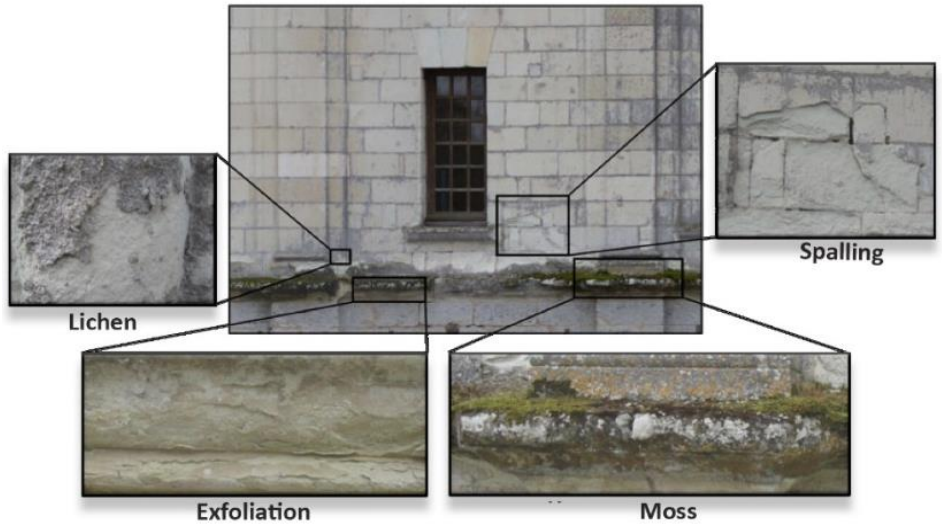

Figure C 3.1 Multiple form of deterioration observed in the external of the east tower of the Chambord castle in France.

In addition to their intrinsic properties, the micro and macro environment that surrounds the stone heritage plays a fundamental role in their patterns of decay; in fact, artefacts or buildings exposed to external conditions commonly show a higher rate of deterioration. Chemical and physical processes added to biological contamination can affect stone works of art, particularly that exposed outdoors. Thermal variations, freezing-thawing processes, salt efflorescence, erosive and corrosive action of both atmospheric pollutants and acid rain are the main physical and chemical causes of the deterioration of stone heritage.[3]

C 3.1.2 Biodeterioration of stone works of art

Microbial colonization of stone works of art has long been considered only as an aesthetic form of deterioration due to the classic chromatic variations associated with them. Unfortunately, biological contaminants not only affect the appearance of cultural heritages but can also induce several damages on the material surface and in the inner porous structure. Moreover, the degree of decay due to these species drastically increases when their growth is coupled with other degradation phenomena.

With particular regard to stone materials, their physical and chemical properties have proved to be strongly linked to the phenomenon of biodeterioration. For this purpose, in 1995 Guillitte coined the term "bioreceptivity" as the property of a material that can lead to anchoring, growth and colonization of flora and/or fauna on its surface. Figure C 3.2 shows the stages of bioreceptivity of stone materials, classified on the basis of their properties as:

- primary bioreceptivity: the initial state properties of the stone materials remained almost unaffected by biodeterioration;
- secondary bioreceptivity: extended and deeper microbial colonization on the stone surface;
- tertiary bioreceptivity refers to anthropogenic activity in terms of biocidal and consolidation treatments of the substrate.[4]

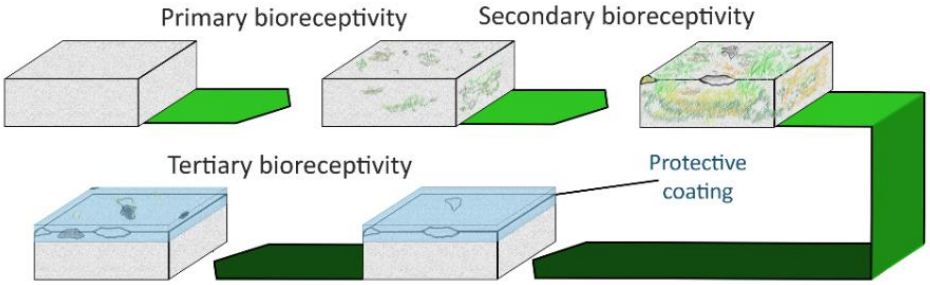

Figure C 3.2: Schematic representation of the stages of bioreceptivity proposed by Guillitte.

The extent to which a stone material can be assessed as bioreceptive is directly related to its open porosity, surface roughness and hygroscopicity, that is all those physical properties involved in the mass transport of water, soil and nutrients, between the stone and the external environment. Furthermore, the composition of the material also plays a crucial role in biological contamination, at least in their first phase. In fact, macro and microelements could mainly favor the growth of some autotrophic microbes which, colonizing the stone surface, lead to the development of higher heterotrophic microbial species. The environmental conditions to which the artefact is exposed also contribute to the growth of microbial contaminants and, moreover, act on the taxonomy of the colonizing species.[5]

Common microbial contaminants

Metabolites, root penetration and the release of pigments are the main phenomena on which the decay induced by the growth of biological contaminants is based. Furthermore, the effect and extent of each of them is often related to well specific microorganisms. Therefore, the knowledge and identification of contaminating microbes is the first requirement to counteract their development and effectively remove them from the biodegraded substrate.[6]

Algae and *cyanobacteria* are often the first colonizers of stone surface. The growth of these photoautotrophic microorganisms is favored in humid environments not directly exposed to light. Through their metabolic activity, stone materials are enriched with nutrients, which can lead to the contamination of heterotrophic microorganisms. *Bacteria* are other microbes commonly involved in the biodeterioration of stone heritage and, depending on their nature, they can use reduced minerals as sources of energy, or grow on microbial colonies capable of fixing atmospheric nitrogen (cyanobacteria).

In addition, *fungi* and *yeast* are common heterotrophic species, which can be found on stone materials, previously colonized by other autotrophic organisms. On the one hand, fungal species preferentially colonize stone materials surrounded by a humid or semi-humid environment, developing their hyphae in the porous matrices of stone materials. On the other hand, yeasts preferentially grow in drier environments, which are more extreme climatic conditions for most fungi. Lastly, *lichens* and *bryophytes* are other typical contaminants of stone materials. The former are symbiotic species derived from the association of fungi (heterotrophs) with algae or cyanobacteria (autotrophs) which coexist in cooperation. The fungal species absorb nutrients from algae metabolism, which in turn are protected from the carbonation process induced by the fungal respiration. The other species, the bryophytes, are commonly non-vascular species capable of growing on the stone surface in a highly humid environment not exposed to sunlight.[6-9]

Morphology of stone microbial colony

Biological species can proliferate on stone artifacts in several macroscopic morphologies according to the degree of contamination. More specifically, two different stages of biodeterioration can be distinguished: microcolonies and patinas (some of which are summarized in Figure C 3.3). The former represents the initial state of biodeterioration and can be classified depending on their appearance in pustules, concealed microbes and irregular strains.

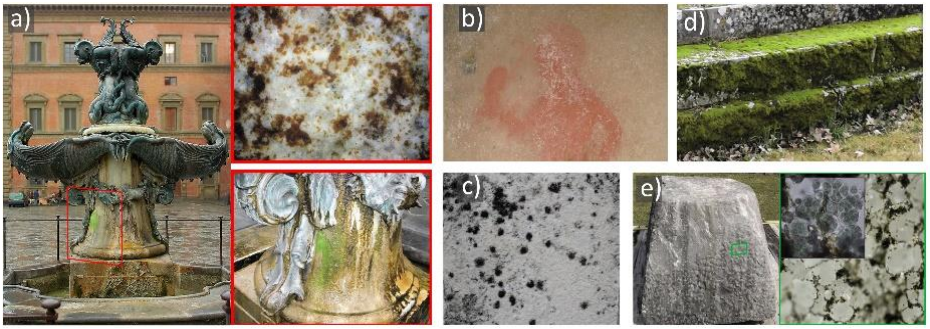

Figure C 3.3: a) Tacca's fountain in Florence colonized by phototropic biofilm (red-below) and brown diatoms appearing both as pustules and brownish strains (red-above); b) whitish strain due to actinomycetes; c) black strains due to fungal growth on marble; d) mosses mats; e) black crusts with microcolonies of cyanobacteria and black fungi.

Pustules are one of the earliest forms of macroscopic biodegradation and usually present a hemispherical morphology with a gelatinous and warty appearance. Figure C 3.3 a represents an example of this pioneering type of colonization, commonly due to the growth of green algae and/or cyanobacteria in humid environments or on substrates submerged in water.

Concealed growth of microbial contaminants is another micro colonial morphology that occurs up to 5 cm from the stone surface. This type of colonization is very difficult to observe because they usually appear similar to salt efflorescence. Highly porous stone artefacts are the materials most affected by this type of biodegradation that give the surface an eroded and granular appearance.

The last main morphology of microcolonies of biological contaminants is the irregular strain. As the name suggests, they appear as irregularly shaped spots that

differ in color due to the deposition of specific organic matter on the stone surface. Black strains are commonly rich in melanin, melanoidins, produced for example by black fungi, while green and greenish spots are attributable to photosynthetic pigments of algae and cyanobacteria. Red and pink colored strains indicate the presence of iron-based pigments often resulting from the metabolism of bacteria, algae and cyanobacteria. Finally, yellowish to brownish strains are generally due to carotenes, carotenoids and other degradation products of chlorophyll.[9]

More complex morphology occurs when the microcolonies grow up to the formation of the patina. The expansion of the pustules leads to the formation of biofilms, which are often considered an intermediate state of biodegradation. The continuous development of the microbial film favors the engraftment of other species up to the formation of microbial mats. Biological contaminants cooperate with each other through their metabolites, which are exchanged through the stratification resulting in a perfect layered organization. Aerobic phototropic microbes colonize the upper layer of the mat, whereas in the deepest layer anaerobic bacteria are the predominant species.[10] Furthermore, the continued growth of microbial mats can lead to the formation of biogenic crusts due to production of a protective layer of calcite on their surface. When this degree of contamination is reached, their removal process becomes much more complex.

Another common morphological form of patinas is due to the combination of previously discussed black crusts with microbial contaminants. In fact, as stated before, thanks to their grater porosity and the presence of organic matter, black crusts are a suitable substrate for bacteria, lichens or black fungi.[9]

Causes and mechanisms of biodeterioration

Stone artifacts are the most common heritages handed down today from ancient times. In particular, the most diffused stone materials used in the construction of monuments and other heritages are typically calcareous (marble and limestone) or siliceous (sandstone and granite) materials. These materials differ greatly in their

intrinsic properties, such as alkalinity, porosity and hardness. As stated before, these characteristics added to environmental conditions favor the growth of microbial contaminants on the stone surface and or in its porous structure, causing different physical and chemical alterations. For instance, roots and hyphal systems, in addition to allowing the anchoring of biocontaminants on the artifact surface, are usually involved in physical damages.[10,11] In fact, by settling and expanding in the stone porosity and in microfractures, they lead to the formations of cracks both on the surface and inside the artifact. The same effect can also be observed for all microorganisms growing within the porous structure of the substrate as observed for the concealed microbial growth, a phenomenon described in the previous section. Another physical decay induced by microbial contaminants on the stone works of art is represented by chromatic alterations, a phenomenon due to the deposition of xenobiotics pigments on the surface of the substrate.[10]

Chemical damages induced by microbes are mainly referred to mineralogical alteration due to the production of metabolites capable of dissolving or chelating the mineralogical components of the stones leading to their solubilization. In this regard, all the biological contaminants described above produce organic acid metabolites, the deposition of which leads to the sequestration of cations from the minerals or to the corrosion of the constituent materials of the substrate by acidolysis:[6]

$$(\text{Mineral}^-)\,M^+ + H^+X^- \longrightarrow H^+(\text{Mineral}^-) + M^+R^-$$

$$X^- = NO_3^-;\ RCOO^-;\ HCO_3^-;\ SO_4^{2-}$$

Furthermore, since bacteria and cyanobacteria are involved in the nitrogen or sulfur cycles, they can oxidize hydrogen sulfide and ammonia to sulfuric and nitric acids, respectively. These two strong acids, after the acidolysis reaction with the stone constituent, will form hygroscopic salts that, accumulated into the stone porosity, lead to the well-known decay from salt efflorescence. In addition sulfuric acid can also be involved in the formation of biogenic gypsum crusts.[11]

C 3.1.3 Removal of biological patina from stone surfaces

The aesthetic and structural maintenance of works of art is an essential point to be respected during any restoration intervention. In this regard, the cleaning procedures of biological colonizers are a delicate and risky process through which the microbial contaminants must be completely removed without altering the treated substrate. To respect this dogma, before any kind of intervention, the study of the stone substrate, microorganisms and interactions between substrate and cleaning agents must carried out.

The most common techniques employed for the removal of biological colonizers from stone heritages, both novel and classic, can be divided into mechanical, physical and chemical methods.

Physical-mechanical methods

Mechanical techniques involve the application of scalpels, spatulas or abrasive particles accelerated towards the stone surface. These methods are widely diffused for the removal of biopatina from stone materials; however, their application is commonly associated with strong peeling effects and causes of stone alteration. Although classified separately, mechanical techniques are generally included in the physical class of treatments as hard methods just for their high abrasive action. Softer physical treatments include microwave heating system, laser and ultraviolet radiation. These treatments are generally considered soft due to the absence of contact between the cleaning agent and the substrates. However, they are no longer safe with works of art because they can induce pigment and substrate surface alterations, thus affecting both the structure and the aesthetic appearance of the artwork.[11,12] Rivas and coworkers tested the effectiveness of laser cleaning methods (soft) with respect to the abrasive action of a scalpel followed by brushing (hard), a common procedure used to remove biopatina from granite heritages. This comparative study was performed on lichen-contaminated granite specimens treated with Nd:YVO_4 laser at a wavelength of 355 nm and with the classic abrasive

technique. Figure C 3.4 shows the cross section of the samples, analyzed by scanning electron microscopy, before and after the treatment with the laser sources, the scalpel and their combination.

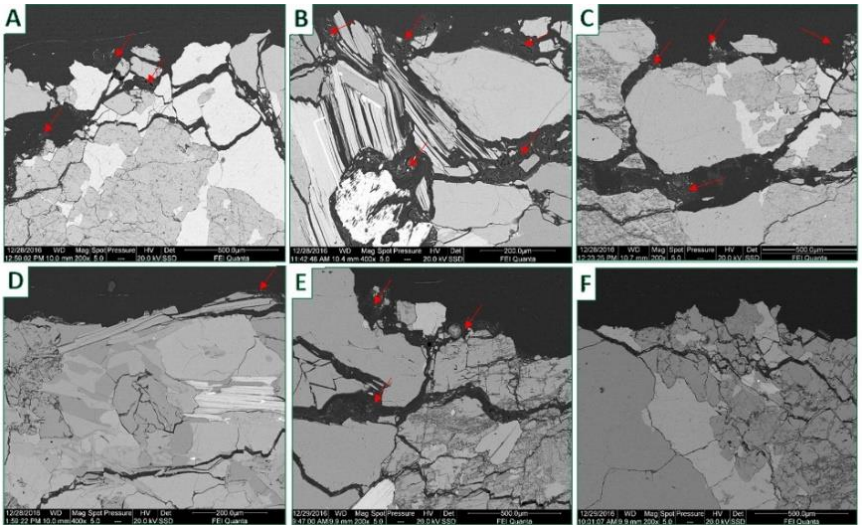

Figure C 3.4: Cross-section of treated granite samples originally contaminated by different lichen species (A-C P. pseudocorallinas and D-F P. amara). A and D sample treated with Nd:YVO_4 laser; B and E treated with scalpel; C and F treated with both methods. The red arrows highlight the residual lichens.

Lichen removal through laser cleaning was only partially observed. The effectiveness of this cleaning method appeared to be related to the taxonomy of lichens. In addition, depending on the laser source, an alteration of the granite samples can be induced, usually due to the degradation of the biotite inclusions. Nevertheless, this new cleaning method proved to be more effective and less aggressive than the traditional treatments.[13]

Chemical methods

Chemical treatments addressed to the inhibition or the removal of biofilms from the surface of stone heritage are performed using bioactive substances, called biocides. These chemicals are classically applied on the artifact as a solution and, interacting with their constituents, are capable to inhibit microbial growth or to degrade microorganisms.[14] Biocides can be classified according to their nature as organic and

inorganic as reported in Table C 3.1, which lists the most common commercial and new biocides.

Table C 3.1: List of some most common substances classified as biocide. both commercially available and novel; represent a mixture of different compounds.

	CLASS	BIOCIDE	STRUCTURE
		ORGANIC	
SYNTHETIC	Organometallic salts	Tri-n-butyl tin oxide	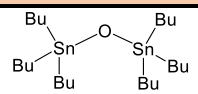
	Heterocycles	Hexazinone	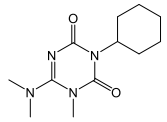
	Quaternary ammonium salts	Benzalkonium chloride	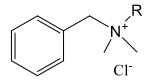
NATURAL	Essential oils	*Mentha piperita L.* *Origanum majorana L.* *Lavandula sp.*	mixtures of different compounds
	Organic acids	Pelargonic acid	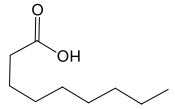
		Zosteric acid	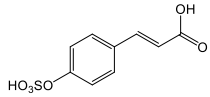
	Alkaloids	Capsaicin	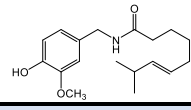
		INORGANIC	
	Oxidizing agents	Hypochlorous acids and its salts Hydrogen peroxide Titanium dioxide Zinc oxide	HClO NaClO; $Ca(ClO)_2$ H_2O_2 TiO_2 ZnO

As reported in the table, organic biocides are commonly divided into synthetic molecules and natural extracts, while the main used inorganic bioactive molecules are oxidizing agents.[15,16] Another distinction between biocide must be made on the basis of their mechanism of action against microorganisms; some of them interfere with the metabolic activity of the microbes while others, such as oxidizing agents, damage or degrade cellular components.[15]

The extent of the effectiveness of bioactive substances compared with hard and soft physical cleaning methodology is provided by Mascalchi and coworkers.[17] They evaluated the effectiveness in removing biodeteriogens (lichens and biofilms) from sandstone and marble, the constituent materials of some tombs located in the English Cemetery in Florence. The degree of contamination was assessed before and after the treatment with abrasive techniques, localized microwave heating system (LMW) and the commercially available biocide ROCIMA™ 103 composed of a concentrated mixture of 2-octyl-2H-isothiazolin-3-one and didecyldimethylammonium chloride in propan-2-ol and formic acid. The authors argued that although the biocidal treatment shows better results than the physical treatment, repeated cycles of LMW can be considered safer for the heritage and the environment. In fact, despite biocides are commonly used in restoration interventions due to their typical high efficiency against biodeteriogens, their application can lead to several complications.

Regardless of their nature, biocides must be applied homogeneously on the surface of the stone heritage in order to obtain the same efficiency over the entire treated surface and to avoid degradation phenomena due to high local amounts of biocide. To allow a homogeneous dispersion it is often necessary to use dangerous organic solvents. Moreover, the use of biocides often involves the deposition of hygroscopic salts and side products in the porosities of stone materials leading to well-known degradation phenomena.[18] These undesirable products can be transported within the porous matrix of the stone substrate and, in addition to causing the phenomenon of salt efflorescence, they could act as a source of carbon favoring fungal contamination.[19]

Novel biocidal systems

A growing number of research groups are recently turning their attention to the development of technologies and systems applicable in the field of cultural heritage with the aim of reducing the impact of classical procedures. In fact, nowadays it is

essential to adopt safer products for works of art and operators as well as for the environment. With particular regard to cleaning interventions, the use of new technologies to implement the classical bioactive chemicals and treatments is receiving considerable interest. For instance, the bioactivity of some ionic liquids (ILs) has recently been evaluated as a function of their structure on microbial strains typical of stone, highlighting the crucial role played by the hydrophobic behavior of anion, dodecyl benzyl sulfonate (DBS), and cation, derivatives of cholinium. The selected ILs have been tested on mixed stabilized microbial suspensions calcareous stone specimens. By increasing the lipophilicity of the IL constituents, the biocidal activity of the ionic liquid seems to increase. This effect can be explained by considering the lower wettability of the substrate induced by the hydrophobic behavior of the ILs, a parameter that plays a crucial role in biodeterioration phenomena.[20]

Recently controlled biocidal delivery systems based on the application of mesoporous silica has been developed. MCM-41 mesoporous silica characterized by a large volume of specific pores organized in hexagonal structures have shown good properties as chemicals releaser. Moreover, through proper functionalization of MCM-41, the biocide retention can be increased, leading to a more controllable system. Dresler and coworkers recently studied this system in the field of cultural heritage in order to develop systems capable of slowly releasing commercial biocidal products. They compared the release behavior of the commercial biocide from MCM-41 and its functionalized derivatives, one with carboxyl groups and the other with amino ones, observing the lowering of the biocide release (MCM-41 > MCM-41-COOH > MCM-41-NH_2). Nevertheless, applying the unfunctionalized mesoporous silica loaded with 0.75 % of Biotin T (a commercially available biocide) on the contaminated stone fragment, a strong reduction of the viable bacterial count, of about 99.2%, has been observed.[21]

Other recent advances in the application of biocides are the employment of photoactivable nanoparticles added to the matrices of protective coatings

commonly applied on the stone surface.[20] For this purpose, zinc and titanium oxides (ZnO and TiO_2) have been used to develop a protective coating capable of inhibiting the microbial growth, preventing biodegradation and decay. Zinc oxide and titanium dioxide, applied on calcareous specimens, show very promising inhibitory properties against *Aspergillus niger* and, in addition, ZnO has also proved to be a good inhibitor of *Penicillium sp.*. [22,23]

C 3.1.4 Role of hydrogels in cultural heritage cleaning

Cleaning processes are probably the most risky and irreversible intervention for precious works of art that can lead to future undesirable effects. For instance, common treatments applied in the removal of dirt from paintings mainly involves organic solvents and/or brushing agents. Unfortunately, these classic cleaning processes usually lead to the swelling and leaching of the structural constituents, thus damaging the artifact. In this regard, several research groups addressed increasing attention to the reduction of these common side effects commonly ascribed to cleaning treatments.

If on the one hand the replacement of classic treatments with safer and more controllable chemicals can be considered a promising alternative, on the other hand the controlled application of cleaning agents using thickeners or gelators can lead to very powerful results thanks to the combination of both chemical and soft mechanical actions. Since the early 90s, supporting materials were applied to cultural heritages to increase the efficacy of typical cleaning products, reducing their possible degradative effects.

The application of organic solvents for the removal of hydrophobic contaminants was often performed with wax-solvent paste in order to reduce solvent penetration and surface alteration. Moreover, cellulose and its derivatives have been covered for an important long-term role as hydrophilic thickeners to which suitable chemicals, selected on the basis of contamination, were added.[24] An example is reported by Baglioni and coworkers who developed a gelling system composed by

polyethylenimine for the removal of degraded varnish from a painted wooden sculpture dating back to the 18th century. Using this gelled system, based on polyethylenimine as a thickening agent (gelator) and 1-pentanol as continuous phase, the varnish was successfully removed from the artefact surface avoiding the side effect encountered with the classic treatments.[25]

As also described in Chapter A 1, hydrogels nowadays play an important role in several fields and, thanks to their intrinsic properties, such as easy encapsulation and transport of chemicals through their three-dimensional network, they can be very promising materials applicable in conservation interventions of cultural heritages.[26-29]

The combination of biocidal effect and soft mechanical action is probably the main advantage of biocide-based hydrogels. In addition, the longer biocide-surface contact time allows to reduce the amount of biocide. At the same time, being a surface treatment, all the side effects due to the penetration of the cleaning agents and the by-products can be avoided, thus reducing the undesirable effects commonly associated with classic treatments.

The works presented in the following sections are part of a wider project focused on "Product and process innovation for maintenance, preservation and sustainable programmed restoration of cultural heritage" (Smart Cities and Communities and Social Innovation on Cultural Heritage project). It aimed at investigating the chemical and physical interactions between restoration products and biodegraded calcareous stones, on the one hand, and at searching for alternative systems to minimize their impact on the building materials, the environment and operators, on the other. In particular, novel approaches to reduce microbial colonization from stone materials using oxidant biocidal agents, supported in alginate hydrogels were proposed. This gel matrix greatly improves the efficacy of the biocide, increasing its action time, allowing its use in low amounts and overcoming the drawbacks associated with its application as aqueous solution.

C 3.2 Alginate-biocide hydrogel for the removal of biofilms

One of the main problems encountered during the removal processes of microorganisms is represented by the concomitant presence of several species that can form a biological patina. In this sense, chemical treatments involving widespread biocides can be applied to counteract the proliferation of biological species. As reported by Faimon and coworkers, oxidant agents such as hydrogen peroxide and sodium hypochlorite are low cost and powerful biocides capable of effectively eradicating the most common microbial species, degrading the organic matter of which they are composed through the reaction represented below:

$$(CH_2O)_n + 2n\ OX \longrightarrow nCO_2 + nH_2O + 2n\ RED$$

in which $(CH2O)_n$ is a hypothetical form of organic matter and OX is an oxidant species capable of transferring one electron reducing itself to the RED species.[30]

Although these chemicals show a good biocidal power, they can also be very aggressive towards the substrate surface, the operators' health and the environment.[11] In particular, when these biocides are applied as an aqueous solution, some by-products remain on the surfaces leading to a degradative effect such as salt efflorescence or corrosion of the artefact surface.[18]

In this first part of the work, a viscous alginate hydrogel supporting hypochlorite ions was optimized. Adhesion of the gel to the stone surface could allow both to decrease the amount of biocide agent, as its action times were prolonged, and to apply it on vertical surfaces, thus reducing the dangerous side effects of this biocide. In this way a powerful biocide agent, no longer used for its negative effects both for human health and for the artwork, was applied to remove biofilms from calcareous stone surfaces reducing its quantity but keeping its cleaning capacity unchanged.

Before applying the optimized hydrogels "*in situ*", it was necessary to test them on substrates as similar as possible to the real cases, to determine any modification of the treated surfaces. Lecce stone is of high interest for stone conservation studies because it is one of the main construction materials of historical Baroque buildings

in southern Italy which undergoes noticeable aesthetical and structural decay problems, mostly related to biofouling and chemical pollution.

As stone items can absorb or release water, their properties are largely affected by environmental moisture content. Water is also the principal degradation agent for materials vulnerable to moisture and air pollutants.[31] Therefore, the knowledge of their response to environmental conditions and their capillary properties is essential for testing their conservation state, for planning appropriate conservation activities and for determining the durability and efficacy of cleaning, consolidation and/or protective treatments.

In this view, NMR relaxometry techniques are particularly useful, especially if working with a surface probe that can guarantee a non-destructive approach.[32,33] The distinctive features that make the NMR technique sensitive to confined state of water rely on the differences in dynamics and magnetic interactions that molecules experiment near a pore wall with regard to the bulk.[33] In fact, NMR relaxation can give information on chemical and geometrical properties of the confinement surface, on the hydration degree of the matrix itself, and even on porosity and pore-size distribution when the porous media are fully water-saturated.[34-37]

C 3.2.1 Materials and Methods

Lecce stone calcarenite samples of approximately 5×5×2 cm^3, composed of 93-97% calcium carbonate and a porosity of about 35%, with two Gaussian pore size distribution centered at 0.5-4 μm and 0.1-0.2 μm respectively,[38-40] were purchased from DÉCOR, Monteroni (LE), Italy.

Induced biofouling of stone samples

Three samples were stored as references, while the others were subjected to biofouling and/or differently treated. All samples were kept at room temperature and RH = 40% until moisture content stability, and then weighed to define the zero point (W_0).

The biological colonization was induced by soaking the stone samples in a glass chamber, containing backwater added with fertilizers ($Mg(NO_3)_2$, K_2HPO_4 and $(NH_4)_2CO_3$ at about 1 wt% each) and exposed to the sunlight to favor the growth of microorganisms, which was evaluated every week until different colonization levels were achieved.

The specimens were labeled as 'LS' followed by '0' for the three reference stones and by "1", "2" and "3" for stones, three samples each, with increasing biofouling. The time of incubation, which depends on the season, was about 1-2 months for LS1-B (low degree of biodegradation), about 3 months for LS2-B (moderate degree of biodegradation) and more than 6 months for LS3-B (high degree of biodegradation).

The identification of phototrophic microorganisms forming the artificially induced biofilms on the Lecce stones has been carried out by direct microscopy observations of the patina present on the specimens. Moreover, in order to better identify the colonizing microorganisms, the biofilms grown on the stone specimens were also inoculated on nutrient media, BG11[41] and observed after 1 month of growth.

The samples were observed with a Zeiss AxioScope light microscope (40x; acquiring images with a Canon EOS 600D) and also with IXplore SpinSR SoRa + ScanR (AI) Super Resolution Confocal Live Cell Imaging combined with High-Content Imaging System with Deep Learning AI and the identification performed following the current taxonomy.[42,43]

Preparation of alginate-biocide hydrogels and cleaning procedure

Alginic acid sodium salt from brown algae with low viscosity (characterized as described in the Section B) and calcium hypochlorite were purchased from Sigma-Aldrich. We used all reagents and chemicals as received.

Different formulations were designed and tested by varying the amounts of alginate and calcium hypochlorite to obtain hydrogels with adequate consistency and effectiveness. Two different biocide hydrogels were optimized:

Biocide-1: Sodium alginate (5 wt%) and $Ca(ClO)_2$ (0.4 wt%)

Biocide-2: Sodium alginate (5 wt%) and $Ca(ClO)_2$ (1 wt%)

Sodium alginate (5 g) was dissolved in 80 mL (alginate-1) or 50 mL (alginate-2) deionized water at nearly 1000 rpm at 25 °C. A 2 wt% $Ca(ClO)_2$ solution in 1.5 wt% glacial acetic acid was prepared and 20 mL and 50 mL were slowly added to alginate-1 and alginate-2 to obtain Biocide-1 and Biocide-2, respectively. The $Ca(ClO)_2$ solution was added using a burette, under vigorous stirring to obtain a more homogeneous hydrogel.

The appropriate hydrogel, chosen depending on the degree of biofouling, was applied to the specimen with a brush, inserting a cotton gauze and left for about 12 h until it dried. The use of a gauze facilitated the removal of the dry gel, leaving no residue on the stone surface and without affecting the biocide action of the gel. The cleaning treatment was applied to all the three samples for each level of colonization.

The hydrogel has to be used within around 24 h as its biocidal activity decreases over time. Hypochlorite, in fact, is consumed by oxidizing the matrix of alginate, also causing the gel to lose its consistency.

For comparison purpose, two more low colonized samples (LS1-B) were progressively cleaned with an aqueous solution of 2.5% ClO^- to determine the minimum amount of hypochlorite solution required to achieve the same cleaning effect obtained with Biocide-1.

Photographic and stereomicroscopic images

To assess the degree of biodegradation of stone materials and the effectiveness of hydrogel treatments, preliminary digital photos were taken with Canon EOS 1300D. Moreover, microscopic images were achieved using a Leica S8APO stereomicroscope equipped with EC3 in reflecting mode, which allows to examine even thicker, non-measurable samples through transmission microscopes, as in the case of our samples.

Colorimetric measurements

We performed color measurements using a Konica Minolta Chroma Meter CR-5 (Minolta, Osaka, Japan) equipped with D65 illuminator on the reflectance setting with a 30 mm aperture. For each sample, color analyses were fulfilled on three different points, covering 75% of total surface, in SCE mode with a 10° standard observer. The colorimetric parameters in CIELAB color space were determined according to UNI EN15886:2010.[44] For the sake of completeness L*, C* and h* (CIELCh color space) parameters were also estimated: (chroma: $C^*=[(a^*)^2+(b^*)^2]^{1/2}$, hue: h=atan(b*/a*)).

Measurements of hygroscopic properties by NMR

The NMR equipment is a mq-ProFiler (Bruker, Italy), consisting of a surface probe and a portable electronic apparatus. The coil in use works at a Larmor frequency of 17.8 MHz, which can excite the sample up to a depth of about 2 mm and with a sensitive volume (x, y, z) of about 2 × 2 × 0.8 cm^3. We studied hygroscopic behavior of the samples under analysis thorough NMR transverse relaxation time (T_2) measurements during moisture[45] and water uptake[46], without removing the equipment from the dry condition up to saturation. Both NMR analyses were realized inside a glove box with controlled relative humidity levels to avoid samples dehydration.

We followed the moisture and water uptake experiments at fixed adsorption times varying from the dry condition (t_0) up to equilibrium moisture content at 90% RH and water saturation condition (t_{eq}), respectively. We performed the capillary water absorption according to UNI EN 15801:2009[47] each stone sample was placed on filter paper (1 cm thick and 9 cm in diameter), dipped in distilled water up to approximately 0.5 cm.

For the water capillary absorption kinetics, we put the air-dried samples in contact with the water source through the selected surface and the NMR instrument on the opposite face. In both experiments, water absorbed by the samples was checked by

weighing them before (W_0) and after (W_T) each T_2 measurement through the gravimetric ratio GR = (W_T - W_0)/W_0%. Figure C 3.5 shows the apparatus employed for the measurements.

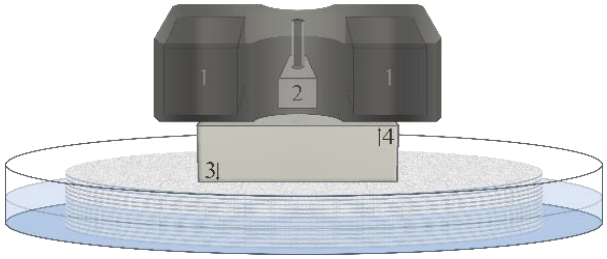

1 *Permanent magnet*
2 *RF coil*
3 *Absorbing surface*
4 *Measuring surface*

Figure C 3.5: Scheme of the kinetics of water absorption and of the ^{1}H-NMR apparatus.

We gained transverse relaxation data through the CPMG pulse sequence ($\pi/2$-τ_E-(π-τ_E-acquisition-τ_E-)$_n$) using the shortest half echo-time τ_E = 22μs to reduce the diffusion effect. For every measurement, it was necessary to acquire n = 2000 echoes to cover the entire relaxation curves. Moreover, each sequence was repeated every 2 s for 512 times to maximize the signal-to-noise ratio, within a reasonable measurement time (~ 15 min). The NMR signal decays were then Laplace inverted by using the algorithm UPEN (UpenWin, villiam.bortolotti@unibo.it) in order to obtain the T_2 distributions.[48] In the graphic representation of the data, the abscissa provides the relaxation time value and the ordinate the normalized spin density. The corresponding integral *i.e.* the extrapolated equilibrium magnetization, in arbitrary units, allows valuating the material's moisture content in the sensitive volume of the NMR surface probe.[49]

Preliminary "in situ" tests

Preliminary field tests, aimed at verifying the effectiveness of the optimized hydrogels, were accomplished inside the church of San Pietro Barisano, also called in Veteribus, the largest rupestrian church in the city of Matera (Figure C 3.6). In particular, attention was focused on a high relief decoration of the balustrade that separates the central nave from the right lateral chapel (red circle in Figure C 3.6) heavily colonized by green biofilms. A small sample was scraped off the surface

nearby the treated zone and observed at the light microscope to evaluate which biofilm-forming microorganisms were responsible of the colonization of the stone.

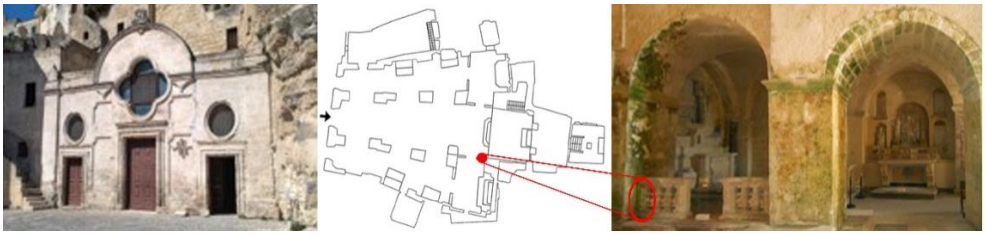

Figure C 3.6: On the left San Pietro Barisano Church (Matera); at center map of the interior of the church, on the right balustrade between central nave and right chapel with, in the red circle, the little stone statue, object of the on-site cleaning procedure.

C 3.2.2 Results and discussion

Alginate-biocide hydrogel

We developed hydrogels containing bioactive substances able to inhibit the growth of biological patina and to remove it from stone surfaces. Alginate hydrogels were prepared by adding an acidic solution of calcium hypochlorite to the polysaccharide solution, exploiting the abilities of calcium ions as crosslinking agents (details are reported in Materials and Methods section). The biocide agent was solubilized in an acetic acid solution to avoid capturing of atmospheric CO_2 and the subsequent precipitation of calcium carbonate. The composition of the gel was varied in terms of concentration of sodium alginate and calcium ions, to modulate its mechanical properties, and of biocide, to adjust its bioactive properties. Biocide-1 was suitable on low-biodegraded surfaces, while we used Biocide-2 when particularly resistant microorganisms were present on the stones.

Effects of alginate-biocide hydrogel on reference Lecce stone specimens

We fulfilled preliminary colorimetric tests to evaluate the side effects of the alginate-biocide hydrogel (Biocide-1) and of the oxidant agent (hypochlorite) in solution (2.5% ClO^- in water) once applied on reference Lecce stones. The amount of hypochlorite solution sprayed on the sample was empirically determined by evaluating its cleaning performance on a low-biodegraded sample LS1-B (see below).

Colorimetric measurements were accomplished on several specimens of reference stone (LS0), on the same stones after the application of hydrogel (LS0-T) and on samples treated with hypochlorite solution (LS0-S). Mean values of the chromatic coordinates of LS0, L*, a* and b*, were 80.7±0.5, 2.2±0.1 and 15.5±0.6, respectively. In Table C 3.2 the mean changes of colorimetric parameters between the reference (LS0) and the two set of treated samples (LS0-T, LS0-S) are reported with the corresponding color differences:

$$\Delta E^*_{ab} = \sqrt{\Delta L^{*2} + \Delta a^{*2} + \Delta b^{*2}} = \sqrt{\Delta L^{*2} + \Delta C^{*2} + \Delta H^{*2}}$$

Table C 3.2: Chromatic coordinates; mean changes of LS0-T and LS0-S samples with reference to LS0 one's and the corresponding color difference ΔE^*_{ab}.

	ΔL*	Δa*	Δb*	ΔC*	ΔH*	ΔE_{ab}*
LS0-T	0.1	-0.1	1.0	1.0	0.2	1.0
LS0-S	0.6	-0.2	1.9	1.8	0.7	2.0

The ΔE^*_{ab} values of LS0-T and LS0-S ($1 < \Delta E^*_{ab} < 2$) are both below the threshold perceived by the human eye (e.g. $\Delta E^*_{ab} \geq 5$).[50] Notwithstanding, the sample LS0-S, treated with the oxidant in solution, presents a ΔE^*_{ab} value that is twice that of the samples treated with the hydrogel, LS0-T. This effect is mainly due to an increase of the b* coordinate that establishes a prompting action in the yellow direction.

The T_2 signal amplitudes and values were measured to identify adsorbed water populations and their mobility inside the porous space of the stones. Therefore, by comparing the T_2 distribution profiles of untreated, biodegraded and cleaned samples, it was possible to study the effects of the cleaning operations on hygroscopic properties of porous structure.

The ^1H transverse relaxation measurements were performed on LS0, LS0-T and LS0-S samples at fixed adsorption times varying from the dry condition (t_0) up to equilibrium moisture content (t_{eq}) at 90% RH. As mentioned before, the single-sided probe was kept inside the glovebox where the samples were exposed to moisture adsorption to minimize changes in the sample's moisture content during NMR signal acquisitions. In Figure C 3.7 the kinetics of moisture absorption for the reference and

the treated samples (LS0-T and LS0-S) were compared. In addition, the figure also shows the comparison between the initial and equilibrium of water uptake for LS0 and LS0-T.

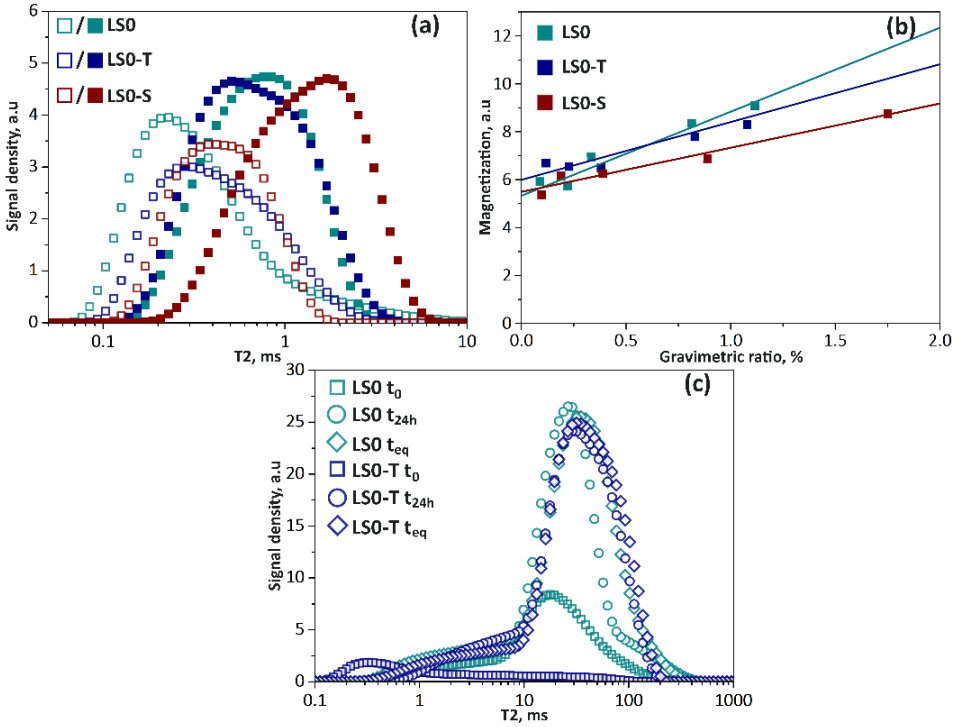

Figure C 3.7: a) Evolution from dry condition up to equilibrium moisture content at 90% RH of the ^1H T_2 distributions for the reference sample, LS0, and the treated reference samples, LS0-T and LS0-S. b) Time evolution of magnetization versus gravimetric ratio until the equilibrium moisture content is reached in reference and treated samples. c) Evolution from the dry up water-saturated condition of the ^1H T_2 distributions for the reference sample, LS0, and the treated sample, LS0-T. The signal decays have been acquired with the single-sided device from a layer of about 2 mm near the surface opposite to that in contact with the water source.

The T_2 distributions of the three samples, detectable only after twenty minutes of water sorption (Figure C 3.7a, open symbols), are narrowed at short T_2 values with a slightly peaked shape centered at nearly 0.3 ms. With increasing sorption time up to equilibrium moisture content at 90% RH, the ^1H signal density of LS0 and LS0-T (Figure C 3.7a, symbols ■ and ■) slowly raises, even if the T_2 distribution limits to T_2 times < 1 ms. These results suggest that the amount of water in both samples is

characterized by a rather low molecular mobility, as it is expected for molecules mainly adsorbed on pore surfaces.[45]

Differently, the T_2 distribution of LS0-S sample at increasing sorption times develops toward longer T_2 peak values, up to equilibrium values of about 3 ms (Figure C 3.7a, symbol ■) revealing the progressive evolution of larger volumes of mobile water inside the pores. This effect can be related to the presence of a hygroscopic salt within the stone material, which modifies the wettability mechanisms of the porous substrate.[45,51] It is reasonable to associate this outcome to the formation of hygroscopic calcium chloride from the hypochlorite solution.

Figure C 3.7b shows the linear relationship between the evolving equilibrium magnetization and the gravimetric ratio during water sorption (acquisitions at t_0, 1h, 4h, 24h, t_{eq}). While the gravimetric water content refers to the entire sample volume, the ^{1}H-NMR signal arises only from water absorbed within the sensitive volume of the single-sided probe. Therefore, data show that the water distribution throughout the sample, at surface and at inner regions remains continuously uniform.

At longer absorption times, the water amount in LS0-S is much greater than in the other samples. As the relationship between the evolution of equilibrium magnetization and of the gravimetric ratio is the same for all the samples, the hygroscopic salt in LS0-S spreads consistently inside the sample. Notwithstanding, it must be observed in Figure C 3.7b, the linear proportionality factor between magnetization and gravimetric data of LS0-S is significantly smaller than the one of two other samples. This effect suggests that part of the adsorbed water in LS0-S is NMR undetectable. It is to notice that, as liquescence goes on, crystallization water becomes part of inner solvation shells of salt ions to which it tightly bounds, and therefore, it still remains invisible to NMR detection.[45]

The water uptake kinetics in the sensitive volume was then followed over the course of time, ranging from dry up to water-saturated condition, without interrupting the

absorption process, simply by keeping the device on the opposite surface to that in contact with the water source.

In LS0 sample, within the first hour of absorption (Figure C 3.7c, symbol □), signal amplitude is present at shorter relaxation times (T_2 in the range 1÷10 ms), which can be assigned to the smallest pores and/or from larger pores only partially water filled.[46] On the contrary, in LS0-T sample, (Figure C 3.7c, symbol □) within the first hour of absorption no meaningful signal amplitude is detected near the unwetted surface, except a small signal amplitude at the shortest detectable relaxation times (T_2 ~ 1 ms).

This result proves that, initially, the capillary rise of water in LS0-T sample scales down by the apparent presence of hydrophobic residual products and is limited to water molecules mainly adsorbed on pore surfaces. However, after few hours of absorption, the water molecules encounter a way through the hydrophobic barrier and can occupy the pore volume available at regular pressure. In fact, after 1 day of absorption (Figure C 3.7c, symbols ○ and ○), both the signal amplitudes increase, and the distributions are shifted towards greater values of transverse relaxation times. With time, the amount of water near the analyzed surface builds up, and larger pores are gradually filled. The shift to larger relaxation times reflects the progressive ingress of water in pores previously only partially filled until the equilibrium condition (Figure C 3.7c, symbols ◇ and ◇).

Induced biofouling of Lecce stone specimens

Lecce stone samples were subjected to biodeterioration for different times to get three different degrees of biofouling: LS1-B (low biodegradation), LS2-B (moderate biodegradation) and LS3-B (high biodegradation). The images of the samples obtained with the stereomicroscope at two different magnifications are shown in the first two rows of Figure C 3.8. Although the main surface of LS2-B presents a moderate biodegradation (see Figure C 3.10a), in the stereomicroscope image shown in Figure C 3.8 (4X) the most colonized area has been magnified.

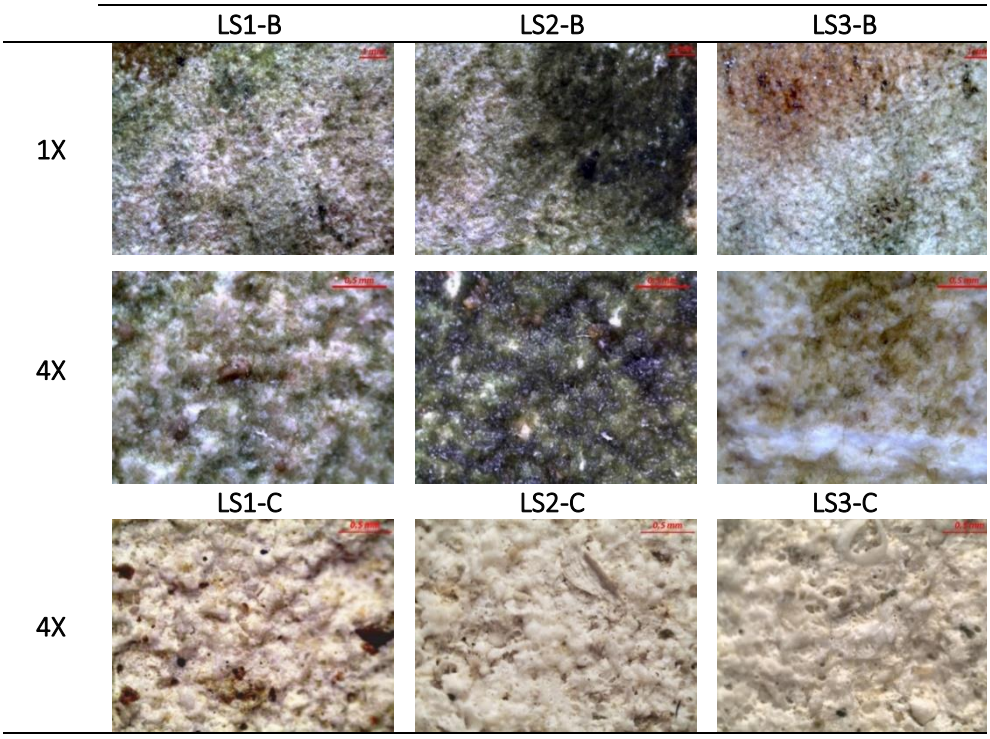

Figure C 3.8: Stereomicroscope images of LS1-B (low biodegradation), LS2-B (moderate biodegradation) and LS3-B (high biodegradation) samples with magnification 1X and 4X, respectively. Third row: Cleaned samples, LS1-C, LS2-C and LS3-C, with magnification 4X.

In presence of light, the first colonizers of lithic surfaces are phototrophic microorganisms, responsible of the discolouration of the stone. Besides the aesthetic problem, the growth of photosynthetic biomass provides extracellular organic matter reach in carbohydrates and nutrients that favours the growth of heterotrophic microorganisms (bacteria, fungi, lichens and mosses) and their biodeterioration activities. We can consider these biofilms as a complex community formed by photoautotrophic and heterotrophic microorganisms, all embedded in an extracellular polymeric matrix that allowed their survival on the stone but contributes to the decay of the substrata.[52]

The observations carried out at the microscopes, both on the biofilms scraped off by the specimens and on the microorganisms grown on the nutrient media, showed the presence of two main groups of colonizing microorganisms (Figure C 3.9). In particular, the artificially induced biofilm was formed by filamentous Cyanobacteria

belonging to the order *Oscillatoriales*, genus *Leptolyngbya* sp., along with green microalgae belonging to the phylum Chlorophyta, order *Chlorellales*, genus *Chlorella* sp. These phototrophic microorganisms are very common colonizers both on outdoor and indoor stone monuments with the cyanobacteria playing a pivotal role in the colonization of the substratum due to their ability to produce extracellular polymeric substances that stabilize and favour the adhesion of the biofilm.[52-54]

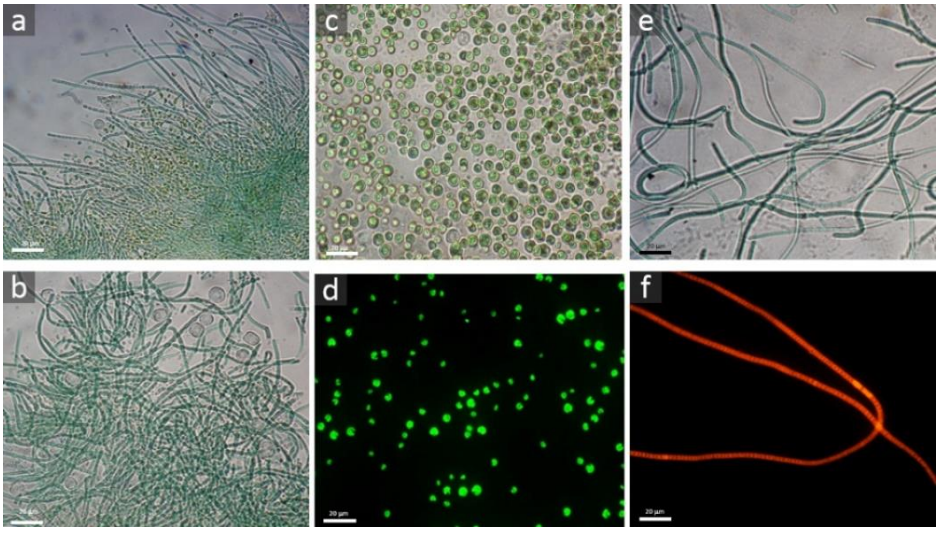

Figure C 3.9: Images of the biofilms scraped off the stone samples showing the presence of filamentous cyanobacteria along with green microalgae (a) and fungal spores (b); the observations of samples grown on nutrient media confirmed the presence of green microalgae of the genus Chlorella sp. (c, d) and cyanobacteria of the genus Leptolyngbya sp. (e, f). The green microalgae (d) and the cyanobacterium (f) present autofluorescence thanks to the photosynthetic pigments, useful for the characterization of the microorganisms; bars = 20 μm.

From LS1-B to LS3-B we observed the transition from a patchy appearance to a more homogeneous covering. The three types of colonized stones varied in amount of cover, but the microorganisms responsible for the colonization were the same independently from the time of exposure.

Effects of alginate-biocide hydrogel on biodeteriorated Lecce stone specimens

We used Biocide-1 to clean the low-biodegraded sample, LS1-B, and it proved effective to completely remove the biopatina from the surface of the sample, as can

be seen from the stereomicroscope image reported in the third row of Figure C 3.8. As partially described previously, samples that present a low biodegradation were cleaned with an aqueous solution of 2.5% ClO^- and to reach a complete removal of the microorganisms from the stone, an amount of oxidizing agent about 10 times higher than that present in the hydrogel Biocide-1 should be employed. Thus, the presence of the biocide inside the hydrogel network permits the use of a lower concentration of oxidizing agent since the adhesion of the gel to the stone surface allows a longer contact time with the microbial contaminants and limits the absorption of water by the stone.

Biocide-1 was then applied on LS2-B sample (Figure C 3.10a), in which some areas were more colonized, as showed in Figure C 3.8 (magnification 4X). As a result of this treatment, some green spots remained in the treated area, indicating that some microbial species were resistant to the biocide action (Figure C 3.10b).

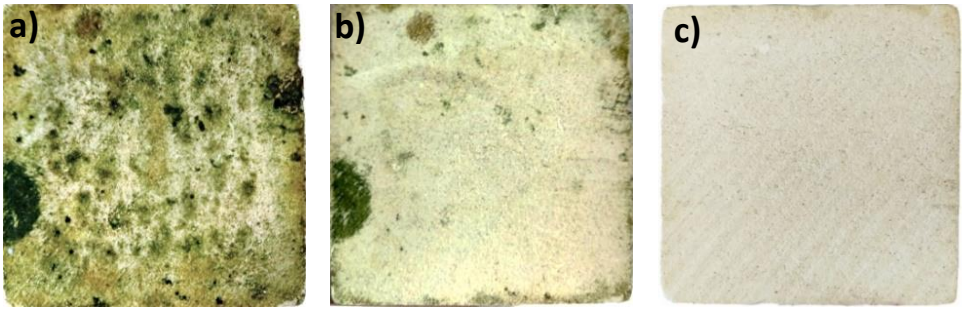

Figure C 3.10: Photographs of a) LS2-B (moderately biodegraded specimen) and LS2-C, the cleaned sample, after: b) a first treatment with Biocide-1, c) a second treatment with Biocide-2.

To check whether this resistance was imputable to the concentration of oxidizing agent, we used the Biocide-2, containing 1 wt% $Ca(ClO)_2$ to clean the LS2-B stone surface. The treated surface was then totally cleaned as can be observed from Figure C 3.10c and from the stereomicroscopic image reported in the third row of Figure C 3.8. Biocide-2 was also adopted for the cleaning of highly colonized stones (LS3-B) and, in this case, a single treatment was enough to get the complete removal of the biopatina from the stone surface (Figure C 3.8). These results illustrate that the two

optimized hydrogels are effective in eliminating microorganisms from the stone surface and that the amount of the oxidizing agent to be added in the hydrogel is dependent on the extent of biocolonization. In Table C 3.3 we reported the mean changes of colorimetric parameters between the reference, LS0, and the three cleaned samples set (LS1-C, LS2-C and LS3-C), along with the corresponding color differences, with values of ΔE^*_{ab} always lower than 1.

Table C 3.3: Chromatic coordinates; mean changes of LS1-C, LS2-C and LS3-C samples with reference to LS0 one's and the corresponding color difference ΔE^*_{ab}.

	ΔL*	Δa*	Δb*	ΔC*	ΔH*	ΔE_{ab}*
LS1-C	0.2	-0.2	0.7	1.0	0.3	0.8
LS2-C	0.1	-0.1	0.9	0.9	0.3	0.9
LS3-C	0.6	-0.2	0.2	-0.2	0.2	0.6

The T_2 profiles acquired during the water uptake from the dry (t_0) up to water-saturated condition (t_{eq}) of the two sets of data LS1 and LS3 are reported in Figure C 3.11 a and b respectively. The T_2 distributions at the initial stage and in equilibrium condition of the reference sample LS0 was added for comparison.

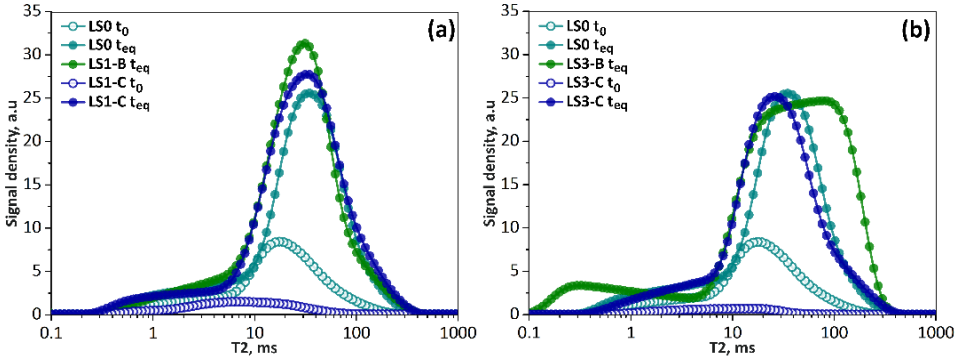

Figure C 3.11: ^1H T_2 distributions from dry up water-saturated condition for the reference sample, LS0, and the two sets of samples a) LS1 and b) LS3. The signal decays have been acquired with the single-sided device from a layer of about 2 mm near the surface opposite to that in contact with the water source.

For both data sets, we didn't perform NMR acquisitions for the dry biodegraded samples, *i.e.* LS1-B and LS3-B, since the drying procedure could modify the natural status of the microorganisms. At water saturation condition the LS1-B profile in

Figure C 3.11a (symbol ●) is very similar to the corresponding LS0 one, even if a larger integral value is clear. Indeed, in Table C 3.4, where magnetization and gravimetric values are listed, its magnetization results ~15% greater.

Concerning the LS3 set, the main differences arise by comparing the equilibrium profiles LS0 t_{eq}, LS3-B t_{eq} and LS3-C t_{eq} (symbols ● , ● and ● in Figure C 3.11b) and the data in Table C 3.4. The high biodegraded sample exhibits a T_2 profile more large-scale than that of the reference sample. The biofouling increases the water content on the surface of the sample and both magnetization and gravimetric ratios increase over 30% of the corresponding values of LS0. Notwithstanding, the effects of the cleaning procedure on LS3-B are eye-catching. The T_2 distribution of LS3-C shows a drastic reduction of the water content at water-saturation condition and its profile returns to the characteristics of T_2 distribution of LS0. In particular, magnetization (M) and gravimetric ratio (GR) of LS3-C are equal to LS0 values within the experimental errors (< 5%) as can be observed in Table C 3.4.

Table C 3.4: Magnetizations in dry (M t_0) and water saturation condition (M t_{eq}) of the reference stone LS0, LS1 and LS3 samples, -B (biodegraded) and -C, (cleaned) and gravimetric ratios of the same samples.

	M t_0	M t_{eq}	GR
LS0	17.7	59.7	19.6
LS1-B	-	68.1	20.5
LS1-C	4.4	63.8	19.2
LS3-B	-	80.4	26.0
LS3-C	1.9	58.2	19.3

On-site application of alginate-biocide hydrogel

The final phase of the Smart Cities project involves testing new products or different application methods of long-standing ones, on stone buildings belonging to “Sassi of Matera” (UNESCO World Heritage Site). In the case of Matera, several papers discussing biodeterioration phenomena and biocide treatments were produced. Among them, studies on rupestrian churches in Matera, focused their attention on the “Crypt of the Original Sin”, an excellent example of rock art.[55,56]

The site identified for our preliminary tests, aimed at evaluating effectiveness of the optimized formulations, was a section of an altar rail in the rupestrian Church of San Pietro Barisano, a perfect example of the "Sassi of Matera" peculiar architecture, which presented a green biofilm mainly composed of green microalgae and some filamentous cyanobacteria, thus very similar to the phototrophs colonizing the Lecce stones used for lab tests.

Many differences emerged comparing laboratory tests with field tests. Unlike the laboratory conditions, the rupestrian environment is characterized by hard microclimates such as high relative humidity, capillary rise, water infiltration and poor ventilation. The main drawback of these surroundings is that the quarry stone surfaces are wet with moisture content, measured with a contact hygrometer, over 90%. The effectiveness of Biocide-1 was firstly assessed on a small portion of the sculpture. The high surface moisture of the stone prevented the complete drying of the hydrogels, even after 24 h. Nevertheless, the biocidal activity remains unchanged and only one application was adequate to remove the biopatina. A thermo-convector was used to dehydrate the gel and remove it completely from the statue's surface. We then applied this new cleaning procedure to the entire surface of the stone relief and the various stages of our cleaning intervention are reported in Figure C 3.12.

Figure C 3.12: Different phases of the application and removal of Biocide-1.

The application of Biocide-1 was very promising with the removal of the phototrophic biofilms from the stone surfaces. More researches need to be carried

out to evaluate if the biocides developed are effective also against bacteria and fungi that have been often detected as responsible of stone biodeterioration also in Matera churches.[57]

C 3.2.3 Conclusion

In this first part of the work, alginate hydrogels containing hypochlorite ions, as biocide agent, were applied to Lecce stone specimens artificially colonized by cyanobacteria and green microalgae. We reproduced different degree of colonization on stone samples under laboratory conditions and developed two main formulations, which differ in active chlorine content, capable of removing microorganisms from the stone surface.

The effectiveness of cleaning treatment was assessed by optical microscopy observations, colorimetric and NMR relaxation measurements, which revealed the efficacy of the hydrogels on the biodeteriogens and the absence of interference with the substrates, in terms of chromaticity and capillary properties.

This cleaning approach allowed us employing an inexpensive biocide agent, such as hypochlorite, since its side effects are bypassed by its entrapment in the gel network. The adhesion of the gel on the stone surface, and then the extended action times, enabled the use of a very low concentration of oxidizing agent to get the complete removal of the biopatina. Finally, the biocidal activity of the alginate hydrogel at lower biocide concentration (BIOGEL-1) was successfully tested on a “real case”, a little stone relief of a balustrade in the rupestrian Church of San Pietro Barisano in the “Sassi of Matera”, confirming the potentiality of the cleaning treatment.

C 3.3 Improvement of oxidative alginate-biocide hydrogels

The results previously described showed that the developed alginate-hypochlorite hydrogels were able to eliminate microbial contaminants from the stone surface. Moreover, unlike what was observed after the application of the oxidant in solution, the chromaticity and capillary properties of the cleaned stones were very similar to

the untreated ones. The entrapment of biocide in the alginate network allows a reduction of the amount of oxidizing agent by about ten times than in aqueous solution and therefore the side effects. The adhesion properties of the hydrogel on the stone surface, which extend the treatment time, prevent the penetration of hygroscopic salts within the stone material and limit the well-known side reactions of the hypochlorite ions.[30] However, the oxidative action of hypochlorite ions also acts on the alginate structure by fluidifying the gel and causing the rapid loss of its biocidal activity, limiting the applicability of this biocidal product, which must be used within the first hours of its preparation.

In this regard, this second part of the work was aimed to the replacement of the hypochlorite salts with other oxidant biocides capable of exerting a more controllable oxidizing action being also not aggressive towards the substrate. For this purpose, we selected two oxidant species: titanium dioxide (TiO_2) and sodium dichloroisocyanurate (NaDCC).

The photocatalytic oxidation performed by the first compound has a great potentiality, being an effective process for removing and reducing biofouling on stones. When irradiated, the photocatalytic particles are in direct contact with or close to microorganisms, hence they are the primary target of the initial oxidative attack.[58] TiO_2 is one of the main photocatalysts used in paints, cements, or in other products for its sterilizing, deodorizing and antifouling properties.[59] Compared to other semiconductors, superior electronic properties, photostability, low-cost manufacturing, non-toxicity and environmental friendliness make TiO_2 a suitable candidate for cleaning and coatings of cultural heritage.[23,60-63] However, the efficiency of TiO_2-based nanocoatings strongly depends on the porosity and roughness of the substrate, which can be greatly reduced especially when applied on building materials of cultural heritage. In fact, to avoid the anesthetic appearance, it is necessary to use them in low amounts that may not be enough to clean the stone support and slow down the proliferation of microorganisms.[65]

Concerning the other oxidative biocide, the slow decomposition reaction of NaDCC can allow to moderate the amount of free hypochlorous acid in the hydrogel, as shown below:

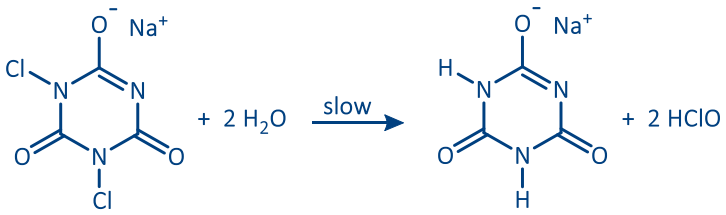

Therefore, the side reactions responsible for the loss of hydrogel stability, observed using hypochlorite salts, should be drastically reduced. A comparative study between sodium dichloroisocyanurate and sodium hypochlorite highlighted their similar bacteriostatic and bactericidal activity.[65] Furthermore, Clasen and Edmondson proposed NaDCC tablets as an alternative tool to the classic hypochlorous salts for the treatment of domestic drinking water, since, even if less available compared to hypochlorite salts, it is safer and has better dosage capacity.[66]

We evaluated the effectiveness of the hydrogels containing the two different biocides for the treatment of Lecce stone samples biodeteriorated with an artificially induced biofilm formed by filamentous cyanobacteria and green microalgae, characterized in the previous part of the work (paragraph C 3.2).

Digital photos and stereomicroscopic images were firstly taken to evaluate the efficacy of the treatments on the substrate surfaces and colorimetric tests were performed to evaluate any color variations compared to the untreated samples. SEM/EDS analyses were executed to verify the presence of any hydrogel or biocide residues on the stone support. NMR analyses were then carried out to assess the hygroscopic properties of the porous space of the stone before and after the biofouling and cleaning procedures.

C 3.3.1 Materials and Methods

Alginic acid sodium salt from brown algae (low viscosity), sodium dichloroisocyanurate dihydrate and calcium chloride anhydrous were purchased

from Sigma Aldrich; titanium dioxide was obtained from Degussa in the form of anatase photocatalyst P25 (nanocrystalline anatase with surface area of 50 m^2/g and a particle size of about 20 nm). For the activation of TiO_2, a Philips TL 6W BLB wood lamp with an emission range between 340 and 400 nm was used. Lecce stone calcarenite samples of approximately 5×5×2 cm^3, composed of 93-97% calcium carbonate and a porosity of about 35%, were purchased from DÉCOR, Monteroni (LE), Italy. Sodium alginate low viscosity and the Lecce stone samples come from the same batch used in the first part of this work.

Induced biocolonization of stone samples

Three calcarenite samples were stored as references (identified by label LSR), while others were subjected to biocontamination (identified by LSB) and/or differently cleaned (identified by LSC).

As previously described (subparagraph C3.2.1), we carried out the biofouling by soaking the stone samples in a glass chamber, containing backwater added with fertilizers ($Mg(NO_3)_2$, K_2HPO_4 and $(NH_4)_2CO_3$ at about 1 wt% each) and exposed to the sunlight for about 3 months to favor the growth of microorganisms.

The phototrophic microorganisms forming the artificially induced biofilms on the Lecce stones were identified in filamentous cyanobacteria and green microalgae as main components.

Hydrogel preparations and applications

Hydrogels were prepared by dispersing sodium alginate in distilled water under vigorous magnetic stirring at room temperature. When a homogeneous solution was formed, the biocide was added. For what concern sodium dichloroisocyanurate as biocide, a solution obtained by mixing NaDCC and calcium chloride was added dropwise to the alginate solution, while in the case of titanium dioxide it was dispersed as a powder directly in the sol system, and the resulting suspension was crosslinked with calcium chloride solution, added drop by drop. A homogeneous crosslinking was obtained by vigorous magnetic stirring. Different hydrogel

formulations were designed by varying the amounts of alginate, calcium ions and biocides (NaDCC or TiO_2).

All the biocidal hydrogels (BIOGELs) were applied on the stone surface with the aid of a cotton gauze to facilitate their removal and after approximately 24 h the dried gels were removed from the stone surface. The effect of the gel composition on biodegraded Lecce stones was evaluated to find the optimum cleaning procedure for both the hydrogels.

Viscosimetric analysis

To evaluate the stability in terms of consistency of the biocidal hydrogels, viscosimetric measurements were performed using Fungilab Viscolead ADV "L" rotational viscosimeter every day for one week. In this regard, the viscosity trend over time of the hydrogel formulations developed in the first part of this work (Biocide 1 and 2), the new formulations (BIOGELS) and the hydrogels prepared without biocide (only for TiO_2 and NaDCC) was compared. All samples were stored at 4°C and the viscosity values were taken at 25°C.

Photographic and stereomicroscopic images

To assess the degree of biodegradation of stone materials and the effectiveness of hydrogel treatments, preliminary digital photos were taken with Canon EOS 1300D. Moreover, microscopic images were achieved using a Leica S8APO stereomicroscope equipped with EC3 in reflecting mode.

Color variations

Colorimetric values of the analyzed samples were determined by using the CIELAB color space proposed in 1976 by the International Lighting Commission (CIE) (UNI EN 15886, 2010).[44] The color modification was calculated as previously described ($\Delta E^*_{ab}=\sqrt{\Delta L^{*2}+\Delta a^{*2}+\Delta b^{*2}}$) in order to evaluate the extent of the chromatic alterations and their possible perceptibility to the human eye ($\Delta E^*_{ab} > 5$).[50]

The Sama Tools SA230 portable colorimeter was used for colorimetric analyses; measurements were made in SCE mode with an 8° standard observer, light D65 (average daylight, including the UV region, with the relative color temperature of 6504 K). The instrument was calibrated with the white reference. The measurements were performed in reflectance and 25 points per sample were taken in order to cover an overall surface of 60%.

SEM/EDS analyses

Scanning electron microscopy in combination with energy-dispersive X-ray spectrometry (SEM/EDS) is a proven forensic tool and is used to analyze several kinds of trace evidence. The X-ray detector, or more specifically, the EDS technique is used to determine qualitatively, and more often "semi-quantitatively", the elemental composition of an area of interest.[67] To examine the surface topography and composition of the samples, Zeiss GeminiSEM 500 equipped with EDS OXFORD Aztec Energy with INCA X-ACT detector was used with a working distance of 8.5 mm and accelerating voltage of 15 KeV.

Measurements of hygroscopic properties by unilateral NMR

We studied hygroscopic behavior of the samples under analyses through NMR transverse relaxation time (T_2) measurements during water uptake.[46] The T_2 relaxation signal profiles and the equilibrium magnetization values can identify adsorbed water populations and their mobility. Therefore, by comparing the T_2 distribution profiles of untreated, biodegraded and cleaned samples, it is possible to study the effects of the biofouling and cleaning operations on hygroscopic properties of the lithotype porous structure.

The NMR equipment is the mq-ProFiler (Bruker, Italy), consisting of a surface probe and a portable electronic apparatus previously described. The kinetics of water uptake in the sensitive volume were followed over the course of time keeping the device on the surface opposite to that in contact with the water source, starting from dry up to water saturated condition (Figure C 3.5).

The capillary water absorption was performed according to the procedure described in the European Standard (UNI EN 15801, 2009);[47] samples were dried in oven at 40 °C until a constant weight was reached. Each stone sample was placed on filter paper (1 cm thick and 9 cm in diameter) and put in contact with the water source (dipped up to approximately 0.5 cm), through the selected surface, and with the NMR instrument on the opposite face. Details about the protocol used to determine the hygroscopic properties were previously reported (subparagraph C 3.2.1).

C 3.3.2 Results and discussion

Preparation of hydrogels

A preliminary study was performed to find the optimal conditions that would allow the cleaning of the Lecce stone samples.

Unlike the hydrogel described in the first part of this work, in which calcium ions, used as crosslinking agents, were added with the oxidizing biocide, in the form of $Ca(ClO)_2$, in this work they were added in quantities independent of each other. For both hydrogels the concentrations of alginate (2.5 ÷ 5.0%) and calcium ions (0.15 ÷ 0.3%) were ranged, in order to obtain a hydrogel with suitable properties, in terms of consistency and adhesion to the stone surface. In the case of hydrogel added with titanium dioxide, other parameters were changed: the concentration of TiO_2 (0.5 ÷ 2.0%), the distance of the sample from the light source (2 ÷ 16 cm), so that the intensity of the radiation reaching the surface was sufficient to stimulate the photocatalytic activity of titanium dioxide, and the irradiation time.

For what concern NaDCC, its concentration was ranged from 0.2 to 0.8%. Both resulting hydrogels were tested on biodegraded samples to find the optimal condition needed for the complete removal of the biopatina. The powerful effect was obtained with the following compositions:

BIOGEL-1: Sodium alginate (5 wt%), TiO_2 (2 wt%) and $CaCl_2$ (0.15 wt%)

BIOGEL-2: Sodium alginate (5 wt%), NaDCC (0.4 wt%) and $CaCl_2$ (0.4 wt%)

Samples treated with BIOGEL-1 must be place at a distance of 2 cm from the light source and irradiated with the wood lamp for 24 hours.

These new formulations, stored at 4 °C and, as regards BIOGEL-1, in the dark to avoid TiO_2 pre-activation, were tested over time to verify their effectiveness, and, after more than a week of storage, the two hydrogels retained both consistency and biocidal activity, overcoming the drawbacks encountered with hypochlorite-based hydrogels.

Stability of biocidal hydrogels

As previously described, the oxidative action exerted by the biocides is capable of degrade also the alginate matrix affecting the stability of the hydrogels both in term of biocidal activity and consistency. Viscosimetric measurements were performed to compare the stability of the new BIOGELs (1 and 2) and the hypochlorite-based hydrogels.

Table C3.5 shows the viscosity values measured for all freshly prepared hydrogels and their relative behavior in one week of storage. The table also displays the viscosities of alginate hydrogels prepared using the same calcium content of the two BIOGELs but without biocide; these gels, indicated as Alg-HG 1 and Alg-HG 2, are ionically crosslinked with 0.15 and 0.3% wt%, respectively.

Table C 3.5: Comparison between the viscosity of different freshly prepared hydrogel formulations (expressed in Poise) and the relative viscosity trend for each one hydrogel stored at 4°C for one week. This last parameter was taken as indicator of consistency.

↓Time (d)	Alg-HG 1	Alg-HG 2	Biocide 1	Biocide 2	BIOGEL 1	BIOGEL 2
η (P) t_0 →	139.6	1092.8	659.7	661.9	166.5	778.3
1	147%	97%	49%	53%	130%	86%
3	151%	75%	26%	10%	122%	60%
7	111%	66%	18%	2%	121%	31%

As expected, a rapid decrease in viscosity was detected for the two hypochlorite-based hydrogel formulations depending on the hypochlorite content. This evidence

highlights the already known rapid loss of consistency of Biocide 1 and Biocide 2. On the contrary, although the initial viscosity is lower, BIOGEL-2 shows a behavior similar to that of the hydrogel with the same calcium content and without biocide (Alg-HG 2). Furthermore, compared to Biocides 1 and 2 it always remains much more viscous.

An anomalous behavior was observed for the BIOGEL-1 formulation which, since its preparation, increases its viscosity by about double after one day. However, this effect, probably due to a better homogenization of the hydrogel at "rest", can be observed, to an almost equal extent, for its homologous formulation prepared without TiO_2. This evidence suggests that this effect is independent of the presence of the biocide. This hypothesis is also supported by the similar behavior of the two formulations (BIOGEL-1 and Alg-HG 1) observed after the first day of the test. After this time, in fact, the viscosity of both hydrogels remains unchanged until the seventh day of storage, when the viscosity values have decreased, reaching values approximately equal to the initial ones, of the freshly prepared hydrogels.

Photographic and stereomicroscopic images

The evaluation of the efficacy of the treatment was initially based on photographic and stereomicroscopic analyses on contaminated stones, before and after treatment, in order to evaluate both with macroscopic and microscopic vision the effectiveness of the cleaning treatments Figure C 3.13.

Figure C 3.13a shows the photographs of one of the reference stones (LSR), of two biodeteriorated stones, LSB-A and LSB-B, and, of the same two samples, after their treatment with, respectively, BIOGEL-1 (LSC1-A) and BIOGEL-2 (LSC2-B). These hydrogels proved to be very effective in removing artificially-induced biofilms on Lecce stone specimens. Moreover, thanks to the 4x magnification stereomicroscope images, shown in Figure C 3.13b, it is evident that both optimized hydrogels are able to remove the biopatina from the stone surface and that the cleaning was effective even for the microbial species present in the deepest pores.

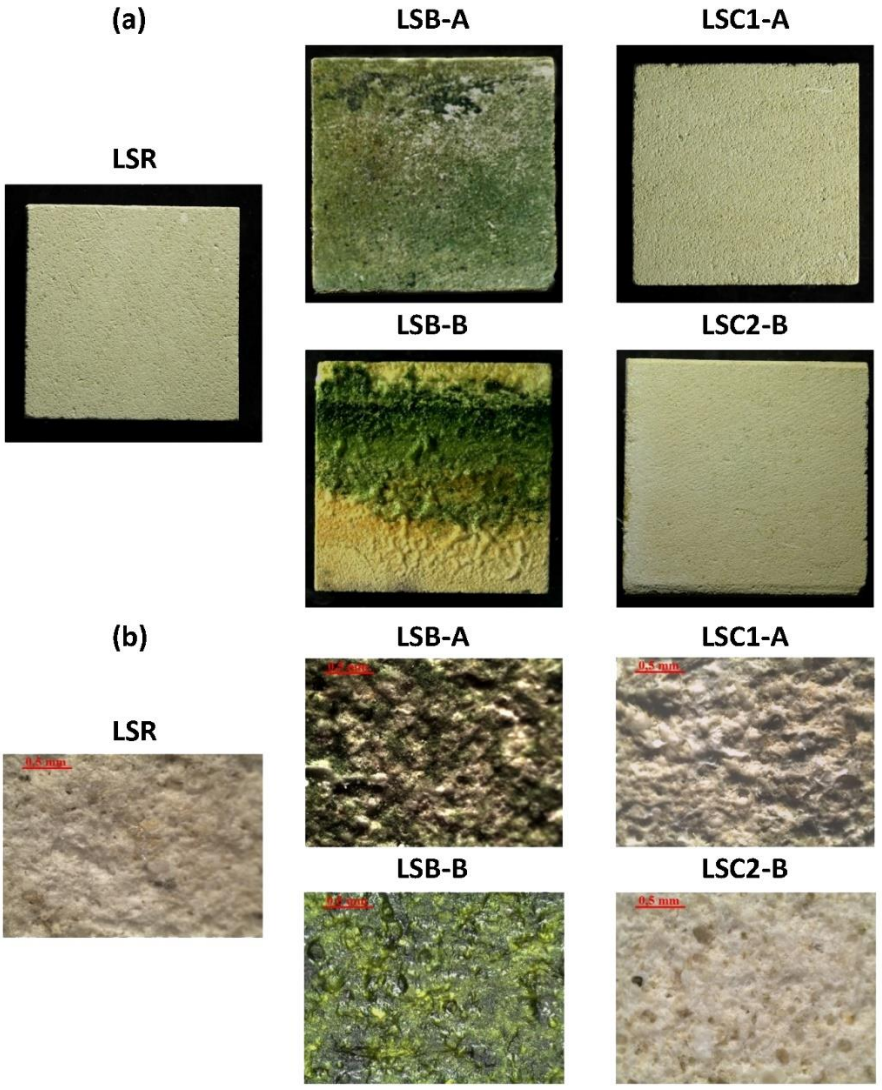

Figure C 3.13: (a) Photographs and (b) stereomicroscopic images (magnification 4x) of the reference LSR, biodegraded: LSB-A and LSB-B and cleaned: LSC1-A and LSC2-B samples, being LSC1-A and LSC2-B the stones cleaned respectively with BIOGEL-1 and BIOGEL-2.

Color variations

Biodeteriorated and treated Lecce stone surfaces were investigated in order to evaluate the color variations with respect to untreated samples.

As previously mentioned, the maximum allowed value of ΔE^*_{ab} is 5, otherwise for higher values there will be a variation in the perception of color by the observer with

unaesthetic consequences for the sample. Colorimetric measurements were performed on several Lecce stone specimens taken as references.

The average values of chromatic coordinates L*, a* and b* were respectively 80.5±0.5, 3.3±0.1 and 11.4±0.4. Table C 3.6 shows the mean changes of colorimetric parameters between the reference (LSR), biodegraded (LSB-A and LSB-B) and cleaned samples (LSC1-A and LSC2-B), along with the corresponding color differences, ΔE^*_{ab}.

Table C 3.6: Chromatic coordinates - mean changes of LSB-A, LSB-B. LSC1-A, LSC2-B with reference to LSR one's and the corresponding color difference ΔE^*_{ab}.

	ΔL*	Δa*	Δb*	ΔE^*_{ab}
LSB-A	-34±9	-4±3	-4±5	35±8
LSB-B	-36±6	2±5	15±4	40±4
LSC1-A	-0.8±0.3	-0.45±0.02	-0.5±0.4	1.06±0.04
LSC2-B	0.2±0.6	-0.7±0.2	-0.8±0.6	1.2±0.3

The ΔE^*_{ab} value of the both biodegraded samples, as expected, is very high but, after the treatments with the two different hydrogels, the ΔE^*_{ab} values of LSC1-A and LSC2-B, that are 1.06 and 1.2 respectively.

These results strengthen those obtained from the microscopic analyses, since the color difference between cleaned and reference samples resulted always well below the perceptible threshold of the human eye, indicating the safeguard of the color of the stone surface.

SEM and Elemental analysis

The SEM/EDS analyses were carried out on the reference sample, LSR, and on two stones treated with the two hydrogels to evaluate the possible presence of residues after the cleaning procedure.

Figure C 3.14 shows the SEM images of the untreated (LSR) and treated samples with BIOGEL-1 (LSC1-A) and BIOGEL-2 (LSC2-B) and the elemental analysis of some different areas selected for each specimen.

a) LSR

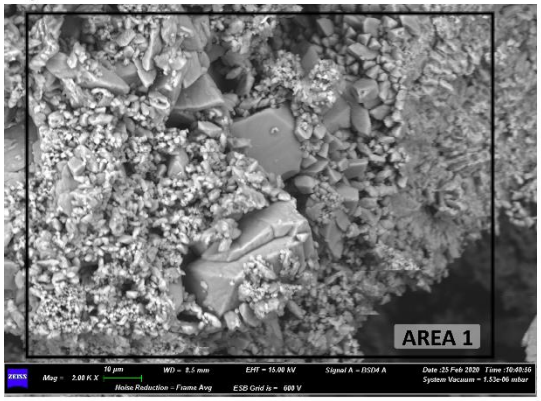

AREA 1	
	Wt%
O	50.0
Ca	38.3
C	10.0

b) LSC1-A

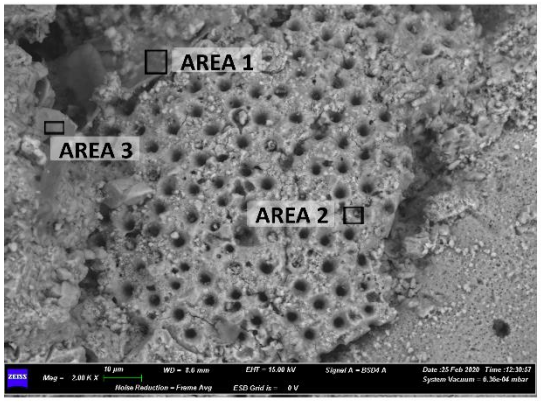

AREA 1		AREA 2		AREA 3	
	Wt%		Wt%		Wt%
O	47.4	O	55.7	O	47.6
C	22.0	Ca	31.7	C	22.3
Ca	18.2	C	11.2	Ca	20.7
Na	6.5	Ti	0.5	Na	4.2
Ti	3.9			Cl	3.1
Cl	1.6			Ti	0.8

c) LSC2-B

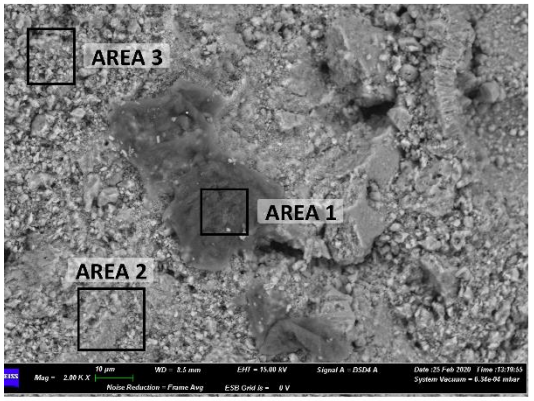

AREA 1		AREA 2		AREA 3	
	Wt%		Wt%		Wt%
O	32.4	O	50.0	O	49.6
C	31.9	Ca	38.3	C	36.3
Ca	17.5	C	10.0	Ca	8.1
Na	3.8			Na	0.9
Cl	3.7			Cl	0.8

Figure C 3.14: On the left, SEM images of the LSR (a), LSC1-A (b) and LSC2-B (c) samples, being LSC1-A and LSC2-B, the stones cleaned respectively with BIOGEL-1 and BIOGEL-2. On the right, the results of the elemental analysis, performed on some selected areas of the corresponding SEM image and underlined by black frames.

The image and elemental composition corresponding to Area 1, shown in Figure C 3.14a, relating to LSR, are typical of a calcarenite. On the other hand, images of the two treated samples (Figure C 3.14b and c) showed some matted areas, randomly distributed, deserving to be investigated through the local elemental analysis. Areas 1, 2 and 3 (Figure C 3.14b) correspond to three different examined zones of the Lecce stone sample treated with BIOGEL-1, LSC1-A. Low amounts of titanium were observed in the corresponding spectra, especially in the matted areas, highlighting the deposition of biocidal residues on the stone surface after the treatment.

Moreover, the elemental analysis in both Lecce stone specimens treated with BIOGEL-1 and BIOGEL-2, highlights non-negligible percentages by weight of sodium and chlorine and an increase in the relative carbon content compared to the LSR sample. The presence of these elements is attributable to small residues of hydrogel mainly located in the matted regions of Figure C 3.14b and c.

The deposition of biocidal residues inside the stone pores after the treatments, could not be considered a negative effect. First of all because very few residues were found on the entire surface of the analyzed sample. In addition, for what concern the presence of titanium dioxide, this is a side effect that cannot be considered unfavorable since titanium dioxide has been employed sometimes in the coating of stone cultural heritage to prevent the growth of microbial contaminants.[23,61,62]

Measurements of hygroscopic properties by Unilateral NMR

To study the effects of the biofouling and cleaning operations on hygroscopic properties of the lithotype porous structure, a set of T_2 profiles of all samples were acquired during the water uptake until the water-saturated conditions were reached.

In panels a and b of Figure C 3.15, the mean LSR data is reported and used to compare its behavior with those of the biodegraded (LSB, Figure C 3.15a) and the cleaned (LSC1 and LSC2 Figure C 3.15b) samples.

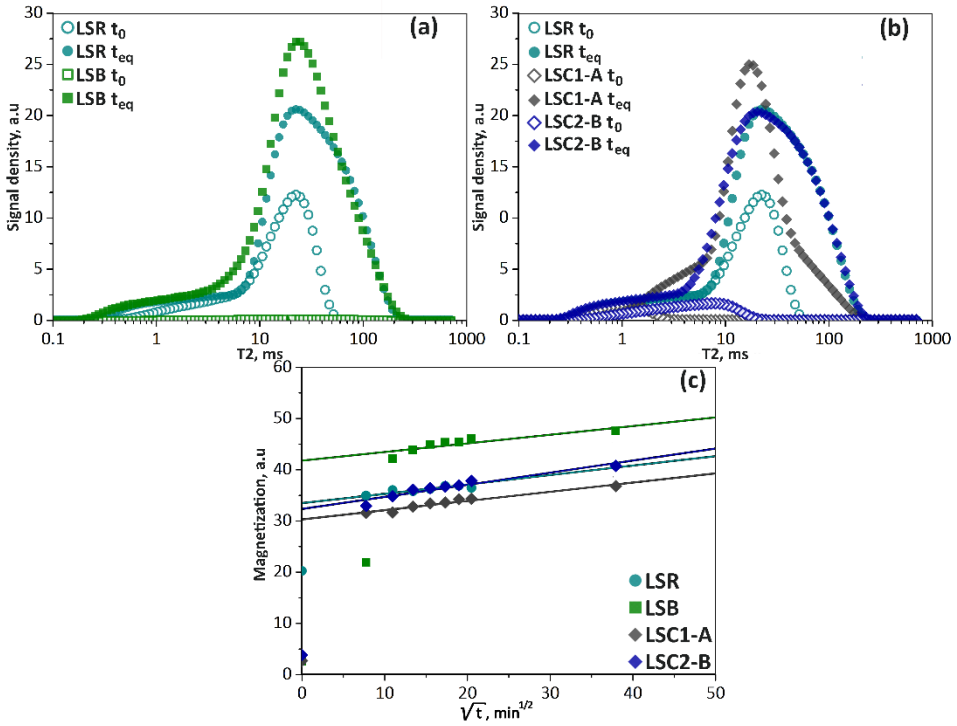

Figure C 3.15: T_2 distributions during water uptake, at dry (t_0) and saturation conditions (t_{eq}), for Lecce stones: (a) in reference, LSR, and biodegraded, LSB, samples; (b) in LSR and cleaned, LSC1 and LSC2, samples. (c) Magnetization evolution during the first day of water uptake in LSR, LSB, LSC1-A and LSC2-B.

Within the initial stage of LSR hydration, specifically at t_0 (symbol ○), the mean signal amplitude reveals a T_2 population in the range 1÷50 ms, which should be assigned to the small pores filled and/or from large pores only partially hydrated.[46] On the contrary, for the LSB samples, within the first hour of absorption (symbol □), no signal is detectable, indicating that microorganisms strongly affect the capillarity properties of the stone samples. After the cleaning treatment (Figure C 3.15b) with BIOGEL-1 (LSC1-A symbol ◇) and BIOGEL-2 (LSC2-B symbol ◇), an appreciable difference compared to the reference is observed. There is a lowering of the signal in t_0 curve attributable to the capillary rise inhibited by the presence of residual products, as evidenced also by SEM/EDS analyses, which slightly affect the surface porosity. At the end of water absorption, t_{eq}, the LSR's signal amplitude (symbol ●) increases and the distribution is shifted towards larger values of transverse

relaxation times because, in the course of water uptake, the amount of water near the analyzed surface increases, and larger pores are gradually filled. The saturation condition for LSB samples (Figure C 3.15a, symbol ■) shows a different behavior: the T_2 range is equal, but the corresponding magnetization values, that can be interpreted in terms of water content, override those of the reference sample.

In Figure C 3.15b, the saturation conditions for both stones treated with the two different hydrogels are compared with the reference one. While the curve of LSC1 (symbol ◆) appears shifted to lower value of relaxation time, sharp and higher than the reference, that of LSC2 t_{eq} (symbol ◆) overlaps the LSR profile.

The area under the T_2 distribution gives the total magnetization and, as we have just mentioned, it is proportional to the mass of water in the lithotype pore spaces inside the sensitive volume of NMR probe. Figure C 3.15c shows the magnetization evolution against the time square root for all the samples. The biodegraded sample (symbol ■) shows a different behavior of hydration compared to the reference (symbol ●). In fact, at lower absorption time, up to two hours of absorption, a clear delay is observed, after which the magnetization values of the biodegraded samples override those of the reference. After the treatment, with both the biocidal hydrogels, the hygroscopic behavior of the stone samples (LSC1-A, symbol ◆ and LSC2-B, symbol ◆), appears restored and comparable to the reference. However, for the sample cleaned with BIOGEL-1 a uniform drop of the time evolution of its magnetization confirms what previously discussed about the presence of titanium dioxide residues on the stone surface. The deposition of biocidal residues inside the stone pores after the treatments, highlighted by SEM/EDS analyses in both the cleaned samples, could justify the lower absorption rate observed in the first hour of the water uptake kinetics.

Despite the presence of hydrogel residues, NMR data ensured that the hygroscopic properties of the reference specimen were restored over time. The different shape of the curve at t_{eq} of LSC1-A could be due to the titanium particles (diameter ~ 25

nm), which, being placed in the largest pores, should decrease their internal volume, thus producing an increasing of porosity proper of shorter T_2.

C 3.3.3 Conclusion

With a particular attention to conservation and restoration of cultural heritage, in the last years we have addressed our attention to the improvement of classical chemical treatments towards their encapsulation in inert matrices. This technique can be used both to limit the problems ascribed to chemical treatments and to preserve the artwork integrity, operator health and environment safeguard.

Two main formulations of alginate hydrogels were prepared by replacing the less controllable hypochlorite ions, used in our previous work, with TiO_2 as photoactivatable biocide and NaDCC as reservoir of hypochlorous acid. The long-term stability of both hydrogels allowed us to use them successfully even a few days after their preparation, overcoming the problems of loss of consistency and effectiveness observed with hydrogels added with hypochlorite ions. Moreover, while TiO_2 dispersed in polymeric matrices has already been used on many stone materials to promote the degradation of biopatina and to create self-cleaning surfaces, this is the first work, to our knowledge, in which NaDCC is applied to remove biofilms from a stone surface and which can therefore be used in the field of cultural heritage. They were successfully tested to clean artificially biodegraded Lecce stones, with cyanobacteria and green microalgae being the main components of the phototrophic artificial biofilms. The effectiveness of the cleaning treatments was evaluated with different techniques, which revealed that the hydrogels not only completely remove the biopatina from the surface of the stone, but do not modify the chromaticity and capillary properties of the treated substrate.

References

1- P. Brimblecombe, "*Environmental assessment and monitoring of cultural heritage*" in "Science and Technology for the Conservation of Cultural Heritage", M.A. Rogerio-Candelera, M. Lazzari, E. Cano Ed., CRC Press, chap. 1, 1-4 (2013);

2- R.W. Le Maitre, A. Streckeisen, B. Zanrttin, M.J. Le Bas, B. Bonin, P. Bateman, G. Bellieni, A. Dudek, S. Efremova, J. Keller, J. Lameyre, P.A. Ssabine, R. Schmid, H. Sørensen, A.R. Woolley, "Igneous rocks a classification and glossary of terms", R.W. Le Maitre Ed., Cambridge University Press (2002);

3- V. Rives, J. García-Talegón, Materials Science Forum, **514-516**, 1689-1694 (2006);

4- O. Guillitte, The Science of Total Environmental, **167**, 215-220 (1995);

5- A.Z. Miller, P. Sanmartín, L. Pereira-Pardo, A. Dionísio, C. Saiz-Jimenez, M.F. Macedo, B. Prieto, Science of the Total Environment, **426**, 1-12 (2012);

6- Th. Warscheid, J. Braams, International Biodeterioration & Biodegradation, **46**, 343-368 (2000);

7- P. Tiano, Seminar article, New University of Lisbon, Department of Conservation and Restoration, 7-12 (2002);

8- A.C. Pinheiro, N. Mesquita, J. Trovão, F. Soares, I. Tiago, C. Coelho, H.P. de Carvalho, F. Gil, L. Catarino, G. Piñar, A. Portugal, Journal of Cultural Heritage, **36**, 275-285 (2019);

9- O.A. Cuzman, P. Tiano, S. Ventura, P. Frediani, "*Biodiversity of stone artifacts*" in "The Importance of Biological Interactions in the Study of Biodiversity", Pujol J. L. Ed., InTech, chap. 19, pp 367-385 (2011);

10- A. Negi, I.P. Sarethy, Microbial Ecology, **78**, 1014-1029 (2019);

11- M.A. Kakakhel, F. Wu, J. Gu, H. Feng, K. Shah, W. Wang, International Biodeterioration & Biodegradation, **143**, 104721 (2019);

12- P. Ortiz, V. Antúneza, R. Ortiz, J.M. Martín, M.A. Gómez, A.R. Hortal, B. Martínez-Haya, Applied Surface Science, **283**, 193–201 (2013);

13- T. Rivas, J.S. Pozo-Antonio, M.E. López de Silanes, A. Ramil, A.J. López, Applied Surface Science, **440**, 467-476 (2018);

14- K. Sterflinger, G. Piñar, Applied Microbiology and Biotechnology, **97**, 9637-9646 (2013);

15- F. Borderie, B. Alaoui-Sossé, L. Aleya, Environmental Science and Pollution Research, **22**, 4144-4172 (2015);

16- M.R. Fidanza, G. Caneva, Journal of Cultural Heritage, **38**, 271-286 (2019);

17- M. Mascalchi, C. Orsini, D. Pinna, B. Salvadori, S. Siano, C. Riminesi, International Biodeterioration & Biodegradation, **154**, 105041 (2020);

18- J.S. Pozo-Antonio, T. Rivas, A.J. López, M.P. Fiorucci, A. Ramil, Science of Total Environment, **571**, 1017–1028 (2016);

19- P.M. Martin-Sanchez, A. Nováková, F. Bastian, C. Alabouvette, C. Saiz-Jimenez, Environmental Science & Technology, **46**, 3762-3770 (2012);

20- S. Lo Schiavo, F. De Leo, C. Urzì, Applied Sciences, **10**, 6568 (2020);

21- C. Dresler, M.L. Saladino, C. Demirbag, E. Caponetti, D.F. Chillura Martino, R. Alduina, International Biodeterioration & Biodegradation, **125**, 150-156 (2017);

22- M.A. Aldosari, S.D. Darwish, M.A. Adam, N.A. Elmarzugi, S.M. Ahmed, Archaeological and Anthropological Sciences, **11**, 3407-3422 (2019);

23- M.F. La Russa, S.A.Ruffolo, N. Rovella, C.M. Belfiore, A.M. Palermo, M.T. Guzzi, G.M. Crisci, Progress in Organic Chemistry, **74**, 186-191, (2012);

24- N. Khandekar, "*Gelled system: theory and early applications*" in "Solvent gels for the cleaning of works of art", V. Dorge Ed., Getty Conservation Institute, chap. 1, 5-11 (2004);

25- P. Baglioni, L. Dei, E. Carretti, R. Giorgi, Langmuir, **25**, 8373-8374 2009;

26- S. Vicini, M. Castellano, M.C.F. Soares Lima, P. Licinio, G. Goulart Silva, Journal of Applied Polymer Sciences, **134**, 44726 (2017);

27- E. Boccalon, M. Nocchetti, M. Pica, A. Romani, K. Sterflinger, Journal of Cultural Heritage, in press, (2020); (https://doi.org/10.1016/j.culher.2020.07.008);

28- P. Baglioni, E. Carretti, D. Chelazzi, Nature Nanotechnology, **10**, 287-290 (2015);

29- P. Baglioni, D. Berti, M. Bonini, E. Carretti, L. Dei, E. Fratini, R. Giorgi, Advances in Colloid and Interface Science, **205**, 361-371 (2014);

30- J. Faimon, J. Štelcl, S. Kubešová, J. Zimák, Environmental Pollution, **122**, 417-422 (2003);

31- C. Hall, W.D. Hoff, Water Transport in Brick, Stone and Concrete, first ed., CRC Press, London, (2002);

32- B. Blümich, J. Perlo, F. Casanova, Progress in Nuclear Magnetic Resonance Spectroscopy, **52**, 197-269 (2008);

33- M. Baias, Magnetic Resonance in Chemistry, **55**, 33-37 (2017);

34- T. Watson, C.T.P. Chang, Progress in Nuclear Magnetic Resonance Spectroscopy, 31, 343-386 (1997);

35- C. Casieri, F. De Luca, L. Nodari, U. Russo, C. Terenzi, V. Tudisca, Journal of Applied Physics, **112**, 084904 (2012);

36- C. Terenzi, C. Casieri, F. De Luca, R. Quaresima, G. Quarta, V. Tudisca, Applied Magnetic Resonance, **46**, 1159-1178 (2015);

37- V. Di Tullio, D. Capitani, N. Proietti, Microporous and Mesoporous Materials, **269**, 180-185 (2018);

38- S. Bugani, M. Camaiti, L. Morselli, E. Van de Casteele, K. Janssens, X-Ray Spectrometry, **36**, 316-320 (2007);

39- S. Bugani, M. Camaiti, L. Morselli, E. Van de Casteele, K. Janssens, Analytical and Bioanalytical Chemistry, **391**, 1343-1350 (2008);

40- A. Calia, M. Laurenzi Tabasso, A.M. Mecchi, G. Quarta, Stone Historic Buildings, **391**, 139-156 (2013);

41- R. Rippka, J. Deruelles, J. Waterbury, M. Herdman, R. Stanier, The Journal of General Microbiology, **111**, 1-61 (1979);

42- J. Komárek, K.Anagnostidis, "*Cyanoprokaryota. 2. Teil: Oscillatoriales*", in "Süßwasserflora von Mitteleuropa", B. Büdel, G. Gärtner, L. Krienitz, M. Schagerl Eds., Elsevier GmbH, München, Bd. 19, pp. 1-759 (2005);

43- F. Leliaert, D.R. Smith, H. Moreau, M.D. Herron, H. Verbruggen, C.F. Delwiche, O. De Clerck, Critical Reviews in Plant Sciences, **31**, 1-46 (2012);

44- UNI EN 15886:2010. Conservation of cultural property - Test methods - Color measurement of surfaces;

45- C. Casieri, C. Terenzi, F. De Luca, Magnetic Resonance in Chemistry, **53**, 15-21 (2015);

46- V. Bortolotti, M. Camaiti, C. Casieri, F. De Luca, P. Fantazzini, C. Terenzi, Journal of Magnetic Resonance, **181**, 287-295 (2006)

47- UNI EN 15801:2009. Conservation of cultural property - Test methods - Determination of water absorption by capillarity.

48- G.C. Borgia, R. J. S. Brown, P. Fantazzini, Journal of Magnetic Resonance, **147**, 273-285 (2000);

49- C. Casieri, L. Senni, M. Romagnoli, U. Santamaria, F. De Luca, Journal of Magnetic Resonance, **171**, 364-372 (2004);

50- G. Vigliano, Graffiti and antigraffiti project [WWW Document]. http://www.icr.beniculturali.it. (2002);

51- M. Gombia, V. Bortolotti, R.J.S. Brown, M. Camaiti, L. Cavallero, P. Fantazzini, Journal of Physical Chemistry B, **113**, 10580-10586 (2009);

52- F. Rossi, E. Micheletti, L. Bruno, S.P. Adhikary, P. Albertano, R. De Philippis, Biofouling, **28**, 215-224 (2012);

53- L. Tomaselli, G. Lamenti, M. Bosco, P. Tiano, International Biodeterioration & Biodegradation, **46**, 251-258 (2000);

54- L. Bruno, D. Billi, S. Bellezza, P. Albertano, Applied and Environmental Microbiology, **75**, 608-617 (2009);

55- M.P. Nugari, A.M. Pietrini, G. Caneva, F. Imperi, P. Visca, International Biodeterioration & Biodegradation, **66**, 705-771 (2009);

56- G. Caneva, F. Bartoli, F. Imperi, P. Visca, Journal of Cultural Heritage, **40**, 59-68 (2019);

57- S.M. Mang, L. Scrano, I. Camele, Sustainability, **12**, 6988 (2020);

58- S.H. Lee, S. Pumprueg, B. Moudgil, W. Sigmund, Colloids Surfaces B: Biointerfaces, **40**, 93-98 (2005);

59- A. Maury-Ramirez, W. De Muynck, R. Stevens, K. Demeestere, N. De Belie, Cement and Concrete Composites, **36**, 93-100 (2013);

60- M.F. La Russa, N. Rovella, M. Alvarez De Buergo, C.M. Belfiore, A. Pezzino, G.M. Crisci, S.A. Ruffolo, Progress in Organic Coatings, **91**, 1-8 (2016);

61- L. Luvidi, A.M. Mecchi, M. Ferretti, G. Sidoti, International Journal of Conservation Science, **7**, 311-322 (2016);

62- G.B. Goffredo, S. Accoroni, C. Totti, T. Romagnoli, L. Valentini, P. Munafò, Building and Environment, **112**, 209-222 (2017);

63- N.T. Padmanabhan, H. John, Journal of Environmental Chemical Engineering, **8**, 104211 (2020);

64- E. Quagliarini, L. Graziani, D. Diso, A. Licciulli, M. D'Orazio, Journal of Cultural Heritage, **30**, 81-91 (2018);

65- I. Heling, I. Rotstein, T. Dinur, Y. Szwec-Levine, D. Steinberg, Journal of Endodontics, **27**, 278-280 (2001);

66- T. Clasen, P. Edmondson, International Journal of Hygiene and Environmental Health, **209**, 173–181 (2006);

67- E.J. Vermeij, P.D. Zoon, S.B.C.G. Chang, I. Keereweer, R. Pieterman, R.R.R. Gerretsen, Forensic Science International, **214**, 96-104 (2012).

Addendum I

Deep Eutectic Solvents

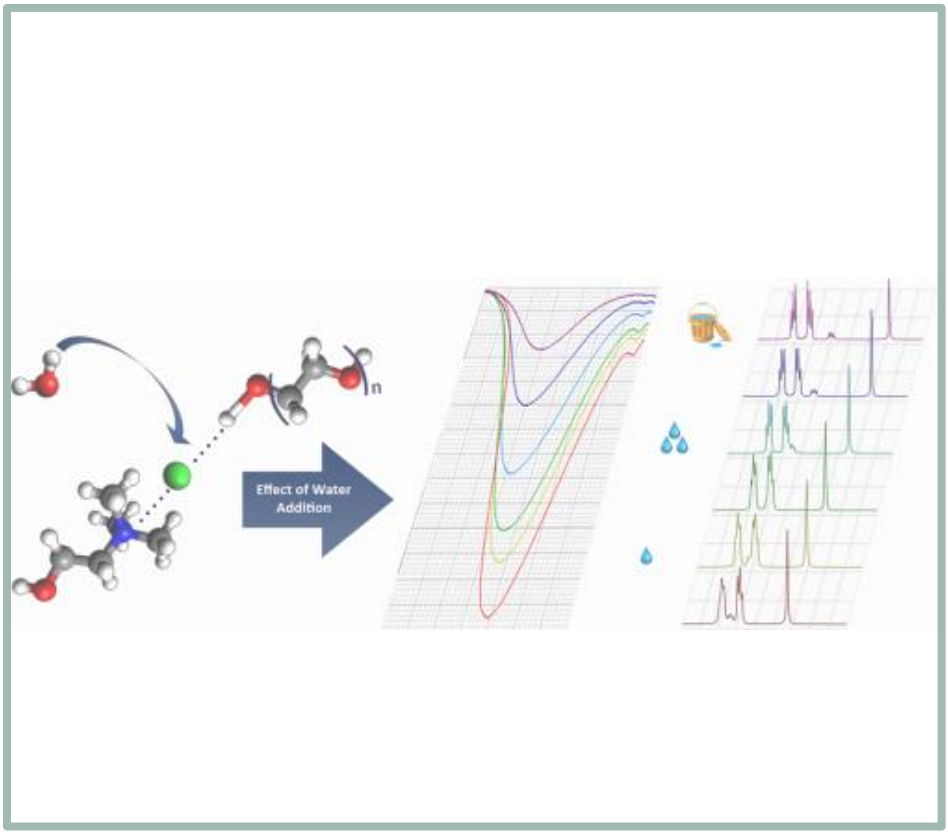

Addendum I

Deep eutectic solvents: a characterization study

In recent decades, even more attention has been paid to the environmental impact attributed to the use of classic solvents both in the academic and industrial processes. Since the 1990s, a growing series of laws and directives has been implemented by the world governments in order to reduce and regulate the use of solvents and other chemicals considered harmful to humans and the environment.[1] However, the role of solvents in chemistry is irreplaceable; they are adopted both as reaction media and in many other processes, such as purification, extraction and cleaning, in which they are used in very large quantities. In order to replace the classical solvents, often considered environmentally unfriendly, nowadays many new media can be found in the literature as a green alternative; starting from the solvents from renewable sources, usually obtained by the treatment of biomass, up to the supercritical fluids (SFs), liquid polymers (LPs), ionic liquids (ILs).[2,3] More recently, deep eutectic solvents (DESs) have emerged as very promising green alternative to the classical organic solvents.[4]

S 1.1 Deep eutectic solvents (DESs)

As previously described, many recent researches are addressed to the development of newer and safer solvent systems. In this field of research, increasing attention has been paid to deep eutectic solvents as a green alternative to the classic volatile organic solvent. They are formed by the mixture of two or more bulky constituents characterized by a low symmetry. In particular, the species involved in the formation of DESs are hydrogen bond acceptors (HBAs) and hydrogen bond donors (HBD) which form a liquid phase close to room temperature when mixed together in appropriate proportions.[5] Deep eutectic solvents can be described by the general formula $Cat^+X^- zY$, where Cat^+X^- is a salt that participates as the hydrogen bond

acceptor, while *zY* represents hydrogen bond donor, where *z* indicates the number of HBD functions or molecules. The hydrogen bond interactions established between the *zY* functions of HBD and the anion of the HBA salt (X^-) are responsible for the weakening of the lattice energy of the components and, as consequence, leads to the formation of molten eutectic. Figure S 1.1 lists some of the main employed components of DESs such as ammonium, phosphonium or sulfonium salts as HBA and neutral molecules with one or more hydrogenated functions capable of establishing hydrogen bonds such as HBD.[5-8]

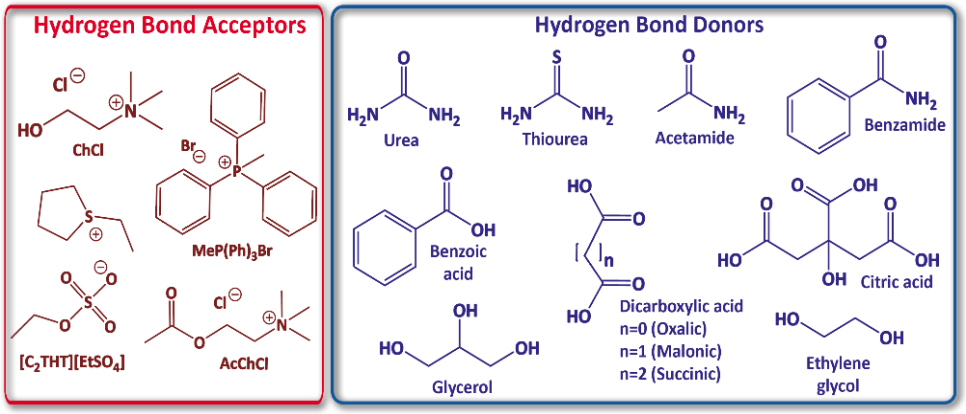

Figure S 1.1: Some of the main HBA and HBD employed in the formation of DESs

Many interesting properties of DESs turn out to be very similar to those exhibited by ionic liquids, such as low vapor pressure and non-flammability.[4,9] Despite there are some similarities, these two species are very different each other from a chemical point of view. On one side, the synthesis of ILs is generally expensive and require careful purification processes. On the other hand, the preparation of DESs cannot be properly defined "synthesis"; they are formed by mixing together the pure constituents under stirring and sometimes by heating the mixture. In fact, being a physical process, no reaction occurs between the constituents of the DES during its formation; therefore, the preparation of the deep eutectic solvent can be considered a waste-free process which does not require purification processes. In addition, the staring materials used for the preparation of DESs are usually inexpensive, biocompatible, biodegradable and much safer compared with those

used for the synthesis of ILs. Nonetheless, recent studies demonstrate that, depending on the nature and ratio of HBA and HBD, some eutectic mixture may show moderate toxicity.[10,11]

Thanks to their unique physicochemical properties and their eco-compatibility, deep eutectic solvents have attracted considerable interest from scientists. In fact, although their industrial applicability is still limited, DESs are widely applied in many fields of research. DESs play an important role in many extraction processes such as the separation of lignin from lignocellulosic waste[12] and of polyphenols from olive leaf.[13] These novel solvent can be used as reaction media not only as solvent or co-solvent but also as reactant and or as organocatalyst.[14,15] Eutectic mixtures were also employed in bioconversion reactions, using both immobilized and non-immobilized enzymes; however, the effect of DES on the catalytic properties of enzymes is not yet well understood and, therefore, much more studies are needed.[16] Moreover, a recent research highlight the good CO_2 absorption ability of deep eutectic solvents based on phenyl acetic acid compared to other analogues DESs prepared with carboxylic acids as HBD.[17]

The ever-growing interest in deep eutectic solvents lies also in the ease of tuning of their physicochemical properties which can be simply modulated by varying the nature of the components, their ratio and/or adding other components to the eutectic mixture.[8,11] Therefore, understanding of how the components of DESs interact with each other is the best way to fully explain their properties and how they can be tuned. For this purpose, many important information arose from both the phase diagram and the hole theory, a predictive method useful for rationalizing the ion mobility as well as for justifying the physicochemical properties of the studied system.

S 1.1.1 Phase diagram

When two components with different melting points are mixed together, the average melting temperature it can be expected to depend linearly on the

composition of the mixture. However, the melting point of a eutectic mixture is much lower than expected, as can be seen from the phase diagram of a binary eutectic showed in Figure S 1.2.

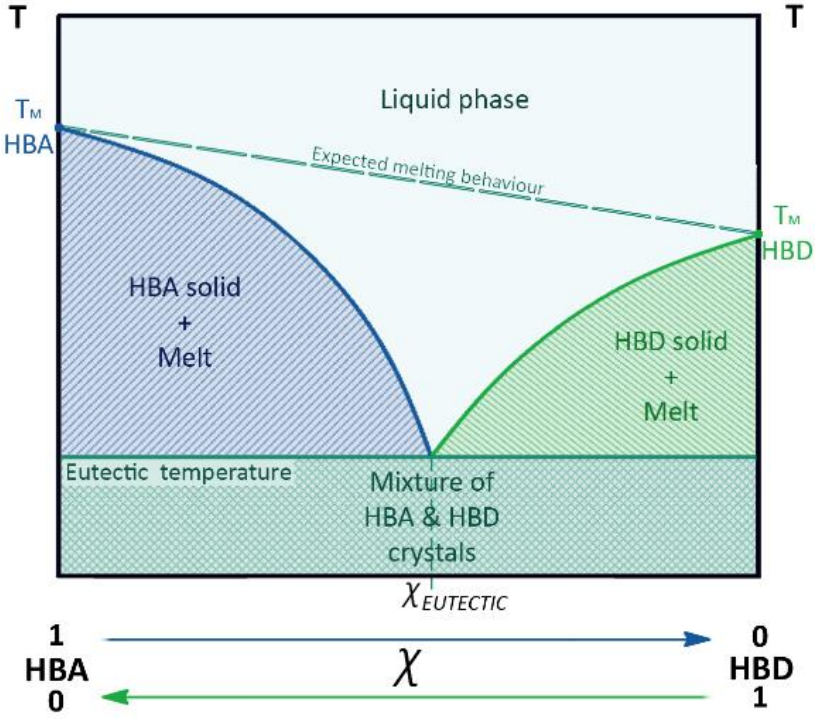

Figure S 1.2: Typical phase diagram of a binary deep eutectic solvent.

The entity of this difference in melting temperature is related to the magnitude of interaction established between the pure constituents.[8] By cooling the DES, three different behaviors can be observed; two of these occur when the HBA or HBD is in excess in the eutectic mixture ($\chi_{HBA}>\chi_{EUTECTIC}$ or $\chi_{HBD}>\chi_{EUTECTIC}$ respectively). Under these conditions, the species in greater amount will precipitate, separating from the mixture, while the liquid phase will be enriched with the other component. Only when the eutectic temperature is reached, the components will crystallize together. Otherwise, if the components are mixed in their eutectic composition ($\chi=\chi_{EUTECTIC}$), the components will solidify together when temperature drops below the eutectic one.[7,8,18]

S 1.1.2 Hole theory

The hole theory represents the most used method to understand and describe the ion mobility of ionic liquids and deep eutectic solvents in relation to the temperature of the system. This theory is based on the assumption that ionic materials are composed of deficiencies of variable size and position, defined as holes and caused by local density fluctuations of the liquid phase.

The average squared radius of these empty spaces is directly related to the temperature of the system and inversely proportional to its surface tension, as indicated in the following relation:

$$\langle r^2 \rangle = \frac{3.5kT}{4\pi\gamma} = \frac{3.5}{a}$$

where *k* indicates the constant of Boltzman, *T* is the absolute temperature, *r* represents the radius and *γ* is the surface tension of the liquid.[19]

An ion can only move when the adjacent hole has adequate dimensions to allow its movement. Ion mobility depends on both the size and the distribution of those empty spaces; thus, at a fixed temperature, the probability P of finding a hole of a given radius r can be determined as:

$$P\,dr = \frac{16}{15\sqrt{\pi}} a^{7/2} r^6 e^{-r^2}\,dr$$

The hole theory can be used to estimate viscosity and its variation as a function of temperature for both molecular and ionic liquid system. Being this property related to the ion mobility and assuming that the thermodynamic contribution of the formation of a hole can be neglected with respect to the probability of finding a suitable one, the viscosity can be easily estimated as shown below:

$$\eta = \frac{m\bar{c}}{2.12\sigma P(r > R)}$$

In this equation, m represents the molecular mass, $\bar{c}$ is the average speed of the molecular species, σ indicates the collision diameter of the molecule and P (r > R) represents the probability of finding a hole with a radius greater than that of the moving species.[19,20]

By applying this model to DESs it is possible to justify their high viscosity, since at room temperature there is a low probability of movement caused by the reduced size of the voids. Likewise, the charge transfer of an ionic liquid is closely related to the availability of the holes, which flow in the opposite direction with respect to the charged species. Electrical conductivity represents the measure of the ion mobility in a liquid system and, independently of the nature of the charged species involved, it is a physical property inversely related to viscosity. As previously stated, at room temperature there is a very low availability of holes that can be approximated with infinite dilution and can be described through the combination of the Stoke-Einstein and Nernst-Einstein equation:

$$\Lambda = z^2 Fe \,/\, 6\pi\eta(R_+ + R_-)$$

where Λ is the molar conductivity, z and e are the ion and electron charge respectively.[20] As indicated by the last equation the conductivity of a DESs is inversely proportional both to the dimension of the constituents and viscosity and, consequently, is directly proportional to the temperature.

S 1.1.3 Effect of water on DESs

Being DESs formed thanks to weak interactions established between the pure constituents, water molecules can establish hydrogen bonds with them affecting the physicochemical properties of the eutectic mixture. Because of its importance, when it comes to the amount of water in DESs, it is necessary to distinguish some cases. Usually, hydrophilic eutectic solvents can contain intrinsic amount of water which arise both from its ability to absorb water from the atmosphere and from the hygroscopicity of the constituents.

Particular attention must be paid to the water content of the constituents, inasmuch some differences can be observed when the eutectic mixtures are prepared starting from hydrated or anhydrous constituents, such as variations in molar ratio to obtain a liquid phase. The degree of intrinsic hydration of a deep eutectic solvent can be easily measured employing the Karl-Fischer titration, a two-step reaction involving

water, iodine and sulphur dioxide.[21] In other cases, water represents properly one of the constituents of the eutectic mixture. Otherwise water can be added as a cosolvent in order to modulate the physicochemical properties of these solvent.[22,23] Being water molecules both HBA and HBD, they can establish strong interactions with the components of DES. Therefore, the increasing addition of water causes a weakening in the deep eutectic solvent networks of hydrogen bonds until the complete disruption of the DES structure.

Dai and coworkers observed that the addition of water usually reduces the viscosity of DESs by increasing their applicability. However, the authors explain that for the systems studied there is a weakening of the interactions between the components of DES as the amount of water increases. In addition, they stated that the structure of the deep eutectic solvent is disrupted when the water amount is increased up to 50 %, beyond which the system can be considered as an aqueous solution of the single constituents.[23]

S 1.2 Choline chloride based DESs

Choline chloride (ChCl) is the most widely used ammonium salt as hydrogen bond acceptor in the preparation of deep eutectic solvents. The interest addressed to this salt is mainly due to its great availability, cheapness and low toxicity.[24,25] In nature, choline salts and their derivates are essential nutrients for both humans and animals. This quaternary ammonium salt in its acetylated form, acetylcholine, plays an important role in neuron signaling as a neurotransmitter. Moreover, phosphatidylcholine is a typical constituent of the phospholipids of which the cell membrane is composed. This ammonium salt is capable of forming many different eutectic mixtures with a plethora of hydrogen bond donor species, such as amides, carboxylic acids, alcohols and glycols. In its first proposed deep eutectic mixture, ChCl was combined in a 1:2 molar ratio with urea to form the so-called *reline*. This DES was characterized by a high melting point depression, compared to the pure constituents, caused by the strong hydrogen bond interactions established between

the two components. In particular, choline chloride and urea as pure substances show high melting point, 302 °C and 134 °C respectively, but when they are mixed together the freezing temperature decreases when the eutectic composition is reached.[26]

Successively, ethylene glycol and glycerol were also used as hydrogen bond donors in combination with choline chloride, also in a 1:2 molar ratio, also forming *ethaline* and *glyceline* respectively. The interaction established between choline chloride and these polyols leads to the formation of eutectic liquids with a freezing point generally much lower than the room temperature. As described in the previous sections, ethylene glycol, glycerin and many other polyols are widely used in various industrial applications due to their safeness and low vapor pressure. Therefore, their application in combination with choline chloride in the preparation of deep eutectic solvents can lead to very a promising green alternative to classic volatile organic solvents.[24]

S 1.3 Aim of the work and future perspective

Since their first evidence, deep eutectic solvents have been considered a valid alternative to the more harmful classical organic solvents. In particular, the high potential of these green solvents lies mainly in their structures and interactions thanks to which they have unique physicochemical properties. Therefore, by studying their interactions it is possible to understand their properties and how they can be fine-tuned in order to improve their applicability.

The present work shows a preliminary characterization performed on three different deep eutectic solvents based on choline chloride as HBA mixed together with three different glycols employed as HBD using the same molar ratio. For these DESs, the role of the structure of the hydrogen bond donors, the effect of the water addition and the temperature on their physicochemical properties have been investigated. For this purpose, measurements of viscosity, conductivity and polarity (by Nile Red dye) were performed; furthermore, structural properties of DESs were analyzed

using Fourier transform infrared spectroscopy (FTIR) and nuclear magnetic resonance spectroscopy (NMR). Diethylene glycol (DEG), triethylene glycol (TEG) and polyethylene glycol 200 (PEG200) have been used as hydrogen bond donors in choline chloride based DESs whose structures are reported in Figure S 1.3.

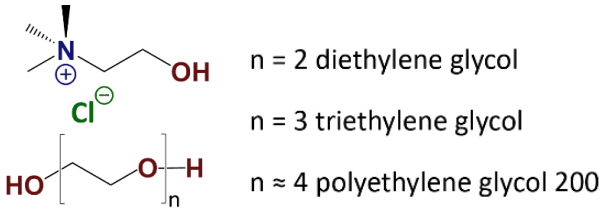

Figure S 1.3: Components of deep eutectic solvents selected in this work.

Particular attention has been paid to the selection of DES constituents and to their ecological and economic sustainability. In fact, as described in this chapter both low molecular weight polyethylene glycols and choline chloride show low or even no toxicity and are easily available and inexpensive materials, which are fundamental prerequisite for developing a green solvent system.

The toxicological aspect of the characterized DESs has been investigated in the literature. Many toxicological studies performed on some of these purposed eutectic mixtures (ChCl/DEG and ChCl/TEG in particular) show their low toxicity towards different strains of fungi, as well as their total harmlessness towards Cyprinus *Cyprinus carpio* fish.[27] Furthermore, no inhibitory effects of ChCl/TEG DES have been observed on different bacterial strains.[28,29]

This work has been performed with the future perspectives of the employment of these DESs for biotransformation reactions. To this end, a good comprehension of the properties of these solvents and their tuneability can lead to a better understanding of the behavior of enzymes when immersed in these unconventional media.

S 1.4 Materials and methods

Choline chloride, diethylene glycol, triethylene glycol and Nile Red are purchased from Sigma-Aldrich and are used as received without further purification. PEG 200,

poly(ethylene glycol) with average molecular weight of 200 and mean ethylene glycol units repetition of 4, is supplied by Merck. All other chemicals used are of analytical grade.

S 1.4.1 Preparation of DES mixtures

DES mixtures were prepared by mixing choline chloride with various HBD partners such as DEG, TEG and PEG 200 at the appropriate HBD/HBA molar ratio and heating the mixtures at 70 °C up to obtain a liquid phase once returned at room temperature. The water content of DES was measured by injecting DES directly into a Karl Fischer titrator (Metrohm 684 KF Coulometer). The water content values given are an average of at least three measurements.

S 1.4.2 Physicochemical properties measurements

The viscosity of the eutectic mixtures was measured using a Fungilab Viscolead mod. ADV L viscometer, equipped with a temperature sensor. Conductivity measures were performed with an Analytical Control ORION Research conductivity meter with a platinum cell (cell constant K = 1.05 cm^{-1}). The effect of water addition on viscosity and conductivity of DESs was evaluated at 25.0 °C in a thermostatic water bath; experiments were performed in triplicate.

Polarity testing were carried out using Nile red as solvatochromic probe. A 0.01 M dye stock solution was prepared in chloroform, and an appropriate amount of the dye solution was transferred to 3 mL volumetric flask. The chloroform was removed by flowing high-purity nitrogen gas directly into the flask. DES mixtures (2 mL) were transferred into the flask and the dye has been solubilized with heating and stirring in an oil bath. The solution was transferred in a 3 mL cuvette and the UV-visible spectra were immediately acquired at 25.0 °C in 400-700 nm range with a Shimadzu UV-160A UV-VIS spectrophotometer. Spectra of Nile red solutions with different amounts of water added to glycols and DESs were also recorded in order to study the influence of the water amount on the wavelength of maximum absorbance (λ_{max})

of Nile red. The polarity parameters of the samples were calculated as molar transition energy (E_{NR}) using the following equation:[30]

$$E_{NR}(kal / mol) = \frac{28591}{\lambda_{max}(nm)}$$

where λ_{max} was the wavelength at the maximum absorbance and was measured in triplicate runs.

S 1.4.3 Structural properties measurements

The infrared spectra were acquired on a Perkin Elmer model Spectrum Two FTIR Spectrometer, based on a Universal Attenuated Total Reflectance sensor (UATR-FTIR). A range from 4000 to 400 cm^{-1} was scanned, with a resolution of 4 cm^{-1} and 4 scans. The spectra of each sample were acquired with six replicates.

The NMR spectra of pure and diluted DESs with a different weigh percentage of deuterium oxide (D_2O) were recorded at 313 K on Bruker Avance III Ascend 400 MHz spectrometer. ^{1}H NMR, ^{35}Cl NMR and ^{14}N NMR spectra were recorded at 400.13, 39.20 and 28.90 MHz, with external D_2O for lock. Chemical shifts for proton are reported in ppm relative to external acetone in D_2O at 2.22 ppm. Chemical shift for ^{35}Cl and ^{14}N signals is imposed respectively at 3.9 and 4.2 ppm.

S 1.5 Effect of water on ChCl:glicol DESs

Triethylene glycol was chosen as HBD molecule for a preliminary screening in order to find the appropriate molar ratio that allowed obtaining a homogeneous, colorless and stable liquid at room temperature. Choline chloride and triethylene glycol were weighed at different molar ratios and they were kept under stirring in an oil bath at 70 °C. At ChCl/TEG molar ratio lower than 1:3, when the temperature drops to room temperature, ChCl crystallized by separating itself from the mixture, as previously reported by Hayyan and coworkers.[31] Therefore, mixtures consisting of ChCl with DEG and PEG 200 were prepared at 1:3 and in both cases homogeneous, colorless and perfectly transparent liquids were obtained.

At first, the water content of the DESs has been determined, since water absorbed by the solvent from the surrounding atmosphere is inevitable during preparation. Moreover, water can act as both hydrogen-bond donor and acceptor and it is therefore likely to interact strongly with the components of DESs. Water amount was found to be between 2 and 5% w/w. The physicochemical and structural properties of these DESs were evaluated as function of added water content.

S 1.5.1 Effect of water addition on DESs conductivity and viscosity

The high viscosity of DESs represents one of the major practical problems due to the slow mass transfer that limits their applications in many fields. Diluting DES with water, which has proved to be an effective way to decrease its viscosity, can solve this problem.

The formation of DES depends on intermolecular hydrogen bonds between the constituent species and simultaneously reduction in the original network of hydrogen bonds existing between the individual components. As water is introduced into the system, hydrogen bonds between the components of DES are broken and new ones are formed between them and water.

At low concentration, water molecules are adsorbed in the molecular matrix of the DESs and hydrogen bonds with ions and HBDs are established. At high water concentration, it establishes strong interactions with the components of the DES, reducing inter- and intramolecular interactions in the liquids and preventing them from interaction between each other. In these conditions, the physicochemical properties of DES change strongly. The viscosity and conductivity of DES diluted with different percentages of water were measured at 25.0 °C and the results are reported in Figure S 1.4.

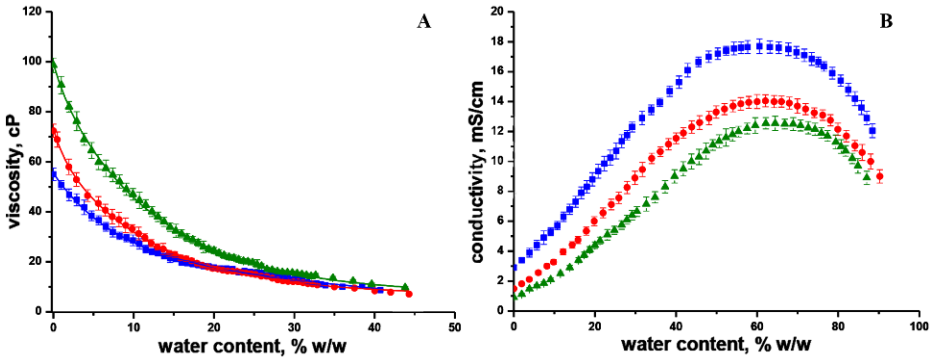

Figure S 1.4: Viscosity (A) and conductivity (B) trends as a function of the percentage of water added (w/w) to DESs at 25.0 °C; (■) ChCl/DEG, (●) ChCl/TEG, (▲) ChCl/PEG 200.

First of all, the figures show that, in the absence of water, the nature of the HBD molecule influenced both viscosity and conductivity of DESs. In fact, at 25.0 °C viscosity increased with the number of oxyethylene units of the glycol, being 55.0, 72.4 and 98.6 cP in ChCl/DEG, ChCl/TEG and ChCl/PEG 200 respectively.

On the other hand, conductivity of ChCl/DEG (2.9 mS/cm) was two times higher than ChCl/TEG (1.49 mS/cm) and three times higher than ChCl/PEG 200 (0.92 mS/cm). The addition of water to DESs greatly affected both viscosity and conductivity, as shown in the above figures. In particular, dilution of DESs with water led to a large decrease in viscosity since hydrogen-bonding interactions between the components gradually weakened. Viscosity value was halved after the addition of about 7-10% water. Moreover, although the initial value was different depending on the glycol used, the viscosity of the DESs was equal when the percentage of water was about 30% and the curves were almost coincident.

The conductivity of DESs diluted with different percentages of water (Figure S 1.4 B) firstly increased with the increasing of water content, reached a maximum at 60% H2O, in which values were 6-15 times higher than that of pure DESs, and then decreased. The initial increase of conductivity was due to the promotion of the ionic dissociation of the components of the DES and the maximum was reached when choline and especially chloride ions were completely dissociated. On the other hand, further water addition caused a dilution of the electrolytes, with a consequent

decrease in conductivity. Similar results were obtained for 1,2-propanediol:choline chloride:water (1:1:1), glucose:choline chloride:water (2:5:5) and sucrose:choline chloride:water (1:4:4) which had the highest conductivity at 60% w/w of water dilution.[23,32]

S 1.5.2 Effect of water addition on DESs polarity

Nile Red is a positive solvatochromic dye; thus, when dissolved in increasingly polar media, the wavelength of its visible absorption maximum (λ_{max}) moves to longer wavelengths (lower energies). Nile Red displays one of the largest shifts in excitation and emission maxima in going from nonpolar to polar solvents. In fact, on changing the solvent from water to pentane, a change in λ_{max} of 110 nm is observed.[31] Figure S 1.5 shows the trend of λ_{max} as a function of the percentage by weight of H_2O for the DESs.

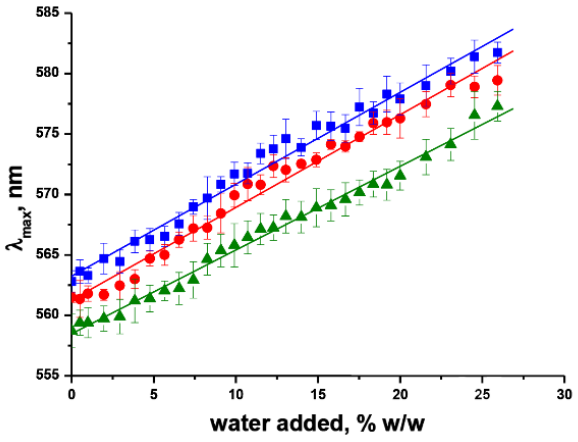

Figure S 1.5: Effect of the percentage of water added on the wavelength of maximum absorbance (λmax) of Nile red in the DESs at 25.0 °C; (■) ChCl/DEG, (●) ChCl/TEG, (▲) ChCl/PEG 200.

As expected, addition of water to DES caused a bathochromic shift of λ_{max}; the change in polarity had a linear trend (R^2 = 0.98÷0.99) as the percentage of water increased for all three investigated systems, independently on the glycol used. Moreover, in Table S 1.1 λ_{max} and E_{NR} values for pure glycols, pure DESs and DESs plus 25% water are displayed. Values in water are also reported for comparison.

Table S 1.1: Polarity parameters of pure glycols, pure DESs and DESs plus 25% water.

		λ_{max}, nm	E_{NR}, kcal/mol
	pure water	593.2	48.20
pure glycols	DEG	558.6	51.18
	TEG	554.6	51.55
	PEG 200	552.9	51.71
pure DESs	ChCl/DEG	562.8	50.80
	ChCl/TEG	561.5	50.92
	ChCl/PEG 200	558.7	51.17
DESs plus 25% water	ChCl/DEG	581.7	49.15
	ChCl/TEG	579.4	49.35
	ChCl/PEG 200	577.3	49.52

Changes in the λ_{max} of the dye reported in the table suggested that the polarity decreased in the order DEG > TEG > PEG 200, both in pure form and as a component of DES. After the addition of 25% water, polarity increased and the molar transition energy (E_{NR}) values were close to that of pure water.

S 1.5.3 Structural properties of DESs: FTIR

The structural features of the DESs have been studied with FTIR-ATR spectroscopy to deepen the interactions that occur between choline chloride and glycols. The spectra showed a strong and wide O-H stretching peak in 3650-3200 cm^{-1} range, C-H stretching at 2900 cm^{-1}, C-H scissor and bending at 1450-1290 cm^{-1} , stretching of alcoholic C-O at 1250 cm^{-1}, C-O-C and C-O-H bending at 1100-1060 cm^{-1} and an absorption peak at 950 cm^{-1}, which is only present in DESs, was attributed to the stretching of ammonium C-N group of choline chloride. Therefore, no significant variations were observed between the spectra of the pure glycols and the relative DESs, except for the stretching vibration band of hydroxyl group between 3700 and 3000 cm^{-1}, as reported in Figure S 1.6.

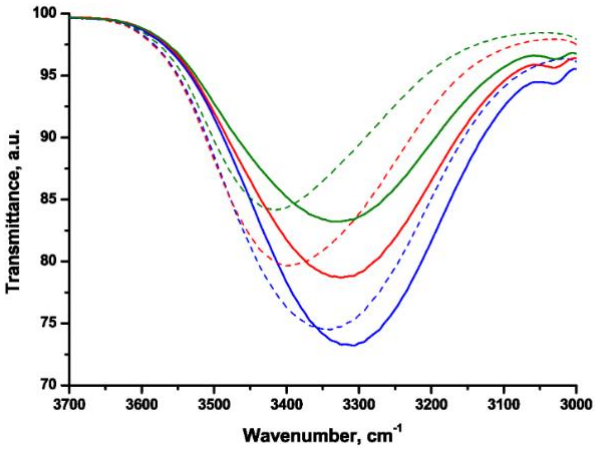

Figure S 1.6: Comparison between the OH stretching vibrational bands between the three pure glycols (dashed lines) and the three DESs (solid lines); (----/—) DEG, (----/—) TEG, (----/—) PEG 200.

Firstly, differences in band intensity of both glycols and DESs were noted, but they were caused by the different concentration of the samples. Moreover, in pure glycols, the O-H stretching bands were centered at 3340, 3400 and 3410 cm^{-1} for DEG, TEG and PEG 200, respectively, and these displacements were due to the hydrogen bond strength. In particular, the O-H band of DEG at lower frequency indicated the formation of intermolecular hydrogen bonds stronger that the other glycols. Moreover, when water was added to the glycols, the O-H band of DEG shifted to higher frequencies up to 3400 cm^{-1} at 50% (w/w) H_2O, as previously reported by Zhang and coworkers,[33] while no differences were detected for both TEG and PEG 200. This result revealed that the strength of intermolecular hydrogen bonds in TEG and PEG 200 is very similar to that of glycol-water and confirmed the presence of much stronger interactions between the hydroxyl groups of pure DEG compared to the other glycols. In the three DESs, the differences between the frequencies of the O-H bands were much smaller, being 3310, 3325 and 3332 cm^{-1} for ChCl/DEG, ChCl/TEG and ChCl/PEG 200, and they are all shifted towards lower values of the corresponding glycols. This result can be explained by the formation of strong hydrogen bonds between the anion chloride and the hydroxyl groups of the HBD, similar in all the samples, as depicted in Figure S 1.7.

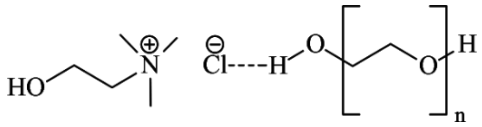

Figure S 1.7: Schematic representation of hydrogen bond established between choline chloride glycols interactions.

Then, the effect of water addition on the three DESs was investigated. In fact, when DESs were diluted, the strong hydrogen bonds between the HBD and the HBA weaken and the frequencies of the O-H stretching bands of glycol should shift towards higher and higher values as the water content increases.

To avoid that the O-H stretching band of water (3300 cm^{-1}), especially at higher percentages, could hide any shift of the O-H band of glycols, D_2O was added instead of H_2O. In Figure S 1.8 are reported the spectra of the three DESs the absorbance peaks of the O-H bands as a function of the amount of added deuterium oxide.

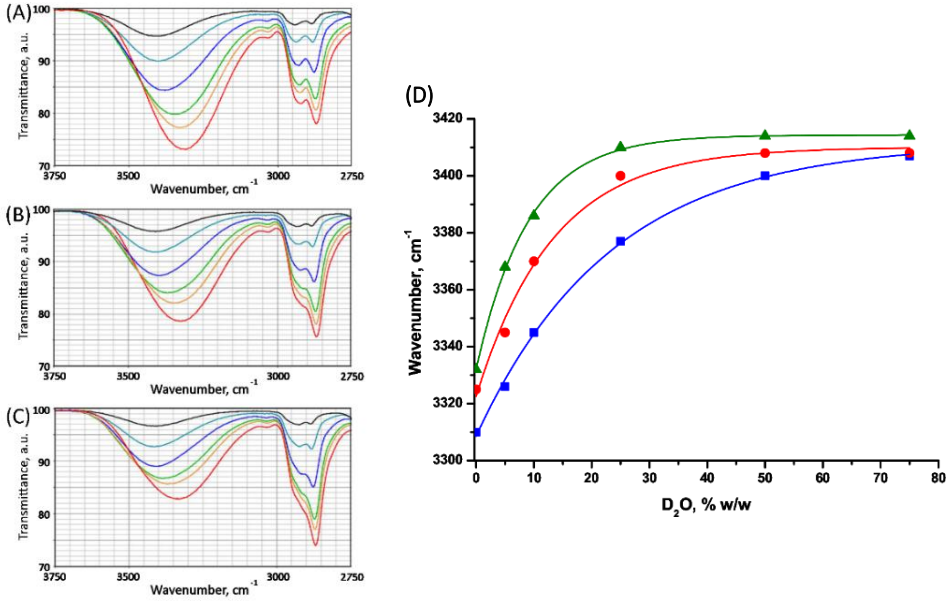

Figure S 1.8: FTIR spectra of DESs (molar ratio 1:3) diluted with deuterium oxide at 0% (—), 5% (—), 10% (—), 25% (—), 50% (—), 75% (—) (w/w) D_2O; (A) ChCl/DEG, (B) ChCl/TEG, (C) ChCl/PEG 200; Dependence of the frequencies of the bands due to O-H stretching on D_2O % w/w; (■) ChCl/DEG, (●) ChCl/TEG, (▲) ChCl/PEG 200 (D).

The O-D stretching band is centered at 2500 cm^{-1} and then, even if the strength of hydrogen or deuterium bonds with the components of DESs is different, this should

not significantly interfere with a possible displacement of the band. The trend of the curves clearly showed a substantial hypsochromic shift of the absorbance peaks pertaining to O-H stretching, between 85 and 100 cm^{-1}. In particular, these shifts were very noticeable up to 25% w/w of added D_2O (70-75 cm^{-1}), indicating that the interactions between the DES components are weakened non-linearly as D_2O was introduced. Further water additions did not significantly change the absorption frequencies and above 50% (w/w) of D_2O added DES-water interactions overcame DES-DES ones.

S 1.5.4 Structural properties of DESs: NMR

In order to further explore the effect of water on the supramolecular structures of the DESs, the eutectic mixtures were diluted with D_2O and investigated with NMR. ^1H NMR spectroscopy has been previously used to characterize H bond interactions in some DESs, NADESs (natural deep eutectic solvents) and ionic liquids[34-37] showing its utility for investigation of microstructure and interaction at molecular level. In a previous study, involving choline chloride and 1,2-propanediol, authors showed in HOESY and NOESY signals corresponding to proximity, less than 5 Å, in a ternary mixture ChCl:1,2-propanediol:water (1:1:1 molar ratio), of the methyl group of 1,2-propanediol with both the methyl carbon and methylene carbon of choline chloride.[38] It is well known that the strength of H-bonds affects the chemical shifts of different peaks in the DES mixtures.[39] Then following the upfield or downfield movement of the chemical shifts of different peaks it is possible to explore the characteristic of the H-bond of this sort of mixtures characterized by two types of proton donors, hydroxyl groups in the glycols and weak C_α–H in the ammonium cation mediated by chloride ion. The interaction between ChCl and glycols investigated by NMR showed a common trend on D_2O addition. As shown in Figure S 1.9, in all cases signals of the N-methylene and methyl groups of ChCl shifted upfield, whereas signals of -CH_2OH and methylene of glycols were quite insensitive

to dilution, indicating the strength of the hydrogen bond mediated by chloride ion as $Cl^{-}\cdots Me_3NCH_2$-.

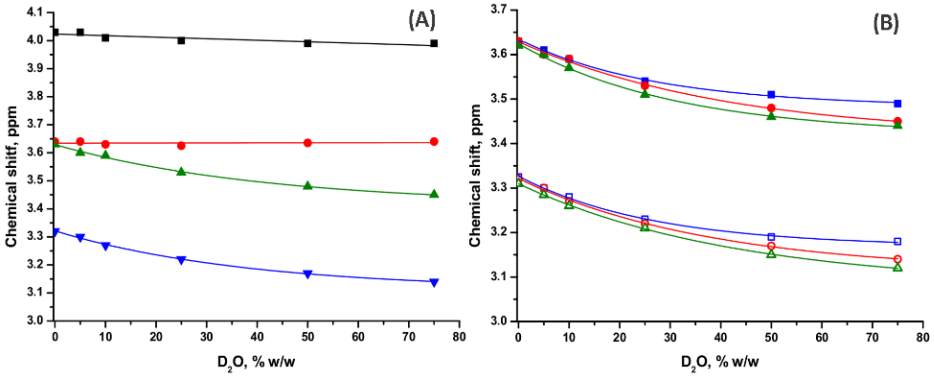

Figure S 1.9: chemical shifts in ^{1}H NMR spectrum of: (A) ChCl/TEG DES; (●) CH2-OH of TEG and (■) CH2-OH (▲) CH2-N$^+$, (▼) CH3-N$^+$ of choline; (B) CH2-N$^+$ (filled symbols) and of CH3-N$^+$ (empty symbols) of choline chloride in (■/□) ChCl/DEG, (●/○) ChCl/TEG, (▲/△) ChCl/PEG 200.

The upfield shift of signals on dilution reveals that in pure DES there was a halide ion-HBD supramolecular complex, in fact, a strong interaction deshielded methyl and methylene protons on ChCl. The progressive disruption of such complexes was evident also on downfield shift of the hydroxyl protons of ChCl and glycols the progressive hydration of the hydroxyl groups, by D_2O, with new hydrogen bonds formation, deshields hydroxyl protons.[40] Similarly, pulsed field gradient NMR experiments performed on ChCl/ethylene glycol DES showed that, when water is added to DES, hydroxyl proton diffuses faster than parent Ch^+ and ethylene glycol, approaching that of pure water, indicating that hydroxyls are in strong exchange with water and no DES structure survives.[41]

These results demonstrated that there are intensive H-bonding interactions and dilution with D_2O caused the interactions weaken gradually up to around 50% (w/w) of D_2O added, but with the supramolecular complex structures to some extent preserved; with the subsequent additions the interactions disappeared completely at around 75% (w/w) of D_2O added. Looking at the behavior of the hydroxyls we come to the same conclusion; in fact, they are non-exchangeable up to a certain

amount of D_2O added, depending from glycol, indicating that they are involved in a strong H-bond.

^1H NMR data revealed, also, different interaction between ChCl and glycols; in fact, upfield shift intensity and non-exchangeable behavior were different for DEG, TEG and PEG 200 being more similar that of TEG and PEG 200. For TEG and PEG 200 the intensity of upfield shift for N-methylene and methyl groups of ChCl, on D_2O addition, was higher than that generated in ChCl-DEG and hydroxyls remained no-exchangeable up to 50% (w/w) of D_2O added, showing a stronger interaction between ChCl and glycol with increasing ethylene units.

^1H NMR data was in accordance with the decrease of viscosity ascribed to the breakage of hydrogen bonds between molecules upon addition of water. Further investigation on ^{35}Cl and ^{14}N NMR showed strong ion-paring interaction between the choline cation and the chloride ion. In fact, line width (LW) of quadrupolar nuclei are strongly affected by electric density symmetry around them and one can expect their broadening when they are involved in interactions that will destroy such symmetry. When chloride ions are hydrated with high symmetry, as in aqueous KCl and NaCl solutions, the line half-width of the ^{35}Cl signals is relatively narrow, ca. 12 Hz, over a wide concentration ranges, from 3×10^{-3} to 10 M[42], indicating that also in a two layer separated ions line half-width for ^{35}Cl remains unchanged.

Also in dilute solution of pure ChCl (5×10^{-3} M) the LW was 10 Hz. Moreover, the magnitude of the field gradient due to the counterion is strongly dependent on interionic distance; then, solvent-separated ion pairs yield a line broadening that is negligible when compared with the effect of ions in contact.

As seen for methylene and methyl groups of choline chloride proton chemical shift (Figures S 1.9 A and B), in Figure S 1.10 the line width at half height of ^{35}Cl and ^{14}N as a function of D_2O added is reported.

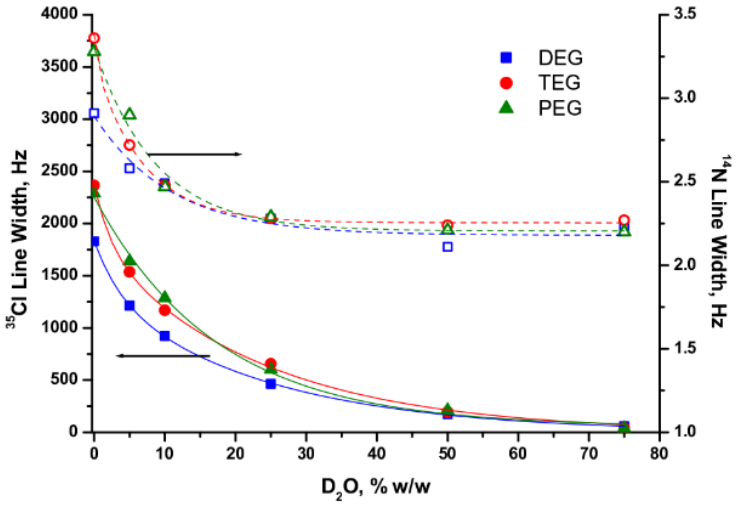

Figure S 1.10: Dependence of linewidth of ^{35}Cl (filled symbols) and ^{14}N (empty symbols) on D_2O % w/w; (■/□) ChCl/DEG, (●/○) ChCl/TEG, (▲/△) ChCl/PEG 200.

Values for peak width at half height (LW) of ^{35}Cl showed a clearly strong ion-paring interaction for all investigates pure DESs; in fact, LW was 2289, 2365 and 1830 Hz for DES ChCl/PEG 200, ChCl/TEG and ChCl/DEG respectively. ^{35}Cl-LW, as expected, decreased on dilution up to ca 40 Hz at 75% (w/w) of D_2O added. It has been previously observed that the ^{35}Cl line width due to KCl in 20% aqueous PEG 200 was about 60 Hz[43] and such evidence seems to confirm that at 75% (w/w) of D_2O added there was not more ChCl-glycol strong interactions. As comparison, for pure ChCl at the same concentration of DES at 75% (w/w) of D_2O added, but without glycols, the ^{35}Cl-LW was 20 Hz.

Results for ^{14}N-LW showed a less sensitive variation for line broadening on dilution, because of the shielding by surrounding methyl and methylene groups. Figure S 1.10 showed the trend for both ^{35}Cl and ^{14}N line width. After a steep decrease up to 25% (w/w) of D_2O added for ^{14}N LW and 50% (w/w) of D_2O added for ^{35}Cl LW, values reached a steady state confirming the substantial hydration of system up to 50% (w/w) of D_2O added. As already mentioned, the ^{14}N LW is less sensitive to interaction changes, whereas ^{35}Cl LW reflected more closely the structural changes.

As seen for ^{1}H NMR, also ^{14}N and ^{35}Cl LW showed the different interaction between ChCl and glycols, in fact the initial line with for ChCl-DEG was smaller than that of ChCl-TEG and ChCl-PEG 200 that conversely were similar, confirming the stronger interaction of ChCl-TEG (PEG 200) system.

S 1.7 Conclusion

In this study, the effect of water addition on the properties of three deep eutectic solvents consisting of choline chloride and glycols was evaluated. Both physicochemical and structural studies clearly indicated that in the absence of water strong interactions between choline chloride and glycols are established. Dilution with water caused a weakening of these hydrogen bonds and many properties of DES drastically change. In particular, as a result of water adding, their viscosity notably decreased, while an increase of their conductivity was observed. Such evidence can be explained with a weakening of the strong inter- and intramolecular interactions between the components of DES and new ones began to form between them and water. Besides, the responses of the Nile Red solvatochromic probe dissolved in three DESs showed a good polarity of these media which could be further increased after the addition of water.

The results obtained by means of FTIR and NMR spectroscopies on the effect of water addition on the nanostructure of DESs and the gradual changes during dilution clearly showed that the intensive H-bonding interactions weaken gradually up to around 50% (w/w) of D_2O added, even if the complex supramolecular structures seemed partly preserved. Further water additions produced the complete disappearance of such interactions and the DES components were completely dissociated and hydrated. Moreover, NMR studies revealed that the interactions between ChCl and glycols are dependent on the number of oxyethylene units, being stronger between ChCl and both TEG and PEG 200 than those existing between ChCl and DEG. In conclusion, water, the most environmental friendly solvent, may be used as a cosolvent to modify the physicochemical properties of choline chloride-based

DESs in an effective and favorable manner, by decreasing viscosity, one of the main limits to the use of DESs for practical applications, such as extraction processes and enzyme reactions.

References

1- F.M. Kerton, R. Marriott, "*Green solvents – Legislation and certification*" in "Alternative Solvents for Green Chemistry: 2nd Edition", The Royal Society of Chemistry, chap 2, pp. 31-50 (2013);

2- C.J. Clarke, W. Tu, O. Levers, A. Bröhl, J.P. Hallett, Chemical Reviews, **118**, 747-800 (2018);

3- S. Das, A. Mondal, S. Balasubramanian, Current Opinion in Green and Sustainable Chemistry, **5**, 37-43 (2017);

4- H. Vanda, Y. Dai, E.G. Wilson, R. Verpoorte, Y.H. Choi, Computes Rendus Chimie, **21**, 628-638 (2018);

5- Q. Zhang, K. De Oliveira Vigier, S. Royer, F. Jérôme, Chemical Society Reviews, **41**, 7108-7146 (2012);

6- M. Antunes, A.S. Campinhas, M. Sá Freire, F. Caetano, H.P. Diogo, R. Colaço, L.C. Branco, B. Saramago, Journal of Molecular Liquids, **295**, 1117281 (2019);

7- Y. Liu, J.B. Friesen, J.B. McAlpine, D.C. Lankin, S.N. Chen, G.F. Pauli, "Journal of Natural Products, **81**, 679-690 (2018);

8- E.L. Smith, A.P. Abbott, K.S. Ryder, Chemical Reviews, **114**, 11060-11082 (2014);

9- F. Chemat, M.A. Vian *, H.K. Ravi, B. Khadhraoui, S. Hilali, S. Perino, A.S.F. Tixier, Molecules, **24**, 3007 (2019);

10- B. Socas-Rodríguez, Á. Santana-Mayor, A.V. Herrera-Herrera, M.Á. Rodríguez-Delgado, "*Deep eutectic solvents*" in "Green Sustainable Process for Chemical and Environmental Engineering and Science", Inamuddin, A.M. Asiri, S. Kanchi Ed., Elsevier, chap. 5, pp 123-177 (2020);

11- Y.P. Mbous, M. Hayyan, A. Hayyan, W.F. Wong, M.A. Hashim, C.Y. Looi, Biotechnology Advances, **35**, 105-134 (2017);

12- Z. Chena, A. Ragauskas, C. Wan, Industrial Crops & Products, **147**, 112241 (2020);

13- M.E. Alañón, M. Ivanović, A.M. Gómez-Caravaca, D. Arráez-Román, A. Segura-Carretero, Arabian Journal of Chemistry, **13**, 1685-1701 (2020);

14- D. Krištofíková, V. Modrocká, M. Mečiarová, R. Šebesta, ChemSusChem, **13**, 2828-2858 (2020);

15- A. Di Crescenzo, M. Tiecco, R. Zappacosta, S. Boncompagni, P. Di Profio, V. Ettorre, A. Fontana, R. Germani, G. Siani, Journal of Molecular Liquids, **268**, 371-375 (2018);

16- I. Juenidi, M. Hayyan, M.A. Hashim, Process Biochemistry, **66**, 33-60 (2018);

17- G. Siani, M. Tiecco, P. Di Profio, S. Guernelli, A. Fontana, M. Ciulla, V. Canale, Journal of Molecular Liquids, **315**, 113708 (2020);

18- K. De Oliveira Vigier, F. Jérôme, "*Synthesis and Properties*" in "Deep eutectic solvents: synthesis, properties, and applications, First Edition", D.J. Ramón and G. Guillena Ed., Wiley-VCH, chap. 1, pp 1-23 (2020);

19- A.P. Abbott, ChemPhysChem, **5**, 1242-1246 (2004);

20- A.P. Abbott, R.C. Harris, K.S. Ryder, "Journal of Physical Chemistry, **111**, 4910-4913 (2007);

21- G. García, S. Aparicio, R. Ullah, M. Atilhan, Energy Fuels, **29**, 2616–2644 (2015);

22- C. Ma, A. Laaksonen, C. Liu, X. Lu, X. Ji, Chemical Society Reviews, **47**, 8685--8720 (2018);

23- Y. Dai, G.J. Witkamp, R. Verpoorte, Y.H. Choi, Food Chemistry, **187**, 14-19 (2015);

24- Y. Wang, C. Ma, C. Liu, X. Lu, X. Feng, X. Ji, Journal of Chemical & Engineering Data, **65**, 2446–2457 (2020);

25- O.S. Hammond, K.J. Edler, "*Structure and implications*" in "Deep eutectic solvents: synthesis, properties, and applications, First Edition", D.J. Ramón and G. Guillena Ed., Wiley-VCH, chap. 2, pp 25-42 (2020);

26- A.P. Abbott, G. Capper, D.L. Davies, R.K. Rasheed, V. Tambyrajah, Chemical Communications, 70-71 (2003);

27- I. Juneidi, M. Hayyan, O. Mohd Ali, Environmental Science and Pollution Research, **23**, 7648–7659 (2016);

28- M. Hayyan, M.A. Hashim, A. Hayyan, M.A. Al-Saadi, I.M. Al Nashef, M.E.S. Mirghani, O.K. Saheed, Chemosphere, **90**, 2193–2195 (2013);

29- B.Y. Zhao, P. Xu, F.X. Yang, H. Wu, M.H. Zong, W.Y. Lou, ACS Sustainable Chemistry & Engineering, **3**, 2746–2755 (2015);

30- J.F. Deye, T.A. Berger, A.G. Anderson, Analytical Chemistry, **62**, 615-622 (1990);

31- M. Hayyan, T. Aissaoui, M.A. Hashim, M.A.H. AlSaadi, A. Hayyan, Journal of the Taiwan Institute of Chemical Engineers, **50**, 24-30 (2015);

32- A. Cicci, G. Sed, M. Bravi, Chemical Engineering Transactions, **57**, 61-66 (2017);

33- J. Zhang, Q. Li, Z. Guo, K. Li, M. Xu, N. Zhang, T. Zhang, X. Wei, Industrial & Engineering Chemistry Research, **50**, 674-679 (2011);

34- D. Yang, S. Zhang, X. Sun, D. Jiang, S. Dai, Journal of Molecular Liquids, **274**, 414-417 (2019);

35- R. Xin, S. Qi, C. Zeng, F. Iqbal, B. Yang, Y. Wang, Food Chemistry, **217**, 560-567 (2017);

36- M. Lozynski, J. Pernak, Z. Gdaniec, B. Gorska, F. Be, Physical Chemistry Chemical Physics, **19**, 25033-25043 (2017);

37- R. Lungwitz, S. Spange, ChemPhysChem, **13**, 1910-1916 (2012);

38- Y. Dai, J. Van Spronsen, G. Witkamp, Analytica Chimica Acta, **766**, 61-68 (2013);

39- E. Posada, R.J.J. Riobóo, M.C. Gutiérrez, M.L. Ferrer, F. Monte, Journal of Molecular Liquids, **276**, 196-203 (2019);

40- J.E. Del Bene, S.A. Perera, R.J. Bartlett, Q.T. Project, V. Uni, V. Gaines, Journal of Physical Chemistry A, **103**, 8121–8124 (1999);

41- C.D. Agostino, L.F. Gladden, M.D. Mantle, A.P. Abbott, I. Ahmed, A.Y.M. Al-murshedi, R.C. Harris, Physical Chemistry Chemical Physics, **17**, 15297–15304 (2015);

42- F.T. Yudasaka Masako, S. Tadashi, I. Hiizu, Bulletin of the Chemical Society of Japan, **54**, 1933-1938 (1981);

43- T. Sugawara, M. Yudaeaka, Y. Yokoyama, T. Fujiyama, H. Iwamura, Journal of Physical Chemistry, **86**, 2705-2709 (1982).

Addendum II

α-Chymotrypsin

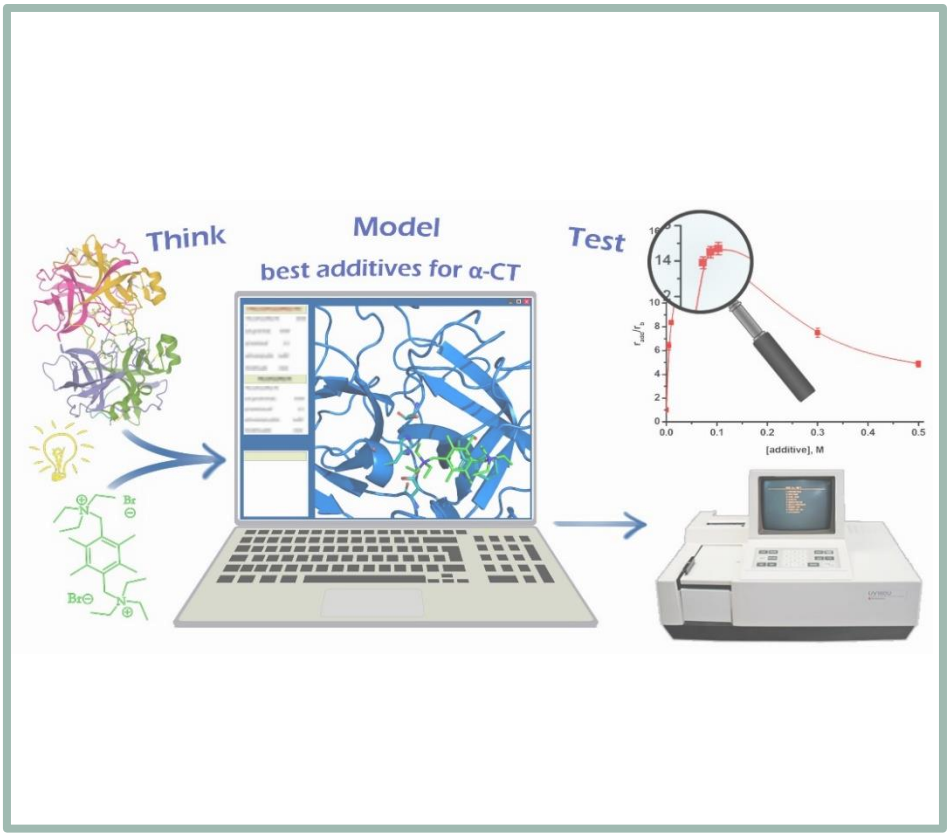

Addendum II

Refine the model to design α-chymotrypsin superactivators

S 2.1 α–Chymotrypsin

Proteases are enzymes commonly involved in the hydrolysis of peptide bonds. Most of these enzymes are classified as serine proteases due to the presence of a nucleophilic serine residue in their active site that is composed of the catalytic triad His 57, Ser 195 and Asp 102. Various enzymes such as trypsin, chymotrypsin, subtilisin, carboxypeptidase Y and Clp protease belong to the class of serine proteases. These enzymes are not only capable of hydrolyzing peptide bonds, but they can also cleave the bonds of other acyl compounds, such as amides, anilides, esters and thioesters.

Serine proteases are widely involved in several important physiological processes such as digestion, homeostasis, apoptosis, signal transduction, reproduction and immune response. Moreover, protease cascade activations are involved in blood coagulation, fibrinolysis, development, matrix remodeling, differentiation and wound healing. These different physiological roles require a high specificity, which is conferred to this class of enzymes by the topology of their binding site, linked to the active site by a network of hydrogen bonds.[1]

α-Chymotrypsin (α-CT) (EC 3.4.21.1), a hydrophilic globular serine protease, represents one of the most studied model enzymes, and its structure and mechanism of action are well-known since the 1970s.[2-4] This enzyme is composed by 245 amino acid residues and is synthetized as a zymogen (its inactive form). In this form the protein is composed of four deformed segments, commonly called activation domain, which are the N terminals of residues 19, 142-152, 184-193 and 216-223.

At the beginning of the proteolytic process the zymogen is activated thanks to the release of the N-terminal Ile 16 which forms a salt bridge with Asp 194; in this way a

conformational change occurs. This process orders the activation domain by forming the "*oxyanion hole*" and the binding site of the substrate. In fact, the deprotonation of the N terminus, due to high pH, and the consequent breakdown of the salt bridge Ile 16-Asp 194 can cause the loss of enzyme activity, due to the formation of inactive zymogen.[1] Figure S 2.1 shows the α-chymotrypsin three-dimensional structure, obtained from X-ray analysis.

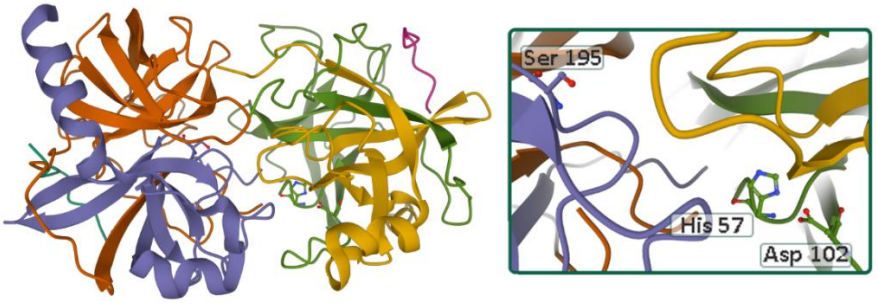

Figure S 2.1: Three-dimensional structure of α–chymotrypsin.

This enzyme has an ellipsoidal shape with dimensions of 50 Å along the crystallographic side *a* and of 40 Å along the sides *b* and *c*. The active site of the molecule is slightly flattened and there is a hole on its surface; this latter feature plays an important role in the binding of specific substrates.

In chymotrypsin, the structure of the antiparallel pleated sheet is quite common, but large regions with regular pleated sheets are not present. There are two folded units represented by six antiparallel lines. Within these units, hydrogen bonds are formed between these lines, according to the model of the antiparallel pleated sheet. Additional hydrogen bonds are present between the sixth and the first line of the same unit, thus forming a distorted cylinder of hydrogen bonds with a hydrophobic core. In the α-CT structure, hydrogen bonds are also very frequent between an amide group and the carbonyl group of the third residue behind, especially at the end of the loop in which the polypeptide chains turn and go back almost in parallel way to the original ones.

All charged groups are present on the protein surface, except for the α–amino group of Ile 16 and the carboxyl group of Asp 102 and Asp 194. In general, the hydrophobic

groups are buried within the protein and the polar ones are externally, although there are also some hydrophobic residues, such as Phe 39 and Phe 41, on the protein surface. In addition, many water molecules are trapped inside the structure. In Figure S 2.2 the active site of α-CT is schematically represented focusing on its catalytic triad (His 57, Ser 195 and Asp 102) and on the oxyanion hole.

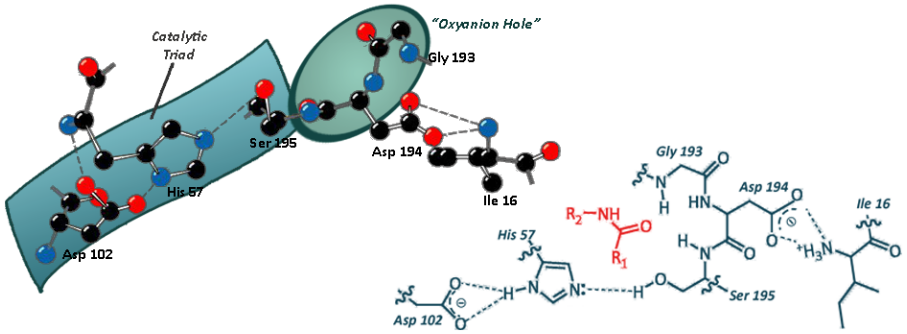

Figure S 2.2: Schematic representation of the catalytic site of α-chymotrypsin in which the catalytic triad and the oxyanion hole are highlighted.

The active site of α-CT is formed by an extensive network of hydrogen bonds between Nδ1-H of His 57 and Oδ1 of Asp 102 and between OH of Ser 195 and Nε2-H of His 57, although the protonation of His 57 causes the loss of the latter hydrogen bond. Other hydrogen bonds were observed between the Oδ2 of Asp 102 and the NH of the main chains of Ala 56 and His 57, which could contribute to the orientation of Asp 102 and His 57.

The catalytic triad is linked to the oxyanion hole, a positively charged pocket formed by the NH backbone of Gly 193 and Ser 195; it can activate the carbonyl of the scissile peptide bond and stabilize the negative charge of the tetrahedral intermediate, which is formed by the proteolysis. The oxyanion hole is also linked to the Ile 16/Asp 194 salt bridge through Ser 195.[1] The α–amino group of Ile 16, formed by the triple cleavage that activates the chymotrypsinogen, forms an ion pair with the carboxylate group of Asp 194 (Figure S 2.2).[3]

The reaction mechanism of α-chymotrypsin, a general mechanism accepted for all serine proteases, is shown in Figure S 2.3.

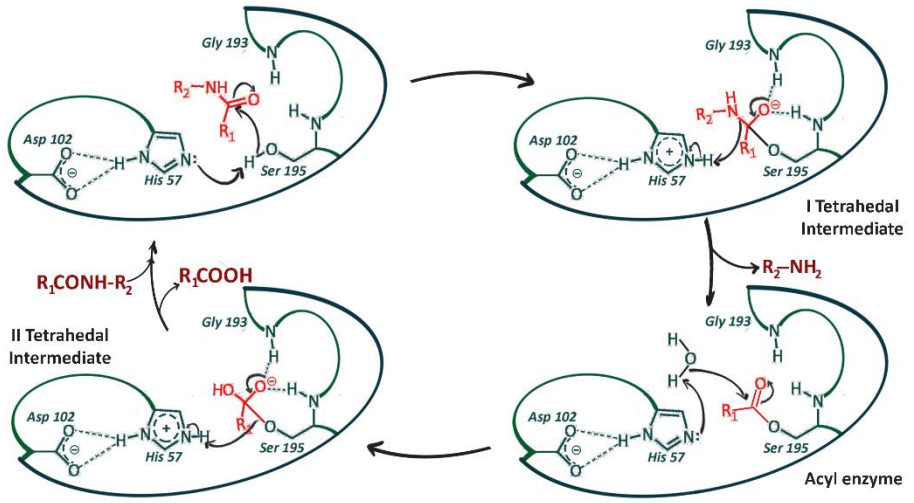

Figure S 2.3: Catalytic mechanism of serine protease.

At first the enzyme acylation occurs, in which the nucleophilic attack of Ser 195 to the carbonyl group of the substrate takes place, assisted by His 57 that acts as a common base; as a result, a tetrahedral intermediate is generated. The protonated His 57 is stabilized by hydrogen bond with Asp 102. Then, the NHs main chain of the oxyanion hole stabilizes the oxyanion of the first tetrahedral intermediate, which, subsequently, collapses expelling the leaving group; this step is assisted by protonated His 57 that act as acid, giving acyl enzyme intermediate. Finally, water attacks the acyl enzyme, with His 57 acting as a general base; thus, a second tetrahedral intermediate is formed and stabilized by oxyanion hole. Then, this intermediate collapse, the carboxylic acid is expelled, using the protonated His 57 as a common acid, and deacylation occurs.[1]

S 2.2 α–Chymotrypsin previous study

Being one of the most studied enzymes, the effect of additives and new reaction media on α–chymotrypsin catalytic properties has been extensively studied and reviewed. Many papers in the literature have been devoted to the superactivating effect of hydrophilic additives on α-CT, such as cationic single-chain and gemini surfactants and polyamines.[5-12] The enhancement of enzyme catalytic activity

induced by these additives has been attributed to hydrophobic interactions between the additives and the protein and this effect was mainly due to an increase of the enzyme catalytic activity.

Polyelectrolytes are also able to induce α-CT superactivation, modifying the electrostatic fields around the enzyme.[13,14] The favorable interactions between enzyme and substrate led to an increase in both affinity (K_M) and catalytic constant (k_{cat}). In particular, kosmotropes were able to stabilize the tertiary structure of the enzyme and to increase hydrophobic interactions between the enzyme and the substrate. Recently, the effect of co-solvents, stabilizers, pressure and temperature on the α-CT hydrolysis of peptide bond was also investigated.[15-17]

For many years our research group has been studying the effect of hydrophilic additives on the activity and stability of α-CT; enzyme was proved to be superactivated by a number of cationic surfactants and a bulky hydrophobic head group seemed to play a decisive role.[18,19] In fact, in the presence of cetyltributilammominium bromide (CTBABr), the enzyme instantaneous activity increased by 8 times compared to the buffer. However, further studies indicated that the amphiphilic nature of the additives was not essential, since ammoniums salts, like tetrabutylammonium bromide (TBABr), which possesses the same head group of CTBABr, but lacks the long hydrocarbon chain, led to the same significant superactivation (*i.e.* 8-fold increase of instantaneous activity) and, in addition, enzyme superactivation is maintained for over two months.[19]

The effect produced by the "big head" additives on the activity of α-CT with natural substrates was also assessed using electron spray ionization mass spectrometry (ESI-MS) and with model substrates containing more amino acid residues than the model substrate, N-glutaryl-(*L*)-phenylalanine *p*-nitroanilide (GPNA) used in previous studies.[20,21] The activating effect of the "big head" additives was rationalized by assuming that the proximity of the additive to the active site led to an increase in its hydrophobicity and therefore to a greater nucleophilicity of the Ser 195 hydroxyl group, the main responsible for the enzymatic activity.

More recently, cationic ammonium-based additives bearing a benzylic group were synthesized and tested.[22] The effect of benzyltrimethylammonium bromide (BzTMABr), benzyltributylammonium bromide (BzTBABr) and benzyldodecyldimethylammonium bromide (BzDDABr) was investigated. A significant increase in GPNA hydrolysis instantaneous rate was observed, with a greater effect for BzTBABr. However, this effect was accompanied by a faster deactivation of the enzyme compared to pure buffer. In addition to benzyl-substituted ammonium salt, two novel dicationic salts, (1,8-bis(tributylammonium)octane dibromide (bisBOAB) and 1,4-bis(tributylammonium)xylene dibromide (bisBAB)) were also synthesized and tested.[22] The major difference between the two dicationic salts was in the linker moiety, which was flexible and rigid, respectively. bisBOAB, which can be considered as a dimer of TBABr, induced similar superactivation and stabilization effects if compared to the monomer, but at lower concentration. In the case of the more rigid bisBAB, the superactivation effect was reduced compared to the more flexible bisBOAB and enzyme deactivation was faster.

The collected data were used to perform molecular modelling studies aiming at rationalizing the observed kinetic effects. The proposed *in silico* model[22] suggested that the residue tryptophan 215 (Trp 215), which is located adjacent to the catalytic site, may represent the anchor point for the quaternary ammonium salts possessing a superactivation effect. More precisely, small size quaternary ammonium-based additives with reduced flexibility (e.g. BzTBABr) were proposed to interact with Trp 215. Due to this binding mode, an increase in the hydrophobicity of the catalytic site occurs, with a consequent increase in the k_{cat} value. For dicationic ammonium salts, the greater flexibility of the spacer in bisBOAB induced alternative binding modes for the alkyl chains, while the rigid structure for bisBAB seemed not optimized to simultaneously interact with Trp 215 and with the hydrophobic region generated by His 57. Therefore, the binding poses for dicationic ammonium salts resulted in agreement with the lower superactivation effect. These modelling studies and

experimental evidences suggested that enzyme catalytic properties could be strongly influenced not only by several structural features of the additive (*i.e.* charge, charge density, size, hydrophobic/hydrophilic balance), but also by specific additive/enzyme interactions.

This work aimed at validating the previously generated hypotheses and the proposed *in silico* model for the interaction between ammonium-based additives and α-CT. To this aim, novel ammonium-based additives were designed, synthesized and tested to validate the hypothesized binding mode. The effect of additives on α-CT catalyzed hydrolysis of GPNA was studied and the determination of kinetic parameters allowed us to better understand the reasons for enzyme superactivation and to estimate the predictive capacity of the model used.

S 2.3 Materials and methods

Crystalline bovine pancreatic α-chymotrypsin (EC 3.4.21.1) (α-CT, 24.8 kDa, type II: 3 times crystallized, dialyzed and lyophilized), N-glutaryl-(*L*)-phenylalanine-*p*-nitroanilide (GPNA), Tris used for buffer preparation and *p*-nitroaniline used for molar absorption coefficient determinations were purchased from Sigma-Aldrich (St. Louis MO, USA). Buffered solutions of enzyme and substrate were freshly prepared immediately before use. All chemicals and solvents, all of analytical grade, were purchased from Merck, and were used as received without further treatments.

S 2.3.1 Synthesis of additives

Mono- and dicationic quaternary ammonium salts were synthesized by the quaternization of the respective tertiary amines with the appropriate bromo derivatives. Melting points were determined on Barloworld Scientific Stewart SMP3 apparatus and are uncorrected. ^{1}His NMR spectra were registered on a Bruker AVANCE DRX 400 instrument using $CDCl_3$, CD_3OD or D_2O as solvents at 25.0 °C. Chemical shifts are given in ppm relative to the residual ^{1}H solvent signal. *Trimethyl(3-phenylpropyl)ammonium bromide (PhPrTMABr)* was obtained by

reaction of (3-bromopropyl)benzene (50 mmol) with trimethylamine (molar ratio 1:1.5) in EtOH, under magnetic stirring for 12 h at room temperature. After removal of the solvent, the solid was purified by crystallization. Yield 12.1 g, 94%, m.p. 150-152 °C (ethyl acetate-methanol). δH (400 MHz, CD_3OD) 2.10-2.18 (2H, m, CH_2), 2.73 (2H, t, CH_2), 3.12 (9H, s, N^+ $(CH_3)_3$), 3.33-3.38 (2H, m, Ph-CH2); 7.33-7.20 (5H, m, Ph).[23]

Tributhyl(3-phenylpropyl)ammonium bromide (PhPrTBABr) was obtained starting from (3-bromopropyl)benzene (50 mmol) by reaction with tributylamine (molar ratio 1:1.5) in CH_3CN; the mixture was refluxed for 3 days. The reaction raw product after elimination of the solvent was taken up with ethyl ether until a solid was obtained; the latter was purified by double crystallization from a mixture of ethyl acetate/ethyl ether. Yield 13.8, 72%, m.p. 79-81 °C (ethyl acetate-ethyl ether). δH (400 MHz, CD_3OD) 0.99 (9H, t, $3CH_3$), 1.36 (6H, m, $3CH_2$), 1.53 (6H, m, $3CH_2$), 2.10 (2H, m, Ph-CH_2- CH_2-), 2.73 (2H, t, Ph-CH_2), 3.21 (8H, m, $4CH_2$), 7.39-7.17 (5H, m, Ph).

Hexamethylene bis(triethylammonium) dibromide (bisEHAB) was synthesized by quaternization of 1,6-dibromohexane (41 mmol) with triethyl amine (molar ratio 1:2.1) in CH_3CN; the mixture was refluxed under magnetic stirring for 8 h. After removal of the solvent, the solid was purified by crystallization from an acetone/ethyl ether mixture. Yield 14.1 g, 75%, m.p. 267-268 °C decompn (acetone-ethyl ether). δH (400 MHz, CD_3OD) 1.36 (18H, t, $6CH_3$), 1.55 (4H, m, $2CH_2$), 1.84 (4H, m, $2CH_2$), 3.24 (4H, m, $2CH_2$). 3.40 (m, 12H, $6CH_2$).[24]

Hexamethylene bis(tributylammonium) dibromide (bisBHAB) was prepared by quaternization of 1,6-dibromohexane (41 mmol) with tributylamine (molar ratio 1:2.2) in CH_3CN; the mixture was refluxed under magnetic stirring for 6 days. After removal of the solvent, the solid was purified by several crystallization from an acetone/ethyl ether mixture. Yield 8.8 g, 50%, m.p. 168-170 °C decompose (acetone-ethyl ether). δH (400 MHz, D_2O) 0.95 (18H, t, $6CH_3$), 1.37 (16H, m, $8CH_2$), 1.66 (16H, m, $8CH_2$), 3.21 (16H, m, 8 CH_2).[25]

bisEDuEAB and bisEOMeEAB were obtained from durene and 1,4-dimethoxybenzene respectively. These compounds were initially converted into dibromo derivatives with formaldehyde and hydrobromic acid by reflux into acetic acid, according to the procedure described in the literature.[26]

1,4-bis(bromomethyl)-2,3,5,6-tetramethylbenzene, purified by crystallization, m.p. 216-218 °C (ethyl acetate), yield 96%. δH (400 MHz, $CDCl_3$) 2.33 (12H, s, $4CH_3$), 4.60 (4H, s, $2CH_2$). 1,4-bis(bromomethyl)-2,5-dimethoxybenzene, purified by crystallization, m.p. 202-203 (methanol) °C, yield 86%. δH (400 MHz, $CDCl_3$) 3.87 (6H, s, $2OCH_3$), 4.53 (4H, s, $2CH_2$), 6.86 (s, 2H, Ph).

[(2,3,5,6-tetramethyl-p-phenylene)dimethylene]bis[triethylammonium bromide] (bisEDuEAB) was synthesized by reaction of 1,4-bis(bromomethyl)-2,3,5,6-tetramethylbenzene (32 mmol) with triethylamine (molar ratio 1:2.1) in CH_3CN; the mixture was refluxed for 6 h. Purified by double crystallization from an acetone-methanol mixture. Yield 11.5g, 88%, m.p. 206-208 °C decompn. δH (400 MHz, D_2O) 1.23 (18H, s, $6CH_3$), 2.44 (12H, s, $4CH_3$), 3.34 (12H, m, $6CH_2$); 4.89 (4H, s, $2CH_2$).

[(2,5-Dimethoxy-p-phenylene)dimethylene]bis[triethylammonium bromide] bisEOMeEAB was synthesized by reaction of 1,4-bis-(bromomethyl)-2,5-dimethoxybenzene (31 mmol) with triethylamine (molar ratio 1:2.1) in CH_3CN; the mixture was refluxed under magnetic stirring for 10 h. Purified by double crystallization. Yield 9.8 g, 75%, m.p. 218-220 °C (acetone-methanol). δH (400 MHz, CD_3OD) 1.46 (18H, t, $6CH_3$), 3.48–3.29 (12H, m, $6CH_2$), 3.98 (6H, s, $2OCH_3$), 4.57 (4H, s, Ph-CH_2-N), 7.30 (2H, s, Ph).[27]

S 2.3.2 α–Chymotrypsin activity assay

The α-CT activity assay was already described elsewhere. [22] Briefly, α-CT activity was measured spectrophotometrically at 25.0±0.1 °C, monitoring the increase in absorbance at 410 nm related to *p*-nitroaniline (*p*NA), the hydrolysis product of GPNA. The molar absorption coefficient (ε at λ = 410 nm) of *p*NA is 8800 $M^{-1}cm^{-1}$ in pure buffer. Absorbance variations in the presence of the additives at the tested

concentrations were evaluated and used in rate values estimations. A Shimadzu UV-160A UV-VIS spectrophotometer equipped with a thermostated cell was used in this study. The α-CT activity assay mixture was prepared in 0.1 M Tris-HCl buffer at pH 7.75, with an enzyme concentration of 0.2 mg/ml (8 μM) and a concentration of the substrate GPNA of 2.5×10^{-3} M. The pH of the mixture remained constant during analysis. The linear increase of absorbance at 410 nm due to *p*NA formation was recorded as a function of time for 5 minutes. Concerning the parameters discussed in this study, the reaction rate of α-CT (*i.e.* moles of *p*NA formed per unit of time) was calculated from the slope of the initial linear curve of *p*NA concentration vs time. The kinetic parameters k_{cat} and Km in pure buffer and in presence of additives were derived by linear regression analysis of the double reciprocal Lineweaver-Burk plots in a range of substrate concentration between 0.1×10^{-3} M and 2.5×10^{-3} M. Experiments were reproduced at least three times and the differences between duplicates in each experiment were always below 5%.

S 2.3.3 Molecular modelling studies

The possible binding poses of the tested additives in the surrounding of the α-CT catalytic site were explored using the FLAP (Fingerprints for Ligands and Proteins) software (Molecular Discovery Ltd., UK).[28] The docking procedure to study the α-CT/additive interaction was described elsewhere.[22] Briefly, the x-ray α-CT structure (pdb code: 4CHA) was processed in FLAP to describe the catalytic cavity in terms of the GRID Molecular Interaction Fields (MIFs).[29,30] Probes used to generate the MIFs were H (shape), DRY (hydrophobic interactions), N1 (His bond donor) and O (His bond acceptor) interactions. Thus, the binding poses of the additives in the α-CT cavity were generated using FLAP in the structure-based mode,[31-33] with 50 conformations for each additive considered. The 10 top-ranked poses according to the Glob-Prod descriptor for each additive were visually inspected. The same approach was used in this study to predict the most probable binding mode of GPNA into the α-CT cavity.

S 2.4 General design approach

The design of novel ammonium-based additives was performed based on a molecular modelling approach previously described.[22] Briefly, in that study the FLAP software was used to evaluate the most probable binding pose of four ammonium based additives, aiming at identifying the molecular interactions potentially responsible for the catalytic effect. Figure S 2.4 shows the four tested additives represented three scaffolds: a) aromatic substituted quaternary ammonium additives (BzTMABr, BzTBABr); b) diammonium-based additives with flexible linker (bisBOAB) and c) diammonium-based additives with rigid linker (bisBAB). Here, the previously generated models for each additive were used as a starting point for a rational design of new analogues, aiming not only at optimizing the catalytic effect, but also at validating the hypothesis previously generated. Using the FLAP editing tool, two new additives for each scaffold were designed, trying to optimize their interaction with the α-CT cavity (pdb code: 4CHA) in terms of maximum overlap of GRID molecular interaction fields. The structure of the new additives is also shown in Figure S 2.4.

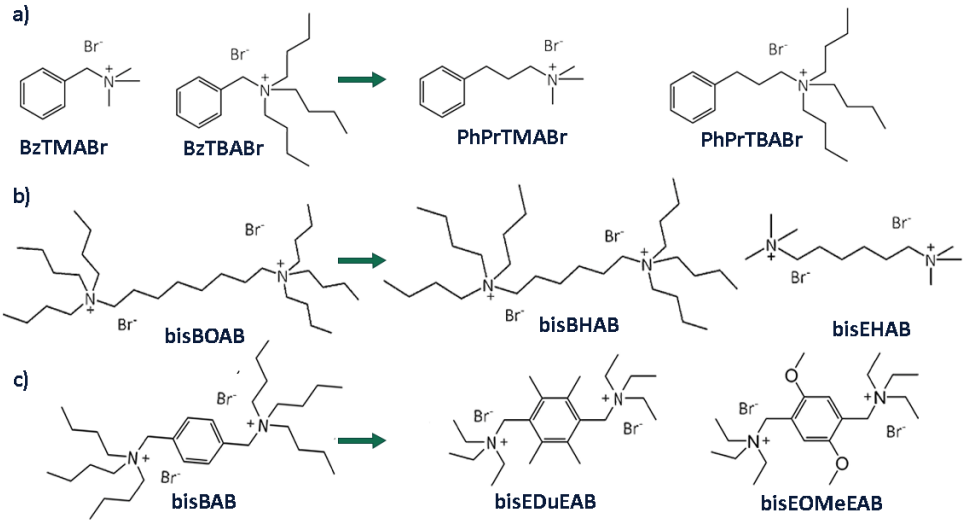

Figure S 2.4: Design of new ammonium additives. Previously tested compounds are shown on the left, while designed structures are illustrated on the right. a) aromatic substituted

quaternary ammonium additives; b) diammonium-based additives with flexible linker; c) diammonium-based additives with rigid linker.

S 2.5 Design of additives and their effect on α-CT activity

S 2.5.1 Phenyl-based ammonium additives

Concerning the phenyl-based ammonium additives (Figure S 2.4 a), previous studies demonstrated a superactivating effect of benzyl-substituted ammonium salts, especially BzTBABr, and modelling suggested the interaction of the phenyl ring with Trp 215 and the orientation of the tributylammonium moiety towards the catalytic triad as key factors in superactivation. Therefore, we used the interaction model to evaluate whether a longer linker between the ammonium and the phenyl moiety could be favorable or detrimental for superactivation to occur. In particular, due to synthetic accessibility, the new additives PhPrTMABr and PhPrTBABr were designed and their most probable binding poses and similarity scores were compared to corresponding BzTMABr and BzTBABr, as showed in Figure S 2.5.

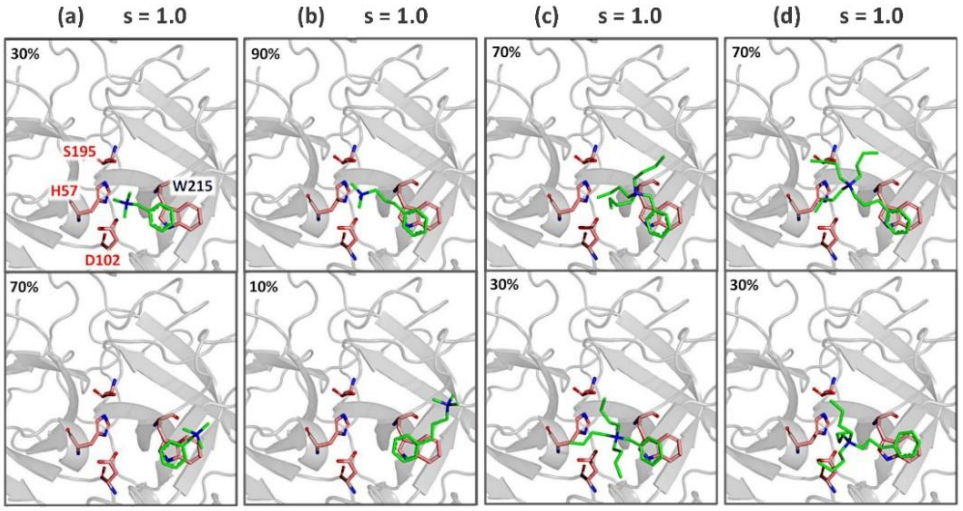

Figure S 2.5: Most probable binding poses for BzTMABr (a), PhPrTMABr (b), BzTBABr (c) and PhPrTBABr (d). For each additive, the ten top-ranked binding poses were analyzed and clustered in the two most different poses, associated to a percentage of occurrence. The similarity score S calculated according to the Glob-Prod descriptor of FLAP is provided (S195: Ser 195; H57: His 57; W215: Trp 215; D102: Asp 102).

Our model suggested that the presence of a propane linker still allows the ammonium moiety of the additive to interact with the hydrophobic moiety corresponding to His 57 closes to the catalytic triad. In the case of the trimethylammonium head groups (Figure S 2.5, a-b) the propane linker seems to facilitate such interaction, increasing the percentage of poses oriented towards the triad. However, compared to the benzyl analogues, PhPrTMABr and PhPrTBABr are located much closer to the catalytic site. Therefore, we decided to synthesize PhPrTMABr and PhPrTBABr, which were predicted to be α-CT superactivators, but the extent of superactivation was uncertain, due to the location of the ammonium group that resulted very close to the catalytic site. Thus, PhPrTMABr and PhPrTBABr were synthesized and their effect on α-CT activity was studied to compare the new results with those obtained for BzTMABr and BzTBABr. Figure S 2.6 illustrates the behavior of the ratio between the reaction rate in the additive solution and in pure buffer (r_{add}/r_b) as a function of the additive concentration for PhPrTMABr and PhPrTBABr.

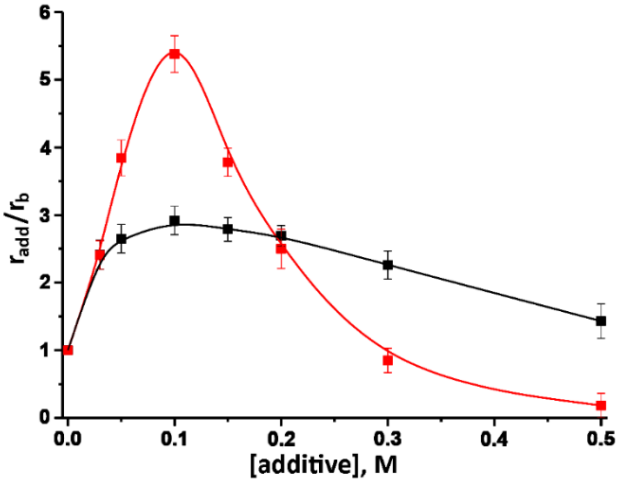

Figure S 2.6: Effect of PhPrTMABr (black) and PhPrTBABr (red) concentration on the activity of α-chymotrypsin in 0.1 M Tris-HCl buffer, pH 7.75 at 25.0 °C.

As predicted by the *in-silico* design, both additives produced an activating effect on the enzyme, and a bell-shaped trend was observed as the concentration of the

additive increased; the maximum of activity was recorded at 0.1 M for both additives. Comparing these results with those previously obtained with the benzyl analogues, however, it was observed that the presence of a propane linker produced a notable decrease in superactivity, almost 40% (from 4.7 to 2.9) for the trimethyl derivative and more than 50% (from 12.4 to 5.4) for the tributyl one. Moreover, the positive effect of a bulky and hydrophobic ammonium group was less evident compared to benzyl additives. Kinetic parameters were determined to deeply understand the effect of these novel additives on enzyme activity and the cause of their lower superactivation with respect to BzTMABr and BzTBABr.

Table S 2.1 reports enzyme-substrate affinity (Michaelis constant, K_M), turnover number (k_{cat}), ratio between k_{cat} values in the presence of additive and in pure buffer ($k_{cat(add)}/k_{cat(b)}$) and k_{cat}/K_M values. Experiments were performed at the additive concentration that produced the maximum superactivation effect.

Table S 2.1: α-Chymotrypsin kinetic parameters in the presence and absence of additives in 0.1 M TRIS-HCl buffer (pH 7.75) at 25.0 °C.

Additive	Km, mM	10^2 k_{cat}, s^{-1}	$k_{cat(add)}/k_{cat(b)}$	k_{cat}/K_M
-	0.44	1.46	-	33.2
BzTMABr 0.4 M[22]	1.37	8.70	5.96	63.5
PhPrTMABr 0.1 M	3.71	10.27	7.03	27.7
BzTBABr 0.15 M[22]	1.99	31.10	21.3	156.3
PhPrTBABr 0.1 M	5.00	24.80	17.00	49.6

Enzyme-substrate affinity decreased significantly in the presence of the two additives but, at the same time, an increase of turnover number than in pure buffer was also found. These trends were very similar to those observed with the benzyl analogues. As regards k_{cat}, trimethylammonium-based derivatives showed similar values, while a decrease of only 20% was observed from BzTBABr to PhPrTBABr. In summary, the lower superactivation produced by the new additives was mainly due to the enhancement in K_M, which was much more pronounced. In particular, the increase in K_M in the presence of BzTMABr and BzTBABr was of about 3- and 4.5-fold

with respect to buffer, respectively, while with PhPrTMABr and PhPrTBABr was 8.4- and 11-fold higher than in buffer. A possible explanation for such increase in the K_M values for PhPrTMABr and PhPrTBABr is that, when a propane linker is used, the access of the substrate to the catalytic cavity is partially hampered reducing the enzyme-substrate affinity. Alternatively, the additive may interact with GPNA making the interaction between enzyme and substrate less efficient. A crystal structure of the GPNA/α-CT complex is not available so far. Thus, the FLAP software was used to predict the most probable binding mode of GPNA that was represented in Figure S 2.7.

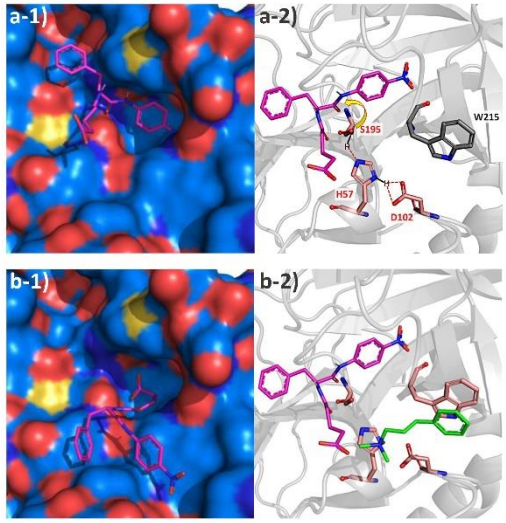

Figure S 2.7: Most probable binding poses for GPNA according to FLAP predictions (a- and b-1); a-2) depiction of the mechanism of hydrolysis of GPNA, according to the GPNA reactive pose; b-2) Simultaneous visualization of GPNA and PhPrTMABr docked into the α-CT cavity, with the protein in cartoon mode to highlight the proximity between the ammonium moiety of the additive and the carboxylate moiety of the substrate.

Two most probable poses were found (Figure S 2.7 a-1 and b-1), whose only one was a potentially reactive pose (Figure S 2.7 a-1), with the corresponding mechanism of hydrolysis depicted in Figure S 2.7 a-2. Indeed, it is well-known that several binding modes are commonly associated to a substrate, but only a few poses generally are compatible with a reactive event catalyzed by the enzyme. Once the most probable reactive pose for GPNA has been determined, this pose was visualized in the α-CT

cavity together with PhPrTMABr, PhPrTBABr, BzTMABr and BzTBABr, as reported in Figure S 2.8.

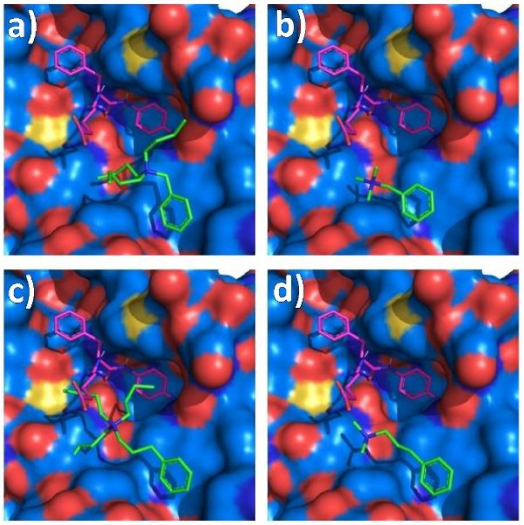

Figure S 2.8: Simultaneous visualization of GPNA and the additives docked into the α-CT cavity. GPNA is shown in purple. Most probable binding pose for BzTBABr (a), BzTMABr (b), PhPrTBABr (c), and PhPrTMABr (d).

This figure is not a real simulation of the interaction of the three molecules (enzyme, additive and substrate), as the substrate and the additive were docked into the protein cavity independently from each other.

However, considering that the additive is added to the enzyme buffered solution before the substrate, Figure S 2.8 suggests that, while BzTBABr and BzTMABr are positioned well at the bottom of the region of interaction of the substrate, simply defining its bottom edge (Figure S 2.8 a and b, respectively), PhPrTBABr and PhPrTMABr are localized much close to the substrate (Figure S 2.8 c and d, respectively). In particular, PhPrTBABr partially occupies the substrate region, and indeed this additive is associated to the highest K_M value in the series (Table S 2.1). In the case of PhPrTMABr, the reduced size of the head group does not induce an overlap of the poses for the additive and the substrate; however, the N-trimethyl moiety of PhPrTMABr is very close to the carboxylic function of GPNA, suggesting a

potential electrostatic interaction that could perturb the orientation of the substrate into the catalytic cavity (Figure S 2.8 d).

S 2.5.2 Diammonium additives with flexible linker

Concerning the diammonium additives with flexible linker (Figure S 2.4 b), the superactivation effect of bisBOAB was found to be lower than the one observed for BzTBABr, and we previously hypothesized that this could be related to the greater flexibility. Thus, the design aimed at verifying the most probable binding modes for two analogues of bisBOAB, having a hexane linker with a triethyl moiety (bisEHAB) or a tributyl moiety (bisBHAB), to modulate hydrophobicity and/or flexibility. The most probable binding poses for bisBOAB and its analogues are shown in Figure S 2.9.

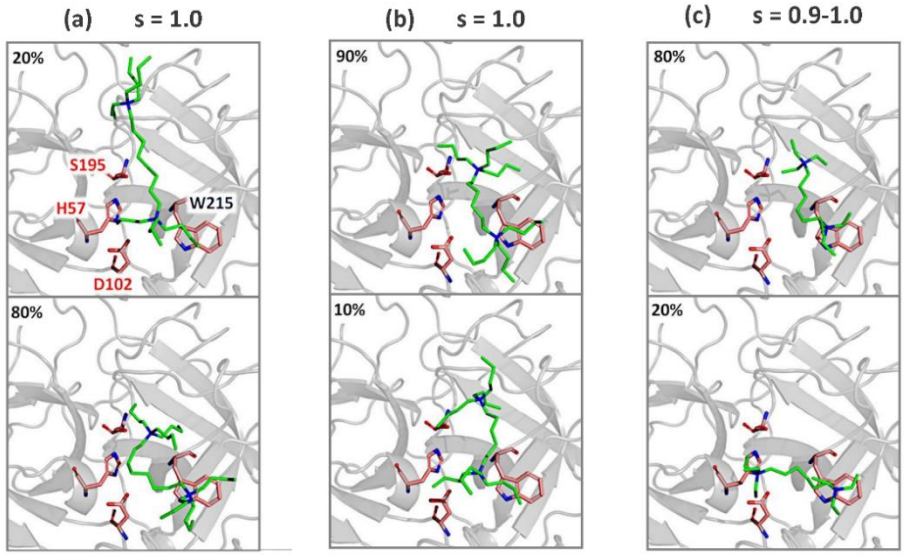

Figure S 2.9: Most probable binding poses for bisBOAB (a), bisBHAB (b), bisEHAB (c). For each additive, the ten top-ranked binding poses were analyzed and clustered in the two most different poses, associated to a percentage of occurrence. The similarity score S calculated according to the Glob-Prod descriptor of FLAP is provided.

The analysis of the binding poses indicated that the shortening of the linker still allows one tributylammonium-based derivatives to anchor Trp 215 and orients the

other towards the catalytic cavity where substrate is usually located (Figure S 2.9 a-b). In particular, the most probable pose for bisBOAB (Figure S 2.9 a, bottom panel) is actually very similar to the most probable one for bisBHAB (Figure S 2.9 b, top panel), as bisBOAB makes a c-curve with the linker that results spatially very similar to the C6-length. Concerning bisEHAB, however, the reduced hindrance at the ammonium level and the shorter linker makes the binding poses much more variable (Figure S 2.9 c), suggesting a lower catalytic effect.

Figure S 2.10 shows the activity profile of α-CT in the presence of buffered solutions of newly synthesized bisEHAB and bisBHAB at varying concentrations.

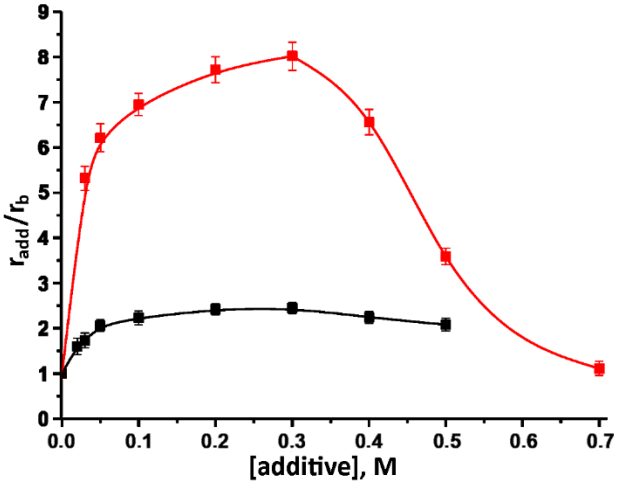

Figure S 2.10: Effect of bisEHAB (black) and bisBHAB (red) concentration on the activity of α- Chymotrypsin in 0.1 M Tris-HCl buffer, pH 7.75 at 25.0 °C.

The two observed trends were rather different. Indeed, in the presence of bisEHAB, the relative rate increased by just a factor of 2 and then remained almost constant in a wider concentration range. On the other hand, a bell-shaped trend of activity was obtained by varying bisBHAB concentration with a maximum activity observed at 0.3 M, in which enzyme superactivation was about 8-fold compared to pure buffer. This behavior was similar to that previously obtained with 0.4 M TBABr and 0.1 M bisBOAB.[22] The presence of the three additives, in fact, increased the rate of the hydrolysis reaction by about 8 folds, confirming once again the essential role

played by the tributyl head group. As previously described,[22] a comparison of the kinetic parameters of TBABr with bisBOAB indicated that, despite of a similar superactivation, the addition of bisBOAB increased the enzyme-substrate affinity, but also decreased k_{cat} value. Thus, the effects of bisEHAB and bisBHAB on enzyme kinetic parameters were also determined and results are shown in Table S 2.2.

Table S 2.2: α-Chymotrypsin kinetic parameters in the presence and absence of additives in 0.1 M TRIS-HCl buffer (pH 7.75) at 25.0 °C.

Additive	Km, mM	10^2 k_{cat}, s^{-1}	$k_{cat(add)}/k_{cat(b)}$	k_{cat}/K_M
-	0.44	1.46	-	33.2
bisEHAB 0.3 M	0.70	3.28	2.25	46.9
bisBOAB 0.1 M[21]	1.86	19.29	13.21	103.8
bisBHAB 0.3 M	1.96	18.44	12.63	94.1

As would be expected, in bisEHAB solutions the two-fold activation with respect to buffer was essentially due to an increase in k_{cat} value, with K_M value that increase of about 70%. The effect of bisBHAB on both enzyme-substrate affinity and turnover number was very similar to that observed in bisBOAB, despite the increase in the concentration required to achieve the same superactivation. This result seemed to confirm the outcomes of modeling studies, according to which the linker length did not significantly change the binding poses of the two additives and therefore their effect on α-CT performance.

S 2.5.3 Diammonium additives with rigid linker

Concerning the diammonium additives with rigid linker (Figure S 2.4 c), we aimed at investigating the effect of substituents in the aromatic moiety. Therefore, having bisBAB as reference compounds, a first *in silico* study was performed to evaluate the binding poses for analogue additives bisEDuBAB and bisEOMeBAB, bearing a durene or a 1,4-dimethoxybenzene scaffold instead of the dibenzyl moiety respectively. According to our model, the replacement of four aromatic hydrogens with methyl groups in bisEDuBAB led to a similarity score, which was identical to that of BisBAB

(S=1), and very similar poses as well. Both for bisBAB and bisEDuBAB, a tributylammonium moiety was involved in the interaction with Trp 215, with the additive displaying two different orientations in the cavity. However, for bisEDuBAB the pose having the aromatic moiety located closer to the catalytic site was more favored. When polar substituents are added to the bisBAB scaffold, molecular modelling studies indicated that a totally different binding mode is preferred. In addition, the similarity score for bisEOMeBAB was lower than the ones for bisBAB and bisEDuBAB, suggesting a less efficient interaction with the protein. The reduced similarity score seems to be mainly related to the lack of interaction with Trp 215, which induces bisEOMeBAB to move towards the inner part of the cavity competing with GPNA. Unfortunately, synthetic accessibility and solubility issues hampered the investigation of bisEDuBAB and bisEOMeBAB; thus, the triethyl analogues bisEDuEAB and bisEOMeEAB were synthesized and tested instead. Figure S 2.11 shows the FLAP most probable binding poses for the two tested compounds, and the poses for bisBAB are also provided for reference.

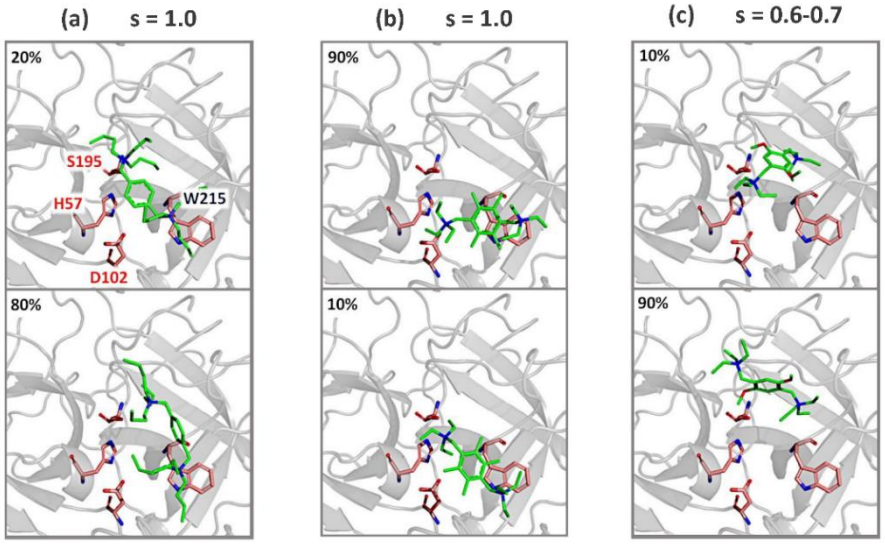

Figure S 2.11: Most probable binding poses for bisBAB (a), bisEDuEAB (b) and bisEOMeEAB (c). For each additive, the ten top-ranked binding poses were analyzed and clustered in the two most different poses, associated to a percentage of occurrence. The similarity score S calculated according to the Glob-Prod descriptor of FLAP is provided.

For bisEDuEAB a similarity score of 1 was obtained, as for bisBAB and bisEDuBAB (S=1). Nevertheless, the hypothesized binding modes were rather different, with bisEDuEAB being not able to reach the oxyanion hole region. This effect seems to be due not to the substituents but to the triethyl ammonium head group, as suggested by comparison with the bisEDuBAB binding poses. Concerning bisEOMeEAB, the similarity score was even lower than that for the tributyl analogue and again lower than the ones for bisBAB and bisEDuAEB, suggesting a less efficient interaction with the protein depending not only on the substitution with polar groups but also on the head group size. As for bisEOMeBAB, an interaction with Trp 215 was not observed. Based on these considerations, a lower catalytic effect was expected for bisEDuEAB and bisEOMeEAB compared to bisBAB. Figure S 2.12 reports the activity profile of α-CT in the presence of bisEOMeEAB and bisEDuEAB as a function of additive concentration.

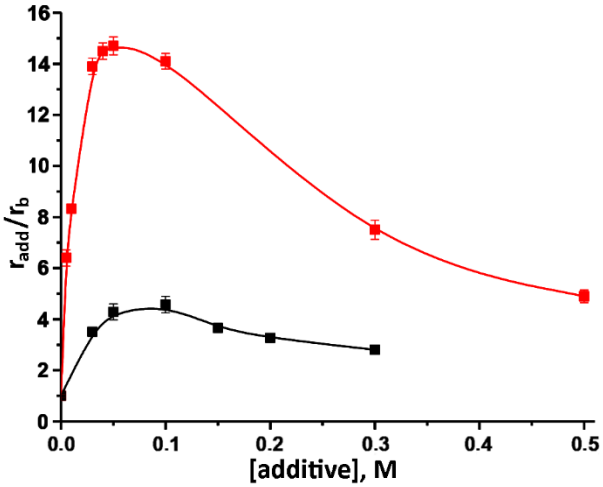

Figure S 2.12: Effect of bisEOMeBAB (black) and bisEDuEAB (red) concentration on the activity of α- Chymotrypsin in 0.1 M Tris-HCl buffer, pH 7.75 at 25.0 °C.

Results obtained with the two diammonium additives having a rigid linker were quite different from each other and compared with bisBAB, the reference additive previously studied.[22] Both curves of reaction rate *versus* surfactant concentration were bell-shaped, with a maximum of activity at additive concentration of 0.1 M and

0.05 M for bisEOMeEAB and bisEDuEAB, respectively. However, superactivation effect produced by the most hydrophobic additive, bisEDuEAB (about 15-fold), not only was higher than bisEOMeEAB (4.5-fold) and bisBAB (6-fold), but it was the highest ever obtained with cationic additives, both surfactants and salts, studied so far. In this case, the hydrophobicity was not due to the bulky tributyl head groups, but to the hydrophobic substituents linked to the aromatic ring. On the other hand, the presence of two methoxy groups, capable of forming hydrogen bonds, probably made the catalytic site much more polar, with a consequent decrease in enzymatic superactivity. Kinetic parameters were also determined and results are provided in Table S 2.3.

Table S 2.3: α-Chymotrypsin kinetic parameters in the presence and absence of additives in 0.1 M TRIS-HCl buffer (pH 7.75) at 25.0 °C.

Additive	Km, mM	10^2 k_{cat}, s^{-1}	$k_{cat(add)}/k_{cat(b)}$	k_{cat}/K_M
-	0.44	1.46	-	33.2
bisBAB 0.1 M[21]	1.49	12.00	8.20	80.5
bisEDuEAB 0.05 M	0.96	24.80	16.99	258.3
bisEOMeEAB 0.3 M	0.96	6.59	4.51	68.6

Enzyme-substrate affinity for both additives was lower than buffer, K_M being double compared to the reference, but was lesser than other superactivating additives, which for BzTBABr and bisBOAB was about 2 mM and for cetyltributylammonium bromide (CTBABr)[17] and tetrabutylammonium bromide (TBABr)[19] were 3.7 mM and 6.1 mM, respectively. An increase in k_{cat} was observed for both additives, but their effects were very different, *i.e.* 4.5-fold for bisEOMeEAB and 17-fold for bisEDuEAB. The value of the turnover number obtained with bisEDuEAB was not the highest reached, since in the presence of BzTBABr and TBABr, was equal to 31×10^2 s^{-1} but, given the greater affinity of the enzyme for the substrate, the catalytic efficiency was certainly the highest reached till now. These results seemed to confirm once again the key role of hydrophobic moieties on the structure of the additive in the superactivation of α-CT, which can increase the nucleophilicity of the catalytic

serine. On the other hand, however, one or more bulky head groups hinder the access of the substrate into the active site, slightly reducing the superactivity.

S 2.6 Conclusion

In this work, an *in silico* model previously used to rationalize kinetic behaviors and superactivation effects of a few quaternary ammonium salts toward α-CT was applied to design new ammonium-based additives of three different chemical series, with the double aim of testing the predicting capabilities of the model and to get new insights on the key interaction in α-CT superactivation. The *in silico* prediction well correlated with experimental findings not only based on the similarity scores obtained, but especially when a binding mode analysis is performed. Regarding phenyl-based additives, the significant reduction in enzyme superactivity observed when a propane linker replaced a methylene was due to an increase in K_M, and molecular modelling studies suggested that these additives partially occupy the substrate interaction region, hindering its access to the active site. The hydrophobic interaction resulted to be critical to improve superactivation, and this was especially evident for the series of diammonium additives bearing a rigid linker. Indeed, bisEDuEAB, which was designed, synthesized and tested in this study, is the most effective ammonium additive studied so far. In addition, bisEDuEAB contrasts the paradigm that bulky hydrophobic head groups are needed to increase the superactivation effect, since the overall hydrophobicity seems to play a role. The presence of hydrophobic substituents linked to the aromatic ring instead of to the head group produced a more hydrophobic microenvironment with a consequent increase in the nucleophilicity of the catalytic serine residue and also allowed an easier entry of the substrate into the active site (lower K_M value than tributyl additives). The amino acid Trp 215 was confirmed to be a key residue for interaction

with superactivating additives. Finally, kinetic parameters were interpreted for the first time also taking into account the potential binding mode of the substrate.

References

1- L. Hedstrom, Chemical Reviews, **102**, 4501-4524 (2002);

2- D.G. Herries, Biochemical Education, **13**, 146 (1985);

3- D.M. Blow, "*The Structure of Chymotrypsin*" in "The Enzymes", P.D. Boyer Ed., ACADEMIC PRESS New York, chap. 6, pp. 185-212 (1971);

4- D.M. Blow, "*Chymotrypsin-Chemical Properties and Catalysis*" in "The Enzymes", P.D. Boyer Ed., ACADEMIC PRESS New York, chap. 7, pp. 213-248 (1971);

5- S.K. Verma, K.K. Ghosh, Kinetics and Catalysis, **52**, 6-10 (2011);

6- M.S. Celej, M.G. D'Andrea, P.T. Campana, G.D. Fidelio, M.L. Bianconi, Biochemical Journal, **378**, 1059-1066 (2004);

7- E. Abuin, E. Lissi, C. Calderón, Journal of Colloid and Interface Science, **308**, 573-576 (2007);

8- S.K. Verma, B.K. Ghritlahre, K.K. Ghosh, R. Verma, S. Verma, X. Zhao, International Journal of Chemical Kinetics, **48**, 779-784 (2016);

9- Y.A. Valiullina, E.A. Ermakova, D.A. Faizullin, A.B. Mirgorodskaya, Y. F. Zuev, Russian Chemical Bulletin, **63**, 273-279 (2014);

10- G.Y. Bai, J.L. Liu, J.X. Wang, Y.J. Wang, Y.N. Li, Y. Zhao, M.-H. Yao, Acta Physico-Chimica Sinica, **33**, 976-983 (2017);

11- T. Kurinomaru, T. Kameda, K. Shiraki, Journal of Molecular Catalysis B: Enzymatic, **115**, 135-139 (2015);

12- A. Endo, T. Kurinomaru, K. Shiraki, Journal of Molecular Catalysis B: Enzymatic, **133**, S432-S438 (2016);

13- A. Endo, T. Kurinomaru, K. Shiraki, Molecular Catalysis, **455**, 32-37 (2018);

14- A. Wangler, R. Canales, C. Held, T.Q. Luong, R. Winter, D.H. Zaitsau, S.P. Verevkin, G. Sadowski, Physical Chemistry Chemical Physics, **20**, 11317-11326 (2018);

15- C. Held, T. Stolzke, M. Knierbein, M.W. Jaworek, T.Q. Luong, R. Winter, G. Sadowski, Biophysical Chemistry, **252**, 106209 (2019);

16- M. Knierbein, C. Held, G. Sadowski, The Journal of Chemical Thermodynamics, **148**, 106142 (2020);

17- N. Spreti, F. Alfani, M. Cantarella, F. D'Amico, R. Germani, G. Savelli, Journal of Molecular Catalysis B: Enzymatic, **6**, 99-110 (1999);

18- F. Alfani, M. Cantarella, N. Spreti, R. Germani, G. Savelli, Biotechnology and Applied Biochemistry, **88**, 001-016 (2000);

19- N. Spreti, P. Di Profio, L. Marte, S. Bufali, L. Brinchi, G. Savelli, European Journal of Biochemistry, **268**, 6491-6497 (2001);

20- F. De Angelis, A. Di Tullio, P. Del Boccio, S. Reale, G. Savelli, N. Spreti, Organic and Biomolecular Chemistry, **1**, 3125-3130 (2003);

21- N. Spreti, M.V. Mancini, R. Germani, P. Di Profio, G. Savelli, Journal of Molecular Catalysis B: Enzymatic, **50**, 1-6 (2008);

22- L. De Matteis, F. Di Renzo, R. Germani, L. Goracci, N. Spreti, M. Tiecco, RSC Advances, **6**, 46202-46211 (2016);

23- J. Weinstock, Journal of Organic Chemistry, **21**, 540-542 (1956);

24- H.J. Barber, K. Gaimster, Journal of Pharmacy and Pharmacology, **3**, 663-669 (1951);

25- T. Iwaguchi, Yakugaku Zasshi, **81**, 925-927 (1961);

26- L. Brinchi, R. Germani, L. Goracci, G. Savelli, C.A. Bunton, Langmuir, **18**, 7821-7825 (2002);

27- N.N.P. Mel'nikov, M.V., Zhurnal Obshchei Khimii, **29**, 3746-3752 (1959);

28- M. Baroni, G. Cruciani, S. Sciabola, F. Perruccio, J.S. Mason, Journal of Chemical Information and Modeling, **47**, 279-294 (2007);

29- P.J. Goodford, Journal of Medicinal Chemistry, **28**, 849-857 (1985);

30- E. Carosati, S. Sciabola, G. Cruciani, Journal of Medicinal Chemistry, **47**, 5114-5125 (2004);

31- G. Muratore, L. Goracci, B. Mercorelli, A. Foeglein, P. Digard, G. Cruciani, G. Palu, A. Loregian, Proceedings of the National Academy of Sciences U.S.A., **109**, 6247-6252 (2012);

32- S. Massari, G. Nannetti, L. Goracci, L. Sancineto, G. Muratore, S. Sabatini, G. Manfroni, B. Mercorelli, V. Cecchetti, M. Facchini, G. Palù, G. Cruciani, A. Loregian, O. Tabarrini, Journal of Medicinal Chemistry, **56**, 10118-10131 (2013);

33- C.G. Fortuna, C. Bonaccorso, A. Bulbarelli, G. Caltabiano, L. Rizzi, L. Goracci, G. Musumarra, A. Pace, A. Palumbo Piccionello, A. Guarcello, P. Pierro, C.E.A. Cocuzza, R. Musumeci, European Journal of Medicinal Chemistry, **65**, 533-545 (2013).

Curriculum Vitae et Studiorum

Francesco Gabriele

Personal information

Citizenship:	*Italian*
Date of birth:	*January 30th, 1990*
Address:	*Via Roma 105, Castelliri (FR), 03030*
Phone number:	*+39 3496090546*
e-mail addresses:	*francesco.gabriele@graduate.univaq.it* *francesco.gabriele.90@gmail.com*

Education and Training

24 CFUs- Teaching courses-Teacher Training: September, 2020

University of L'Aquila, Italy

Scholarship on hydrogel Applications: May – October 2017

University of L'Aquila, Italy

Master's degree in Chemical Sciences (LM54): April 8th, 2017

University of L'Aquila, Italy Summa Cum Laude

Thesis: Development of biocompatible hydrogels for cultural heritage applications

Tutor: Prof. Nicoletta Spreti

Bachelor's degree in Chemical and Material Sciences and Technologies (L27): October 24th, 2014

University of L'Aquila, Italy 103/110

Thesis: Effect of water-soluble additives on the activity of Bovine Carbonic Anhydrase

Tutors: Prof. Nicoletta Spreti and Prof. Raimondo Germani

High School-Chemical technical specialist diploma: July, 2008

Istituto di Istruzione Superiore "Tulliano" Arpino 75/100

Communications to Conferences

F. Gabriele, A. Vetrano, L. Bruno, C. Casieri, R. Germani, N. Spreti "*Effectiveness of oxidative alginate-biocide hydrogels for the removal of microbial contaminants from calcareous stone materials*" European Conference on Biodeterioration of Stone Monuments (ECBSM 2020) (November 5^{th} – 6^{th}, 2020) - remote mode. The scientific committee awarded me for as 'second ex aequo best presentation' of the ECBSM2020 PhD Awards;

F. Di Donato, A.A. D'Archivio, N. Spreti, C. Casieri, F. Gabriele. "*MULTIMETHODOLOGICAL NMR-DSC-IR APPROACH FOR THE CHARACTERIZATION OF TYPICAL PECORINO CHEESES*" XLVIII National Congress on Magnetic Resonance, L'Aquila (September 11^{th} – 13^{th}, 2019);

F. Gabriele, C. Casieri, M. Chiarini, N. Spreti, M. Tortora. "*^{1}H-NMR-RELAXATION AS A POWERFUL TOOL FOR ASSESSING CONSERVATION MATERIALS*" XLVIII National Congress on Magnetic Resonance, L'Aquila (September 11^{th} – 13^{th}, 2019);

L. Goracci, F. Gabriele, M. Tiecco, R. Germani, N. Spreti. "*A structure-activity relationship study on the α-Chymotrypsin superactivation by quaternary ammonium salts*", XXXVIII Convegno Nazionale della Divisione di Chimica Organica, Milano (September 9^{th} – 13^{th}, 2018).

Pubblications

F. Gabriele, N. Spreti, T. Del Giacco, R. Germani, M. Tiecco, "*Effect of Surfactant Structure on the Superactivity of Candida rugosa Lipase*", *Langmuir*, 34, 11510−11517 (2018);

F. Gabriele, M. Chiarini, R. Germani, M. Tiecco, N. Spreti, "*Effect of water addition on choline chloride/glycol deep eutectic solvents: Characterization of their structural and physicochemical properties*", *Journal of Molecular Liquids*, 291, 111301 (2019);

F. Gabriele, L. Goracci, R. Germani, N. Spreti, "*Refining the model to design a-chymotrypsin superactivators: the role of the binding mode of quaternary ammonium salts*", *New Journal of Chemistry*, 44, 20823-20833 (2020);

F. Gabriele A. Donnadio, M. Casciola, R. Germani, N. Spreti, "*Ionic and covalent crosslinking in chitosan-succinic acid membranes: Effect of physicochemical properties*", *Carbohydrate polymers*, 251, 117106 (2021);

F. Gabriele, M. Tortora, L. Bruno, C. Casieri, M. Chiarini, R. Germani, N. Spreti, "*Alginate-biocide hydrogel for the removal of biofilms from calcareous stone artworks*", *Journal of Cultural Heritage*, submitted;

F. Gabriele, A. Vetrano, L. Bruno, C. Casieri, R. Germani, L. Rugnini, N. Spreti, "*New oxidative alginate-biocide hydrogels for calcareous stone*", manuscript in preparation;

A. Vetrano, F. Gabriele, R. Germani, N. Spreti, "*Characterization of Candida rugosa lipase entrapped in alginate beads to enhance its thermal stability and recyclability*", manuscript in preparation.

School

Scuola di Microscopia Applicata ai Beni Culturali (Programma ZEISS Academy) L'Aquila (May 13th -17th, 2019);

V scuola Nazionale di "Chimica dell'Ambiente e dei Beni Culturali", Ravenna (January 23th -26th, 2018).